

**Sedimentological study of a fluvial succession of the Eocene–Oligocene
Bayah Formation, West Java: Reconstruction of paleohydrological
features of an ancient fluvial system using empirical equations developed
from modern fluvial systems in the Indonesia islands**

January 2018

**Chiba University
Graduate School of Science**

**Division of Geosystem and Biological Sciences
Department of Earth Sciences**

Billy G. Adhiperdana

(千葉大学審査学位論文)

Sedimentological study of a fluvial succession of the Eocene–Oligocene
Bayah Formation, West Java: Reconstruction of paleohydrological
features of an ancient fluvial system using empirical equations developed
from modern fluvial systems in the Indonesia islands

2018 年1 月

千葉大学大学院理学研究科

地球生命圏科学専攻地球科学コース

Billy G. Adhiperdana

Contents

Contents	i
List of figures	iv
List of tables	xvi
Abstract	xvii
General Introduction	1
Part 1. Sedimentological Features of a Fluvial Succession of the Eocene–Oligocene Bayah Formation in the Sukabumi High, West Java	
1. Introduction	4
1.1. Background	4
1.2. Research area and datasets	8
2. Geologic Setting	12
2.1. Tectonic framework	12
2.2. Stratigraphy	15
2.3. Regional paleoclimate	18
3. A Fluvial and Lacustrine-Delta Succession	20
3.1. Lithofacies associations	20
3.1.1. Facies association 1: Conglomerate deposits	21
3.1.2. Facies association 2: Conglomeratic sandstone deposits	22
3.1.3. Facies association 3: Sandstone dominated deposits	23
3.1.4. Facies association 4: Interbedded carbonaceous mudstones with laminated mudstones and siltstones	24
3.1.5. Facies association 5: Carbonaceous mudstones with thin lignite traces and thin sandstone intercalations	25
3.1.6. Facies association 6: Crudely stratified gravelly sandstones and bioturbated sandstones with soft sediment deformation structures	27
3.1.7. Facies association 7: Sandy siltstones interbedded with carbonaceous mudstones	29
3.1.8. Facies association 8: Interbedded dark-coloured organic-rich mudstones with plant fragments	30

3.2. Facies relations and depositional systems	32
3.3. Temporal variation in fluvial deposits	35
3.4. Variation in geometry of channel-fill deposits	36
3.4.1. Lenticular and tabular conglomerate-dominated package	37
3.4.2. Tabular and lenticular conglomeratic sandstone package	38
3.4.3. Tabular and lenticular sandstone-dominated package	39
4. Sandstone Petrography and Clay Mineralogy	41
4.1. Variation in sandstone compositions	41
4.2. Variation in clay mineralogy	45
4.2.1. Kaolinite/Illite basal-peak intensity ratio (001)	48
4.2.2. Illite crystallinity index ($^{\circ}\Delta 2\theta$)	52
4.2.3. Illite chemistry index ($5\text{\AA}/10\text{\AA}$)	53
5. Discussion and Conclusions	56
 Part 2. Hydrological Features of Modern Fluvial Systems in the Indonesian Islands	
6. Introduction	61
6.1. Background	61
6.2. Geomorphologic and climatic setting	63
6.3. Data and methods	66
7. Results	70
7.1. Discharges relative to bankfull channel widths	70
7.2. Bankfull channel width and channel depth	71
7.3. River bed and bank materials and bankfull channel width and channel depth	72
8. Discussion	74
8.1. Relationships between bankfull channel width and discharges	74
8.2. Relationships between channel width and mean-channel depth	75
8.3. Comparison of empirical relationships	77
9. Conclusions	81
 Part 3. Application of Hydrological Parameters to the Bayah Formation Fluvial System	
10. Paleohydrologic Reconstruction	84

10.1. Paleohydrological parameters	84
10.2. Paleochannel reconstruction	86
10.3. Paleodischarge reconstruction	89
11. Discussion and Conclusions.	91
General Conclusions	93
Acknowledgements	97
References	98

List of figures

Fig. 1. (A) Present day plate-tectonic setting of Indonesian archipelago. The map was modified from Hall (1996; 2012). The study area is situated at the western part of Java Island, in the southern margin of the Sundaland. (B) Simplified geographical map of the West Java. The study area is located at the southwestern part of West Java, which is indicated by a red-coloured box.	119
Fig. 2. (A) Global climatic changes based on oxygen-isotope records and eustatic sea-level curves (Miller et al., 2005; Kominz et al., 2008; Zachos et al., 2008; Cramer et al., 2009). (B) Regional tectonic and climatic settings of the Late Eocene–Early Oligocene for the SE Asian continental margin. Modified from Hall (1998) and Boucot et al. (2013).	120
Fig. 3. Simplified map of morphotectonic units of the Western part of Java island (modified from Baumann et al., 1973). These units are defined based on the presence of high relief morphology and depressions, which correspond to structural high and low, respectively. The study area is indicated by black-colour rectangle, and situated in the Sukabumi high morphotectonic unit.	121
Fig. 4. Geological map of the study area in the Sukabumi high morphotectonic unit. Modified from Effendi et al. (1989). This map shows the distribution of the Bayah Formation in the Sukabumi high. Outcrops of the Bayah Formation extends along 19 km from the northwest to southeast, forming a homoclinal ridge structure dipping to the south.	122
Fig. 5. Generalized stratigraphic column of the study area in the Sukabumi high (adapted from Adinegoro, 1973; Samuel and Mudjito, 1975; Effendi et al., 1989; Morgenroth et al., 2007; Hendrizan et al., 2012; Morley, 2012).	123
Fig. 6. Summary of facies associations (FA1–FA4) recognized in the Bayah Formation.	124
Fig. 7. (A–C) Outcrop photographs of conglomerates (FA1). Person with yellow circle for scale. (D–E) Close-up photographs of FA1, showing crude foreset bedding (D) and cross-stratified conglomerates (E).	125

Fig. 8. (A) Outcrop photograph of conglomeratic sandstones (FA2). Person with red circle for scale. (B–C) Close-up photographs of FA2, showing crudely graded stratification (B) and poorly bedded conglomeratic sandstones (C).	126
Fig. 9. Outcrop photograph of sandstone-dominated deposits (FA3). Person with yellow circle for scale guide. (B) Close-up photograph of FA3, showing distinct trough cross-stratification. Hammer for scale. (C–D) Current ripples on the top of bedding surfaces the FA3 deposits (C) and a fining-upward pattern to the overlying mudstones (D).	127
Fig. 10. (A) Outcrop photograph of interbedded carbonaceous mudstones with laminated mudstones and siltstones (FA4). Person with yellow circle for scale. (B–D) Close-up photographs of FA4, showing current ripple-laminated siltstones (B and D), carbonaceous fragments (C), and soft-sediment deformation structures (D).	128
Fig. 11. Summary of the facies associations (FA5) recognized in the Bayah Formation.	129
Fig. 12. (A) Outcrop photograph of carbonaceous mudstones with thin lignite layers and thin sandstone intercalations (FA5). Person with yellow circle for scale. (B–D) Close-up photographs of FA5. (E–G) Intercalated sandstone bed types in FA5. Person with yellow circle for scale.	130
Fig. 13. Summary of the facies associations (FA6–FA8) recognized in the Bayah Formation.	131
Fig. 14. (A) Outcrop photograph of crudely stratified gravelly sandstones and bioturbated sandstones with soft-sediment deformation (FA6). Person with yellow circle for scale. (B–C) Close-up photographs of FA6, showing conglomerates and gravelly sandstone with foreset bedding.	132
Fig. 15. (A) Outcrop photograph of crudely stratified gravelly sandstones and bioturbated sandstones with soft-sediment deformation (FA6). Person with yellow circle for scale. (B–E) Close-up photographs of FA6, showing soft-sediment deformation (B and E), load structures (C), and bioturbation (D).	133
Fig. 16. (A) Outcrop photograph of sandy-siltstones interbedded with carbonaceous mudstones (FA7). Person with yellow circle for scale. (B) Close-up photograph of	

FA7, shows rhythmically interlaminated sandy siltstones and mudstones. (C)	
Close-up photograph of FA7, shows intensely bioturbated mudstones.	134
Fig. 17. (A) Outcrop photograph of interbedded dark-coloured, organic-rich mudstones with plant fragments facies (FA8). Person with yellow circle for scale. (B) Close-up photograph of FA8, showing black-coloured, plate-like laminated organic rich mudstones. (C) Close-up photograph of FA8, showing carbonaceous mudstones with papery parting.	135
Fig. 18. Schematic diagram illustrating a generalized model of nonmarine depositional system and facies belts in the Bayah Formation in the study area. Relationships between facies associations and facies belts are shown in this diagram.	136
Fig. 19. Diagram composed of photo panel, interpreted outcrop panel, and log section, which show geometry and stratigraphic relationship of facies associations. The outcrop section represents field relationship between FA3 and FA5. Thick FA5 is encased in FA3. Inclined bedding represents lateral accretion of bar deposits characterizing FA3. Thin type 3 sandstone intercalations present in this FA5.	137
Fig. 20. Diagram composed of photo panel, interpreted outcrop panel, and log section, which show geometry and stratigraphic relationship of facies associations. The outcrop section shows the field relationships between FA1, FA2, and FA5. Distinct erosional surfaces that mark the base of intervals in the base of FA1, which incised into FA5 mudstones.	138
Fig. 21. Diagram composed of photo panel, interpreted outcrop panel, and log section, which show geometry and stratigraphic relationship of facies associations. The outcrop section represents field relationships between FA1, FA3, FA4, and FA5. Fining-upward sandstone deposits of FA3 in the lower part were underlain by mudstone of FA4, and fine upward into FA5 mudstone of floodplain deposits.	139
Fig. 22. Diagram composed of photo panel, interpreted outcrop panel, and log section, which show geometry and stratigraphic relationship of facies associations. The outcrop section represents field relationships between FA3, FA4, and FA5. The lateral offset stacking between the lower FA3 package and the upper FA3 package are characterized by the presence of transitional deposits that consists of interbedded laterally accreted deposits of FA4 mudstones.	140

Fig. 23. Diagram composed of photo panel, interpreted outcrop panel, and log section, which show geometry and stratigraphic relationship of facies associations. The outcrop section represents field relationships between FA3 and FA5. The log section shows coarsening-upward mudstone-dominated deposits of FA5 in the lower part and change upward into the laterally accreted deposits in the FA5 sandstones.	141
Fig. 24. Diagram composed of photo panel, interpreted outcrop panel, and log section, which show geometry and stratigraphic relationship of facies associations. The outcrop section represents vertically stacked relationships between FA8 in the lower part and FA6 in the upper part, which incised into the underlain FA8 mudstones.	142
Fig. 25. Diagram composed of photo panel, interpreted outcrop panel, and log section, which show geometry and stratigraphic relationship of facies associations. The outcrop section represents vertically stacked relationships between FA6 in the lower part, which incised into the underlying FA8 mudstones.	143
Fig. 26. Stratigraphic correlation of the fluvial–lacustrine–delta succession of the Bayah Formation. The succession is divided into 7 intervals (IV1–IV7 in ascending order) based on mapping of 6 distinct erosional surfaces (ESs) (i.e., ES1 to ES6 in ascending order). These erosional surfaces are defined in the base of channel-fill or mouth-bar deposits, which are coarser than those developed beneath each erosional surface. Inset map in the lower right shows locations of measured sections.	144
Fig. 27. (A–B) Example of distinct erosional surfaces at the base of the intervals (ES1 and ES5). These erosional surfaces are defined in the base of channel-fill deposits (FA2 and FA1), which are coarser than those developed beneath each erosional surface.	145
Fig. 28. (A–C) Example of distinct erosional surfaces at the base of the intervals (ES5, ES3, and ES4). In addition to the presence of coarse-grained facies, which developed above the mudstone facies, the distinct erosional surfaces are also characterized by distinct scouring surfaces (A and C).	146

Fig. 29. Interpreted outcrop panel showing larger-scale inclined stratifications, which consist of smaller-scale laterally accreted deposits. These deposits are commonly associated with FA3 and show both tabular and lenticular external geometry. This outcrop is situated within the interval 1 (IV1).	147
Fig. 30. Interpreted outcrop panel showing composite sets of cross-stratification, which represent downstream-accreted deposits. These deposits are associated with FA2 and show tabular geometry. This type of deposits is common in the lower part of the interval 2 (IV2).	148
Fig. 31. Interpreted outcrop panel showing large-scale inclined stratifications, which consist of smaller-scale laterally accreted deposits. These deposits are associated with FA3 and show lenticular geometry. These laterally accreted sandstones are interbedded with mudstones in the upper part. This type of deposits is common in the upper part of the interval 2 (IV2).	149
Fig. 32. Interpreted outcrop panel showing thick high-angled foreset cross-stratifications that represent downstream-accreted deposits. These deposits are associated with FA1 and show sheet-like, and tabular geometry. This type of deposits is common in the interval 3 (IV3).	150
Fig. 33. Interpreted outcrop panel showing composite sets of cross-stratification, which represents downstream-accreted deposits. These deposits are associated with FA2 and show tabular geometry. This type of deposits is common in the interval 4 (IV4).	151
Fig. 34. Interpreted outcrop panel showing large-scale inclined stratifications in the lower part and composite sets of cross-stratification, which represents laterally accreted deposits. These deposits are associated with FA3 and show lenticular geometry. These laterally accreted sandstones are interbedded with mudstones in the upper part. This type of deposits is common in the interval 5 (IV5).	152
Fig. 35. Interpreted outcrop panel showing large-scale inclined stratifications, which consist of smaller-scale laterally accreted deposits. These deposits are associated with FA2 and show tabular geometry. This type of deposits is common in the upper part of the interval 6 (IV6).	153

Fig. 36. Interpreted outcrop panel showing large-scale inclined stratifications, which consist of smaller-scale laterally accreted deposits. These deposits are associated with FA3 and show tabular and lenticular geometry. The laterally accreted sandstones are interbedded with mudstones in the upper part. This type of deposits is common in the interval 7 (IV7).	154
Fig. 37. Schematic block diagram illustrating three types of distinct geometry and style of channel-fill deposits of the Bayah Formation fluvial succession. (A) Lenticular and tabular conglomerate-dominated packages (Type 1 channel-fill deposits). (B) Tabular and lenticular conglomeratic-sandstone packages (Type 2 channel-fill deposits). (C) Tabular and lenticular sandstone-dominated packages (Type 3 channel-fill deposits).	155
Fig. 38. Stratigraphic positions of rock samples for laboratory examination. Stratigraphic horizons of mudstone samples for XRD measurements are represented by green-coloured circles, and those of sandstone samples for petrographic examination are represented by red-coloured circles.	156
Fig. 39. Ternary sandstone classification diagram (Pettijohn et al., 1987) based on quartz grains (Q), feldspar grains (F) and rock fragments (L). The grey-shade area was enlarged to show the sample subdivision into three compositional types i.e. (1) quartz-arenite sandstones, (2) sublithic-arenite sandstones and (3) lithic-arenite sandstones.	157
Fig. 40. Ternary sandstone plots to infer provenance types (Dickinson et al., 1983). (A) Plot based on total quartz (Q = monocrystalline quartz + polycrystalline quartz), feldspar (F = K-feldspar + plagioclase) and rock fragment (L). (B) Plot based on quartz monocrystalline (Qm), Feldspar (F = K-feldspar + plagioclase), and total rock fragment (Lt = rock fragment + quartz polycrystalline).	157
Fig. 41. Map of the Mesozoic basement rocks in the Northwest Java basin and adjacent areas (modified from Hamilton, 1979; Schiller et al., 1991; Hall, 2012). Study area is indicated with a small black-coloured rectangle. The Mesozoic basement rocks consist primarily of granitoid, metamorphic, and volcanic rocks ...	158
Fig. 42. Microscopic photographs representing examples of typical sandstone groups of the Bayah Formation according to the ternary classification. (A) and (B)	

indicate quartz-arenite sandstones ($Q_{97}F_0L_3$ and $Q_{96}F_1L_4$ respectively). (C) and (D) indicate sublithic-arenite sandstones ($Q_{86}F_1L_{13}$ and $Q_{71}F_1L_{29}$ respectively). (E) and (F) indicate lithic-arenite sandstones ($Q_{54}F_5L_{41}$ and $Q_{61}F_2L_{37}$ respectively)	159
Fig. 43. Microscopic photographs representing examples of quartz framework grains of the Bayah Formation sandstones. (A) and (B) show various petrographic aspects of monocrystalline quartz (Qm), indicated by white arrows. (A) and (B) show various petrographic aspects of polycrystalline quartz (Qp), indicated by white arrows.	160
Fig. 44. Microscopic photographs representing various petrographic aspects of feldspar framework grains observed in the Bayah Formation sandstones. (A) Grid twinning of microcline feldspar, indicated by white arrows. (B) myrmekitic texture of K-feldspar, indicated by white arrows. (C) and (D) polysynthetic twinning of plagioclase, indicated by white arrows.	161
Fig. 45. Microscopic photographs representing various classes of sedimentary rock fragments (Ls) observed in the Bayah Formation sandstones. (A) and (B) graywacke fragments, indicated by white arrows. (C) and (D) cryptocrystalline-siliceous rock and chert fragments respectively, indicated by white arrows.	162
Fig. 46. Microscopic photographs representing various classes of metamorphic rock fragments (Lm) and volcanic rock fragments (Lv) observed in the Bayah Formation sandstones. (A) and (B) quartzite and mica-schist fragments respectively, indicated by white arrows. (C) and (D) trachytic and rhyolitic volcanic rock fragments respectively, indicated by white arrows.	163
Fig. 47. Temporal variation in framework composition of sandstones for the eastern sections (locations A, B, C, D, and E are indicated in Fig. 4).	164
Fig. 48. Temporal variation in framework composition of sandstones for the western sections (locations F, G, and H are indicated in Fig. 4).	165
Fig. 49. (A) Bivariant log-plot of the Bayah Formation sandstones to discriminate compositional maturity based on grain types ratios, which are the most sensitive to climatic control (Suttner and Dutta, 1986). (B) Log ratio plot between grain types to indicate the importance of weathering according to Weltje et al. (1998).	

(C) Weathering-index factors are defined in terms of climate and physiographic parameters.	166
Fig. 50. Log-plot between rock fragment–quartz ratio (L/Q) and feldspar–quartz ratio (F/Q) according to Garzanti et al. (2013). The diagram can be used to evaluate the relative importance of climate on detrital mode by estimating the substantial loss of feldspar and rock fragments during weathering of the parent rock lithology in source areas.	166
Fig. 51. Five X-ray diffractograms of mudstone samples of the Bayah Formation. The diffractogram patterns represent five groups of the clay mineral assemblages. This is reflected by the variation in the estimated volume percentages between illite, kaolinite, and smectite. Gradual changes in illite and kaolinite in each group are indicated by pie diagrams.	167
Fig. 52. Mudstone samples for XRD measurement were taken from four predominant types of mudstones of the Bayah Formation. (A) Type 1 mudstones, characterized by thin-bedded, structureless mudstones with white–purplish colours and rootlets. (B) Close-up photo of the type 1 mudstones. (C) Type 2 mudstones, characterized by greyish-laminated mudstones with thin sandstone intercalations. (D) Close-up photo of the Type 2 mudstones.	168
Fig. 53. (A) Type 3 mudstones consist of greyish black, structureless mudstones with minor lignite and plant remains. (B) Close-up photo of the Type 3 mudstones. (C) Type 4 mudstones consist of rhythmite-bioturbated mudstones with concretions and plant remains. (D) Close-up photo of the Type 4 mudstones.	169
Fig. 54. (A) Log-plot of peak-area counts between kaolinite and illite for five clay mineral groups. Each mineral group is distributed nearly parallel to the kaolinite–illite ratio lines. (B) Log-plot of peak-area counts between kaolinite and illite for four different types of mudstone deposits. Two predominant types of mudstone deposits (Types 2 and 3) are distributed nearly parallel to the kaolinite–illite ratio lines.	170
Fig. 55. (A) Temporal and spatial variation in kaolinite–illite ratios for mudstone types of the Bayah Formation. (B) Temporal and spatial variation in kaolinite–illite ratios for clay mineral groups of the Bayah Formation (western sections refer to	

locations F, G, and H; central sections refer to location D; eastern sections refer to locations A, B, C, D, E in Fig. 4).	171
Fig. 56. (A) Temporal and spatial variation in the illite crystallinity index for mudstone types of the Bayah Formation. (B) Temporal and spatial variation in the illite crystallinity index for clay mineral groups of the Bayah Formation.	172
Fig. 57. (A) Temporal and spatial variation in the illite chemical index for mudstone types of the Bayah Formation. (B) Temporal and spatial variation in the illite chemical index for clay mineral groups of the Bayah Formation.	173
Fig. 58. Maps showing the tectonic and geomorphological setting of the Indonesian islands. (A) A plate-tectonic framework of the Indonesian islands. Simplified from Hall (1997). Rectangles show locations used for the collection of hydrological and geomorphological data. (B) Geomorphological features of Java. (C) Geomorphological features of Sumatra. (D) Geomorphological features of Kalimantan. Figures B, C and D are simplified from wikimedia.org (2007), and inset maps show the locations of the islands in the Indonesian archipelago.	174
Fig. 59. Locations of measurement sites for discharges in Java. Site numbers are listed in Table 1.	175
Fig. 60. Locations of measurement sites for discharges in Sumatra. Site numbers are listed in Table 1.	176
Fig. 61. Locations of measurement sites for discharges in Kalimantan. Site numbers are listed in Table 1.	177
Fig. 62. (A) An example of the measurement of a bankfull channel width (W_b) from an aerial photograph Mahakam River in Melak, Kalimantan (site 641 in Table 1) (Google Earth). (B) An example of the cross-sectional geometry of a river channel in the middle reaches of the Mahakam River at Melak, Kalimantan (site 641 in Table 1), illustrating definition of cross-sectional parameters. See Table 4 for list of symbols.	178
Fig. 63. Locations of measurement sites for cross-sectional geometry of fluvial channels in Java. Site numbers are listed in Table 2.	179
Fig. 64. Locations of measurement sites for cross-sectional geometry of fluvial channels in Sumatra. Site numbers are listed in Table 2.	180

Fig. 65. Locations of measurement sites for cross-sectional geometry of fluvial channels in Kalimantan. Site numbers are listed in Table 2.	181
Fig. 66. River bed and bank materials at the measurement sites for discharges in Java. Site numbers are listed in Table 1.	182
Fig. 67. River bed and bank materials at the measurement sites for discharges in Sumatra. Site numbers are listed in Table 1.	183
Fig. 68. River bed and bank materials at the measurement sites for discharges in Kalimantan. Site numbers are listed in Table 1.	184
Fig. 69. An example of the comparison of river morphology using topographic maps and satellite images from the early 20th century, the end of 20th century, and the present to evaluate the degree of engineering modification of fluvial systems. The Citarum River at Tanjungpura is shown in (A) 1917, (B) 1999, and (C) 2015 (site 63 in Fig. 2 and Table 1). Map A is from the 1:50,000 Topografische Dienst. Batavia, surveyed from 1908 to 1917, and reprinted by the U.S. Army Map Service. Map B is from the 1:25,000 Indonesian Agency for Geospatial Information topographic map, surveyed in 1999 and map C is from a Google Earth's aerial photograph. The Bengawan Solo River at Bojonegoro is shown in (D) 1922, (E) 1999, and (F) 2016 (site 271 in Fig. 2 and Table 1). Map D is from the 1:50,000 Topografische Dienst. Batavia, surveyed in 1922, and reprinted by U.S. Army Map Service. Map E is from the 1:25,000 Indonesian Agency for Geospatial Information topographic map, surveyed in 1997, and map F is from a Google Earth's aerial photograph.	185
Fig. 70. (A) Relationships between bankfull channel width (W_b) and mean discharge (Q_{mean}) and (B) between W_b and the bankfull discharge (Q_b) for northward-flowing and southward-flowing rivers in Java and for all rivers in Java.	186
Fig. 71. Comparison of the regression lines for northward-flowing and southward-flowing rivers, and for all rivers in Java. Data are shown in Fig. 70.	186
Fig. 72. Relationships between W_b and Q_{mean} (A) and between W_b and Q_b (B) for westward-flowing and eastward-flowing rivers in Sumatra, and for all rivers in Sumatra.	187

Fig. 73. Comparison of the regression lines for westward-flowing and eastward-flowing rivers, and all rivers in Sumatra. Data are shown in Fig. 72.	187
Fig. 74. Relationships between W_b and Q_{mean} , and W_b and Q_b for all rivers in Kalimantan.	188
Fig. 75. (A) Relationships between W_b and Q_{mean} , and W_b and Q_b for all rivers in Java, Sumatra, and Kalimantan. (B) Comparisons of the regression lines for hydrological data given in A.	188
Fig. 76. Relationship between mean bankfull channel depth d_m and maximum bankfull channel depth (d_b) in (A) Java, (B) Sumatra, and (C) Kalimantan rivers. Relationship between W_b and the maximum bankfull channel depth (d_b) in (D) Java, in (E) Sumatra, and in (F) Kalimantan rivers. Relationship between W_b and d_m in (G) Java, in (H) Sumatra, and in (I) Kalimantan rivers.	189
Fig. 77. (A–C) Empirical relationships between hydrological parameters in Indonesian rivers, and (D–F) comparison of regression lines for these relationships.	190
Fig. 78. Relationships between river bed and bank materials and d_b , W_b , Q_{mean} , and Q_b	191
Fig. 79. Mean annual rainfall data from 2000 to 2013 in Java, Sumatra, and Kalimantan. Data are from Indonesia Central Bureau of Statistics (2015).	192
Fig. 80. Comparison of empirical relationships between hydrological parameters obtained from different regions for (A) Q_{mean} and W_b , (B) Q_b and W_b , and (C) W_b and d_m	192
Fig. 81. Example 1 (IV 5) of log section measurement and interpretation of compound-bar thickness to estimate bankfull-channel depth. The interpreted maximum paleochannel depth associated with this channel-bar deposits was estimated at 3.1 m. Person with black circle give scale guide to the photograph	193
Fig. 82. Example 2 (IV 1) of log section measurement and interpretation of compound-bar thickness to estimate bankfull-channel depth. The interpreted maximum paleochannel depth associated with this channel-bar deposits was estimated at 16.4 m. Person with black circle give scale guide to the photograph ...	194
Fig. 83. Example 3 (IV 2) of log section measurement and interpretation of compound-bar thickness to estimate bankfull-channel depth. The interpreted	

maximum paleochannel depth associated with this channel-bar deposits was estimated at 19.3 m. Person with black circle give scale guide to the photograph ...	195
Fig. 84. Result of the paleochannel dimension and paleodischarge reconstruction using data from the fluvial succession of the Bayah Formation.	196
Fig. 85. Diagram indicating relationships between paleohydrological features of the Indonesian modern river and the reconstructed paleohydrological features of the Bayah Formation.	196
Fig. 86. Schematic illustration of temporal variation in paleohydrological parameters of the Bayah Formation. Each schematic channel dimension represents average paleohydrological parameter values of the intervals (IV1–IV7). Illustrations of paleochannel cross-section and plan-view sinuosity were scaled according to the parameter values.	197
Fig. 87. A schematic summary diagram of temporal variations in framework composition of sandstones, clay mineral composition, and paleohydrological features of the Bayah Formation fluvial–lacustrine–delta succession in relation to its component intervals (IV1–IV7). See Fig. 26 for the definition of the intervals...	198
Fig. 88. The relationships between relative changes in sea level, intensity of weathering, and precipitation for the development of the Bayah Formation fluvial–lacustrine–delta succession in a convergent margin setting influenced by a low-latitude tropical climatic condition during a transitional period from greenhouse to icehouse stages at the Eocene–Oligocene time. IV1–IV7 denote component intervals of the formation defined in Fig. 26.	199
Fig. 89. Summary diagram illustrating the interaction of external factors that control spatial and temporal variations in channel-fill deposits, fluvial styles, and framework composition of the Bayah Formation. Fluctuation in the rate of subsidence, changes in rainfall seasonality, and relative sea level seem to have been the most significant factors of allogenic controls for the development of the Bayah Formation.	200

List of tables

Table 1. Hydrological data from river channels in the Indonesian islands. The numbers correspond to the site numbers in Figs. 59, 60, and 61.	201
Table 2. Cross-sectional data for river channels in the Indonesian islands. The numbers correspond to the site numbers in Figs. 63, 64, and 65.	212
Table 3. Relative percentages of spatial distribution of river bed and bank materials in Java, Sumatra, and Kalimantan islands.	213
Table 4. List of symbols used in the present study.	214
Table 5. Width–discharge relationships in river channels in the Indonesian islands.	214
Table 6. Width–depth relationships in river channels in the Indonesian islands.	215
Table 7. Empirical equations for the relationships between discharge parameters (Q_{mean} and Q_b) and bankfull channel width (W_b) and channel depth (d_m) and channel width (W_b) obtained from different regions.	216
Table 8. Summary of the calculated paleohydrologic parameters of fluvial succession of the Bayah Formation.	217

Abstract

This study intends to (1) clarify the spatial and temporal variation in depositional facies, fluvial styles, and framework compositions of the Eocene–Oligocene Bayah Formation, and (2) reconstruct paleohydrological features of the formation using empirical equations developed from modern rivers in the Indonesia islands, which can characterize hydrological features of fluvial systems developed in a convergent margin under the influence of a low-latitude tropical climate.

The Bayah Formation developed in an active convergent margin setting influenced by a low-latitude tropical climate. It is up to 915 m thick and classified into 8 major lithofacies associations (FA1–FA8), which indicate that the formation formed as a fluvial–lacustrine-deltaic succession and is subdivided into 7 intervals (IV1–IV7) based on 6 distinct erosional surfaces (ES1 to ES6). Temporal variation in channel-fill deposits and framework compositions of the Bayah Formation document complex interaction between relative sea-level, climate, and tectonics in a convergent margin setting.

The mean discharge and bankfull width ($Q_{\text{mean}}-W_b$) relationship has distinct variations within the Indonesian rivers, and reflects regional variations in annual rainfall of a tropical climate. The bankfull discharge and bankfull width (Q_b-W_b) relationship does not show any regional variations regardless of their tectonic and climatic settings, and indicates that fluvial morphology is controlled by flood-related episodic discharge rather than by annual mean discharge. The bankfull and maximum depth (W_b-d_b) and bankfull width and mean depth (W_b-d_m) empirical relationships show distinct variation within the islands, and reflect specific climatic and tectonic settings of each islands. Higher d_m relative to a given

W_b in the Indonesian rivers reflect the combination of high water discharge, overbank protection by thick vegetation cover, and active tectonic movement.

The Bayah Formation shows slight temporal variations in maximum bankfull-channel depths, bankfull-channel widths, maximum bankfull discharges, and channel sinuosity. These variations are interpreted to have induced by the fluvial system similar to some of the eastward-flowing rivers in the alluvial plain of Sumatra and western Kalimantan. Slight temporal variation in paleohydrologic features of the Bayah Formation is more likely to represent temporal variations in paleodischarges, which were associated with the ever-wet–seasonal transition periods of the equatorial climate in the Sundaland region under an overall change from greenhouse to icehouse condition in global climates.

General Introduction

This study intends to (1) clarify the spatial and temporal variation in depositional facies, fluvial styles, and framework compositions of the Eocene–Oligocene Bayah Formation, and (2) reconstruct paleohydrological features of the formation using empirical equations developed from modern rivers in the Indonesia islands, which can characterize hydrological features of fluvial systems developed in a convergent margin under the influence of a low-latitude tropical climate.

The major purposes of the present study have been driven by three main motivations. The first motivation is that the Eocene–Oligocene Bayah Formation is considered to have developed in an active convergent margin of the SE Asian continent (Fig. 2), which represent quite different fluvial deposits to other fluvial deposits of an active convergent margin such in Japan and South-American margin. Detailed depositional processes and environments of Cenozoic nonmarine deposits in the southern margin of SE Asian continental margin is still poorly understood because a detailed outcrop-based study on these deposits has not yet been conducted. Moreover, representative outcrops are scarce, and most of the Paleogene nonmarine deposits have not been exposed on outcrops. Consequently, the outcrop of the Bayah Formation in the study area provides an only representative nonmarine Paleogene deposits in Java Island. The second motivation is that up to the present, most of the empirical equations regarding fluvial hydrology were developed based on modern fluvial systems in passive margin and/or interior continent under the influence of mid- to high-latitude climatic conditions. Those empirical equations can not be directly applied to ancient fluvial deposits, which were developed in an active

convergent margin under the influence of low-latitude climatic condition in the tropical region. The third motivation is that the reconstruction of paleohydrological features of the Bayah Formation fluvial deposits, because the Bayah Formation developed during the Eocene to Oligocene times. This is an important period when the global climate shifted from greenhouse to icehouse conditions, and it should be a great value to better understand what happened in tropical nonmarine environment during this period. Because the tectonic and climatic settings for the sedimentation of the Bayah Formation can be considered to have been equivalent to those in the modern fluvial systems in the Indonesian islands, it is also important to clarify how the interaction between the tectonic, climate and sea-level changes controlled the nonmarine sedimentation in an active convergent margin in a tropical region.

To clearly address those motivations, the present study is divided into three main parts (Part1–Part3) that represent different aspects of the significance of the present study as follows: Part 1: sedimentological features of the Eocene–Oligocene Bayah Formation, Part 2: hydrological features of modern fluvial systems in the Indonesian Islands, and Part 3: the application of hydrological parameters to the Bayah Formation fluvial system, respectively.

Part 1.

**Sedimentological Features of a Fluvial Succession of the
Eocene–Oligocene Bayah Formation in the Sukabumi High,
West Java**

1. Introduction

1.1. Background

The geology of sedimentary basins and their hinterlands in the Indonesian archipelagoes have been widely studied since the Dutch-colonial era in the early 20th century until recently (Ben-Avraham and Emery, 1973; Katili, 1989; Hall and Morley, 2004) (Fig. 1). These studies have been motivated primarily by their potentials as prolific oil and gas producing basins, and coal-bearing deposits (Atkinson et al., 2006; Doust and Noble, 2008; Hall, 2009). However, the interests of these studies have also focused on regional geology and tectonics, which have intended to better understanding of regional geology, geologic composition, tectonics, and volcanology of the islands (e.g., van Bemmelen, 1963; Katili, 1971; 1989; Hamilton, 1979; Wight et al., 1997; Davis et al., 2007). Geological researches on sedimentary basins in West Java Island are largely a part of these studies. The sedimentological studies of oil- and gas-producing basins in Indonesia began in the Early Eocene successions (Hamilton, 1979; Martodjojo, 1984; Whateley and Jordan, 1989; Hall and Morley, 2004; Hall, 2009). The prominent characteristic of the sedimentation history of these Early Eocene basins is represented by the common infilling of nonmarine depositional systems. (Butterworth and Atkinson, 1993; Cole and Crittenden, 1997; Longley, 1997; Witts et al., 2012; Morley and Morley, 2013). The early sediment history of these nonmarine depositional systems covering alluvial-fan, lacustrine, and fluvial deposits. These nonmarine deposits are widely distributed from the North Sumatra basin to the north, through Central and South Sumatra basins, Northwest Java basin, Barito basin, and Central Kalimantan, to East Kalimantan

basins (Whateley and Jordan, 1989; Cole and Crittenden, 1997; Longley, 1997; Witts et al., 2012; Morley and Morley, 2013).

By now, geological studies on these Paleogene nonmarine sediments have only focused on reservoir and oil source rocks for oil and gas explorations. Moreover, those studies are generally conducted based on subsurface data, such as drilling and wireline-log data, which were stratigraphically limited only to hydrocarbon-bearing stratigraphic intervals. (e.g., Whateley and Jordan, 1989; Butterworth and Atkinson, 1993; Young et al., 1995; Carter, 2003; Atkinson et al., 2006; Darmadi et al., 2007). A scientifically detailed and comprehensive study, in terms of sedimentology and genetic stratigraphy of the nonmarine Paleogene deposits in the western Indonesia basins, has not yet been conducted on the basis of detailed outcrop analyses. An outcrop based study on temporal and spatial variations in lithofacies, fluvial styles, compositional framework and paleohydrologic reconstruction are critical steps to a better understanding of sedimentary history and basin development in the Indonesia islands.

The nonmarine Paleogene sedimentary rocks that document depositional history of the Indonesian basins are rarely exposed on onshore outcrops. Some exceptional well exposed outcrops, which represent extensive lateral variations in geometry and lithofacies organization of nonmarine deposits, have commonly been situated in quarries and coal mines. In the Sumatra and Kalimantan islands, outcrops of nonmarine Paleogene deposits have been reported only in several locations. In the Java island, representative outcrops of nonmarine Paleogene deposits have also only been reported in a few localities in the southern parts of the West Java island (Martodjojo, 1984; Schiller et al., 1991; Kusumahbrata, 1994; Effendi et al., 1998). In contrast, well-exposed outcrops are available

in the Sukabumi-high of the West Java island, and can provide an opportunity to conduct detailed outcrop-based analyses of nonmarine deposits (Figs. 1 and 4).

The interaction between tectonic, relative sea-level and climates is an important controlling factor of spatial and temporal variations in fluvial sedimentation. Tectonic activity controls the rate and magnitude of subsidence and uplift of a sedimentary basin. In contrast, a climatic factor controls rainfall, erosion, and vegetation, and is also considered to affect fluvial sedimentation (e.g. Blair, 1987; Shanley and McCabe, 1994; Leeder and Stewart, 1996; Catuneanu and Elango, 2001; Macklin et al., 2012; Foreman et al., 2012; Blum & Törnqvist, 2000). These two major factors have been interpreted to control spatial and temporal variations in channel dimension, channel patterns, vertical stacking, facies organization, and composition of fluvial deposit (e.g. Rust and Gibling, 1990; Allen et. Al., 2014; Foix et. Al., 2013; Fabuel-Perez, 2009; Ghazi and Mountney, 2011).

Sedimentological studies focusing on spatial and temporal variations in fluvial sedimentation in terms of the interaction between climate, tectonics, and relative sea-level changes are generally conducted mainly on fluvial successions developed in continent interior and passive margin setting, and also in some basins that are associated with a collisional orogenic setting (Miall, 1996).

Detailed sedimentological studies in an active, convergent-margin setting is fewer than those in other tectonic settings, except for a few case studies such as Santra et al. (2013) who studied the Eocene fluvial deposits located in the Tyee forearc basin of the North American plate. The Eocene fluvial deposits in the Tyee basin are characterized by alternations of incisional fluvial-dominated channel deposits with only thin and minor mudstones intercalations and underlain by shallow-marine deposits. Another example of fluvial deposits formed in a forearc region is the Jurassic–Lower Cretaceous fluvial

deposits formed in a subduction zone of the Gondwana margin (Nichols and Cantrill, 2002). This is the Jurassic–Lower Cretaceous fluvial deposits, and is characterized by the development of very thick braided river deposits over the underlain shallow-marine deposits with a distinct erosional contact that is considered to have formed in response to a sudden base-level fall in association with a regional uplifting process.

Better understanding of fluvial depositional models from different tectonic setting and different climatic conditions is very important in hydrocarbon exploration and production, because they have played an important role in oil-producing basins worldwide, and fluvial deposits are important reservoir and source rock deposits. A significant volume of oil and gas has been discovered in fluvial-sandstone reservoirs in the North Sea, Alberta, Gulf Coast, the Gulf of Thailand, and in the Northwest Java basin as well (Bustin and Chonchawalit, 1995; Miall, 2006; Doust and Sumner, 2007). The Eocene–Oligocene fluvial succession of the Bayah Formation provides an additional example of fluvial records that developed in a forearc setting of an active continent margin under the influenced of a tropical climatic condition in a low-paleolatitude, equatorial setting (Hall, 1996; 2013; Morley, 1998; 2012; 2013). In addition, the Bayah Formation in the study area provides an opportunity to document detailed geometry, lithofacies organization, and heterogeneity of fluvial deposits, which can be used for a better understanding of the sub-surface fluvial deposits that have served as important hydrocarbon plays in hydrocarbon producing basins of the northwest Java.

By the integration of data consisting of sedimentologic log sections from moderately to well exposed sedimentary rock outcrops, sandstone petrographic examination, and clay mineral analyses using an X-ray diffraction measurement, this study intends to (1) describe detailed lithofacies associations and the relationships between facies associations in the

fluvial succession, (2) clarify the stratigraphic subdivisions in the fluvial succession, (3) identify lithofacies characteristics, and spatial and temporal variations in thickness and geometry of fluvial channel-fill deposits, (4) document spatial and temporal variations in framework composition of sandstones and clay mineral composition for clarifying provenance and climatic settings of the deposits, (5) reconstruct paleohydrology of fluvial deposits in terms of channel dimensions and paleodischarge parameters, and (6) discuss possible allogenic factors for the development of the fluvial sedimentation in the Bayah Formation in terms of the interaction between climatic, tectonic and sea-level changes.

In fluvial sedimentation of a nonmarine depositional system, climates have played an important role in the intensity of weathering and erosion in a provenance terrane (Weltje et al., 1998; Garzanti et al., 2013). Moreover, climates may also have been an important role as a control of hydraulic factors, such as slope gradient and water discharges (Blum & Törnqvist, 2000; Bridge, 2003; Shibata et al., 2010).

1.2. Research area and datasets

A study area is located at the outcrop exposures of the Bayah Formation in the Sukabumi high. In the Sukabumi high, the Eocene–Oligocene Bayah Formation is also known as the Walat Formation. The study area is situated in the 12-km west from the nearby city, Sukabumi. The outcrop of the Bayah Formation at the study area forming a 15-km-long and 4.5-km-wide homoclinal ridge with the inclined strata dipping to the south. This homoclinal ridge appears as an elongated hill which is oriented in the WNW–ESE direction. The local geographic name of this hills is the Walat hill. Therefore, the

Bayah Formation in the Sukabumi high is also known as the Walat Formation (Martodjojo, 1984; Effendi et al., 1989). This homoclinal ridge represents a northern limb of a larger synclinal form (Fig. 4) with an axial line oriented in the E–W direction. In contrast to the northern limb, the Bayah Formation is not exposed in the surface in the southern limb of the syncline. In this southern part of the syncline, the Bayah Formation is covered with younger rocks, such as limestone and marl deposits of the Rajamandala Formation, and volcanic deposits of the Jampang Formation.

Composite stratigraphic profiles were obtained from several geological traverses, crossing from the north to the south intersecting strike of bedding of the Bayah Formation that almost parallel to the long axis of the homoclinal ridge. The sections of these geological traverses pass through several main quarries for mining quartz grain deposits. The relatively well-exposed outcrops are commonly occurred at quarries of the quartz mines, which are widely operated along the homoclinal ridge of the Walat hill. Together with the quarries, outcrops are also found locally in the roadcuts and rivercuts. There are twelve main locations of the quarries mining for quartz deposits in the study area. The locations of these main quarries are divided into two major areas in the eastern and western parts of the Walat ridge. Eight main stratigraphic sections are distributed in these twelve locations of the main quarries (A–H, in alphabetical order). In the western part (Fig. 4), well exposed outcrop locations that situated in the main quarries are as follows (from south to north): (1) Sekarwangi, (2) Bantarmuncang, and (3) Pasir Bongkok, respectively. In the eastern part (Fig. 4), well exposed outcrop locations that situated in the main quarries are as follows (from south to north): (1) Cimenteng, (2) Cantayan, (3) Kampungkemang, (4) Padaasih–Gunung Kerud, (5) Pasirpogor, (6) Selagombong, (7) Kadupugur–Cibatu river, and (8) Cipicung. Each designated by the letters F, G, and H, respectively.

The Bayah Formation in the Sukabumi-structural high attains a total thickness of 915 meters based on measured sections in the outcrops which are located in the quarries, hill sides, roadcut, and rivercut within the eight major locations of geological traverses (A–H). In addition to the exposures of mudstone deposits, the outcrop conditions of sandstone and conglomerate bodies that represent channel-fill deposits are not entirely well exposed. In general, the outcrops of these sandstone bodies (packages) and conglomerate bodies (packages) are only partially exposed. However, these partially exposed geometry and internal characteristics of these channel-fill deposits in the Bayah Formation can be clearly identified in the limited outcrop belts. In some of the well exposed outcrops in the quarry areas, the extent of lateral dimensions of these sandstone and/or conglomerate packages are exposed on the surface of more than 200 lateral extent, with the thickness of more than 100 meters in some sites, such as Bantarmuncang, Sekarwangi, Pasirbongkok, Kadupugur, and Pasirpogor.

In addition to the measured sections and lithologic description, sketching internal organization of sandstone and conglomerate bodies, taking mosaic photographs, paleocurrent measurements, and rock sampling were also conducted at the outcrop locations. Hand-specimen samples were obtained from sandstone beds for petrographic examination and from mudstone deposits for X-ray diffraction (XRD) measurement. Eighty four mudstone samples were used for clay mineralogic analysis by XRD measurement. Eighty seven sandstone samples were prepared in thin sections for petrographic examination. Several thin section samples were stained with the alizarin red-S to distinguish between plagioclase and potassium feldspar.

Framework grain composition for provenance analysis and for sandstone classification in petrographic examination were obtained from modal analyses using counting grid-point

intersections on petrographic parameters in the samples. Point-counting procedure in this study were performed following the Gazzi-Dickinson method (Ingersoll et al., 1984). Grid-intersection points of 450–560 counts were counted for each sample. Point-counting were performed to several petrographic parameters following the parameters of Dickinson and Suczek (1979). The XRD patterns of the mudstone samples were measured using a Rigaku Geigerflex X-ray diffraction spectrometers with Cu K α radiation. The data were measured from 5 to 40° 2 θ for the samples that were treated with ethylene-glycol solvation. Samples were determined and semi-quantitatively calculated by using X Powder Pro software.

2. Geologic Setting

2.1. Tectonic framework

According to a morpho-structural setting of the western part of Java island, the study area is situated in the Sukabumi high structural unit (Bauman, 1973) (Figs. 3 and 4). The morpho-structural subdivision of the West Java was defined mainly based on the presence of subsurface high- and low-structures. The Sukabumi high represents morpho-structural high that was created by the Neogene structural inversion processes (Samuel and Mudjito, 1975; Martodjojo, 1984). Within a framework of the regional geology of West Java, the Bayah Formation represents a succession of nonmarine siliciclastic deposits of the Eocene–Oligocene epoch, which have been exposed in the Sukabumi high (Baumann et al., 1973; Samuel and Mudjito, 1975), and is the oldest stratigraphic unit in the Sukabumi High.

Kusumahbrata (1994) stated that the Sukabumi high is a part of the Southwest Java basin, which is situated at the southern part of the Bogor basin (Martodjojo 1984). The sedimentary basins of the western part of Java were situated at the southern edge of the Sundaland that formed close to Cenozoic subduction margins (Fig. 1A), and appears to have formed in a backarc setting during the Paleogene (Clements and Hall, 2007; Clements and Hall, 2011; Hall and Morley, 2004). The Sundaland is the continental core of SE Asia (Hamilton, 1979) formed by the accretion of blocks to the Eurasian margin by the Late Triassic (Hall, 1996; Clements & Hall, 2007). The Sundaland contains a large number of Cenozoic sedimentary basins, which formed from the Paleogene to the Middle Miocene (Hall & Morley, 2004).

The Southwest Java basins, which were a part of the larger Bogor basin, have been initially developed in the Early Eocene in a forearc region, which is characterized by faulted blocks that infilled with nonmarine deposits (Martodjojo, 1984; longley, 1997; Hall and Morley, 2004). During the Oligocene time, this basinal area changed into shallow-marine area over the continental crust. Shallow-marine limestone deposits of the Oligocene Rajamandala Formation represent platform carbonate deposits that conformably overlie the Bayah Formation. At a later development phase during Miocene, this basinal area was characterized by the presence of northward verging thrust faults at the southern part of the basin that indicate the initiation of a retroarc basin. During this basinal development phase, a volcanic arc shifted to the southern part of the basin, in association with the orogenic wedge (Dickinson and Suczek, 1979; Martodjojo, 1984; DeCelles and Giles, 1996; Clements et al., 2009). In this phase, the Bogor basin became to be represented mainly by marine environments. Volcaniclastic sedimentation sourced from the volcanic arc in the southern part of basin was also commenced during this phase. Among volcaniclastic deposits, the Jampang Formation is represented by mass-transport deposits and is considered to represent a deepwater setting of the basin development (Martodjojo, 1984).

From the Eocene onwards numerous sedimentary basins formed throughout the Sundaland. Cenozoic sediments were deposited on a variety of basement rocks ranging from granites to ophiolites. The sedimentary records typically begin at the Eocene or Oligocene, and the older parts of most sedimentary successions are terrestrial (Hall & Morley, 2004). Much of the southern Sundaland was a site of deposition of alluvial, fluvial, and deltaic sediments (Hall, 1998; 2009; 2013).

The most prominent structural elements on the Sunda Shelf were faults or block faulting, which clearly controlled the basins distribution. Some fault may have been

originated as strike-slip faults, but others are mainly normal faults to configure a series of blocks. Graben-like basins that include the Sunda and West Java basins are considered to have formed by tensional forces (Ben-Avraham and Emery, 1973). Late Cretaceous–Paleocene basement rocks for the Cenozoic basins in the Northwest Java have been identified based on drilling and subsurface data. These Late Cretaceous–Paleocene basement rocks consist mainly of granitoid rocks and low-grade metamorphic rocks (Patmosukismo and Yahya, 1975; Hamilton, 1979). The Paleogene volcanic rocks of the Jatibarang Formation has also been identified in the Northwest Java basin based on the subsurface data, together with the Mesozoic basement rocks (Soeria-Atmadja et al., 1998; Soeria-Atmadja and Noeradi, 2005).

The presence of coeval plutonic and volcanic rocks to the north in the Northwest Java basin are considered to represent subduction-related magmatic arc in the Early Cenozoic. The west Java–Sumatra active continental margin has features similar to an Andean-type continental margin (Soeria-Atmadja et al., 1998). The Andean-type continental margin of the West Java is characterized by the presence of plutonic rocks in association with metamorphic rocks as an arc massif, which is overlain by volcanic rock successions, together with accumulation of sedimentary deposits formed on the arc massif. Depositional setting of these sedimentary succession was in between an arc massif–trench system, and can be defined as a forearc region (cf. Dickinson and Seely, 1979). The basinal area where the sedimentation of fluvial succession of the Bayah Formation took place is considered to have been situated at the forearc basin, according to this tectonic framework of the Northwest Java basin. In terms of a plate tectonic framework of the continental-margin and arc-trench system, this basinal area is also known as the continental-margin

arc-massif basin, in which nonmarine deposits were initially developed (cf. Dickinson and Seely, 1979).

2.2. Stratigraphy

In the southern part of the SE Asian continental margin, Cenozoic rocks rest on older rocks with distinct unconformities. Rocks beneath the unconformity are considered to be basement rocks that consist mainly of the Cretaceous and older granites, Mesozoic sedimentary rocks, accreted ophiolitic and arc rocks, and pre-Mesozoic metamorphic rocks (Ben-Avraham and Emery, 1973; Hamilton, 1979; Hall, 2012). Sedimentary rocks above the unconformity are the Eocene and younger, which were deposited mainly in block-faulting induced sedimentary basins along the Sundaland continental margins. However, their depositional ages are poorly constrained (Clements et al., 2011).

At the southwestern side of the West Java, the Paleogene succession is generally dominated by quartzose clastic fragments derived from the crystalline basement of the Sunda Shield to the north. At Gunung Walat of the Sukabumi structural high, the succession is represented mainly by fluvial and/or fluvio-deltaic sediment (cf. Martodjojo, 1984 & 1986), while near Bayah it is represented much more by deltaic to shallow-marine sediments. To the further west in Cihara, the same succession changes mainly into shallow-marine deposits. To the south in the Ciletuh, it is represented by coarse clastics deposits, which are believed to have formed in a submarine-fan environment (Schiller et al., 1991).

The West Java is divided into ten major structural elements, comprising highs and lows. The Bayah Formation is situated in a small elevated structural inversion called the Sukabumi high, to the south of prominent volcanoes in the West Java (Baumann et al., 1973). Quartz sandstone of the Bayah Formation in the Walat hill, which is the oldest outcropping unit in the Sukabumi high, is barren of marine fossils and is thought to have been deposited as a fluvial succession. Some spores and pollens indicate that its most probable age is early Oligocene in the Sukabumi high (Figs. 3, 4, and 5). In this high, this unit is conformably succeeded by marine marls of the Batuasih Formation and its age is considered to be late Oligocene according to scattered planktonic foraminiferal fauna. This formation is overlain unconformably by a fairly thick reefal limestone that is defined as the Rajamandala Limestone (Adinegoro, 1973; Baumann et al., 1973).

Effendi et al. (1989) described the Bayah Formation at the Walat hill in Sukabumi as a unit that is characterized mainly by cross-stratified quartz sandstones and conglomerates, carbonaceous claystones, lignite and thin coal seams and represented by an overall showing coarsening-upward succession. According to the pre-war Dutch geological report, the Bayah Formation at the Walat hill was assigned to an Early Oligocene age, an oldest formation found in the area, and the thickness was estimated to be between 1000 and 1373 meters (Effendi et al., 1989). The Bayah Formation at the Sukabumi high is unconformably overlain by a limestone unit equivalent to the Rajamandala Formation and shales of the Batuasih Formation. The limestone unit was developed over the Bayah Formation in response to a transgression (Martodjojo, 1986; Effendi et al., 1989). The basal contact of the Bayah Formation with the Mesozoic basement rocks is not visible in the Sukabumi high, the lowermost part of the formation and the basal unconformable contact with the

Mesozoic rocks were buried by extremely thick Quaternary pyroclastics and their reworked deposits in the north.

A generalized stratigraphic column of the study area in the Sukabumi high (Figs. 4 and 5) was proposed by the previous workers. (Adinegoro, 1973; Samuel and Mudjito, 1975; Effendi et al., 1989; Morgenroth et al., 2007; Hendrizan et al., 2012; Morley, 2012). Based on spores and pollen found in quartzose sandstones in the upper part of the Bayah Formation at the Pasir Bongkok site, including *Florschuetzia trilobata*, *Monocalpites medius* (pollen) and *Verrumonoletes usmensis* (spore), the age of the Bayah Formation was assigned to be the Early Oligocene (Samuel and Mudjito, 1975; Martodjojo, 1984). In contrast, the palynology records which were taken from the lower part of the formation at the Gunung Walat site, contain *Meyeripollis nayarkotensis*, *Proxapertites operculatus* and *Palmapollenites kutchensis*, indicating the age of the formation as the Late Eocene (Morley, 2012). Calcareous nanno plankton and planktonic foraminifera samples, which were taken from marine deposits of the Batuasih Marl that conformably overlies the Bayah Formation give CP18 and P19 paleontologic zones, respectively (Morgenroth et al., 2007; Hendrizan et al., 2012). These zones represent Early Oligocene–Late Oligocene and this age gives age constraint for the end of the nonmarine depositional system of the Bayah Formation.

Detrital geochronology based on the apatite fission-track dating from the Bayah Formation in the Sukabumi high revealed an age of 35 ± 8 Ma (Middle Eocene to Early Oligocene), and this records a thermo-tectonic age of annealing temperature of apatite grain during burial (Soenandar, 1997). This geochronologic age indicates that a burial stage of a part of the Bayah Formation started at between 40–25 Ma.

2.3. Regional paleoclimate

Regional palaeoclimate of the SE Asian continental margin are summarized below for two reasons. The first reason is that climate is very important factors to control the sedimentation of nonmarine deposits even during the Paleogene. The second reason is that the SE Asian continental margin has experienced distinctive paleogeographic changes in association with global climatic changes that may also have influenced the climate in studied region (Hall, 1998; Morley, 2012; Morley and Morley, 2013). The information on the paleoclimatic conditions during Paleogene in the Sundaland region was obtained from palynological records from coal deposits, which were sampled from several locations in the Sumatra, Java, and Kalimantan islands (Morley, 2012; Boucot et al., 2013).

The affinities of the Paleogene flora of Kalimantan and Sumatra are essentially pantropical, and suggest a difference from an Australian affinity. Palynological evidence is therefore suggests that the islands of Sumatra and Borneo maintained an equatorial position, in contact with an Asian landmass throughout the Cenozoic, and the position of the Java island was situated slightly south of the equator at low latitude (Morley, 1977, Boucot et al., 2013).

In the Eocene, equatorial climate in the Sundaland region developed from a subhumid everwet to seasonal, which was reflected by the common occurrence of coals (Morley, 1998; Morley, 2012). In the Cenozoic climatic and environmental history of the Southeast Asian continental margin, the occurrence of coals coincided with periods of everwet climate (Morley, 2012). Based on the widespread occurrence of the low-pollen vegetation from Sumatra to West Java (*Barringtonia*), Oligocene climates in some parts of Sumatra

and Java Sea developed from subhumid seasonal to everwet conditions (Morley, 2012; Morley and Morley, 2013). The presence or absence of seasonal floods characterized either everwet or seasonal climates, respectively. In addition to the regional paleoclimatic setting, the eustatic curves show an overall sea level fall during the Late Eocene–Early Oligocene (± 38 –30 Ma), (Miller, et al., 2005; Kominz et al., 2008).

3. A Fluvial and Lacustrine-Delta Succession

3.1. Lithofacies associations

Sedimentology of the fluvial–lacustrine-delta succession of the Bayah Formation was analyzed by classifying eleven main lithofacies types, and they were grouped into eight classes of lithofacies associations (Figs. 6–17). Each lithofacies association is defined primarily by the grain sizes, grain and clast fabric, sedimentary structures, composition, and geometry. The fluvial–lacustrine-delta succession of the Bayah Formation in the study area attains a total thickness of 915 m, and can be subdivided into eight major lithofacies associations. These facies associations are: (FA1) Conglomerate deposits, (FA2) Conglomeratic sandstone deposits, (FA3) Sandstone-dominated deposits, (FA4) Interbedded carbonaceous mudstones with laminated mudstones and siltstones, (FA5) Carbonaceous mudstones with thin lignite traces and thin sandstone intercalations, (FA6) Crudely-stratified gravelly-sandstones and bioturbated sandstones with soft-sediment deformation, (FA7) Sandy-siltstones interbedded with carbonaceous mudstones, and (FA8) Interbedded dark-coloured organic-rich mudstones with plant fragments. Description and interpretation of the facies associations are summarized in Figs. 6, 11 and Fig. 13. These lithofacies associations are interpreted to represent fluvial channel-fill deposits (FA1–FA3), abandoned channel deposits (FA4), flood-plain deposits (FA5), delta-front deposits (FA6–FA7), and lacustrine muddy deposits (FA8) (Fig. 18). These eight major lithofacies associations show variations in the thickness, lateral continuity, and in vertical stacking patterns (Figs. 19–25).

3.1.1. Facies association 1: Conglomerate deposits

Description: This facies association is characterized by the presence of medium- to very thick-bedded (0.6–16 m thick) clast- and matrix-supported conglomerates and pebbly sandstones. The gravel-size clasts consist largely of coarse pebbles, and fine cobble were occasionally observed. A clast framework is poorly sorted to moderately sorted, and intraformation mudclast are occasionally found near the base. Clast composition is represented primarily by milky quartz grains, chert, schist, phyllite, and minor granite rock fragments are also locally present. Crudely horizontal and trough cross-stratification are commonly observed sedimentary structures. Inclined foreset bedding is also locally observed (Fig. 7D). In addition, indistinct clast size grading as commonly observed, and clast imbrications are also locally observed. The bed boundaries are defined by sharp-basal surfaces, which show either irregularly scoured or flat-horizontal surfaces (Fig. 28B). Amalgamation developed a thicker unit of this association. The presence of thin and discontinuous sandstone layers, which have crude cross stratification, is occasionally observed. The conglomerate bodies display an overall tabular geometry. Log type and representative outcrop photographs of this association are shown in Figs. 6 and 7.

Interpretation: The amalgamated nature of the conglomerate deposits of FA1 indicates a series of cut-and-fill events as a result of fluctuating floods (Rasmussen, 2000). Crudely graded stratified gravels with thin sandstone intercalations is interpreted to have formed as a response to migration of low-relief, longitudinal bars with high velocity flows (Hein and Walker 1977). Sand intercalations were deposited on gravel bar surfaces during waning flow stages. The dominance of coarse-grained, gravelly channel-fill deposits is characteristic of braided streams, or channel-fills deposited at a distal portion of an alluvial

fan system (Rust, 1978) that is represented by gravelly longitudinal bar deposits (Ramos and Sopena, 1983; Pope and Wilkinson, 2005).

3.1.2. Facies association 2: Conglomeratic-sandstone deposits

Description: This facies association consists of medium- to very thick-bedded (0.7–14 m thick), medium- to coarse-grained sandstones, with very commonly interbed granule and pebble-sized layers. The most commonly observed sedimentary structures are crudely horizontal stratification and trough cross-stratification, and gently inclined foreset stratification that has sigmoid geometry (Figs. 8 and 33). Although smaller-scale laminations are very rare, large current ripple structures are locally observed. Sets of poorly defined fining-upward sandstone beds are common. The sandstone beds have planar to undulate upper surfaces, the basal surfaces are commonly sharp and erosional. Intercalations of muddy deposits (5–20 cm thick) are locally observed (Fig. 33). Overall, the conglomeratic sandstone beds are characterized by lenticular and/or tabular geometry. A representative log type and outcrop photographs are shown in Figs. 6 and 8.

Interpretation: The dominant coarse-grained sandstones with conglomerate interbeds can be attributed to be a product of short and intense bedload-dominated events, such deposition occurred in a shallow, scoured depressions associated with fluvial channels (Hampton and Horton, 2007). The shallow bottom scours may have been induced by channelised stream flow. These shallow channels commonly represent a very low sinuosity fluvial system that is characterized by progressive downstream shoaling and broadening (Tunbridge, 1984). Rarely observed internal lamination may indicate rapid deposition

through the deceleration of high discharge of suspended sediment loads (Rasmussen 2000). The presence of large current ripple structures may indicate waning stage ripples superimposed on a top of dunes formed during a flood stage (Cant, 1982). Conglomeratic sandstone channel-fill deposits with gently inclined foreset stratification is considered to have formed as downstream migration and aggradation of coarse-grained bar deposits. (Rust, 1978; Cant, 1982; Rust and Gibling, 1990). In a similar way, the presence of sigmoidal foresets with parallel topsets may reflect conditions of vertical bed accretion in association with the downstream dune migration under an upper flow regime (Rasmussen, 2000).

3.1.3. Facies association 3: Sandstone-dominated deposits

Description: This facies association is characterized by medium- to very thick-bedded (0.8–12 m thick) sandstones. The sand size of this lithofacies consists primarily of fine- to medium-grained sand, locally associated with coarsed sand and minor pebbles. Sedimentary structures are typically represented by the presence of trough-cross stratification with inclined accretional surfaces. Gently inclined stratification with mudstone partings are also very common in this association. These thin mudstone interbeds (10–40 cm thick) are whitish or greyish colored, and are locally intercalated within this sandstone dominated deposits. In some localities, internal physical sedimentary structures are not obvious. The sandstone beds have flat and sharp basal bed boundaries and the bases are locally distinctly erosional. The sandstones with a fining-upward pattern of more than 1 m thick change gradationally upward into muddy deposits of FA 4 or FA 5.

In some localities, the sandstone beds are amalgamated to form very thick-bedded sandstone bodies. These sandstone-dominated deposits display lenticular and tabular geometry. A representative log type and outcrop photographs are shown in Figs. 6 and 9.

Interpretation: The fining-upward sandstone beds that is characterized by a composite set of trough cross-stratification, in association with larger inclined foreset bedding, are interpreted to represent point-bar deposits (Cant and Walker 1978). Lateral accretion surfaces also indicate the development of lateral migration of bars superimposed on point-bar deposits. The local presence of fine-grained muddy deposits reflect deposition from suspended loads during intervals of lateral migration of point bars. (Jackson, 1976; Stewart, 1981; Halfar et al., 1998; Roberts, 2007). These sandstone-dominated deposits are attributed to point-bar deposits of high sinuosity, mixed-load, meandering channels. The thicker, vertically-stacked superimposed sandstones may imply deposition within a meander belt complex during periods of reduced subsidence (Puigdefabregas & Van Vliet, 1978; Ghosh, 1987; Kraus & Middleton, 1987).

3.1.4. Facies association 4: Interbedded carbonaceous mudstones with laminated mudstones and siltstones

Description: This facies association consists primarily of interbedded dark grey mudstones with parallel arranged carbonaceous fragments or dispersed organic matters, which are commonly represented by thin, laterally discontinuous lignite intercalations (0.5–3 cm thick). Internally, the mudstones vary from structureless to parallel and/or current ripple laminations. The laminations are characterized by alternation of streaks of siltstones and

mudstones. Soft-sediment deformation structures are locally observed. The mudstone beds show sharp upper and basal boundaries, and display laterally thinning out lenticular geometry. A representative log type and outcrop photographs are shown in Figs. 6 and 10.

Interpretation: The mud dominated deposits with minor physical sedimentary structures are interpreted to represent deposits of waning current stages, which were weak enough to deposit mud and silt size detritus from suspension (e.g., Ashley, 1990; Bridge and Gabel, 1992; Skelly et al., 2003). The thin parallel lamination of alternating siltstone and claystone laminae indicates overall deposition from suspension over the upper parts of sandstone bar deposits and/or abandoned flood plains (Allen, 1964; Jackson, 1981). Soft-sediment deformation may have occurred in response to desiccation or the formation of shrinkage cracks (Thomas et al., 2002; Bridge, 2006). These mudstone-dominated lithofacies features likely represent a deposits formed in a mud-filled abandoned channel. Fine-grained sedimentation is considered to represent deposition from suspended loads during intervals of channel shifting and/or channel-belt avulsion. (Dunagan and Turner, 2004; Ghosh, 2006; Jinnah and Roberts, 2011).

3.1.5. Facies association 5: Carbonaceous mudstones with thin lignite traces and thin sandstone intercalations

Description: This facies association is composed primarily of interbedded dark grey carbonaceous mudstones, siltstones, kaolinite mudstones, lignite traces, and thin sandstones intercalations (sandstone beds types 5A–5C). This facies association is laterally extensive, and is up to a few tens meter in thickness. Current-ripple cross-lamination and

faint parallel lamination with local associations of soft-sediment deformation structures are commonly observed physical sedimentary structures (Figs. 11 and 12). Coarsening-upward patterns (0.4–1 m thick) are commonly observed. Thin sandstone intercalations within this facies association can be classified into three major types (types 5A–5C). Type 5A is characterized by thin-bedded sandstones with basal scours and has lenticular geometry (Fig. 12E). The grain size is typically fine- to medium-grained with occasional intercalations of pebbles. Type 5B is represented by sheet-like sandstone bodies with locally scoured bases, and encased in dark-grey carbonaceous mudstones (Fig. 12F). Internally, plane-parallel and trough cross-, and current-ripple cross-laminations are commonly developed. Type 5C is characterized by thin-bedded, medium-grained sandstones with current-ripple cross-laminations and small trough cross-stratification. Type 5C sandstone beds commonly show undulated, distinct basal and upper surfaces. A representative log type and outcrop photographs are shown in Figs. 11 and 12.

Interpretation: This facies association represents deposits formed in a mud dominated floodplain environment. The sandstone interbeds are interpreted to represent sedimentation as distal crevasse splay deposits formed in some areas that were affected by occasional active sand transportation over a floodplain during flood events. Some sandstone interbeds that have thinning- or thickening-upward patterns may have formed in response to a change in location of the main channels (Bridge, 1984). The muddy deposits that encase the thin sandstone interbeds were also formed from fine-grained suspension during flood events. In addition, some carbonaceous-rich sediments are considered to have accumulated in swamp environment within a floodplain. The thin-bedded lenticular sandstone intercalations (sandstone type 5A) and thin sheet-like sandstone intercalations (sandstone

type 5B) are interpreted as a fill of small-scale channels and a crevasse splay deposits respectively on a floodplain environments during flood stages (Farrell, 1987; Miall, 1996; Bentham, 1993; Griffing et al., 2000; Tooth, 2005; Hampton and Horton, 2007). Sandstone type 5C is considered to have formed as deposition and migration of small-scale bedforms by waning flows from overfilled channels with low relief levees.

3.1.6. Facies association 6: Crudely stratified gravelly sandstones and bioturbated sandstones with soft-sediment deformation structures

Description: This facies association is composed primarily of sharp-based, laterally extensive sandstones and gravelly sandstones. Sandstone deposits generally consist of moderately sorted, medium- to coarse-grained sandstones, showing downstream-inclined stratification that is associated with thin mudstone intercalations. Current ripple cross-lamination, plane-parallel stratification, low-angled and trough cross-stratification characterize this facies association. Large-scale load structures (40 cm thick and 1 m wide), which forms ball-and-pillow structures are also locally present. The lateral extent of the thickest sandstone bodies is laterally mappable for more than 250 m. The sandstones packages display fining-upward patterns. Vertical burrows and large-scale load structures (40 cm thick and 80 cm wide) are locally developed. Internally, these sandstone beds are characterized by lenticular and sheet-like geometry. Another important feature of the thick-bedded sandstone beds is undulated erosional bases, which distinctly incise underlying mudstones. Thinner sandstone beds of this facies association display flat and sharp basal surfaces. On the erosional basal surfaces, gravel lag deposits at bases that consists of

admixture of extra-formation clasts and intra-formational mudstone clasts within a sandstone matrix are also locally present. A representative log type and outcrop photographs are shown in Figs. 13, 14, and 15.

Interpretation: In general, the interbedded deposits may be attributed to the gravelly sandstones and sandstones of a proximal delta-front mouth-bar deposits formed in response to high sediment discharges from a river channels into a standing water. (Farquharson, 1982; Shomacker et al., 2010; Tänavsuu-Milkeviciene and Sarg, 2012). Laterally extensive sandstone deposits are considered to have formed as mouth bar deposits in a delta-front environment (e.g., Farquharson, 1982; Shomacker et al., 2010; Tänavsuu-Milkeviciene and Sarg, 2012). The presence of thin mudstones intercalations may indicate that each sandstone beds may be originated from high discharged sedimentation, which was interrupted by periods of low discharge and mud settling (e.g., Farquharson, 1982; Shomacker et al., 2010). The presence of sparse vertical burrows in the sandstone beds may document opportunistic colonization with a high-energy delta-front environment (e.g., Buatois and Mángano, 2009). The sharp-based lower boundaries between mudstones and sandstones imply subaqueous erosion by fast flowing currents during flood stages (e.g., Kovacic et al., 2004; Schomacker et al., 2010). The erosional lower boundaries which display undulated basal scour surfaces, with coarse-grained sandstones and gravel-lag deposits, suggest a channelized deposit. Small relative fall in lake level may have induced downward shift of a fluvial system on a delta plain basinwards and produced trough-shaped scours into the underlying lacustrine deposits (e.g., Shomacker et al., 2010).

3.1.7. Facies association 7: Sandy siltstones interbedded with carbonaceous mudstones

Description: This facies association is composed primarily of organic matter-rich layers and faintly laminated rhythmites intercalated in massive mudstones and bioturbated sandy-siltstones. The interbeds of faintly laminated rhythmites, carbonaceous mudstones, and bioturbated siltstones show an overall coarsening-upward pattern. In the lower part of the Pasir Bongkok-section site, this association consists of eight coarsening upward cycles. Each cycle differs one another in thickness and the presence or absence of rhythmites. These cycles, in general, grade upward from rhythmites in the base, which is overlain by organic-rich carbonaceous mudstones intercalated with greyish mudstones and bioturbated muddy sandstones locally associated with sparsely distributed pale-brown nodules. Greyish mudstones contain less carbonaceous matter upsection. Bioturbated siltstones generally coarsen upward, and grade into silty sandstones to be dominant in thickly bedded toward upperhalf intervals. Current ripple-laminations with streaks of carbonaceous matter are the dominant sedimentary structures in the bioturbated siltstone beds. Rhythmites are composed of interlaminated dark-colored mudstones and paler brownish colored siltstones. The individual laminae thickness is between a few mm to 10 mm. Alternation between different laminae display a stripe appearance. The contact between laminae is commonly sharp. Bioturbation is not found or very minor in rhythmites package. A representative log type and outcrop photographs are shown in Figs. 13 and 16.

Interpretation: In general, the fine-grained muddy interbeds are considered to be a distal delta front deposits formed in a lacustrine environment. (Lambert and Hsü, 1979; Haszeldine, 1984; Tye and Coleman, 1989; Hamblin, 1992; Benvenuti, 2003). Coarsening-

upward successions from rhythmites to bioturbated muddy sandstones are interpreted to represent a shallowing-upward environmental change formed in response to progradation of a deltaic system. The thinly laminated rhythmites have been reported from both ancient and modern lacustrine delta environments and are considered to be formed in response to flood events or seasonal climatic variations (e.g., Lambert and Hsü, 1979; Haszeldine, 1984; Benvenuti, 2003). These flood-induced suspension sediments might have been delivered into a lacustrine environment from a fluvial feeder. The absence of bioturbation within the rhythmites generally implies poor-oxygenated conditions, or a high rate of sedimentation (e.g., van Houten, 1973). The presence of burrows in the upper part of shallowing-upward deposits represents slow deposition of background fine-grained sediment particles in more oxygenated conditions (e.g., Hamblin, 1992). Reddish brown mudstones indicate the presence of iron oxide mineral pigmentation. Particles of iron oxide or iron hydroxide minerals have been transported together with suspended-sediment loads in a marginal lacustrine deltaic environment (e.g., Whateley and Jordan, 1989; Martinek et al., 2006; Abels et al., 2009).

3.1.8. Facies association 8: Interbedded dark-colored organic-rich mudstones with plant fragments

Description: This facies association is composed primarily of a combination of thick (up to 7 m in thickness) and laterally extensive organic-rich mudstones that show papery parting, which is characterized by the presence of finely plant remain debris and contains carbonaceous mudstones with minor laminations. These mudstone-dominated deposits

show sharp-based bed boundaries. Algal palynomorph (*Pediastrum* sp.) has been reported from carbonaceous mudstones of this facies association (Isnaniawardhani, 2014, Laboratory of Palaeontology–Padjadjaran University, personal communication). This facies association are typically developed at the lower and middle intervals of the Pasir Bongkok site. A representative log type and outcrop photographs of this facies association are shown in Figs. 13 and 17.

Interpretation: The facies association 8 deposits are interpreted to have formed in a stagnant condition associated with limited water circulation in a lacustrine environment. Minor laminations and grading are interpreted to reflect flocculation process influenced by fluctuation of terrigenous and organic input into a lacustrine environment. Finely plant-remain debris may result from subaerial alteration during pond-drying periods (Jerrett et al., 2011). These suspension-related fine-grained depositional processes appear to have occurred in an oxygen-depleted condition below a thermocline in a lake. The presence of fine-grained sediments may have been primarily supplied from a deltaic system. (Hamblin, 1992; Basilici, 1997; Cole and Crittenden, 1997; Anadon, 1998; Johnson and Graham, 2004). Some deposits similar to the present example have been interpreted to have formed in small lakes with nearby highly vegetated peaty substratum (Moore and Chater, 1969). Algal palynomorph (*Pediastrum* sp.) found in the muddy deposits of this facies association indicates freshwater-lake deposits and can support the above interpretation (Morley and Morley, 2013).

3.2. Facies relations and depositional systems

The interpretations of depositional systems for the Bayah Formation in the study area are based on detailed sedimentological analysis, geological and facies mapping, detailed stratigraphic sections, and paleocurrent analyses. The results indicate that the succession may have been deposited in three major facies belts (Fig. 18). Facies belts constitute combination of several facies associations. These are: (1) a braidplain, (2) a meandering river and floodplain, and (3) a lacustrine-delta.

A braid-plain facies belt is dominated by FA1 with associations of FA2 and FA5. A diagram in Fig. 20 is an example of photo panel, interpreted outcrop panel, and log section, which show geometry and stratigraphic relationship of FA1 and FA2 as a braid-plain facies belt. These facies associations are typically present in the eastern part of the study area (Fig. 26), where the thickest succession of this facies belt is present, and the belt represent a lower half interval of the fluvial succession. In a complete section, such as a section at the Pasirpogor and Cantayan locations, the braided channel succession displays a sharp-erosional base scoured into the underlain overbank mudstones. Conglomerate and cross-bedded pebbly sandstones overly this basal surface. These coarse-grained deposits pass upward into thick-bedded sandstones consisting of coset of cross-bedded sandstones with gravel-lag deposits at reactivation surfaces. Conglomerate deposits occur again upsection, and are finally overlain by cross-bedded sandstones. Large (up to 40 cm wavelength and 6 cm height), but thin current ripple-laminated sandstones are found in the top of these cross-bedded sandstones. Desiccation cracks and thin overbank mudstones are occasionally present in the upper surface of these sandstone beds. Paleocurrent measurements reveals a paleocurrent pattern with a dominant flow to the south-southwest and to the south

directions (Fig. 26). Following this direction laterally to the southwest, this facies belt become thinner, and passes into thickly bedded sandstones and pebbly sandstones, which are separated by mudstone deposits. Lateral decrease in thickness and lateral change into sandstones to the southwest may indicate a downstream-directed transition from braidplain system to meandering river system and its associated flood basin. An abrupt change into mudstones upsection is observed in some localities, together with an overall fining-upward conglomerate succession, can be interpreted to have been caused by slope retreat in the near-source area and decrease in sediment supply.

Meandering river and floodplain systems comprises five facies associations (FA3–FA5), with local association of FA1 and FA2. A diagram in Figs. 19 and 21–23 are an example of photo panel, interpreted outcrop panel, and log section, which show geometry and stratigraphic relationship of FA3, FA4, and FA5 as a meandering river and floodplain facies belt. The deposits of this facies belt are typically developed in the eastern and central parts of the study area, and occur in the middle and the upper parts of the Bayah Formation. In the fluvial system of the Bayah Formation, several styles of the sandstone-dominated deposits are present. They differ mainly in thickness and internal geometry. Deposits that are found in three different locations represent different styles of meandering channel deposits. At the Sekarwangi location, the sandstone-dominated channel-fill deposits are characterized by sheet and lenses geometry, and are dominated by sandstones. In the lower part in these deposits, the sandstone sheets are dominant with subhorizontal basal surfaces. This part passes upwards into packages bounded by low angled inclined accretion surfaces. Toward the tops, meandering channel-fill deposits display fining-upwards patterns, which fine upward into the carbonaceous mudstone dominated deposits. At the Cimenteng location, internal geometry of channel-fill deposits is characterized by

less distinct lateral accretion packages, and formed mainly by thick tabular bodies, which are separated into several units by discontinuous bounding surfaces. These bounding surfaces are defined by changes in dips and strikes, and are not represented commonly by distinct erosional contacts. Where these boundaries are identified, they generally display low angled inclined accretion surfaces, and forms sheets and wedge-like geometry. Individual sandstone packages are 0.6 to 1.7 m in thickness.

A third type of channel-fill deposits are well defined in a section at the Kadupugur location. In this location, the sandstone-dominated channel-fill deposits forms elongated tabular geometry, and consists mainly of medium- to coarse-grained sandstones. This type of sandstone bodies is represented by less complex internal and external organization, and is represented by less laterally extensive thin sandstone sheets and lenses. The bounding surfaces of these sandstone sheets and lenses are occasionally separated by thin mudstone interbeds. The channel margins abruptly pinch out or pass laterally into overbank muddy deposits. The lateral extension of the sandstone bodies is up to several meters.

Lacustrine-delta systems are composed mainly by three facies associations (FA6–FA8). A diagram in Figs. 24–25 are an example of photo panel, interpreted outcrop panel, and log section, which show geometry and stratigraphic relationship of FA6, FA7, and FA8 as a lacustrine-delta facies belt. This depositional system occurs in the upper stratigraphic interval of the Bayah Formation (Fig. 26), and is developed mainly in the westernmost part of the study area (i.e., at the Pasir Bongkok section). The deposits of this facies belt are typically developed at the lower and middle intervals of the Pasir Bongkok section, which represented by vertically stacked relationships between FA8 in the lower part and FA6 in the upper part, and incised into the underlain FA8 mudstones. The lower

boundary of FA6 and FA7 with the underlying thick-bedded sandstones and conglomerates is characterized by distinct sharp contact.

3.3. Temporal variation in fluvial deposits

Based on geological mapping from an outcrop, the fluvial–lacustrine–delta successions of the Bayah Formation can be subdivided into 7 intervals (IV1–IV7 in ascending order) by 6 distinct erosional surfaces (ES) (ES1 to ES6 in ascending order) (Figs. 26). These erosional surfaces are defined in the base of channel-fill deposits or mouth-bar deposits, which are coarser than those developed beneath each erosional surface (Figs. 27 and 28). Facies associations beneath each distinct erosional surface are commonly represented by mudstone-dominated deposits (FA4–FA5 or FA7–FA8). The intervals show temporal variation in thicknesses (Fig. 26). The fluvial deposits in the intervals show an overall decrease in thickness from IV1 to IV6, and an increase in thickness from IV6 to IV7. Within each interval (IV1–IV7), coarser-grained channel-fill deposits develop on the basal erosional surfaces and commonly pass upward into sandstone-dominated channel-fill deposits in association with the increase in mudstones deposits. The stratigraphic relationships between fluvial deposits within each interval are considered to be relatively conformable, representing continuous vertically stacked deposits. Each interval, in general, coarsens to the north-eastern upstream direction and is represented by channel-fill deposits encased in flood-plain muddy deposits (FA4), and by mouth-bar deposits in association with delta-front and lacustrine muddy deposits.

Muddy facies associations (FA4 and FA5) are generally dominant in the interval IV1, and in the upper parts of IV2, IV5, and IV7. In the middle parts of the intervals (IV3–IV4), gravelly channel-fill deposits (FA1 and FA2), which developed in the E–NE area are laterally grade into sandstone-dominated channel-fill deposits (FA3) in the W–SW area. In contrast, lacustrine-muddy deposits are mainly developed only in the western area in the intervals IV4 to IV6. The lacustrine muddy deposits (FA7 and FA8) were replaced upward by sandstone-dominated channel-fill deposits (FA3) in the uppermost interval (IV7). The uppermost fluvial deposits in the interval IV7 is thicker than fluvial deposits in the intervals IV5 and IV6. The fluvial deposits of the IV7 were overlain by coastal and shallow-marine sandy deposits with a ravinement surface in their base (Fig. 26). The coastal and shallow-marine sandy deposits fine upward to shallow-marine muddy deposits, which were subsequently replaced by reefal carbonates as a response to a forced regression and the ensuing transgression (Fig. 26).

The Bayah formation fluvial deposits in the Sukabumi high show a fairly consistent paleoflow direction through the whole section and S–SW-directed paleocurrents are dominant.

3.4. Variation in geometry of channel-fill deposits

Channel-fill deposits are one of the important depositional elements of fluvial depositional system, and reflect the cumulative effects of fluvial sedimentations (Jackson, 1975; Miall, 1996; Bridge and Tye, 200; Gibling, 2006). Although cross-sectional geometry of channel-fill deposits of the Bayah Formation is not necessarily observed

everywhere in the study area, some distinctive features of packages of channel-fill deposits can be identified on the outcrops based on the geometry and internal organization of channel and bar deposits (Miall, 1985; 1996; Marzo et al., 1988).

Packages of sandstone–conglomerate fluvial bodies in the Bayah Formation are subdivided into three major types, based on internal lithofacies organizations and geometry of the deposits (e.g., Nami and Leeder, 1978; Friend et al., 1979; Marzo et al., 1988): (1) lenticular and tabular conglomerate-dominated packages, (2) tabular and lenticular conglomeratic-sandstone packages, and (3) tabular and lenticular sandstone-dominated packages. Each type is interpreted to represent a different style of sedimentation, as follows: (1) a bedload-dominated sedimentation in braided river, (2) longitudinal and transversal bars that developed in a transitional area between braided and sinuous rivers, and (3) a mixed-load sedimentation in meandering rivers. Schematic illustration representing these three types of major channel-fill deposits are shown in Fig. 37. Although these three types of channel-fill deposits have tabular and lenticular forms, they differ in dominant grain size, internal lithofacies organizations, and stratigraphic positions within the Bayah Formation fluvial succession.

3.4.1. Lenticular and tabular conglomerate-dominated package

This package consists mainly of thick, laterally extensive bodies of conglomerates. Individual beds can reach a thickness of more than 8 m, with the lateral extent can be traced for more than 250 m. FA1 is the dominant facies association of this package, although FA2 is also commonly observed in some locations.

Internal organization of the deposits is characterized by the presence of vertically-stacked high-angled foreset bedding together with through cross-stratification in some part and graded-stratified conglomerates. Such a composite set has multiple vertical stacking. The deposits do not show a distinct fining-upward pattern. Repetition of vertical increase and decrease in gravel size are common. Southwest to south-directed paleocurrents are dominant. This type of channel-fill deposits is interpreted to represent bedload-dominated sedimentation in braided rivers (e.g., Cant, 1982; Rust et al., 1990; Miall, 1996), and is very commonly observed in the interval IV3, and in the lower parts of the IV4 and IV6. A schematic diagram in Fig. 37A shows internal lithofacies organizations and geometry of the lenticular and tabular conglomerate-dominated package.

3.4.2. Tabular and lenticular conglomeratic sandstone packages

This package consists mainly of thick, laterally extensive bodies of conglomeratic sandstone deposits, and up to more than 3 m in thickness. Its lateral extent can be traced for more than 100 m. FA2 is a dominant facies association, although FA1 and FA2 are also commonly observed in some locations. Internal organization of the deposits is characterized by the presence of high-angled foreset bedding, indicating downstream-accreted deposits in association with the trough cross-stratification and crudely stratified conglomeratic sandstones. Composite set of these foreset bedding are arranged in multiple-stacking pattern, which show an overall tabular geometry. These channel-fill deposits are common in the lower part of the interval IV4, in which the conglomeratic sandstone deposits show a thinning-upward pattern in association with less lateral extension. This type of channel-fill deposits (Figs. 33 and 37B) is commonly observed in the lower part of

the intervals IV2 and IV4. The basal part of this type is characterized by conglomerates that incise into the underlain muddy deposits of FA5.

This type of channel-fill deposits is interpreted to represent longitudinal- and transversal-bar deposits, which may have been formed in a transitional areas between braided and sinuous rivers (e.g., Cant, 1982; Ramos and Sopena, 1983; Ramos et al., 1986). A schematic diagram in Fig. 37B shows internal lithofacies organizations and geometry of the tabular and lenticular conglomeratic sandstone packages.

3.4.3. Tabular and lenticular sandstone-dominated packages

This type of channel-fill deposits is characterized by either tabular or lenticular geometry. The tabular-shaped deposits are commonly very thick bedded and laterally extensive (Figs. 36 and 37C). In contrast, the lenticular-shaped deposits are commonly thinner and their lateral continuity is less extensive. FA3 is the dominant facies associations, and FA2 is only locally observed above the internal-scouring surfaces. Although outcrops are limited for this type, the thickest deposits can be laterally traced for more than 200 m. The basal part of this type channel-fill deposits is characterized by pebbly sandstones, which incised into the underlain muddy deposits of FA5 having either concave-upward or planar-shaped basal surfaces. Some complete exposures of this type clearly show fining-upward patterns, and the deposits pass upward into the interbedded thin sandstone and mudstone deposits (FA3), and are finally covered with thick carbonaceous mudstone deposits of either FA4 or FA5. Internally, the tabular-shaped deposits commonly show thickly vertically stacked, large-scale sets of inclined-stratification or nearly horizontal-stratification, which are bounded by either lateral-

accretion surfaces or intercalations of thin (< 5 cm thick) laterally discontinuous mudstone beds.

A schematic diagram in Fig. 37C shows internal lithofacies organizations and geometry of the tabular and lenticular sandstone-dominated packages. The presence of laterally accreted deposits suggests that this type of channel deposits developed from mixed-load sedimentation in meandering rivers (e.g., Cant, 1982; Miall, 1996; Bridge, 2003). This type of channel-fill deposits is commonly observed in the interval IV1, in the upper part of the intervals IV2, IV5, and IV7.

4. Sandstone Petrography and Clay Mineralogy

4.1. Variations in sandstone compositions

Petrographic examination was conducted using 87 sandstone samples which were obtained from the fluvial succession. Relative stratigraphic positions of the sandstone samples are shown in the Fig. 38. Together with the Gazzi-Dickinson method (Ingersoll et al., 1984), this study also used a conventional point-counting procedure. Grid-intersection points of 450–560 are counted for each sample. The point-counting data were used to calculate several petrographic parameters following the parameters of Dickinson and Suczek (1979).

Based on the petrographic examination, the Bayah Formation sandstones are classified into three compositional groups, according to the classification scheme of Pettijohn et.al. (1987): (1) quartz-arenite sandstones ($Q_{94}F_1L_5 - Q_{98}F_0L_2$), (2) sublithic-arenite sandstones ($Q_{76}F_0L_{24} - Q_{93}F_1L_6$), and (3) lithic-arenite sandstones ($Q_{48}F_6L_{46} - Q_{74}F_0L_{26}$). On the QFL ternary diagram for the sandstone classification (Fig. 39), the framework composition does not exhibit distinct temporal variation between the intervals. Slight temporal and spatial variations in framework composition are also evident as illustrated in Figs. 47 and 48. Lithic arenite and sub-lithic arenite are dominant in the lower intervals (IV1–IV2). In response to the decrease in lithic-arenite and sublithic-arenite, quartz-arenite becomes dominant in the intervals IV3 and IV4, and finally, the intervals IV5–IV7 are represented by sublithic-arenite.

In contrast, sandstones from the deposits belong to the transgressive phase, which occurred above the ravinement surfaces (Fig. 47 and 48), classified into three

compositional groups as follows (1) quartz-arenite sandstones, (2) lithic-arenite sandstones, and (3) sublithic-arenite sandstones.

The most prominent rock fragments in the sandstones of the Bayah Formation are metamorphic rocks and meta-sedimentary rock fragments. The low grade metamorphic rock fragments are the most common relative the other types of rock fragments (96%). Lithic fragments consist dominantly of metamorphic rock fragments (Lm) (Fig. 46), and minor amounts of sedimentary rock fragments (Ls) and volcanic rock fragments (Lv) (Figs. 45 and 46). Microscopic photographs in Figs. 45–46 represent various class of sedimentary rock fragments (Ls) observed in the Bayah Formation sandstones. Graywacke rock fragments and altered fine-grained sedimentary rocks, cryptocrystalline siliceous rock and chert fragments are commonly observed compared with other types of sedimentary rock fragments. More commonly observed metamorphic rock fragments are quartzite, schistose quartz rock fragments, and micaceous schist fragments. Volcanic rock fragments, are only occurred in the uppermost interval of the Bayah Formation, and they are represented by grains with trachytic and rhyolitic textures.

The Bayah Formation sandstones can be tentatively classified into either feldspar-poor sandstones or quartz-rich sandstones (Girty and Pardini, 1987; Chandler, 1988; Hossain et al., 2010), because they only have less than 7% feldspar and contain relatively much more quartz grains (quartz average = 81%) (Figs. 42 and 43). Thus, compositional variations in the Bayah Formation sandstones are defined by increase and decrease in rock fragments relative to increase and decrease in quartz grains (Fig. 39).

Potassium feldspar is more common feldspar grains than plagioclase feldspar, which is characterized by grid twinning, myrmekitic textures, and polysynthetic twinning, respectively (Fig. 44).

Major provenance types of the Bayah Formation sandstones were investigated using the criteria given by Dickinson et al. (1983) on the QFL and QmFLt ternary diagrams (Figs. 40A and 40B). In general, the QFL diagram emphasizes maturity aspects of sandstones, and the QmFLt diagram is useful for identifying the provenance aspects. In the QmFLt plot, polycrystalline quartz, chert and quartzite are assigned to rock fragments (Lt) (Graham et al., 1976). On the QFL diagram, the Bayah Formation sandstones are divided into two groups. Most of the sandstones belong to the recycled orogen provenance, and minor sandstones indicate their provenance type as the craton interior. In contrast, the sandstones are classified into three groups on the QmFLt diagram (Fig. 40B).

In general, the majority of the Bayah Formation sandstones are grouped into the recycled-provenance type. The Paleozoic–Mesozoic basement rocks of the Sundaland continent margin are situated to the north of the Bayah Formation fluvial basin (Hamilton, 1979; Schiller et al., 1991; Hall, 2012). The basement rock terrain, which consists primarily of granitoid rocks, metasedimentary, and low-grade metamorphic rocks (Patmosoekismo and Yahya, 1974; Hamilton, 1979), seems to have a potential as a provenance for detrital fragments of the Bayah Formation fluvial basin in the south (Fig. 41). The basement rocks to the north consist primarily of granitoid rocks, metasedimentary and low-grade metamorphic rocks (Patmosoekismo and Yahya, 1974; Hamilton, 1979).

In addition to provenance factors, sandstone composition is also controlled by other factors, such as weathering and climatic conditions (Chandler, 1988; Weltje et al., 1998; Garzanti et al., 2013). The feldspar-poor sandstones of the Bayah Formation contradict with the existence of the feldspar-bearing provenance to the north. To identify the potential of the other factors, the framework composition of the sandstones can be analyzed in several different methods.

The bivariate ratio of polycrystalline quartz (Qp) and total quartz (Q) to feldspar (F) plus rock fragments (L) (Suttner and Dutta, 1986) was used to interpret paleoclimatic conditions of the provenance terrane (Fig. 49A). The present-day maximum distance between the Mesozoic basement rocks to the north and the Bayah Formation at the Sukabumi high is approximately 300 km. The bivariate log-plot can discriminate compositional maturity of the Bayah Formation sandstones based on grain types ratios, which are sensitive to a climatic control. The diagram in Fig. 49A can discriminate four climatic condition in terms of precipitation (Suttner and Dutta, 1986). This diagram also indicates that chemically most stable grains (quartzose) are five or more than fifty times more than unstable grains (feldspar plus rock fragments). The majority of the Bayah Formation sandstones are classified in a humid field on the diagram, and minor other sandstones are in a semi-humid field (Fig. 49A).

With a similar reasoning method, the log ratio plot in Figs. 49B–49C between grain types, which are the most sensitive to climatic control, also indicates the importance of weathering effect (Weltje et al., 1998). The weathering index in this diagram is calculated as a function between relief and climate. On this diagram, the majority of the Bayah Formation sandstones are concentrated in a field that is indicated by the numbers 2 and 4. According to the classification scheme (Fig. 49C), the sand grains are interpreted to have formed in a moderately–intensely weathering under subhumid–tropical humid climatic condition in association with a moderate–low relief conditions.

The variation in the relative proportion of unstable to stable sand grains between the intervals can not be identified based on the climatic and weathering indices (Fig. 49). On the weathering index in terms of the log-plots between rock fragment–quartz ratio (L/Q) and feldspar–quartz ratio (F/Q) according to (Garzanti et al., 2013), minor variation in the

relative proportion of unstable to stable sand grains between the intervals can be identified (Fig. 50). Moreover, this diagram can be used to evaluate the relative importance of climate on detrital composition by estimating substantial loss of feldspar and rock fragments during weathering in the source area. Although some overlaps between the intervals (IV1–IV7) are present, the decrease feldspar grains relative to quartz grains can be identified on the diagram (Fig. 50). This diagram also indicates a decrease in feldspar grains and rock fragments relative to quartz grains from IV1 to IV3–IV4. This variation corresponds to the increase in the degree of weathering from strong to extreme states, and is followed by the increase in feldspar grains and rock fragments relative to quartz grains from IV3–IV4 to IV5 and IV7. Feldspar grains are not evidently observed in the majority of sandstones formed during the transgression phase such as those of sand ridge deposits and shoreface deposits developed below the limestones. These sandstones are classified in an extreme-weathering field on the diagram.

4.2. Variation in clay mineralogy

Clay mineral composition of mudstones from all of the mudstone-bearing facies associations (FA4–FA5 and FA7–FA8) and some samples from thinly interbed mudstones within coarse-grained facies associations (FA2 and FA3) was determined by an X-ray diffractometry. The analysis of clay mineralogy of mudstones was conducted to investigate spatial and temporal variations in clay mineral composition, and to evaluate potential allogenic factors, such as climatic and weathering controls (Singer, 1984; Sáez et al., 2003; Do Campo et al., 2007; Liu et al., 2008; 2012). Clay minerals are common products of

earth surface processes, such as weathering and authigenesis, and the clay mineral assemblages in terrestrial deposits are the result of the complex interactions between provenance, relief, depositional environments, and paleoclimates (Chamley, 1989).

Mudstone samples were pulverized into powder to 2 μm or less. Unoriented powder slides and solvated with ethylene glycol were prepared for each sample. The proportions of different clay minerals present in the mudstone samples are semi-quantitatively estimated using X Powder Pro software. Spatial and temporal variations in clay mineral composition of the Bayah Formation fluvial deposits were evaluated using a kaolinite to illite ratio (K/I), an illite-crystallinity index, and an illite-chemistry index. The kaolinite to illite ratio (K/I) was estimated based on peak areas of the basal reflections (Ruffel and Worden, 2000; Liu et al., 2008; Nagel et al., 2014). The illite crystallinity was measured using the full width at half maximum (FWHM) of the 001 basal illite peak (Li et al., 2012; Kübler and Jaboyedoff, 2000; Limmer et al., 2012). The illite chemistry index refers to an intensity ratio of the 5 Å and 10 Å peak areas (Gingele, 1996; Gingele et al., 2001; Liu et al., 2008). Variations in the semi-quantitative clay mineral analyses were not affected by the variation in grain size, because all of the samples for the X-ray diffraction are derived from mudstone deposits. Thus increase and/or decrease in kaolinite and illite in each sample may not have been influenced by diagenetic transformation, because diagenetic alteration of clay minerals are characteristically occurred in porous sandstone deposits (Lintnerova et al., 2013).

The patterns of diffractogram curves obtained from 84 X-ray diffraction measurements can be classified into five major diffractogram types (Fig. 51). The five major diffractogram types reflect the variations in the estimated volume percentages between illite, kaolinite and smectite. Gradual changes in illite and kaolinite in each group are

indicated by pie diagrams. The diagram in Fig. 51 indicates variation in illite relative to kaolinite with minor smectite from the lowermost to the top diffractograms. Illite proportion decreases from the bottom to top, in association with the increase in kaolinite proportion.

The distinction between five groups of clay mineral assemblage are indicated by gradual transition of peak-basal reflections of major clay minerals, mainly represented by the illite (001) and kaolinite (001) reflections (Fig. 51). In addition to the five clay-mineral types, the XRD mudstone samples belong to four major types of mudstone deposits (Figs. 52–53). Type 1 samples are characterized by thin-bedded, structureless, white-purplish mudstones with rootlets, and the type 1 mudstones belong to the floodplain deposits of FA5. Type 2 samples are characterized by greyish, current ripple-laminated mudstones with thin sandstone intercalations, and the type 2 mudstones belong to the abandoned-channel deposits and floodplain deposits (FA4–FA5) (Fig. 52). Type 3 samples consist of structureless to contorted mudstones with lignite and plant remains, and the type 3 mudstones belong to the floodplain deposits of FA5. Type 4 samples consist of bioturbated mudstones and rhythmites with plant remains and concretion, and the type 4 mudstones belong to the lacustrine–delta-front deposits (Fig. 53). The variations in relative proportion of illite and kaolinite between the five clay-mineral types and between the four mudstone types were identified using the log-plots of the peak-reflection counts between kaolinite (001) and illite (001) (Figs. 54A–54B). Although some degree of overlap is present between clay mineral assemblages, the five types of clay mineral assemblages are clearly discriminated on the diagram (Fig. 54A). The clay mineral type 1 indicated by a pink colour is distributed below the kaolinite–illite ratio line of 1.4. The clay mineral type 2 indicated by a light-green colour is situated around the kaolinite–illite ratio line of 2.0. The

clay mineral type 3 indicated by a blue colour is situated between the kaolinite–illite ratio line of 1.0 and 2.0. The clay mineral type 4 indicated by a dark-green colour is situated around the kaolinite–illite ratio line of 1.0. The clay mineral type 5 indicated by a yellow colour is distributed above the kaolinite–illite ratio line of 1.0 (Fig. 54A). In addition, a slight increase in smectite is indicated by dark-green, blue, and light-green colours.

In contrast, the four mudstone types of the clay samples are not clearly discriminated on the diagram (Fig. 54B). However, very slight discrimination between mudstone types still can be identified on the diagram. The majority of type 3 mudstones are situated below the kaolinite–illite ratio line of 1.4, and the majority of types 2 and 4 mudstones are distributed above the kaolinite–illite ratio line of 1.4 (Fig. 54B).

In terms of clay mineral assemblages, these diagrams indicate that most of the type 1 and type 3 mudstones are associated with the kaolinite-rich assemblages. In contrast, the type 2 mudstones have two mineralogic affinities, i.e. the kaolinite-rich type 2 mudstones ($K/I > 1.4$) and the illite-rich type 2 mudstones ($K/I < 1.0$). Consequently, mudstone samples, which were taken from the floodplain deposits, tend to be associated with the kaolinite-rich assemblages. The spatial and temporal variations in mudstone types and clay mineral assemblages in the fluvial succession are shown in Figs. 55–57.

4.2.1. Kaolinite/Illite basal-peak intensity ratio (001)

Kaolinite and illite are the main clay minerals in the fluvial succession of the Bayah Formation in contrast to the relative proportion of smectite (0–17%). Kaolinite and illite minerals show significant variations in their relative proportions (2–65% and 22–76%, respectively). Temporal and spatial variations in kaolinite–illite ratios for mudstone types

and for clay mineral groups of the Bayah Formation are shown in Figs. 55A and 55B, respectively. Temporal variation in kaolinite–illite ratios does not show significant difference between the intervals (IV1–IV7).

Temporal variations generally appear to be in a relatively small amplitude (<1). Variations in the kaolinite–illite ratio with larger amplitude (>2), occur mainly in the eastern section above the IV2 and between IV2–IV6. In the central section, temporal variation with a large amplitude occurs in the IV4 interval. Between IV2–IV6 intervals, temporal variations with large amplitude occur below and above the distinct erosional surfaces that characterize interval boundaries (IV3–IV7) in the eastern section. In contrast, the lacustrine–delta deposits in the western section do not show these temporal variations with a large amplitude. In the eastern section, the majority of the kaolinite-rich clay types which are indicated by a pink-colour symbol occur above the IV2 (IV3–IV7) interval. In addition, slight spatial variations in the kaolinite–illite ratio are also occurred within each interval. In each interval, the kaolinite–illite ratio are higher in the western sections than the eastern sections. Although the diagrams indicate that the kaolinite-rich clay mineral types commonly occur in the eastern sections, a slight spatial variation indicate that the western sections have relatively higher kaolinite–illite ratio than the eastern sections.

For the western sections (Fig. 55) in the interval IV1, the kaolinite–illite ratio varies between 1.2 and 2.5, with the average kaolinite–illite ratio value of 1.59. In contrast, in the eastern sections, the kaolinite–illite ratio in IV1 varies between 0.35 and 2.42, with the average kaolinite–illite ratio value of 1.08. For IV1 in the both western and eastern sections, the kaolinite–illite ratio vary between 0.35 and 2.5, with the average kaolinite–illite ratio value of 1.27. For the western sections in the interval IV2, the kaolinite–illite ratio varies between 0.93 and 2.19, with the average kaolinite–illite ratio value of 1.67, and

in the same interval in the eastern sections, the kaolinite–illite ratio varies between 0.78 and 1.53, with the average kaolinite–illite ratio value of 1.3. For IV2 in the both western and eastern sections, the kaolinite–illite ratio varies between 0.78 and 2.19, with the average kaolinite–illite ratio value of 1.55. For the eastern sections in the interval IV3, the kaolinite–illite ratio varies between 1.14 and 2.93, with the average kaolinite–illite ratio value of 1.82.

For the western sections in the interval IV4, the kaolinite–illite ratio varies between 1.23 and 3.2, with the average kaolinite–illite ratio value of 2.12. At the same interval of IV4 in the central sections, the kaolinite–illite ratio varies between 1.35 and 4.32, with the average kaolinite–illite ratio value of 2.12. For the east sections in the interval IV4, the kaolinite–illite ratio varies between 0.53 and 1.34, with the average kaolinite–illite ratio value of 1.03. For interval IV4 from the western to eastern sections, the kaolinite–illite ratio varies between 0.53 and 4.32, with the average kaolinite–illite ratio value of 1.76. For the western sections in the interval IV5, the kaolinite–illite ratio varies between 2.14 and 4.2, with the average kaolinite–illite ratio value of 2.92. At the same interval of IV5 in the central section, the kaolinite–illite ratio varies between 1.34 and 1.67, with the average kaolinite–illite ratio value of 1.53. For the eastern sections in the interval IV5, the kaolinite–illite ratio varies between 1.37 and 1.82, with the average kaolinite–illite ratio value of 1.6. For interval IV5 from the western to eastern sections, the kaolinite–illite ratio varies between 1.34 and 4.2, with the average kaolinite–illite ratio value of 1.96. For the western sections in the interval IV6, the kaolinite–illite ratio varies between 3.14 and 4.11, with the average kaolinite–illite ratio value of 3.47. For the eastern sections in the interval IV7, the kaolinite–illite ratio varies between 1.66 and 2.37, with the average kaolinite–illite ratio value of 1.89. In the same interval of IV7 in the western sections, the average

kaolinite–illite ratio value of 1.83 is dominant. For the interval IV7 in the both western and eastern sections, the kaolinite–illite ratio varies between 1.66 and 2.37, with the average kaolinite–illite ratio value of 1.88. The range and average values of the kaolinite–illite ratio between the intervals indicate an increase in the average value of the kaolinite–illite ratio from the intervals IV1 to IV6, and subsequent decrease in the average value of the kaolinite–illite ratio from the intervals IV6 to IV7.

The overall increase and decrease in the kaolinite–illite ratio occurred in the either western or the eastern sections, although the eastern sections have relatively higher average values of the kaolinite–illite ratio than the western sections. In general, the relative illite ratio increases in the basal part of the intervals, and a significant increase in relative kaolinite contents is commonly observed in the fluvial succession. This temporal change in clay mineral composition appear to have responded to a change from the relatively poorer-drained conditions with alternating humid and dry seasons to warmer and more humid climatic conditions. The relatively higher average values of the kaolinite–illite ratio in the eastern than the western sections is interpreted as a response to spatial change in hydro-geochemistry condition. In the Bayah Formation, a lacustrine depositional environment developed in the western part of the fluvial basin. In general, lake water in a lacustrine environment has more alkaline and higher pH conditions than in either swamp or floodplain areas. Kaolinite is more stable and has a higher potential to be preserved in the lower alkaline and pH conditions (Rimmer and Davis, 1986; Do Campo et al., 2007).

4.2.2. Illite crystallinity index ($^{\circ}\Delta 2\theta$)

Low values of the illite crystallinity index correspond to the well-crystallized illite minerals, and high values of the illite-crystallinity index indicating the poorly-crystallized illite minerals (Chamley, 1989; Huyghe et al., 2011). High temperature and water from precipitation induce more intense weathering and produce poorly-crystallized illite, which are represented by wider X-ray diffraction peaks (Limmer et al., 2012).

Temporal and spatial variations in the illite crystallinity index for mudstone types and for clay mineral groups of the Bayah Formation are shown in Figs. 56A and 56B, respectively. The statistically valid data for the illite crystallinity index ($^{\circ}\Delta 2\theta$) show the highest, lowest, and average states, and are between 0.74–1.42, 0.33–0.42, and 0.50–0.68, respectively. The majority of mudstones of the fluvial succession can be classified into mudstones with poorly crystallised illite (70%), which corresponds to the high index values. In contrast, the remaining 30% of mudstones can be classified into well crystallized illite, which possibly still related to the physical erosion of the parental rocks. Temporal variation in the illite crystallinity index does not show significant difference between the intervals (IV1–IV7). Temporal variations generally appear in a relatively small amplitude ($<0.25^{\circ}\Delta 2\theta$). Temporal variation in the illite crystallinity index is not harmony with that in the kaolinite–illite ratio. The correlation between the illite crystallinity index and kaolinite–illite ratio is very weak, as indicated by small correlation coefficient ($r = 0.29$). In addition, the illite crystallinity index does not vary with the clay-mineral types and mudstone types (Fig. 56). The lowest values of the illite crystallinity index (well-crystallized illite) are only concentrated in the middle part of the fluvial succession, in particular in a horizon just below the interval IV3. In the western sections, the majority of mudstones in the lower

intervals (IV1–IV2) show relatively higher illite crystallinity values than the upper intervals (IV4–IV5). Although the illite crystallinity does not show significant temporal variation, a decrease and an increase in the average values of the illite crystallinity can be identified (Fig. 56). A decrease in the average illite crystallinity index occurred gradually from the interval IV1 (Avg. 0.49 °2 θ) to IV6 (Avg. 0.34 °2 θ), which is followed by an increase in the illite crystallinity in the interval IV7 (Avg. 0.42 °2 θ). The overall increase and decrease in the average values of illite crystallinity index occurred in the both western and eastern sections.

In general, the lower illite crystallinity is interpreted to respond to greater chemical weathering (Pandarinath, 2009). Higher temperature and rainfall cause stronger weathering, and thus wider XRD peaks and lower crystallinity may have developed. Stronger humidity and precipitation are favour for greater hydrolyzation and stronger weathering, which cause a reduction in illite crystallinity (Lamy et al., 1998; Alizai et al., 2012).

4.2.3. Illite chemistry index (5Å/10Å)

The illite chemical index was estimated using an illite ratio for the 5 Å (002) and 10 Å (001) peak areas for the ethylene-glycolated samples. The illite chemistry index above 0.5 indicates Al-rich illites suggests that the muddy deposits were formed under strong hydrolysis condition. In contrast, the illite chemistry index below 0.5 represents Fe- and Mg-rich illites (biotites, micas), which are characteristic for physically eroded, unweathered rocks (Gingele, 1996; Diekmann and Wopfner, 1996; Li et al., 2012).

Temporal and spatial variations in the illite-chemistry index ($5\text{\AA}/10\text{\AA}$) for the mudstone types and clay mineral groups of the Bayah Formation are shown in Fig. 57. Temporal variation in the illite chemistry index does not show significant difference between the intervals (IV1–IV7). Temporal variations generally appears in a relatively small amplitude ($<0.25\ 5\text{\AA}/10\text{\AA}$).

The illite chemistry index for the Bayah Formation mudstones varies between 0.34 and 1.23 with an average of 0.59. The statistically valid data for the illite-chemistry index of the highest, lowest, and average are between 0.86–1.23, 0.34–0.44, and 0.50–0.64, respectively. The majority of the fluvial mudstones has the index values above 0.5, and can be classified into mudstones with a high illite chemistry index (60%). In contrast, the remaining 40% of the mudstones have the index values below 0.5, and can be classified into a low illite chemistry index. The illite crystallinity index and illite chemistry index do not show distinct linear correlation, as indicated by only moderate correlation coefficient ($r = 0.59$). Consequently, temporal variation in the illite crystallinity index does not resemble the temporal variation in the illite chemistry. This imply a higher value of the illite chemistry index must not necessarily correspond to a lower value of the illite crystallinity. Because the majority of the fluvial mudstones can be classified into mudstones with poorly crystallized illite (70%), and the lower illite crystallinity index can have higher illite chemistry index in an extreme weathering conditions. However, the diagram of illite-chemistry index (Fig. 57) indicates an overall increase in the illite chemistry index from the interval IV3 to IV7. A similar increasing pattern in the illite crystallinity is also observed from the interval IV3 to IV7 (Fig. 56).

The mudstones with a relatively smaller value of the illite chemistry index are only observed in the interval IV1 to IV2. The majority of mudstones in the upper intervals

(IV4–IV5) show relatively higher values than the lower intervals. Similar to the illite crystallinity index, the illite chemistry index does not vary between the clay mineral types and mudstone types (Fig. 57).

In the western sections, the smaller values of illite chemistry index (≤ 0.5) are generally associated with the fluvial intervals IV2 and IV7. In contrast, the smaller values of illite chemistry index (≤ 0.5) are associated with the intervals IV1 and IV2 in the eastern sections. In the Bayah Formation fluvial succession, an overall increase in the average values of the illite chemistry index from the intervals IV1 to IV6 is observed. This is followed by a decrease in the average values in the interval IV7. This change may represent an increase in the relative proportion of Al-rich illites to the proportion of Fe- and Mg-rich illites in the mudstones from the intervals IV1 to IV6, followed by a decrease in Al-rich illites relative to Fe- and Mg-rich illites in the interval IV7. The maximum value of the illite chemistry index is associated with the interval IV6 ($5\text{\AA}/10\text{\AA} = 1.22$). This index value (>1) is very high and represents very high proportion of Al-rich illites, suggesting very intense hydrolysis conditions in the interval IV6. Smaller values of the illite chemistry index are generally associated with the presence of smectite (3.7%–14.4%) and mixed layer illite-smectite (14.3%–25.8%) in the intervals IV1–IV3. The high illite chemistry index is associated with Al-rich illites, representing strong hydrolysis condition. In contrast, the low illite chemistry index is associated with Fe- and Mg-rich illites (biotites, micas), representing weakened chemical weathering condition.

5. Discussion and Conclusions

The fluvial–lacustrine-delta succession of the Bayah Formation is interpreted to represent a largely climatic-driven nonmarine sedimentation during the long-term regional everwet climate in Late Eocene (Morley and Morley, 2012), in association with a transition stages of regional-longer term tectonic-related sedimentation between late syn-rift–post-rift stages in the southern margin of the Sundaland continent (Longley, 1997; Doust and Sumner, 2007). The evidently observed freshwater algae (*Pediastrum* sp.), a woody- *Ficus* sp. (*moraceae*), and *rubaceous* shrubs (Isnaniawardhani, 2014; Winantris, 2015, Laboratory of Palaeontology–Padjadjaran University, personal communications) in the fluvial succession, in association with the absence of deposits which indicate tidal influences, suggest that the fluvial succession was likely situated far from the paleoshoreline in the early stage of its sedimentation.

The total thickness of fluvial–lacustrine succession of up to 915 m indicates a sustained nonmarine accommodation. Nonmarine accommodation is generally induced by basin subsidence together with the presence of the increase in sediment loads (Blair, 1987; Shanley and McCabe, 1994; Miall, 1996; Catuneanu and Elango, 2001). Stratigraphic subdivision of the fluvial succession into 7 intervals (IV1–IV7 in ascending order) by 6 distinct erosional surfaces (ES1 to ES 6 in ascending order), in association with temporal variations in grain size, suggest the involvement of other factors in the filling of the nonmarine accommodation. Nonmarine accommodation, which is created primarily by periodic tectonic movements, is mainly characterized by relatively persistence thickness in fluvial cycles, progressive coarsening-upward deposits, a drastic change in dispersal

polarity and paleocurrent directions, a significant incisions and down-cutting erosional surfaces, a shift of depositional environments, and significant variation in detrital framework of sandstones (e.g., Graham et al., 1976; Blair, 1987; Catuneanu and Elango, 2001; Nichols and Cantrill, 2002). In contrast, the fluvial–lacustrine succession of the Bayah Formation is characterized by an overall upward thinning of the intervals (IV1–IV6), and then the thickening in the uppermost interval (IV7). Each interval of the Bayah Formation is represented by an overall fining-upward pattern from sandstone- and conglomerate-dominated deposits in the lower parts to mudstone-dominated deposits in the upper parts. Although distinct erosional surfaces in the base of each interval can be traced laterally for more than 100 m, these surfaces are not considered to develop regionally. These erosional surfaces are similar to those described as a local erosional surface in the base of fourth-order fluvial cycle (e.g., Miall, 1996; Plink-Björklund, 2005). Relief contrast of the distinct basal erosional surfaces of the intervals do not exceed more than 3 m. Moreover, the paleocurrent directions of the fluvial succession show persistent trends in both the fluvial deposits and coastal and shallow marine deposits in the uppermost position. This suggests that tectonic movement may not have been purely a primary controlling factor in the sedimentation of the Bayah Formation.

Sandstones of the Bayah Formation do not show significant temporal variation in detrital framework composition. Although the sandstones show slight fluctuation of the temporal variation in the proportion of quartz relative to rock fragments, this variation is not considered to have reflected changes in provenances. Rapid erosion in association with high discharge period can revitalize supply of clastic sediments, which contain relatively more rock fragments (Suttner and Dutta, 1986; Chandler, 1988). It is interpreted that temporal fluctuation in the increase of rock fragments relative to quartz and feldspar grains

indicate temporal intensification of physical erosion relative to the chemical weathering processes. Bivariant log-plot ratios between the most stable and unstable framework grains indicate that the majority of sandstones were derived from moderately–intensely weathered sands under the influence of subhumid–tropical humid climate, in association with the moderate to low relief conditions (Suttner and Dutta, 1986; Weltje et al., 1998; Garzanti et al., 2013). Similarly, in terms of the weathering effect and climatic factors, variations in clay mineral composition of the Bayah Formation mudstones is interpreted to represent a potential effect of weathering and climatic factors, documented in temporal variations in the kaolinite–illite ratio, illite crystallinity, and illite chemistry index.

Although temporal variations in clay mineralogy do not show significant difference between the intervals, an overall increase and decrease in the kaolinite–illite ratio, illite crystallinity, and illite chemistry index with larger amplitude may indicate temporal variations in the weathering intensity from the alternating humid and dry seasons to a warm and more humid climatic conditions.

Based on geometry and its internal characteristics, the packages of sandstone and conglomerate bodies, which represent channel-fill deposits are subdivided into three types: (1) lenticular and tabular conglomerate-dominated packages, (2) tabular and lenticular conglomeratic sandstone packages, and (3) tabular and lenticular sandstone-dominated packages. Each type represents a different style of sedimentation, as follows: (1) is a bedload-dominated sedimentation in braided river, (2) is characterized by the development of longitudinal and transversal bar that may have been situated in a transitional area between braided and sinuous rivers, and (3) is a mixed-load sedimentation in meandering rivers, respectively. In association with the variation in mineralogy of the deposits that indicate variation in weathering intensity and climates, the variation in channel-fill deposits

of the Bayah Formation is considered to reflect temporal variations in sediment supply and discharges conditions. Change in fluvial styles may be a significant indicator of the change of sediment supply and discharge conditions (Patton, 1987; Miall, 1996; Blum and Tornqvist, 2000; Lewis et al., 2001).

Part 2.

Hydrological Features of Modern Fluvial Systems in the Indonesian Islands

6. Introduction

6.1. Background

Empirical equations between hydrological parameters, such as bankfull channel depth and width, annual mean and bankfull water discharges, have been developed for modern fluvial systems (e.g., Leopold and Maddock, 1953; Leeder, 1973; Ethridge and Schumm, 1978; Osterkamp and Hedman, 1982; Williams, 1984a, b, 1986; Shibata and Ito, 2014). These equations have been used to reconstruct paleohydrological features of ancient fluvial systems; and variations in paleocurrent directions and sinuosity based on analyses of outcrops, cores and log data of fluvial successions (e.g., Van der Neut and Eriksson, 1999; Bridge and Tye, 2000; Bridge, 2003; Adams and Bhattacharya, 2005; Ito et al., 2006; McLaurin and Steel, 2007; Hampson et al., 2013; Holbrook and Wanas, 2014).

These empirical equations have been established based on hydrological data from modern fluvial systems mainly on passive continental margin and continental-interior settings that are influenced by a temperate climate. Consequently, a better understanding of variations in hydrological parameters in fluvial systems requires the establishment of empirical equations for different tectonic and climatic settings (Shibata and Ito, 2014). This enables us to understand spatial and temporal variations better in the paleohydrological features documented in ancient fluvial successions, and how these are related to global environmental change and the tectonic setting of sedimentary basins.

Empirical equations for fluvial paleohydrologic reconstructions have been established in continental margin and continental interior settings and reflect mid- and high-latitude climates (Leopold and Maddock, 1953; Crane, 1982; Osterkamp and Hedman, 1982; Williams, 1984a). Hydrological equations have not yet been developed for active-margin

settings influenced by low-latitude and equatorial climates, which produce thick vegetation, intense rainfalls, and active sediment yield (Sinha et al., 2012; Syvitski et al., 2014), although hydrological parameters have been analyzed in modern fluvial systems in the Pacific coast of the U.S.A., which is represented also by convergent margin tectonics (e.g., Castro and Jackson, 2001; Modrick and Georgakakos, 2014). However, in terms of climatic conditions, the Pacific coast of the U.S.A. are situated in mid-latitude region, which reflect different climatic conditions to the active-margin settings influenced by low-latitude and equatorial climates. According to the Köppen-Geiger climate zonation, the average-annual rainfalls in mid-latitude region is commonly less than 1000 mm. In contrast to the tropical climate in equatorial region, where the average-annual rainfalls can exceed 2000 mm (Peel et al., 2007). Fluvial discharge is very much affected by the level of precipitation. These empirical equations for fluvial hydrology are a crucial step for identifying similarities and differences in the hydrological parameters of fluvial systems formed in different tectonic and climatic settings.

The present study develops empirical equations for hydrological parameters in modern fluvial systems in the three main islands (i.e., Java, Sumatra, and Kalimantan) of the Indonesian archipelago, where these hydrological analyses have not yet been attempted (Fig. 58). These equations are established based on relationships between mean and bankfull discharge, bankfull channel width, and mean and maximum bankfull depth. Although the bankfull channel width and mean and maximum bankfull channel depth have also been analyzed as a function of drainage area (e.g., Dunne and Leopold, 1978; Wohl et al., 2004; Modrick and Georgakakos, 2014), this study mainly analyzed the relationships between bankfull width and depth data and discharge data. In this study, the analyzed relationships were compared with some empirical equations proposed by the previous

studies, which have been used to reconstruct paleohydrological features of ancient fluvial successions. The results provide a case study for modern fluvial systems developed in an active low-latitude convergent margin setting under the influence of a tropical climate.

6.2. Geomorphological and climatic setting

Indonesia is an archipelagic nation with more than 18,000 component islands, including 5 large islands: Sumatra, Java, Kalimantan (Borneo), Sulawesi (Celebes), and West Papua. The present study focuses on fluvial systems in the three largest islands: Sumatra, Java, and Kalimantan. The Indonesian archipelago spans the equator from latitudes 6°N to 11°S (Fig. 58). It is characterized by mountain ranges and plateaus with volcanoes in Sumatra and Java and Paleogene and older sedimentary, volcanic, and metamorphic rocks in Kalimantan. The volcanic ranges form the Sumatra–Banda arc, and extend nearly 7000 km along the archipelago from the northwest to southeast. The volcanic highlands are surrounded by lowland alluvial and coastal plains that are larger in area in retroarc regions, such as the east coast of Sumatra and the northern coast of Java, than in forearc regions on these islands (Laumonier, 1997; Göltenboth and Erdelen, 2006) (Fig. 58). Consequently, fluvial systems in the retroarc regions are larger and longer than those in the forearc regions. The retroarc regions of Sumatra island are larger and longer than those in Java island. In contrast, fluvial systems in Kalimantan drain through a stable region far from the subduction zone (Fig. 58).

The Sumatra and Java islands are situated in front of the Sunda–Java arc subduction zone (Hall, 1997) (Fig. 58), and are characterized by active deformation processes

including intense seismicity and active faulting (e.g., Simandjuntak and Barber, 1996; Soehaimi, 2008; Tjia, 2013; Nguyen et al., 2015). Several studies on seismicity and active-regional faults in Sumatra and Java have reported the presence of an extensive development of fluvial-terrace deposits, which are associated with active faults along the western part of Sumatra and southern part of Java islands (Aribowo and Yudhicara, 2015; Marliyani et al., 2016). In Java, drainages are divided by volcanic ranges that extend in an east–west direction. Northward-flowing rivers drain to the inland sea of Java and southward-flowing rivers drain to the Indian Ocean (Figs. 58 and 59). In Sumatra, volcanic ranges extend in a northwest–southeast direction, and form a drainage divide for the eastward-flowing and westward-flowing rivers (Figs. 58 and 60).

In contrast, because Kalimantan is a part of the Sundaland continental mass (Simandjuntak and Barber, 1996; Hall, 1997), the island does not have active volcanoes. In the centre of the island, Paleogene and older rocks occupy highlands that are surrounded by lowland alluvial and coastal plains (Fig. 61). Consequently, river systems in Kalimantan spread out from the highlands and flow toward marginal inland seas, such as the Java Sea and the Makassar Strait (Figs. 58 and 61). Drainage areas in Kalimantan are covered by dense tropical rainforest, and peneplain processes have been dominant (Göltenboth and Erdelen, 2006). Because the lowlands and alluvial plains in Sumatra and Kalimantan are wider, these two islands also have larger drainage basins than those on the Java. For example, the largest drainage basin in Kalimantan is seven times larger than any in Java (Directorate General of Forestry and Environmental Planner, 2011).

Indonesia is characterized by a monsoon climate in the equatorial region (Tan, 2008; Karmalkar et al., 2010). Regional variations in climate between islands are caused by their geographic positions relative to the equator, the Indian Ocean, and the Australian continent

(Aldrian and Susanto, 2003; Indonesian Agency for Meteorology, Climatology and Geophysics, 2015). According to the Köppen-Geiger climate classification, the climate of the Indonesian archipelago is classified as a tropical rainforest type (Peel et al., 2007; Tan, 2008).

Monsoon climates in Indonesia consist of alternating rainy and dry seasons. The rainy season occurs during 6 consecutive months from December to May in association with the northwest monsoon, and the dry season occurs from June to November during the southeast monsoon (Tan, 2008). The driest months occur from July to September, during which the average rainfall is <60 mm/month. A peak rainy season occurs from January to February, with average rainfall of >250 mm/month. The rainy season is characterized by heavy torrential rain that results in extensive floods (Asian Disaster Preparedness Center, 2000).

Based on the relative duration of dry and rainy seasons, climate in almost all parts of Sumatra and Kalimantan is classified as a per-humid type (Cecil et al., 2003; Tan, 2008). Because dry seasons span only 2–4 months on these islands and are interrupted by rainy days, precipitation is evenly distributed throughout the year. Consequently, the relative ratio between maximum and minimum river discharge does not show distinct annual variations. The ratios vary from 6 to less than 80 in Sumatra and are less than 30 in Kalimantan (Laumonier, 1997; Center for Water Resources Development and Research, 2011). In contrast, because Java has a seasonal climate type (Cecil *et al.*, 2003; Tan, 2008), river discharges have distinct seasonal variations, and the ratio between maximum and minimum discharge varies from 20 to more than 100 (Runtunuwu and Pawitan, 2008).

6.3. Data and methods

Water discharge data were obtained from 649 observation sites in Java ($n = 338$), Sumatra ($n = 247$), and Kalimantan ($n = 64$) (Figs. 59, 60, and 61). The sites in Java and Sumatra are additionally subdivided into two regions: northward-flowing ($n = 233$) and southward-flowing ($n = 105$) rivers in Java, and eastward-flowing ($n = 161$) and westward-flowing ($n = 86$) rivers in Sumatra. The divisions on these two islands follow the geomorphological subdivisions in the two islands with respect to the volcanic highlands (Figs. 58–61; Table 1). Water discharge data used in the present study are mean discharge (Q_{mean}) and bankfull discharge (Q_b). These data are available digitally from the Center for Water Resources Development and Research, Ministry of Public Works and Housing (Center for Water Resources Development and Research, 2011) (Table 1). Q_{mean} is the average of all mean annual discharges observed within a defined period. Mean annual discharges are defined as the sum of average monthly discharge, measured on a daily basis, divided by 12 months of the concerned year. Q_b is commonly taken as a condition forming the shape and morphology of fluvial channels, and is interpreted to be equivalent to the mean annual flood discharges (e.g. Williams, 1978; Van den Berg, 1995). Yamamoto (2004) showed that the mean annual flood-peak discharges are almost equivalent to Q_b using data from Japanese rivers. Xu (2004) also used the mean annual maximum daily discharges as Q_b for analyzing hydraulic geometry of rivers in various countries worldwide. Therefore, Q_b can be estimated from the average of the annual maximum daily discharges during flood seasons within a defined period. Observation periods at hydrological stations vary from 5 to 44 years as listed in Table 1. The first and last observation years also vary between sites. Most records begin between 1983 and 1993 and

end in 2009. In the collection of discharge parameters at the 649 observation sites, bankfull channel width (W_b) was obtained using high-resolution satellite images from Google Earth (<http://www.google.com/earth>) (Fig. 62A), following methodologies in previous studies (e.g., Williams, 1986; Atha, 2014). Distances between the present-day levees in the both sides of fluvial channels, which locally have sandy bars in the satellite images, were measured along 3 to 5 lines across a channel at each observation site, and the average value was used as W_b .

Three parameters of the cross-sectional geometry of fluvial channels, such as bankfull channel depth (d_b), mean bankfull channel depth (d_m), and W_b , were measured at 86 locations (Figs. 63–65), where cross-sectional channel geometry has been documented by the Provincial Public Works Agency, Indonesian Ministry of Public Works and Housing (2012) in non-consecutive years between 1980 and 2012 (Table 2; Fig. 62B). Data are available from 45 sites in Java, 19 sites in Sumatra, and 22 sites in Kalimantan (Table 2; Figs. 63–65). In the present study, d_b is defined as the elevation difference between the thalweg and floodplain, and W_b is defined as the distance between banks. The inside portions of banks are well defined by the “bankfull edges”, which are located at the edge of flat floodplain in a cross section (Fig. 62). The bankfull edges are usually indicated by abrupt changes of slope in a cross section, and the distance between the edges were measured as W_b . The cross-sectional area (A) and wetted perimeter (P) were also calculated for bankfull conditions. The hydraulic radius (R_h) during a bankfull condition is approximated by d_m ($R_h \approx d_m$); (Leopold et al., 1992; Dingman, 2009) and was calculated by dividing A by P (Fig. 62B; Table 2). The present study used “ABViewer” software for measurements of A and P from channel cross sections. At 86 observation sites, W_b was

checked using the satellite images. The relative errors of the W_b estimation between using cross sections and satellite images are from 0.0 % to 47.8 % with an average of 12.7 %.

The nature of sediment types of river beds and banks at the observation sites in the Java, Sumatra, and Kalimantan Islands was also checked using 1:100,000 geological maps (Indonesian Geological Survey, 2004) (Figs. 66–68; Table 3).

Because W_b is closely correlated with discharge parameters (e.g., Osterkamp and Hedman, 1982; Williams, 1984a; Dingman, 2009), the present study analyzed the relationships between W_b and discharge data (Q_{mean} and Q_b) in the Indonesian rivers and established a power function:

$$Q = C W_b^B \quad (1)$$

where Q is discharge (m^3s^{-1}), C is a coefficient, and B is an exponent. Similarly, W_b is also closely correlated with the depth parameters (d_b and d_m) (e.g., Leeder, 1973; Bridge and Mackey, 1993), and Bridge and Mackey (1993) proposed an empirical equation between d_m and d_b . Here, empirical relationships were developed for d_b , d_m , and W_b as follows:

$$d_m = D d_b \quad (2)$$

$$W_b = E d_b^F \quad (3)$$

$$W_b = G d_m^H \quad (4)$$

where D , E and G are coefficients, and F and H are exponents.

In general, the morphology of the Indonesian rivers is preserved in their natural condition. Engineering operation has not given significant modification of the river morphology. The engineering structures, such as the construction of flood-control dams, reservoirs, and irrigation systems, only affect a small portion of fluvial systems in the suburbs and urban areas (Rijsdijk, 2012). We compared topographic maps published in the early 20th century (surveyed in 1908 and 1928) with those were at the end of the 20th century (surveyed between 1977 and 1991) for estimating engineering modification of fluvial geomorphology at five observation sites in each of Java, Sumatra, and Kalimantan (Fig. 69). In this comparison, sinuous bends do not show any distinct change, although channel planforms and shoreline locations locally show slight modifications. Although land use for paddy fields has also made minor modification in fluvial geomorphology that does not show any distinct changes in rural areas. Overall, minor changes in fluvial geomorphology indicate that cross-sectional channel geometry and discharge data from fluvial channels over a time span between 1983 and 2009 can be used to establish empirical equations (1)–(3) in the three largest islands of Indonesia.

The empirical equations were evaluated following a method of Waltham (1994), and the present study used statistical parameters, such as the correlation coefficient (r), the coefficient of determination (R^2), and the significance level (p) of the F -ratio, which describe the relationships between d_b and d_m , and among $\log d_b$, $\log d_m$, $\log Q_{\text{mean}}$, $\log Q_b$, and $\log W_b$. The 95% regression-confidence bounds were calculated and plotted on the diagrams (Figs. 70, 72; and Figs. 74–77). The symbols used in the present study are listed in Table 4.

7. Results

7.1. Discharges relative to bankfull channel widths

Empirical relationships between discharge (Q_{mean} and Q_b) and W_b , are summarized in Figures 70–75 and Table 5. Correlation coefficients (r) for the relationships between discharge parameters and W_b are in the range 0.72–0.97, and are greater than 0.7 for all islands as well as for the two sub-regions of Java and Sumatra. These values indicate that discharge parameters and W_b have a statistically significant relationship (e.g., Inagaki et al., 1992). The coefficients of determination (R^2) for these parameters range from 0.59 to 0.92, indicating that 59% to 92% of the factors, which control discharges, can be explained by the bankfull channel width (W_b). In addition, p values (level of significance) are all less than 0.05, indicating that the empirical equations are statistically significant.

Although the lengths and drainage areas of the northward-flowing rivers in Java and the eastward-flowing rivers in Sumatra are generally larger than those of the southward-flowing rivers in Java and the westward-flowing rivers in Sumatra, the empirical relationships between discharge (Q_{mean} and Q_b) and W_b do not show significant differences between the two fluvial systems in both Java and Sumatra (Figs. 71 and 73). The 95% confidence bounds for the regression curves of the rivers in Java and Sumatra have overlapping regions. In addition, the exponents and intercept values of the equations for northward- and southward-flowing rivers have quite similar values in Java, although the exponent of the equations for eastward-flowing rivers is slightly larger than that for westward-flowing rivers in Sumatra (Figs. 70–73; Table 5). Although the relationships between discharge (Q_{mean} and Q_b) and W_b exhibit slight regional differences in Sumatra,

the relationship between Q_b and W_b calculated using all data from each of the three islands exhibit similar patterns (Figs. 73 and 75). In contrast, the relationship between Q_{mean} and W_b is slightly different between rivers in the three major Indonesian islands (Fig. 75B).

7.2. Bankfull channel width and channel depth

The empirical relationships between maximum bankfull channel depth (d_b) and mean bankfull channel depth (d_m), between d_b and bankfull channel width (W_b), and between d_m and W_b were developed based on cross-sectional measurements of fluvial channels (Figs. 76–77; and Table 2). The three empirical equations and their statistical parameters obtained by the present study are summarized in Table 6.

The correlation coefficients (r) for d_m and d_b range from 0.93 to 0.97, suggesting a strong correlation between d_m and d_b for rivers in Java, Sumatra, and Kalimantan. Furthermore, coefficients of determination (R^2) for these parameters range from 0.86 to 0.94, indicating that 86% to 94% of the factors that control d_m can be determined by d_b . The p values (level of significance) for the relationships are less than 0.05, indicating that the empirical equations between d_m and d_b are statistically significant.

The correlation coefficients (r) for W_b and channel depth (d_m and d_b) range from 0.43 to 0.76, indicating that W_b and channel depth are correlated in rivers in Java, Sumatra, and Kalimantan. Furthermore, the coefficients of determination (R^2) for these parameters range from 0.31 to 0.54, indicating that 31% to 54% of the factors that control the bankfull channel width (W_b) can be explained by both d_m and d_b . In addition, the p values (level of

significance) are less than 0.05, indicating that the empirical equations for W_b and d_m and W_b and d_b are statistically significant.

7.3. River bed and bank materials and bankfull channel width and channel depth

River bed and bank materials in the Java, Sumatra, and Kalimantan islands can be grouped into five major types (Types 1–5) (Table 3; Figs. 66–68, and Fig. 78). Type 1 is Quaternary volcanic deposits. It is represented by unlithified gravel- and sand-sized pyroclastic and volcanoclastic deposits, which were produced primarily by volcanic eruptions, together with lahar deposition. Type 2 is Quaternary alluvial–coastal deposits, which are composed of unlithified sands and gravels. These deposits constitute river-terraces, floodplains, and coasts as reworked sediments of the type 1 and/or were supplied from older rocks in hinterlands. Type 3 is a bedrock of the Neogene and Paleogene sedimentary rocks, such as sandstone, mudstone, and minor carbonate rocks. Type 4 is also a bedrock that is composed mainly of Mesozoic fine-grained siliciclastic sedimentary rocks. Type 5 is the pre-Neogene igneous and metamorphic rocks, which are represented by granite, schist, and argillite. The relative area of the river bed and bank materials in Java Island is generally represented by the type 1 (46%) in association with the type 2 (37%). The rest is occupied by the type 3 (17%). In Sumatra, the river bed and bank materials are occupied by the types 1 and 2, and each of these two types covers about 33% and 35% in area, respectively. The rest is represented by the types 3 (28%) and 5 (4%), respectively. In contrast to Java and Sumatra, the relative area of the river bed and bank materials in

Kalimantan is dominated by the type 2 (44%), together with the type 3 (26%), 4 (14%), and 5 (16%), respectively (Table 3).

8. Discussion

8.1. Relationships between bankfull channel width and discharges

Slight differences in the relationships between discharge (Q_{mean} and Q_b) and W_b occur in westward-flowing and eastward-flowing rivers in Sumatra, although the same relationships for northward-flowing and southward-flowing rivers in Java do not show distinct differences (Figs. 71 and 73). Higher discharge for a given W_b in eastward-flowing rivers in Sumatra is considered to reflect larger drainage areas in the retroarc region in Sumatra than those in Java (Fig. 58). The empirical relationship between Q_{mean} and W_b derived from the total data from each island shows regional variation for Java, Sumatra and Kalimantan. This variation is most distinct for Java and Kalimantan (Fig. 75). That is, Q_{mean} has higher values in Kalimantan than in Java relative to a given W_b .

This regional variation in Q_{mean} relative to W_b is considered to reflect variations in regional climate. Mean annual rainfall data from 2000 to 2013 (Indonesia Central Bureau of Statistics, 2015) shows that among the three islands, Kalimantan has the highest mean annual rainfall, whereas Java has the lowest mean annual rainfall (Fig. 79). The Indonesian archipelago can be divided into three different climatic–rainfall zones based on rainfall peak-cycles (Aldrian and Susanto, 2003; As-syakur et al., 2013). Most of Kalimantan is in a climate zone, having two annual peak rainy seasons caused by movement of the inter-tropical convergence zone (Aldrian and Susanto, 2003). In contrast, Java is in a climate zone, having only one wet and dry monsoon cycle; i.e., one rainy season (Aldrian and Susanto, 2003). Consequently, annual mean discharge is higher in

Kalimantan than in Java, and this regional variation results in differences in empirical equations for Q_{mean} and W_b .

In contrast, empirical relationships between Q_b and W_b do not show significant regional variations for Java, Sumatra, and Kalimantan (Fig. 75). The rivers in Java are generally characterized by smaller drainage basins with shorter river lengths, compared with the rivers in Sumatra and Kalimantan (Cecil et al., 2003; Directorate General of Forestry and Environmental Planner, 2011). In addition, smaller rivers in Java have steeper rivers slopes than the rivers in Kalimantan, which is widely occupied by lowland plains (Directorate General of Forestry and Environmental Planner, 2011). Geomorphological conditions in Java promote a rapid hydrological response to high rainfalls in peak rainy seasons, which may cause large maximum and bankfull discharge (Charlton, 2008). Although rivers in Java, Sumatra, and Kalimantan islands have different geomorphologic conditions in terms of the size of drainage basins, together with the slope and the length of rivers, they do not show significant regional variations in the Q_b – W_b relationships. They imply wide applicability of the relationships for fluvial systems formed in a convergent margin under the influence of a low-latitude tropical climate (Table 5).

8.2. Relationships between channel width and mean-channel depth

The relationships between d_m and d_b do not show any significant differences between rivers in Java, Sumatra and Kalimantan (Figs. 76–77; Table 6). The relationships indicate that mean bankfull channel depth is approximately half of the maximum bankfull depth ($d_m \approx 0.5 d_b$). In contrast, the empirical relationships between d_m and W_b and between d_b and

W_b show some regional variations between the three islands (Fig. 77). The regional variations summarized in Fig. 77 indicate that the rivers in Kalimantan have the largest W_b and those in Java have the smallest W_b relative to given depth parameters (d_b and d_m). This also shows that channel widths tend to increase with increasing discharges (Leopold and Maddock, 1953; Leopold et al., 1992; Charlton, 2008).

The per-humid climatic condition in Kalimantan is characterized by high annual rainfalls throughout the year that result in higher discharge than in Java. Alternatively, wider drainage basins in Kalimantan are also likely controlled by the higher discharges in Kalimantan than in Java. In addition, fluvial systems in tectonically active regions are characterized by active channel incision in response to the uplift of drainage areas (e.g., Amos and Burbank, 2007; Hilley and Arrowsmith, 2008). Active uplift has occurred in Java throughout the Quaternary (Soehaimi, 2008; Tjia, 2013; Nguyen et al., 2015), and this may also have promoted active incision in fluvial systems, resulting in smaller width/depth ratios in Java than in Kalimantan.

In contrast, the increase in W_b with respect to increase in d_m and d_b in rivers in Sumatra is smaller than for rivers in Kalimantan and Java (Fig. 77). Sumatra is also characterized by active Quaternary tectonics and higher discharge than Java. The relative intensity between sediment supply and water discharge is thought to control spatial and temporal variations in depositional and erosional processes in river channels (Blum and Törnqvist, 2000). The combination of these factors in Sumatra has likely promoted active erosion of fluvial channels to form lower width/depth ratios than rivers in Java and Kalimantan.

Erodibility of river bed and bank materials is also considered to control the depth and width of fluvial channels regardless of the magnitude of flood discharges. Although fluvial systems in Java, Sumatra, and Kalimantan are represented by 5 different types of river bed

and bank materials (Fig. 78; Table 3), rivers developed on the type 2 have the highest average values of d_b (4.32 m–11.65 m) and W_b (61 m–84 m), and those on the types 3 and 5 have the lowest average values of d_b (1.32 m–4.45 m) and W_b (33 m–44 m), respectively (Fig. 78). However, spatial variation in these materials have not necessarily influenced the relationships between the width, depth, and discharges in the study areas (Fig. 78). Consequently, the interaction between tectonics and climates is considered to have controlled the relationships between the geomorphological and hydrological parameters in the three islands.

8.3. Comparison of empirical relationships

Empirical relationships between discharge parameters (Q_{mean} and Q_b) and W_b have been proposed based on hydrological data from modern fluvial systems in various tectonic and climatic settings (e.g., Dury, 1976; Osterkamp and Hedman, 1982; Williams, 1984a; Mackey, 1993) (Table 7). Most previous studies have analyzed data from rivers formed in passive continental margin and continental interior settings, which have been influenced mainly by mid- to high-latitude temperate climatic conditions. Recently, Shibata and Ito (2014) proposed empirical equations for modern fluvial systems in the Japanese islands, which have been influenced by mid-latitude temperate and monsoon climates.

Although Shibata and Ito (2014) and the present study focused on modern fluvial systems in a convergent margin setting, the empirical relationships between discharge Q_{mean} and W_b in modern fluvial systems in Indonesia and the Japanese islands show distinct differences (Fig. 80A). In general, modern fluvial systems in Indonesia have higher Q_{mean}

than those in the Japanese islands with respect to a given W_b (Fig. 80). This variation likely reflects regional variations in annual rainfall between Indonesia and Japan, which is controlled by differences in monsoon-influenced climates in low-latitude and mid-latitude regions, respectively. Shibata and Ito (2014) pointed out that empirical relationships between Q_{mean} and W_b have distinct regional variations and are influenced by differences in tectonic and climatic settings (Fig. 80A). They also proposed that regional variations are a result of monthly variations in discharge, reflecting regional climatic conditions within Japan. In contrast, the empirical relationship between Q_b and W_b does not show distinct regional variation, regardless of the tectonic and climatic settings (Fig. 80B). In general, Q_b is interpreted to control geomorphological features of fluvial channels (e.g. Ackers, 1970; Dury, 1976; Bridge, 2003; Yamamoto, 2004), although Pickup and Rieger (1979) claimed that channel forms are a product of the whole series of discharges experienced by fluvial channels. Gupta (1988) reviewed the relationships between channel forming processes and floods in humid tropical regions between the 10° and 30° latitudes, and concluded that high-magnitude floods are extremely important as channel- and valley-forming events in certain parts of the humid tropics. Although such high-magnitude floods were not analyzed by the present study, the slight variation in the Q_b – W_b relationships not only among Indonesian rivers but also among rivers in Japan and continental areas imply that Q_b strongly affect W_b . This supports a general concept that bankfull discharges can be considered as channel-forming discharges.

On the other hand, the empirical relationships between W_b and d_m in both the present and previous studies show distinct variations (Fig. 80C). These variations may reflect specific climatic conditions and tectonic settings of each fluvial system (Fig. 80C; Table 7). The d_m – W_b regression line for Indonesian rivers has a lower gradient than for other

rivers, and is thought to be related to the fact that Indonesian rivers have a wider W_b than shallow rivers ($d_m \leq 5$ m) formed in mid- and high-latitude areas. In other words, Indonesian rivers with a relatively large channel width ($W_b \geq 100$ m) are deeper with respect to a given W_b than rivers formed in mid- and high-latitude areas. This variation likely reflects higher flood discharges during wet seasons in Indonesia and the ensuing erosion of riverbeds by floodwaters. Alternatively, the growth of thick vegetation covers on overbanks and flood plains of tropical rivers can strengthen riverbanks and increase their resistance to bank erosion (Hickin, 1984; Bartley et al., 2008).

Because the empirical equation between d_m and W_b for modern fluvial systems has distinct regional variations in different tectonic and climatic settings, the equation developed in the present study may only capture the relationship for a convergent margin setting influenced by a tropical climate. In contrast, the empirical equation between Q_b and W_b does not show any distinct regional variations. This Q_b – W_b relationship can be applied to other fluvial systems in a convergent margin setting under a tropical climate, although the applicability of this equation has not yet been tested. The bankfull channel depth (d_b) has been reconstructed from outcrops, cores, and wireline-logs using maximum thickness of bar deposits (Allen, 1965; Bridge and Diemer, 1983; Bridge and Mackey, 1993), and/or the thickness of cross bedding (i.e., cross-set thickness: Bridge and Tye, 2000; Leclair and Bridge, 2001; Bridge, 2003) with correction of diagenetic compaction (Ethridge and Schumm, 1978; Lorenz et al., 1985). In contrast, the bankfull channel width (W_b) of ancient channels can not be directly measured in stratigraphic successions, except for well-preserved stratigraphic records and some Holocene deposits (Williams, 1988). Therefore, the empirical equations developed in this study are also used for the reconstruction of

paleochannels and their hydrological features which were deposited in a convergent margin setting under a tropical climate. The appropriate selection of a d_m-W_b equation combined with an appropriate Q_b-W_b equation enables us to reconstruct spatial and temporal variations in fluvial paleohydrological features in stratigraphic successions more precisely than reconstruction using previously proposed equations.

9. Conclusions

The present study established empirical equations for geomorphological and hydrological parameters that characterize fluvial systems formed in a convergent margin setting influenced by a low-latitude tropical climate. This setting is different from those used for previously established empirical equations. The relationship between discharge (Q_{mean} and Q_b) and bankfull channel width (W_b) is investigated using hydrological data from 649 measurement locations in Java, Sumatra and Kalimantan. The relationship between channel depth (d_m and d_b) and the bankfull channel width (W_b) is also investigated based on 86 cross-sections of fluvial channels in Java, Sumatra and Kalimantan.

Although the relationships among discharge parameters (Q_{mean} and Q_b) and W_b do not show distinct variations between rivers in retroarc and forearc regions in Java, some variation is observed in Sumatra. The relationship between Q_{mean} and W_b has distinct variations for rivers in Java, Sumatra, and Kalimantan. These variations are considered to reflect regional variations in annual rainfall under the influence of a monsoon-influenced tropical climate. In contrast, the relationships between Q_b and W_b do not show any regional variations across the three islands. These minor regional variations indicate that fluvial channel geometry in Indonesia have adjusted to bankfull hydrological conditions during rainy seasons. In addition, the empirical equation between Q_b and W_b does not show distinct variations across fluvial systems regardless of their tectonic and climatic settings, although the empirical equation between Q_{mean} and W_b shows distinct variations that reflect tectonic and climatic settings. Consequently, the Q_b – W_b equation indicates that the development of fluvial morphology is controlled by flood-related episodic discharge rather than by annual mean discharge, and is considered to be widely applicable for the modern

and ancient fluvial systems especially for those formed in a convergent margin under the influence of low-latitude tropical climate.

On the other hand, the empirical relationship between W_b and d_b developed by the present study, and between W_b and d_m determined by the present and previous studies shows distinct variation. This variation may reflect specific climatic and tectonic settings. In particular, fluvial systems in Indonesia have a higher mean bankfull channel depth (d_m) with respect to a given W_b than those formed in passive margin and continental interior basins influenced by the mid- and high-latitude climates. Higher d_m with respect to a given W_b in fluvial systems in Indonesia is considered to be related to the combination of high water discharge, overbank protection from thick vegetation cover, and active tectonic movement. In summary, the appropriate selection of a depth–width equation combined with an appropriate discharge–width equation permits us to reconstruct spatial and temporal variations in hydrological features in both modern and ancient fluvial systems more precisely than reconstruction using previously proposed equations.

Part 3.

Application of Hydrological Parameters to the Bayah Formation Fluvial System

10. Paleohydrologic Reconstruction

10.1. Paleohydrological parameters

Paleohydrology can be defined as the study of past hydrologic regimes and hydrologic processes related to science of the earth's water, its composition, distribution and displacement in the ancient landscape, involving rain, erosion, and sediment transport in the drainage basin (Schumm, 1968; Patton, 1987). Hydrological and geomorphological studies of rivers provide the basis of the interpretation of paleohydrology in a fluvial environment and its sedimentation (Schumm, 1968). By analysis of similar contemporary or modern processes, transfer functions are developed and allow the reconstruction of past hydrologic conditions (Patton, 1987; Bridge, 2003). The broad objectives of paleohydrological study are to reconstruct past hydrologic conditions of an ancient fluvial system and to describe its paleogeographic setting of the past fluvial sedimentary system (Williams, 1984b; Bridge, 2003; Garde, 2006).

Empirical equations between hydrological parameters, such as bankfull channel depth and width, annual mean and bankfull water discharges, have been developed for modern fluvial systems (e.g., Leopold and Maddock, 1953; Leeder, 1973; Ethridge and Schumm, 1978; Osterkamp and Hedman, 1982; Williams, 1984a, b, 1986; Shibata and Ito, 2014). These equations have been used to reconstruct paleohydrological features of ancient fluvial systems based on analyses of outcrops, cores and log data of fluvial successions (e.g., Van der Neut and Eriksson, 1999; Bridge and Tye, 2000; Bridge, 2003; Adams and Bhattacharya, 2005; Ito et al., 2006). These empirical equations have been established based on hydrological data from modern fluvial systems mainly on passive continental

margin and continental-interior settings that are influenced by a temperate climate (Fig. 80). Consequently, a better understanding of variations in hydrological parameters in fluvial systems requires the establishment of empirical equations for different tectonic and climatic settings (Shibata and Ito, 2014). Hydrological equations have not yet been developed for active-margin settings influenced by low-latitude and equatorial climates, which produce thick vegetation, intense rainfalls, and active sediment yield (Sinha et al., 2012; Syvitski et al., 2014). These equations are a crucial step for identifying similarities and differences in the hydrological parameters of fluvial systems formed in different tectonic and climatic settings.

The paleohydrologic reconstruction of the fluvial succession of the Bayah Formation is obtained from empirical equations for hydrological parameters that have been developed based on modern fluvial systems of the Indonesian archipelagoes, where these hydrological analyses have not yet been attempted. These equations are established based on relationships between mean (Q_{mean}) and bankfull discharge (Q_b), bankfull channel width (W_b), and mean (d_m) and maximum bankfull depth (d_b) (Figs. 75 and 77). The results provide a case study for modern fluvial systems developed in an active low-latitude convergent margin setting under the influence of a tropical climate. The modern fluvial systems of the Indonesian archipelago are considered to be consistent with the regional setting for fluvial sedimentation of the Bayah Formation that were situated in an active margin of the Sundaland under the Paleogene tropical-climatic condition in equatorial zone (Hall, 1998; Boucot et al., 2013; Morley and Morley, 2013).

Paleohydrologic reconstruction of the fluvial succession of the Bayah Formation intends to understand the past condition of paleochannel dimension and paleodischarge,

and temporal variation in paleohydrologic parameters in fluvial system of the Bayah Formation during the Eocene–Oligocene time.

The important parameters of ancient river hydrology are the river sinuosity, bankfull channel depth, bankfull channel width, channel belt width, and discharge parameters. Among these important parameters, bankfull-channel width (W_b), bankfull-channel depth (d_b), sinuosity (S_n), and maximum bankfull discharge (Q_b) parameters were used for the paleohydrologic reconstruction of the fluvial succession of the Bayah Formation. The critical information, which is used for the estimation of paleohydrological parameters are based on the measurements of stratigraphic thickness of bar deposits (h), following the methods outlined in the Bridge and Tye (2000), Ito et al. (2006) and Kukulski (2012). Some examples of log-section measurements and interpretation of stratigraphic bar thickness to estimate bankfull-channel depth are shown in Figs. 81–83. The correction for stratigraphic thickness to compensate burial compaction were not applied in this study, although the original thickness seems to be greater than the stratigraphic thickness (e.g., Bridge and Tye, 2000; Ito et al., 2006). The symbols for paleohydrologic reconstruction are shown in Table 4.

10.2. Paleochannel reconstruction

Channel dimensions are discussed in terms of the maximum bankfull-channel width (W_b) and bankfull-channel depth (d_b), together with sinuosity. The stratigraphic thickness of bar deposits is interpreted to represent maximum bankfull depth (d_b) of the paleochannel ($d_b \approx h$). Based on the previous empirical relation between d_b – d_m , the mean bankfull depth

(d_m) is approximately half of the maximum depth of paleochannel ($d_m \approx 0.5 d_b$) (Bridge and Tye, 2000; Ito et al., 2006). In contrast, according to the hydrological parameters which have been developed based on modern fluvial systems of the Indonesian archipelago (See Part 2), the d_b – d_m relationship is expressed as $d_m \approx 0.65 d_b$ (Fig. 77). The river sinuosity parameter (S_n) is estimated based on paleocurrent data using the following equation (Bridge et al., 2000; Ito et al., 2006):

$$S_n = 4.84 / (4.84 - \phi^2),$$

where ϕ is half of the maximum paleocurrent range in radian unit. The sinuosity of river channel is an important parameter in the determination of the fluvial styles, increase in sinuosity of a channel is interpreted as response to an increase in the proportion of suspension loads relative to bedloads, and reduction in current strength (Schumm, 1968; Ferguson, 1987). The bankfull-channel width (W_b) is estimated as a function of the mean-channel depth (d_m), using the following equation (Fig. 77 and Table 6):

$$W_b = 52.88 d_m^{0.76} \text{ (m)}.$$

The estimated maximum bankfull-channel depth (d_b) are based on 204 calculations of thickness of interpreted bar deposit (h) from sandstone and conglomeratic sandstone bodies within the intervals (IV1–IV7) (Figs. 81–83). The statistically valid data for the maximum bankfull depth (d_b) indicates the shallowest, deepest, and average bankfull channel depths in the fluvial succession of the Bayah Formation are between 1.7–4.3 m, 9.9–18.5 m, and 5.0–8.3 m, respectively. The shallowest bankfull-channel depths are commonly observed in the interval IV1 and the intervals IV2 and IV7 in the eastern parts. The deepest bankfull-channel depths are commonly associated with the succession in the intervals IV2, IV3, and IV4 in the western parts and the intervals IV5 and IV6 in the eastern parts. The average

maximum bankfull depths for each interval (IV1–IV7) are summarized in the Table 8. The fluvial succession of the Bayah Formation shows minor temporal variation in the maximum bankfull channel depths (Fig 84; Table 8). According to the above statistical description, the temporal variation in the maximum bankfull depths of the intervals are dominantly attributed to average depths. The deepest maximum bankfull depth is only occurred within the interval IV4. An overall increase in average bankfull depth from the intervals IV1 to IV4 and an overall decrease from the intervals IV4 to IV7 are also observed. Schematic illustration of temporal variation in the bankfull channel depths of the Bayah Formation is shown in the Fig. 86. Each schematic channel dimension represents average paleohydrologic parameter values of the intervals. The dimensions of paleochannel cross-section and plan-view sinuosity on this schematic illustration are scaled according to the associated parameter values.

The statistically valid data for the bankfull channel width (W_b) indicates that the narrowest, largest, and average bankfull channel widths in the Bayah Formation fluvial succession are 57–100 m, 211–302 m, and 129–169 m, respectively. Similar to the bankfull-depth parameters, the narrowest bankfull-channel widths are commonly occurred in the interval IV1 and the intervals IV2 and IV7 in the eastern parts. In contrast, the largest bankfull-channel widths are commonly observed in the intervals IV2, IV3, and IV4 in the western parts and the intervals IV5 and IV6 in the eastern parts.

From the 100 selected locations of the paleocurrent measurements, the statistically valid data for the maximum paleocurrent range in radian show that the greatest, smallest and average values are between 1.62–2.79 rad, 0.05–0.94 rad, and 1.10–1.41 rad, respectively. These maximum paleocurrent range values correspond to the highest, smallest, and average sinuosity values (S_n) of 1.2–1.7, 1.0–1.05, and 1.07–1.13,

respectively. The statistics indicates a small standard deviation (0.6 rad) around the mean (1.3 rad) in the maximum paleocurrent range data. In other words, the sinuosity throughout the fluvial succession of the Bayah Formation does not show distinct temporal variation (Figs. 84 and 86; Table 8). Only about 15% of the channel in the fluvial succession can be assigned to the high sinuosity class (S_n 1.3–1.7). The remaining 85% of the maximum paleocurrent ranges are assigned to the low–moderate sinuosity channel (S_n 1.0–1.29). The high sinuosity channels are occurred in the intervals IV1–IV2, IV4 and IV6–IV7.

10.3. Paleodischarge reconstruction

The morphology of a river channel is determined by the behaviour of the water and the type of sediment flowing through it. The maximum bankfull discharge parameter (Q_b) are estimated as a function of the bankfull-channel width (W_b) using the following equation (Fig. 75 and Table 5):

$$Q_b = 1.09 W_b^{1.42} \text{ (m}^3\text{/s)}.$$

The statistically valid data for the mean-annual discharges (Q_b) indicate that the highest, smallest, and average maximum bankfull discharges in the Bayah Formation fluvial succession are 1942–3615 m³/s, 337–820 m³/s, and 1161–1591 m³/s, respectively. Although the fluvial succession shows minor temporal variation in the maximum bankfull discharges, an overall increase in the maximum bankfull discharges from the intervals IV1 to IV4 and an overall decrease from the intervals IV4 to IV7 are observed (Figs. 84 and 86; Table 8). In addition, each interval shows an upward decrease in the maximum bankfull discharges. The higher maximum bankfull discharges are more evenly documented in the

intervals IV3, IV4, and IV6 compared to the higher maximum bankfull discharges in the intervals IV1–IV2, IV5, and IV7.

11. Discussion and Conclusions

Minimum and maximum values of the W_b , d_b and Q_b for the Bayah Formation were compared with hydrologic data obtained from modern fluvial system of the Indonesian islands for identifying the relationships between paleohydrologic features of the Indonesian modern rivers and the reconstructed paleohydrologic features of the Bayah Formation (Fig. 85). On those diagrams, the minimum values of the W_b , d_b and Q_b for the Bayah Formation are equivalent to some of the hydrologic data from the middle reaches of the eastward-flowing rivers in Sumatra Island, and some of the hydrologic data from the middle reaches of the northward-flowing rivers in Java Island. In contrast, the maximum values of the W_b , d_b and Q_b for the Bayah Formation are equivalent to some of the middle and lower reaches of the rivers in the western Kalimantan Island, which has a large Mahakam River basin.

Some of the northward-flowing rivers in Java and the eastward-flowing rivers in Sumatra, which have fluvial hydrologic features similar to the minimum W_b , d_b and Q_b values of the Bayah Formation, are the middle reaches of the Brantas, Cimanuk, Pulau Tagor, Seureula and Bingkuang rivers ($W_b = 71\text{--}112$ m, $d_b = 2.3\text{--}4.6$ m, $Q_b = 124\text{--}842$ m³/s). Some of the large rivers in western Kalimantan Island, which have fluvial hydrologic features similar to the maximum W_b , d_b and Q_b values of the Bayah Formation, are the middle reaches of the Telen, Ancalong and Penyinggahan rivers ($W_b = 255\text{--}292$ m, $d_b = 10.5\text{--}17.4$ m, $Q_b = 1667.5\text{--}3185.5$ m³/s). These large western Kalimantan rivers, which have fluvial hydrologic features similar to the maximum W_b , d_b and Q_b values of the Bayah Formation, are situated within the Mahakam River basin that has a drainage area of 78,716 km². River beds and bank materials of the rivers in Java, Sumatra, and western Kalimantan islands, which have fluvial hydrological features quite similar to those of the

Bayah Formation, are the Quaternary alluvial–coastal deposits that are composed mainly of unlithified sands and gravels. In addition, the positions of those middle-reach rivers are situated in the lowland areas far from the highland mountainous areas (25 km–85 km), and also from the present-day shorelines (33–170 km). Thus, the fluvial succession of the Bayah Formation is interpreted to have been developed under the similar or somewhat smaller fluvial systems that belong to some of the eastward-flowing rivers in the alluvial plain of Sumatra and some of the rivers in western Kalimantan.

Although paleochannel sizes and paleodischarges of the Bayah Formation fluvial system do not show distinct temporal variation, the paleohydrologic features have minor variation within individual intervals. Because the Bayah Formation fluvial system is considered to have develop in a nonmarine basin far from the contemporaneous shorelines, the variations in paleochannel dimension and fluvial stratigraphy of the Bayah Formation do not seem to have been controlled by relative sea- level changes. Although distinct stratigraphic variations in paleochannel dimension were reported as a response to the abrupt global climatic change at the Paleocene–Eocene thermal maximum event (Foreman et al., 2012), palynological and paleontological records of the Paleogene sedimentary rocks of the Cenozoic SE Asian basins do not indicate such abrupt climatic changes around the equatorial region of the SE Asian continental margin (Morley, 1998; 2012; Morley and Morley, 2013). Slight temporal variation in paleohydrologic features of the Bayah Formation is more likely to represent temporal variation in river discharges, which may have been associated with transitions between the ever-wet to seasonal periods and vice versa of the equatorial climate in the Sundaland region (Morley, 1998; 2012; Morley and Morley, 2013).

General Conclusions

The Bayah Formation in the Sukabumi high attains a total thickness of 915 meters, and is subdivided into eight major lithofacies associations (FA1–FA8). These lithofacies associations cover fluvial to lacustrine–delta depositional systems, that may have been deposited in three major facies belts: (1) a braidplain, (2) a meandering river and floodplains, and (3) a lacustrine–delta. The fluvial–lacustrine–delta succession of the Bayah Formation is subdivided into 7 intervals (IV1–IV7 in ascending order) by 6 distinct erosional surfaces (ES1 to ES 6 in ascending order). The fluvial–lacustrine–delta succession of the Bayah Formation is characterized by an overall upward thinning of the component intervals (IV1–IV6), and subsequent thickening in the uppermost interval (IV7). Each interval of the Bayah Formation is represented by an overall fining-upward pattern from sandstone- and conglomerate-dominated deposits in the lower parts and more dominance of mudstone-dominated deposits in the upper parts. The uppermost interval (IV7) is overlain by coastal and shallow-marine sandy deposits and the contact is represented by a ravinement surface. The coastal and shallow-marine sandy deposits fine upward to shallow-marine muddy deposits, which were subsequently replaced by reefal carbonates as a response to a forced regression and the ensuing transgression. Paleocurrent directions of the fluvio-lacustrine–delta succession show a fairly consistent trend from N–NE toward S–SW through the intervals. The overall decrease in thickness of the intervals from I to VI is interpreted to have responded to an overall decrease in nonmarine accommodation, except for the uppermost interval, which is overlain by coastal and shallow-marine successions and indicates ensuing increase in nonmarine accommodation.

Based on geometry and its internal characteristics, the packages of sandstone and conglomerate bodies that represent channel-fill deposits are subdivided into three types: Type 1 is lenticular and tabular conglomerate-dominated packages, Type 2 is tabular and lenticular conglomeratic sandstone packages, and Type 3 is tabular and lenticular sandstone-dominated packages. Each type represents a different style of sedimentation, as follows: Type 1 is a bedload-dominated sedimentation in braided rivers, Type 2 is characterized by the development of longitudinal and transversal bar that may have been situated in a transitional area between braided and sinuous rivers, and Type 3 is a mixed-load sedimentation in meandering rivers, respectively. The three types have a downslope arrangement and also show a vertical succession either from types 1 to 2 or types 2 to 3. These spatial and temporal arrangements of the types of the channel-fill deposits are common in each interval and the vertical arrangement is considered to have responded to an increase in nonmarine accommodation that was replaced by an ensuing abrupt decrease in the nonmarine accommodation.

The Bayah Formation sandstones show temporal variation in detrital framework composition. This variation is not considered to reflect changes in provenances, and is interpreted that temporal fluctuation in the increase of rock fragments relative to quartz and feldspar grains indicate temporal intensification of physical erosion relative to the chemical weathering processes. An overall increase and decrease in the clay minerals suggest temporal variations in the weathering intensity from the alternating humid and dry seasons to a warm and more humid climatic conditions. The temporal variation in channel-fill deposits, sandstones composition, and clay mineralogy of fluvial–lacustrine–delta succession of the Bayah Formation suggest that this variation is considered to have largely been controlled by the complex interaction between relative sea-level, climate, and tectonic

(Figs. 87–89). Namely, the decrease in nonmarine accommodation possibly promoted the intensification of physical erosion in the hinterlands. In contrast, clay mineral composition of the fluvial deposits suggests climatic change from the alternating humid and dry seasons to a warm and more humid conditions, although the depositional period of the Bayah Formation occurred in a transitional stage from greenhouse to icehouse global climatic conditions.

The present study established empirical equations for geomorphological and hydrological parameters that characterize fluvial systems formed in a convergent margin setting influenced by a low-latitude tropical climate based on hydrological data from modern fluvial channels in Java, Sumatra, and Kalimantan islands. The relationship between Q_{mean} and W_b has distinct variations for rivers in Java, Sumatra, and Kalimantan. These variations are considered to reflect regional variations in annual rainfall under the influence of a tropical climate. In contrast, the relationships between Q_b and W_b do not show any regional variations across the fluvial systems regardless of their tectonic and climatic settings. The Q_b – W_b equation indicates that the development of fluvial morphology is controlled by flood-related episodic discharge rather than by annual mean discharge. The empirical relationship between W_b and d_b developed by the present study, and between W_b and d_m determined by the present and previous studies shows distinct variation. This variation reflects specific climatic and tectonic settings. Fluvial systems in Indonesia have a higher mean bankfull channel depth (d_m) with respect to a given W_b than those formed in passive margin and continental interior basins influenced by the mid- and high-latitude climates. Higher d_m with respect to a given W_b in fluvial systems in Indonesia is considered to be related to the combination of high water discharge, overbank protection from thick vegetation cover, and active tectonic movement.

Although hydrological parameters of the Bayah Formation fluvial deposits have minor temporal variations, the maximum bankfull-channel depth, bankfull-channel widths, maximum bankfull discharges, and channel sinuosity do not show distinct changes between the intervals of the fluvial succession (Figs. 86 and 87). The fluvial succession of the Bayah Formation is interpreted to have developed under humid climatic condition in an ancient equatorial region in association with an active convergent margin setting. On the basis of the application of hydrological equations obtained from the modern fluvial systems in the Indonesian islands, the Bayah Formation fluvial systems have hydrological features similar to those of some of the eastward-flowing rivers in the alluvial plain of Sumatra and the rivers in western Kalimantan. Slight temporal variations in paleohydrologic features of the Bayah Formation are more likely to represent temporal variation in river discharges which may have been associated with fluctuation in climatic condition between ever-wet and seasonal periods of the equatorial paleoclimate in the Sundaland region.

In summary, although the nonmarine depositional systems of the Bayah Formation formed during a transitional period from greenhouse to icehouse stages of global environmental changes in the Eocene–Oligocene time, the development of the Bayah Formation nonmarine depositional systems are interpreted to have been controlled by the interaction between relative sea-level changes, climates, and tectonics. These allogenic controlling factors do not seem to have changed in harmony (Figs. 87 and 88), and the intensity of chemical weathering and precipitation in the hinterlands are not considered to have responded to the global environmental changes in the equatorial region in the southern convergent margin of the Sundaland.

Acknowledgements

Firstly, I would like to express my sincere gratitude to my advisor Professor Makoto Ito for his invaluable advice, patience, and immense knowledge throughout the process of my research. I am very grateful to have this excellent research experience, which I have never had before. He has taught me how the study on modern processes can be synergistically assembled to ancient deposits study. I am greatly indebted to him, who has dedicated some of his time helping me with my studies and my everyday life in Chiba.

I would also like to thank my dissertation committee Professor Takahiro Miyauchi, Professor Nobuhiro Kotake, and Professor Nozomu Takeuchi for their constructive advices and comments.

My sincere thanks also goes to Dr. Kenichiro Shibata for sharing ideas concerning study on modern fluvial. I am thankful for his willingness to invite me to be part of his research on fluvial hydrology. I would also thank Dr. Noboru Furukawa for introducing me to laboratory procedures for X-ray diffraction measurements.

I gratefully acknowledge the Indonesian Ministry of Research, Technology and Higher Education for funding the first 3 years of my study in Chiba University, and the Indonesian Center for Water Resources, for providing the river hydrology data. I would also thank colleagues and students at Department of Geology, Padjadjaran University, and all my fellow lab-mates at the Laboratory of Sedimentology and Genetic Stratigraphy, Faculty of Science, Chiba University for the fellowship over the years in Chiba.

Finally, I would like to thank my family for their emotional support throughout my study. They always supported me and encouraged me to do well and to never give up.

References

- Abels, H. A., H. A. Aziz, D. Ventra, and F. J. Hilgen, 2009, Orbital Climate Forcing in Mudflat to Marginal Lacustrine Deposits in the Miocene Teruel Basin (Northeast Spain): *Journal of Sedimentary Research*, v. 79, no. 11, p. 831–847, doi:10.2110/jsr.2009.081.
- Ackers, P., and F. G. Charlton, 1970, Meander geometry arising from varying flows: *Journal of Hydrology*, v. 11, no. 3, p. 230–252, doi:10.1016/0022-1694(70)90064-8.
- Adams, M. M., and J. P. Bhattacharya, 2005, No Change in Fluvial Style Across a Sequence Boundary, Cretaceous Blackhawk and Castlegate Formations of Central Utah, U.S.A.: *Journal of Sedimentary Research*, v. 75, no. 6, p. 1038–1051, doi:10.2110/jsr.2005.080.
- Adinegoro, U., 1973, Reef-Limestones in the Sukabumi Area, *in* Proceedings Indonesian Petroleum Association 2nd Annual Convention: IPA, p. 109–120.
- Aldrian, E., and R. Dwi Susanto, 2003, Identification of three dominant rainfall regions within Indonesia and their relationship to sea surface temperature: *International Journal of Climatology*, v. 23, no. 12, p. 1435–1452, doi:10.1002/joc.950.
- Allen, J. R. L., 1965, a Review of the Origin and Characteristics of Recent Alluvial Sediments: *Sedimentology*, v. 5, no. 2, p. 89–191, doi:10.1111/j.1365-3091.1965.tb01561.x.
- Allen, J. R. L., 1964, Studies in Fluvial Sedimentation: Six Cyclothems From the Lower Old Red Sandstone, Anglowelsh Basin: *Sedimentology*, v. 3, no. 3, p. 163–198, doi:10.1111/j.1365-3091.1964.tb00459.x.
- Allen, J. P., C. R. Fielding, M. R. Gibling, and M. C. Rygel, 2014, Recognizing products of palaeoclimate fluctuation in the fluvial stratigraphic record: An example from the Pennsylvanian to Lower Permian of Cape Breton Island, Nova Scotia: *Sedimentology*, v. 61, no. 5, p. 1332–1381, doi:10.1111/sed.12102.
- Amos, C. B., and D. W. Burbank, 2007, Channel width response to differential uplift: *Journal of Geophysical Research: Earth Surface*, v. 112, no. 2, p. 1–11, doi:10.1029/2006JF000672.
- Anadón, P., F. Robles, E. Roca, R. Utrilla, and A. Vázquez, 1998, Lacustrine sedimentation in the diapir-controlled Miocene Bicorn Basin, eastern Spain: *Palaeogeography, Palaeoclimatology, Palaeoecology*, v. 140, no. 1–4, p. 217–243, doi:10.1016/S0031-0182(98)00045-5.

- Aribowo, S., and Yudhicara, 2015, Development of River Terrace at the Releasing Bend of the Sumatran Fault Zone near Ranau Lake , Southern Sumatra, *in* 1'st International Geological Joint Conference Universitas Padjadjaran and University of Sabah: p. 81–86.
- Ashley, G. M., 1990, Classification of Large-Scale Subaqueous Bedforms: A New Look at an Old Problem: *Journal of Sedimentary Research*, v. 60, no. 1, p. 160–172, doi:10.2110/jsr.60.160.
- Asian Disaster Preparedness Center, 2000, Indonesia Country Study, *in* A. Kishore, K., Subbiah, A.R., Sribimawati, T., Diharto, S., Alimoeso, S., Rogers, P., Setiana, ed., Asian Disaster Preparedness Center (ADPC) Report: Pathumthani, p. 68.
- As-syakur, A. R., T. Tanaka, T. Osawa, and M. S. Mahendra, 2013, Indonesian rainfall variability observation using TRMM multi-satellite data: *International Journal of Remote Sensing*, v. 34, no. 21, p. 7723–7738, doi:10.1080/01431161.2013.826837.
- Atha, J. B., 2014, Identification of fluvial wood using Google Earth: *River Research and Applications*, v. 30, no. 7, p. 857–864, doi:10.1002/rra.2683.
- Atkinson, C., M. Renolds, and O. Hutapea, 2006, Stratigraphic traps in the Tertiary rift basins of Indonesia: case studies and future potential: *Geological Society, London, Special Publications*, v. 254, no. 1, p. 105–126, doi:10.1144/GSL.SP.2006.254.01.06.
- Bartley, R., R. J. Keen, A. A. Hawdon, P. B. Hairsine, M. G. Disher, and A. E. Kinsey-Henderson, 2008, Bank erosion and channel width change in a tropical catchment: *Earth Surface Processes and Landforms*, v. 33, no. 14, p. 2174–2200, doi:10.1002/esp.1678.
- Basilici, G., 1997, Sedimentary facies in an extensional and deep-lacustrine depositional system: the Pliocene Tiberino Basin, Central Italy: *Sedimentary Geology*, v. 109, no. 1–2, p. 73–94, doi:10.1016/S0037-0738(96)00056-5.
- Baumann, P., P. D. E. Genevraye, and L. Samuel, 1973, Contribution to the Geological Knowledge of South West Java, *in* IPA 2nd Annual Convention Proceedings.
- Ben-Avraham, Z., and K. O. Emery, 1973, Structural Framework of Sunda Shelf: *The American Association of Petroleum Geologists Bulletin*, v. 57, no. 12, p. 2323–2366.
- Bentham, P. A., P. J. Talling, and D. W. Burbank, 1993, Braided stream and flood-plain deposition in a rapidly aggrading basin: the Escanilla formation, Spanish Pyrenees: *Geological Society, London, Special Publications*, v. 75, no. 1, p. 177–194, doi:10.1144/GSL.SP.1993.075.01.11.

- Benvenuti, M., 2003, Facies analysis and tectonic significance of lacustrine fan-deltaic successions in the Pliocene-Pleistocene Mugello Basin, Central Italy: *Sedimentary Geology*, v. 157, no. 3–4, p. 197–234, doi:10.1016/S0037-0738(02)00234-8.
- Blair, T. C., 1987, Tectonic and Hydrologic Controls on Cyclic Alluvial Fan, Fluvial, and Lacustrine Rift-Basin Sedimentation, Jurassic-Lowermost Cretaceous Todos Santos Formation, Chiapas, Mexico: *SEPM Journal of Sedimentary Research*, v. Vol. 57, no. 5, doi:10.1306/212F8C83-2B24-11D7-8648000102C1865D.
- Blum, M. D., and T. E. Tornqvist, 2000, Fluvial responses to climate and sea-level change : a review and look forward: *Sedimentology*, v. 47, p. 2–48.
- Boucot, A. J., C. Xu, C. R. Scotese, and R. J. Morley, 2013, Phanerozoic Paleoclimate: An Atlas of Lithologic Indicators of Climate: *SEPM Concepts in Sedimentology and Paleontology*, v. 11, doi:10.2110/sepmcsp.11.
- Bridge, J. S., G. a Jalfin, and S. M. Georgieff, 2000, Geometry, lithofacies, and spatial distribution of Cretaceous fluvial sandstone bodies, San Jorge Basin, Argentina: Outcrop analog for the hydrocarbon-bearing Chubut Group: *Journal of Sedimentary Research*, v. 70, no. 2, p. 341–359, doi:10.1306/2DC40915-0E47-11D7-8643000102C1865D.
- Bridge, J. S., and S. D. Mackey, 2009, A Theoretical Study of Fluvial Sandstone Body Dimensions, *in* *The Geological Modelling of Hydrocarbon Reservoirs and Outcrop Analogues*: Oxford, UK, Blackwell Publishing Ltd., p. 213–236, doi:10.1002/9781444303957.ch14.
- Bridge, J. S., and R. S. Tye, 2000, Interpreting the dimensions of ancient fluvial channel bars, channels, and channel belts from wireline-logs and cores: *AAPG Bulletin*, v. 84, no. 8, p. 1205–1228, doi:10.1306/E4FD4B07-1732-11D7-8645000102C1865D.
- Bridge, J. S., 1984, Large-scale facies sequences in alluvial overbank environments: *Journal of Sedimentary Research*, v. 54, no. 2, p. 583–588, doi:10.1306/212F8477-2B24-11D7-8648000102C1865D.
- Bridge, J. S., 2003, *Rivers and Floodplains: Forms, Processes, and Sedimentary Record*: Blackwell Science Ltd., 504 p.
- Bridge, J. S., and J. A. Diemer, 1983, Quantitative interpretation of an evolving ancient river system: *Sedimentology*, v. 30, no. 5, p. 599–623, doi:10.1111/j.1365-3091.1983.tb00698.x.
- Bridge, J. S., and S. L. Gabel, 1992, Flow and sediment dynamics in a low sinuosity, braided river: Calamus River, Nebraska Sandhills: *Sedimentology*, v. 39, no. 1, p. 125–142, doi:10.1111/j.1365-3091.1992.tb01026.x.

- Buatois, L. A., and M. G. Mángano, 2009, Applications of ichnology in lacustrine sequence stratigraphy: Potential and limitations: *Palaeogeography, Palaeoclimatology, Palaeoecology*, v. 272, no. 3–4, p. 127–142, doi:10.1016/j.palaeo.2008.10.012.
- Bustin, R. M., and A. Chonchawalit, 1995, Formation and Tectonic Evolution of the Pattani Basin, Gulf of Thailand: *International Geology Review*, v. 37, no. 10, p. 866–892, doi:10.1080/00206819509465431.
- Butterworth, P. J., and C. D. Atkinson, 1993, Syn-rift deposits of the Northwest Java Basin: Fluvial sandstone reservoirs and lacustrine source rocks, *in* *Clastic Rocks and Reservoirs of Indonesia : A Core Workshop: IPA*, p. 211–229.
- Cant, D. J., 1982, Fluvial Facies Models and Their Application, *in* P. A. Scholle, and D. Spearing, eds., *AAPG Memoir 31: Sandstone Depositional Environments: AAPG*, p. 115–137, doi:10.1306/M31424C6.
- Carlston, C. W., 1965, The relation of free meander geometry to stream discharge and its geomorphic implications: *American Journal of Science*, v. 263, p. 864–885, doi:10.2475/ajs.263.10.864.
- Carter, D. C., 2003, 3-D seismic geomorphology: Insights into fluvial reservoir deposition and performance, Widuri field, Java Sea: *AAPG Bulletin*, v. 87, no. 6, p. 909–934, doi:10.1306/01300300183.
- Castro, J. M., and P. L. Jackson, 2001, Bankfull discharge recurrence intervals and regional hydraulic geometry relationships: patterns in the Pacific northwest, USA: *Journal of the American Water Resources Association*, v. 37, no. 5, p. 1249–1262, doi:10.1111/j.1752-1688.2001.tb03636.x.
- Catuneanu, O., and H. N. Elango, 2001, Tectonic control on fluvial styles : the Balfour Formation of the Karoo Basin , South Africa FOLD: *Journal of sedimentary geology*, v. 140, p. 291–313.
- Cecil, C. B., F. T. Dulong, R. A. Harris, J. C. Cobb, H. G. Gluskoter, and H. Nugroho, 2003, Observations on climate and sediment discharge in selected tropical rivers, Indonesia, *in* C. B. Cecil, and N. T. Edgar, eds., *Climate Controls on Stratigraphy: SEPM (Society for Sedimentary Geology)*, p. 29–50, doi:10.2110/pec.03.77.0029.
- Chamley, H., 1989, *Clay Sedimentology*: Berlin, Heidelberg, Springer Berlin Heidelberg, 623 p., doi:10.1007/978-3-642-85916-8.
- Chandler, F. W., 1988, Quartz arenites: review and interpretation: *Sedimentary Geology*, v. 58, no. 2–4, p. 105–126, doi:10.1016/0037-0738(88)90065-6.
- Charlton, R., 2008, *Fundamentals of Fluvial Geomorphology*: New York, Routledge, 234 p.

- Clements, B., and R. Hall, 2011, A record of continental collision and regional sediment flux for the Cretaceous and Palaeogene core of SE Asia: implications for early Cenozoic palaeogeography: *Journal of the Geological Society*, v. 168, no. 5, p. 1187–1200, doi:10.1144/0016-76492011-004.
- Clements, B., R. Hall, H. R. Smyth, and M. a. Cottam, 2009, Thrusting of a volcanic arc: a new structural model for Java: *Petroleum Geoscience*, v. 15, no. 2, p. 159–174, doi:10.1144/1354-079309-831.
- Clements, B., and R. Hall, 2007, Cretaceous to Late Miocene stratigraphic and tectonic evolution of West Java: *Proceedings of the Indonesian Petroleum Association*, no. May, p. 1–18.
- Cole, J. M., and S. Crittenden, 1997, Early Tertiary basin formation and the development of Lacustrine and quasi-lacustrine/marine source rocks on the Sunda Shelf of SE Asia: *Geological Society, London, Special Publications*, v. 126, no. 1, p. 147–183, doi:10.1144/GSL.SP.1997.126.01.12.
- Crane, R. C., 1982, A Computer model for the architecture of avulsion-controlled alluvial suites: *University of Reading, University of Reading*, 1029 p.
- Darmadi, Y., B. J. Willis, and S. L. Dorobek, 2007, Three-Dimensional Seismic Architecture of Fluvial Sequences on the Low-Gradient Sunda Shelf, Offshore Indonesia: *Journal of Sedimentary Research*, v. 77, no. 3, p. 225–238, doi:10.2110/jsr.2007.024.
- Davies-Vollum, K. S., and M. J. Kraus, 2001, A relationship between alluvial backswamps and avulsion cycles: An example from the Willwood Formation of the Bighorn Basin Wyoming: *Sedimentary Geology*, v. 140, no. 3–4, p. 235–249, doi:10.1016/S0037-0738(00)00186-X.
- Davis, R. C., S. W. Noon, and J. Harrington, 2007, The petroleum potential of Tertiary coals from Western Indonesia: Relationship to mire type and sequence stratigraphic setting: *International Journal of Coal Geology*, v. 70, no. 1–3 SPEC. ISS., p. 35–52, doi:10.1016/j.coal.2006.02.008.
- DeCelles, P. G., and K. A. Giles, 1996, Foreland basin systems: *Basin Research*, v. 9, no. 2, p. 172–176.
- Dickinson, W. R., and D. R. Seely, 1979, Structure and Stratigraphy of Forearc Regions: *AAPG Bulletin*, v. 63, no. 1, p. 2–31, doi:10.1306/C1EA55AD-16C9-11D7-8645000102C1865D.
- Dickinson, W. R., 1985, Interpreting Provenance Relations from Detrital Modes of Sandstones, *in* Zuffa G.G., ed., *Provenance of Arenites*: Dordrecht, Springer Netherlands, p. 333–361, doi:10.1007/978-94-017-2809-6_15.

- Dickinson, W. R., L. S. Beard, G. R. Brakenridge, J. L. Erjavec, R. C. Ferguson, K. F. Inman, R. A. Knepp, F. A. Lindberg, and P. T. Ryberg, 1983, Provenance of North American Phanerozoic sandstones in relation to tectonic setting: *Geological Society of America Bulletin*, no. February, p. 222–235, doi:10.1130/0016-7606(1983)94<222.
- Dickinson, W. R., and C. A. Suczek, 1979, Plate Tectonics and Sandstone Compositions: *AAPG Bulletin*, v. 63, no. 12, p. 2164–2182, doi:10.1306/2F9188FB-16CE-11D7-8645000102C1865D.
- Diekmann, B., and H. Wopfner, 1996, Petrographic and diagenetic signatures of climatic change in peri- and postglacial Karoo sediments of SW Tanzania: *Palaeogeography, Palaeoclimatology, Palaeoecology*, v. 125, no. 1–4, p. 5–25, doi:10.1016/0031-0182(95)00084-4.
- Directorate General of Forestry and Environmental Planner, 2011, Drainage basin map and drainage data for the rivers in Sumatra, Java and Kalimantan: Jakarta, (digital copy) p.
- Do Campo, M., C. del Papa, J. Jiménez-Millán, and F. Nieto, 2007, Clay mineral assemblages and analcime formation in a Palaeogene fluvial-lacustrine sequence (Maíz Gordo Formation Palaeogen) from northwestern Argentina: *Sedimentary Geology*, v. 201, no. 1–2, p. 56–74, doi:10.1016/j.sedgeo.2007.04.007.
- Doust, H., and H. S. Sumner, 2007, Petroleum systems in rift basins - a collective approach in Southeast Asian basins: *Petroleum Geoscience*, v. 13, no. 2, p. 127–144, doi:10.1144/1354-079307-746.
- Doust, H., and R. A. Noble, 2008, Petroleum systems of Indonesia: *Marine and Petroleum Geology*, v. 25, no. 2, p. 103–129, doi:10.1016/j.marpetgeo.2007.05.007.
- Dunagan, S. P., and C. E. Turner, 2004, Regional paleohydrologic and paleoclimatic settings of wetland/lacustrine depositional systems in the Morrison Formation (Upper Jurassic), Western Interior, USA: *Sedimentary Geology*, v. 167, no. 3–4, p. 269–296, doi:10.1016/j.sedgeo.2004.01.007.
- Dunne, T., Leopold, L., 1978, *Water in Environmental Planning*: San Francisco, W.H. Freeman, 818 p.
- Dury, G. H., 1976, Discharge prediction, present and former, from channel dimensions: *Journal of Hydrology*, v. 30, no. 3, p. 219–245, doi:10.1016/0022-1694(76)90102-5.
- Effendi, A. C., Kusnama, and B. Hermanto, 1998, Geological map of the Bogor quadrangle, Java (1:100,000): Bandung.

- Ehrmann, W., 1998, Implications of the late Eocene to early Miocene clay mineral assemblages in McMurdo Sound (Ross Sea, Antarctica) on paleoclimate and ice dynamics: *Palaeogeography, Palaeoclimatology, Palaeoecology*, v. 139, p. 213–231.
- Ethridge, F., and S. A. Schumm, 1978, Reconstructing Paleochannel Morphologic and Flow Characteristics: Methodology, Limitations, and Assessment: *Fluvial Sedimentology*, v. 5, no. 1977, p. 705–721.
- Fabuel-Perez, I., J. Redfern, and D. Hodgetts, 2009, Sedimentology of an intra-montane rift-controlled fluvial dominated succession: The Upper Triassic Oukaimeden Sandstone Formation, Central High Atlas, Morocco: *Sedimentary Geology*, v. 220, no. 3–4, p. 103–140, doi:10.1016/j.sedgeo.2009.04.006.
- Farquharson, G. W., 1982, Lacustrine deltas in a Mesozoic alluvial sequence from Camp Hill, Antarctica: *Sedimentology*, v. 29, no. 5, p. 717–725, doi:10.1111/j.1365-3091.1982.tb00076.x.
- Farrell, K. M., 1987, Sedimentology and Facies Architecture of Overbank Deposits of the Mississippi River, False River Region, Louisiana: *The Society of Economic Paleontologists and Mineralogists*, p. 111–120, doi:-.
- Foix, N., J. M. Paredes, and R. E. Giacosa, 2013, Fluvial architecture variations linked to changes in accommodation space: Río Chico Formation (Late Paleocene), Golfo San Jorge basin, Argentina: *Sedimentary Geology*, v. 294, p. 342–355, doi:10.1016/j.sedgeo.2013.07.001.
- Foreman, B. Z., P. L. Heller, and M. T. Clementz, 2012, Fluvial response to abrupt global warming at the Palaeocene/Eocene boundary: *Nature*, v. 491, no. 7422, p. 92–95, doi:10.1038/nature11513.
- Friend, P. F., M. J. Slater, and R. C. Williams, 1979, Vertical and lateral building of river sandstone bodies, Ebro Basin, Spain: *Journal of the Geological Society*, v. 136, no. 1, p. 39–46, doi:10.1144/gsjgs.136.1.0039.
- Garzanti, E., C. Doglioni, G. Vezzoli, and S. Andò, 2007, Orogenic Belts and Orogenic Sediment Provenance: *The Journal of Geology*, v. 115, no. 3, p. 315–334, doi:10.1086/512755.
- Garzanti, E., M. Padoan, S. Andò, A. Resentini, G. Vezzoli, and M. Lustrino, 2013, Weathering and Relative Durability of Detrital Minerals in Equatorial Climate: Sand Petrology and Geochemistry in the East African Rift: *The Journal of Geology*, v. 121, no. 6, p. 547–580, doi:10.1086/673259.
- Ghazi, S., and N. P. Mountney, 2011, Petrography and provenance of the Early Permian Fluvial Warchha Sandstone, Salt Range, Pakistan: *Sedimentary Geology*, v. 233, no. 1–4, p. 88–110, doi:10.1016/j.sedgeo.2010.10.013.

- Ghosh, P., S. Sarkar, and P. Maulik, 2006, Sedimentology of a muddy alluvial deposit: Triassic Denwa Formation, India: *Sedimentary Geology*, v. 191, no. 1–2, p. 3–36, doi:10.1016/j.sedgeo.2006.01.002.
- Gibling, M. R., 2006, Width and Thickness of Fluvial Channel Bodies and Valley Fills in the Geological Record: A Literature Compilation and Classification: *Journal of Sedimentary Research*, v. 76, no. 5, p. 731–770, doi:10.2110/jsr.2006.060.
- Gingele, F. X., 1996, Holocene climatic optimum in southwest Africa - Evidence from the marine clay mineral record: *Palaeogeography, Palaeoclimatology, Palaeoecology*, v. 122, p. 77–87, doi:10.1016/0031-0182(96)00076-4.
- Gingele, F. X., P. De Deckker, and C. D. Hillenbrand, 2001, Clay mineral distribution in surface sediments between Indonesia and NW Australia - Source and transport by ocean currents: *Marine Geology*, v. 179, no. 3–4, p. 135–146, doi:10.1016/S0025-3227(01)00194-3.
- Girty, G. H., and C. H. Pardini, 1987, Provenance of sandstone inclusions in the Paleozoic Sierra City mélange, Sierra Nevada, California: *Geological Society of America Bulletin*, v. 98, no. 2, p. 176, doi:10.1130/0016-7606(1987)98<176:POSIIT>2.0.CO;2.
- Göltenboth, F., and W. Erdelen, 2006, Geography, geology and climate, *in* J. M. Friedhelm Göltenboth, Kris H. Timotius, Paciencia P. Milan, ed., *Ecology of Insular Southeast Asia, The Indonesian Archipelago*: Amsterdam, Elsevier, p. 3–26.
- Graham, Stephan A., R. V. Ingersoll, and W. R. D., 1976, Common Provenance for Lithic Grains in Carboniferous Sandstones from Ouachita Mountains and Black Warrior Basin: *Journal of Sedimentary Petrology*, v. 46, no. 3, p. 620–632, doi:10.1306/212F7009-2B24-11D7-8648000102C1865D.
- Grantham, J. H., and M. A. Velbel, 1988, The influence of climate and topography on rock-fragment abundance in modern fluvial sands of the southern Blue Ridge Mountains, North Carolina: *Journal of Sedimentary Petrology*, v. 58, no. 2, p. 219–227, doi:10.1306/212F8D5F-2B24-11D7-8648000102C1865D.
- Griffing, D. H., J. S. Bridge, and C. L. Hotton, 2000, Coastal-fluvial palaeoenvironments and plant palaeoecology of the Lower Devonian (Emsian), Gaspé Bay, Quebec, Canada: *Geological Society, London, Special Publications*, v. 180, no. 1, p. 61–84, doi:10.1144/GSL.SP.2000.180.01.05.
- Gupta, A., 1988, Large floods as geomorphic events in the humid tropics, *in* P. C. Baker, V.R., Kochel, R.C., Patton, ed., *Flood Geomorphology*: John Wiley & Sons, p. 301–315.
- Halfar, J., W. Riegel, and H. Walther, 1998, Facies architecture and sedimentology of a meandering fluvial system: A Palaeogene example from the Weissensteiner Basin,

- Germany: *Sedimentology*, v. 45, no. 1, p. 1–17, doi:10.1046/j.1365-3091.1998.00140.x.
- Hall, R., 2009, Hydrocarbon basins in SE Asia: understanding why they are there: *Petroleum Geoscience*, v. 15, no. 2, p. 131–146, doi:10.1144/1354-079309-830.
- Hall, R., 2012, Late Jurassic-Cenozoic reconstructions of the Indonesian region and the Indian Ocean: *Tectonophysics*, v. 570–571, p. 1–41, doi:10.1016/j.tecto.2012.04.021.
- Hall, R., 1996, *Reconstructing Cenozoic SE Asia*: Geological Society, London, Special Publications, v. 106, no. 1, p. 153–184, doi:10.1144/GSL.SP.1996.106.01.11.
- Hall, R., 1997, Cenozoic plate tectonic reconstructions of SE Asia: Geological Society, London, Special Publications, v. 126, no. 1, p. 11–23, doi:10.1144/GSL.SP.1997.126.01.03.
- Hall, R., 1998, The plate tectonics of Cenozoic SE Asia and the distribution of land and sea: *Biogeography and Geological Evolution of SE Asia*, p. 99–131.
- Hall, R., 2013, The palaeogeography of Sundaland and Wallacea since the Late Jurassic: *Journal of Limnology*, v. 72, no. S2, p. 1–17, doi:10.4081/jlimnol.2013.s2.e1.
- Hall, R., and C. K. Morley, 2004, Sundaland basins, in P. W. and D. H. P. Clift, W. Kuhnt, ed., *Continent-Ocean Interactions Within East Asian Marginal Seas*: American Geophysical Union, p. 55–85, doi:10.1029/149GM04.
- Hamblin, A. P., 1992, Half-graben lacustrine sedimentary rocks of the lower Carboniferous Strathlorne Formation, Horton Group, Cape Breton Island, Nova Scotia, Canada: *Sedimentology*, v. 39, no. 2, p. 263–284, doi:10.1111/j.1365-3091.1992.tb01038.x.
- Hampson, G. J., T. O. Jewell, N. Irfan, M. R. Gani, and B. Bracken, 2013, Modest Change In Fluvial Style With Varying Accommodation In Regressive Alluvial-To-Coastal-Plain Wedge: Upper Cretaceous Blackhawk Formation, Wasatch Plateau, Central Utah, U.S.A: *Journal of Sedimentary Research*, v. 83, no. 2, p. 145–169, doi:10.2110/jsr.2013.8.
- Hampton, B. A., and B. K. Horton, 2007, Sheetflow fluvial processes in a rapidly subsiding basin, Altiplano plateau, Bolivia: *Sedimentology*, v. 54, no. 5, p. 1121–1147, doi:10.1111/j.1365-3091.2007.00875.x.
- Haszeldine, R. S., 1984, Muddy deltas in freshwater lakes, and tectonism in the Upper Carboniferous Coalfield of NE England: *Sedimentology*, v. 31, no. 6, p. 811–822, doi:10.1111/j.1365-3091.1984.tb00888.x.

- Hein, F. J., and R. G. Walker, 1977, Bar evolution and development of stratification in the gravelly, braided, Kicking Horse River, British Columbia: *Canadian Journal of Earth Sciences*, v. 14, no. 4, p. 562–570, doi:10.1139/e77-058.
- Hendrizar, M., P. Praptisih, and S. Putra, 2012, Depositional Environment of the Batuasih Formation on the Basis of Foraminifera Content: A Case Study in Sukabumi Region, West Java Province, Indonesia *Lingkungan Pengendapan Formasi Batuasih Berdasarkan Kandungan Foraminifera: Studi Kasus Daerah Suka*: *Indonesian Journal on Geoscience*, v. 7, no. 1, p. 101–112.
- Hickin, E. J., 1984, Vegetation and river channel dynamics: *The Canadian Geographer/Le Géographe canadien*, v. 28, no. 2, p. 111–126, doi:10.1111/j.1541-0064.1984.tb00779.x.
- Hilley, G. E., and J. R. Arrowsmith, 2008, Geomorphic response to uplift along the Dragon's Back pressure ridge, Carrizo Plain, California: *Geology*, v. 36, no. 5, p. 367–370, doi:10.1130/G24517A.1.
- Hillier, R. D., S. B. Marriott, B. P. J. Williams, and V. P. Wright, 2007, Possible climate variability in the Lower Old Red Sandstone Conigar Pit Sandstone Member (early Devonian), South Wales, UK: *Sedimentary Geology*, v. 202, no. 1–2, p. 35–57, doi:10.1016/j.sedgeo.2007.05.006.
- Holbrook, J., and H. Wanas, 2014, A Fulcrum Approach To Assessing Source-To-Sink Mass Balance Using Channel Paleohydrologic Paramaters Derivable From Common Fluvial Data Sets With An Example From the Cretaceous of Egypt: *Journal of Sedimentary Research*, v. 84, no. 5, p. 349–372, doi:10.2110/jsr.2014.29.
- Hossain, H. M. Z., B. P. Roser, and J. I. Kimura, 2010, Petrography and whole-rock geochemistry of the Tertiary Sylhet succession, northeastern Bengal Basin, Bangladesh: Provenance and source area weathering: *Sedimentary Geology*, v. 228, no. 3–4, p. 171–183, doi:10.1016/j.sedgeo.2010.04.009.
- Huyghe, P., R. Guilbaud, M. Bernet, A. Galy, and A. P. Gajurel, 2011, Significance of the clay mineral distribution in fluvial sediments of the Neogene to Recent Himalayan Foreland Basin (west-central Nepal): *Basin Research*, v. 23, no. 3, p. 332–345, doi:10.1111/j.1365-2117.2010.00485.x.
- Ielpi, A., 2012, Orbitally-driven climate forcing in late Pliocene lacustrine siderite-rich clastic rhythms (Upper Valdarno Basin, Northern Apennines, Italy): *Palaeogeography, Palaeoclimatology, Palaeoecology*, v. 331–332, p. 119–135, doi:10.1016/j.palaeo.2012.03.004.
- Indonesia Central Bureau of Statistics (BPS), 2015, Rainfall intensity (mm) and amounts of daily rainfall data in the rain-gauge station of the Indonesian Agency for Meteorology, Climatology and Geophysics (BMKG) 2000-2013: Jakarta.

- Indonesian Agency for Meteorology Climatology and Geophysics, 2015, Report on Drought Forecast 2015 in Indonesia: Jakarta, 145 p.
- Indonesian Geological Survey, 2004, Indonesian Geological Map: Jakarta, (digital copy) p.
- Ingersoll, R. V., Thomas F. Bullard, Richard L. Ford, J. P. Grimm, J. D. Pickle, and S. W. Sares, 1984, The Effect of Grain Size on Detrital Modes: A Test of the Gazzi-Dickinson Point-Counting Method: *SEPM Journal of Sedimentary Research*, v. Vol. 54, no. 1, doi:10.1306/212F83B9-2B24-11D7-8648000102C1865D.
- Ito, M., M. Matsukawa, T. Saito, and D. J. Nichols, 2006, Facies architecture and paleohydrology of a synrift succession in the Early Cretaceous Choyr Basin, southeastern Mongolia: *Cretaceous Research*, v. 27, no. 2, p. 226–240, doi:10.1016/j.cretres.2005.11.005.
- Jackson II, R. G., 1975, Hierarchical attributes and a unifying model of bed forms composed of cohesionless material and produced by shearing flow: *Geological Society Of America Bulletin*, doi:10.1130/0016-7606(1975)86<1523.
- Jackson II, R. G., 1976, Depositional Model of Point Bars in the Lower Wabash River: *SEPM Journal of Sedimentary Research*, v. Vol. 46, no. September, p. 579–594, doi:10.1306/212F6FF5-2B24-11D7-8648000102C1865D.
- Jackson, R. G., 1981, Sedimentology of muddy fine-grained channel deposits in meandering streams of the American Middle West: *Journal of Sedimentary Petrology*, v. 51, no. 4, p. 1169–1192, doi:10.1306/212F7E5A-2B24-11D7-8648000102C1865D.
- Jerrett, R. M., S. S. Flint, R. C. Davies, and D. M. Hodgson, 2011, Sequence stratigraphic interpretation of a pennsylvanian (upper carboniferous) coal from the central appalachian basin, USA: *Sedimentology*, v. 58, no. 5, p. 1180–1207, doi:10.1111/j.1365-3091.2010.01200.x.
- Jinnah, Z. A., and E. M. Roberts, 2011, Facies Associations, Paleoenvironment, and Base-Level Changes in the Upper Cretaceous Wahweap Formation, Utah, U.S.A.: *Journal of Sedimentary Research*, v. 81, no. 4, p. 266–283, doi:10.2110/jsr.2011.22.
- Johnson, C. L., C. L. Johnson, S. a Graham, and S. a Graham, 2004, Cycles in Perilacustrine Facies of Late Mesozoic Rift Basins, Southeastern Mongolia: *Journal of Sedimentary Research*, v. 74, p. 786–804, doi:10.1306/051304740786.
- Johnsson, M. J., 1990, Tectonic versus chemical-weathering controls on the composition of fluvial sands in tropical environments: *Sedimentology*, v. 37, no. 4, p. 713–726, doi:10.1111/j.1365-3091.1990.tb00630.x.
- Karmalkar, A., C. McSweeney, M. New, and G. Lizcano, 2010, UNDP Climate Change, Country Profiles: Indonesia: New York, 66 p.

- Katili, J. A., 1971, A Review of the Geotectonic Theories and Tectonic Maps of Indonesia: *Earth-Science Reviews*, v. 7, p. 143–163.
- Katili, J. A., 1989, Review of past and present geotectonic concepts of eastern indonesia: *Netherlands Journal of Sea Research*, v. 24, no. 2–3, p. 103–129, doi:10.1016/0077-7579(89)90143-9.
- Kominz, M. A., J. V. Browning, K. G. Miller, P. J. Sugarman, S. Mizintseva, and C. R. Scotese, 2008, Late Cretaceous to Miocene sea-level estimates from the New Jersey and Delaware coastal plain coreholes: An error analysis: *Basin Research*, v. 20, no. 2, p. 211–226, doi:10.1111/j.1365-2117.2008.00354.x.
- Kováčic, M., J. Zupanic, L. Babic, D. Vrsaljko, M. Miknic, K. Bakrac, I. Hecimovic, R. Avanic, and M. Brkic, 2004, Lacustrine basin to delta evolution in the Zagorje Basin, a Pannonian sub-basin (Late Miocene: Pontian, NW Croatia): *Facies*, v. 50, no. 1, p. 19–33, doi:10.1007/s10347-003-0001-6.
- Kraus, M. J., and L. T. Middleton, 1987, Contrasting architecture of two alluvial suites in different structural settings: *SEPM (Society for Sedimentary Geology)*, 253–262 p.
- Kübler, B., and M. Jaboyedoff, 2000, Illite crystallinity: *Comptes Rendus de l'Academie de Sciences - Serie IIa: Sciences de la Terre et des Planetes*, v. 331, no. 2, p. 75–89, doi:10.1016/S1251-8050(00)01395-1.
- Kukulski, R., 2012, Fluvial sedimentology and stratigraphy of the Late Jurassic–Early Cretaceous Monteith Formation: no. August, doi:http://hdl.handle.net/11023/170.
- Kusumahbrata, Y., 1994, Sedimentology and stratigraphy of the Bayah, Walat and Ciletuh formations, southwest Java Basin, Indonesia: *ProQuest Dissertations and Theses*, p. 1.
- Lambert, A., and K. J. Hsu, 1979, Non-annual cycles of varve-like sedimentation in Walensee, Switzerland: *Sedimentology*, v. 26, no. 3, p. 453–461, doi:10.1111/j.1365-3091.1979.tb00920.x.
- Laumonier, Y., 1997, Physical environment and physiographic classification of the vegetation, in M. J. A. Werger, ed., *The Vegetation and Physiography of Sumatra*: Dordrecht, Kluwer Academic Publisher, p. 22–37, doi:10.1017/S0266467498290523.
- Le Roux, J. P., and S. Elgueta, 2000, Sedimentologic development of a Late Oligocene–Miocene forearc embayment, Valdivia Basin Complex, southern Chile: *Sedimentary Geology*, v. 130, no. 1–2, p. 27–44, doi:10.1016/S0037-0738(99)00096-2.
- Leclair, S. F., and J. S. Bridge, 2001, Quantitative interpretation of sedimentary structures formed by river dunes: *Journal of Sedimentary Research*, v. 71, no. 5, p. 713–716, doi:10.1306/2dc40962-0e47-11d7-8643000102c1865d.

- Leeder, M. R., 1973, Fluvialite fining-upwards cycles and the magnitude of palaeochannels: *Geological Magazine*, v. 110, no. 3, p. 265, doi:10.1017/S0016756800036098.
- Leeder, M. R., and M. D. Stewart, 1996, Fluvial incision and sequence stratigraphy: alluvial responses to relative sea-level fall and their detection in the geological record: Geological Society, London, Special Publications, v. 103, no. 1, p. 25–39, doi:10.1144/GSL.SP.1996.103.01.03.
- Leopold, L. B., M. G. Wolman, and J. P. Miller, 1992, *Fluvial processes in geomorphology*: New York, Dover Publications Inc., 507 p.
- Leopold, L. B., and T. Maddock Jr., 1953, The hydraulic geometry of stream channels and some physiographic implications: Washington, D.C., 64 p.
- Lewis, S. G., D. Maddy, and R. G. Scaife, 2001, The fluvial system response to abrupt climate change during the last cold stage: The Upper Pleistocene River Thames fluvial succession at Ashton Keynes, UK: *Global and Planetary Change*, v. 28, no. 1–2, p. 341–359, doi:10.1016/S0921-8181(00)00083-7.
- Li, C. S., X. F. Shi, S. J. Kao, M. Te Chen, Y. G. Liu, X. S. Fang, H. H. Lü, J. J. Zou, S. F. Liu, and S. Q. Qiao, 2012, Clay mineral composition and their sources for the fluvial sediments of Taiwanese rivers: *Chinese Science Bulletin*, v. 57, no. 6, p. 673–681, doi:10.1007/s11434-011-4824-1.
- Limmer, D. R., C. M. Köhler, S. Hillier, S. G. Moreton, A. R. Tabrez, and P. D. Clift, 2012, Chemical weathering and provenance evolution of Holocene-Recent sediments from the Western Indus Shelf, Northern Arabian Sea inferred from physical and mineralogical properties: *Marine Geology*, v. 326–328, p. 101–115, doi:10.1016/j.margeo.2012.07.009.
- Lintnerová, O., J. Michálek, P. Uhlík, J. Soták, and Z. Weissová, 2013, Latest triassic climate humidification and kaolinite formation (western Carpathians, tatra mts.): *Geological Quarterly*, v. 57, no. 4, p. 701–728, doi:10.7306/gq.1123.
- Liu, Z. et al., 2008, Detrital fine-grained sediment contribution from Taiwan to the northern South China Sea and its relation to regional ocean circulation: *Marine Geology*, v. 255, no. 3–4, p. 149–155, doi:10.1016/j.margeo.2008.08.003.
- Liu, Z., H. Wang, W. S. Hantoro, E. Sathiamurthy, C. Colin, Y. Zhao, and J. Li, 2012, Climatic and tectonic controls on chemical weathering in tropical Southeast Asia (Malay Peninsula, Borneo, and Sumatra): *Chemical Geology*, v. 291, p. 1–12, doi:10.1016/j.chemgeo.2011.11.015.
- Longley, I. M., 1997, The tectonostratigraphic evolution of SE Asia: Geological Society, London, Special Publications, v. 126, no. 1, p. 311–339, doi:10.1144/GSL.SP.1997.126.01.19.

- Lorenz, J. C., D. M. Heinze, J. A. Clark, and C. A. Searls, 1985, Determination of Widths of Meander-Belt Sandstone Reservoirs From Vertical Downhole Data, Mesaverde Group, Piceance Creek Basin, Colorado.: American Association of Petroleum Geologists Bulletin, v. 69, no. 5, p. 710–721, doi:10.1306/AD4627EF-16F7-11D7-8645000102C1865D.
- Macklin, M. G., J. Lewin, and J. C. Woodward, 2012, The fluvial record of climate change: Philosophical Transactions of the Royal Society A: Mathematical, Physical and Engineering Sciences, v. 370, no. 1966, p. 2143–2172, doi:10.1098/rsta.2011.0608.
- Marliyani, G. I., J. R. Arrowsmith, and K. X. Whipple, 2016, Characterization of slow slip rate faults in humid areas: Cimandiri fault zone, Indonesia: Journal of Geophysical Research: Earth Surface, v. 121, no. 12, p. 2287–2308, doi:10.1002/2016JF003846.
- Martínek, K., M. Blecha, V. Daněk, J. Franců, J. Hladíková, R. Johnová, and D. Uličný, 2006, Record of palaeoenvironmental changes in a Lower Permian organic-rich lacustrine succession: Integrated sedimentological and geochemical study of the Rudník member, Krkonoše Piedmont Basin, Czech Republic: Palaeogeography, Palaeoclimatology, Palaeoecology, v. 230, no. 1–2, p. 85–128, doi:10.1016/j.palaeo.2005.07.009.
- Martodjojo, S., 1984, Evolusi Cekungan Bogor: Bandung Institute of Technology (ITB), 396 p.
- Marzo, M., W. Nijman, and C. Puigdefabregas, 1988, Architecture of the Castissent fluvial sheet sandstones, Eocene, South Pyrenees, Spain: Sedimentology, v. 35, no. 5, p. 719–738, doi:10.1111/j.1365-3091.1988.tb01247.x.
- McLaurin, B. T., and R. J. Steel, 2007, Architecture and origin of an amalgamated fluvial sheet sand, lower Castlegate Formation, Book Cliffs, Utah: Sedimentary Geology, v. 197, no. 3–4, p. 291–311, doi:10.1016/j.sedgeo.2006.10.005.
- Miall, A. D., 1985, Architectural-element analysis: A new method of facies analysis applied to fluvial deposits: Earth-Science Reviews, v. 22, no. 4, p. 261–308, doi:10.1016/0012-8252(85)90001-7.
- Miall, A. D., 1996, The Geology of Fluvial Deposits, Sedimentary Facies, Basin Analysis, and Petroleum Geology: Berlin, Heidelberg, Springer Berlin Heidelberg, 582 p., doi:10.1007/978-3-662-03237-4.
- Miller, K. G., 2005, The Phanerozoic Record of Global Sea-Level Change: Science, v. 310, no. 5752, p. 1293–1298, doi:10.1126/science.1116412.
- Modrick, T. M., and K. P. Georgakakos, 2014, Regional bankfull geometry relationships for southern California mountain streams and hydrologic applications: Geomorphology, v. 221, p. 242–260, doi:10.1016/j.geomorph.2014.06.004.

- Moore, P. D., and E. H. Chater, 1969, Studies in the vegetational history of Mid-Wales: I. The post-glacial period in Cardiganshire: *New Phytologist*, v. 68, no. 1, p. 183–196, doi:10.1111/j.1469-8137.1969.tb06431.x.
- Morgenroth, P., A. T. Rahardjo, and K. A. Maryunani, 2011, Dinoflagellate cysts from two Oligocene surface sections on Java Island, Indonesia: *Palaeontographica Abteilung B*, v. 284, no. 4–6, p. 125–157, doi:10.1127/palb/284/2011/125.
- Morley, R. J., 1998, Palynological evidence for Tertiary plant dispersals in the SE Asian region in relation to plate tectonics and climate: *Biogeography and Geological Evolution of SE Asia*, p. 211–234.
- Morley, R. J., 2012, A review of the Cenozoic palaeoclimate history of Southeast Asia, *in* S. W. David Gower, Kenneth Johnson, James Richardson, Brian Rosen, Lukas Rüber, ed., *Biotic Evolution and Environmental Change in Southeast Asia*: Cambridge University Press, p. 79–114, doi:http://dx.doi.org/10.1017/CBO9780511735882.006.
- Morley, R. J., and H. P. Morley, 2013, Mid Cenozoic freshwater wetlands of the Sunda region: *Journal of Limnology*, v. 72, no. s2, p. 18–35, doi:10.4081/jlimnol.2013.s2.e3.
- Nagel, S., S. Castelltort, E. Garzanti, A. T. Lin, S. D. Willett, F. Mouthereau, M. Limonta, and T. Adatte, 2014, Provenance Evolution During Arc-Continent Collision: Sedimentary Petrography of Miocene To Pleistocene Sediments In the Western Foreland Basin of Taiwan: *Journal of Sedimentary Research*, v. 84, no. 7, p. 513–528, doi:10.2110/jsr.2014.44.
- Nami, M., and M. R. Leeder, 1978, Changing Channel Morphology and Magnitude in the Scalby Formation (M. Jurassic) of Yorkshire, England, *in* A. D. Miall, ed., *Fluvial Sedimentology*: Canadian Society of Petroleum Geologists, p. 431–440.
- Nguyen, N., J. Griffin, A. Cipta, and P. R. Cummins, 2015, Indonesia's Historical Earthquakes: Modelled examples for improving the national hazard map: Canberra, doi:10.11636/Record.2015.023.
- Nichols, G. J., and D. J. Cantrill, 2002, Tectonic and climatic controls on a Mesozoic forearc basin succession, Alexander Island, Antarctica: *Geological Magazine*, v. 139, no. 3, p. 313–330, doi:10.1017/S0016756802006465.
- Osterkamp, W. R., and E. R. Hedman, 1982, Perennial-streamflow characteristics related to channel geometry and sediment in Missouri River basin.
- Pandarínath, K., 2009, Clay minerals in SW Indian continental shelf sediment cores as indicators of provenance and palaeomonsoonal conditions: A statistical approach: *International Geology Review*, v. 51, no. 2, p. 145–165, doi:10.1080/00206810802622112.

- Patmosoekismo, S., and I. Yahya, 1974, Basement Configuration of the North West Java Area: Proceedings Indonesian Petroleum Association Third Annual Convention, p. 129–152.
- Patton, P. C., 1987, Measuring the Rivers of the Past: A History of Fluvial Paleohydrology: History of Geophysics: Volume 3 - The History of Hydrology, v. 3, no. Figure 1.
- Peel, M. C., B. L. Finlayson, and T. A. McMahon, 2007, Updated world map of the Köppen-Geiger climate classification: Hydrology and Earth System Sciences, v. 11, no. 5, p. 1633–1644, doi:10.5194/hess-11-1633-2007.
- Pettijohn, F. J., P. E. Potter, and R. Siever, 1987, Sand and Sandstone: Springer-Verlag New York, 553 p., doi:10.1007/978-1-4612-1066-5.
- Pickup, G., and W. Rieger, 1979, A conceptual model of the relationship between channel characteristics and discharge: Earth Surface Processes, v. 4, p. 37–42.
- Plink-Björklund, P., 2005, Stacked fluvial and tide-dominated estuarine deposits in high-frequency (fourth-order) sequences of the Eocene Central Basin, Spitsbergen: Sedimentology, v. 52, no. 2, p. 391–428, doi:10.1111/j.1365-3091.2005.00703.x.
- Pope, R. J. J., and K. N. Wilkinson, 2005, Reconciling the roles of climate and tectonics in Late Quaternary fan development on the Spartan piedmont, Greece, *in* A. M. Harvey, A. E. Mather, and M. Stokes, eds., Geological Society, London, Special Publications: Geological Society of London, p. NP-NP, doi:10.1144/GSL.SP.2005.251.01.16.
- Provincial Public Works Agency, 2012, Discharge and River Cross Sectional Survey of Java, Sumatra and Kalimantan, unpublished report (Year 1980–2012): Bandung.
- Puigdefabregas, C., and A. Van Vliet, 1978, Meandering stream deposits from the Tertiary of the southern Pyrenees: Canadian Society of Petroleum Geologists Memoir, v. 5, p. 469–485.
- Ramos, A., and A. Sopena, 1983, Gravel Bars in Low-Sinuosity Streams (Permian and Triassic, Central Spain), *in* Modern and Ancient Fluvial Systems: Oxford, UK, Blackwell Publishing Ltd., p. 301–312, doi:10.1002/9781444303773.ch24.
- Ramos, A., A. Sopena, and M. Perez-arlucea, 1986, Evolution of Buntsandstein fluvial sedimentation in the northwest Iberian ranges (Central Spain): Journal of Sedimentary Petrology, v. 6, p. 862–875.
- Rasmussen, H., 2000, Nearshore and alluvial facies in the Sant Llorenç del Munt depositional system: Recognition and development: Sedimentary Geology, v. 138, no. 1–4, p. 71–98, doi:10.1016/S0037-0738(00)00144-5.

- Raucsik, B., and A. Varga, 2008, Climato-environmental controls on clay mineralogy of the Hettangian-Bajocian successions of the Mecsek Mountains, Hungary: An evidence for extreme continental weathering during the early Toarcian oceanic anoxic event: *Palaeogeography, Palaeoclimatology, Palaeoecology*, v. 265, no. 1–2, p. 1–13, doi:10.1016/j.palaeo.2008.02.004.
- Research Center for Water Resources Development and, 2011, Hydrology Year Book: Annual River Discharge of Sumatra, Java and Kalimantan Year 1968–2011: Bandung, Ministry of Public Works and Housing, Republic of Indonesia, (digital copy) p.
- Rijsdijk, A., 2012, Surface runoff and sediment yields from tropical volcanic upland watersheds as influenced by climatic, geological and land-use factors, *in* D. Higgitt, ed., *Perspectives on Environmental Management and Technology in Asian River Basins* (Springer Briefs in Geography): Dordrecht, Springer, p. 69–91, doi:10.1007/978-94-007-2330-6.
- Rimmer, S. M., and A. Davis, 1986, Geologic Controls on the Inorganic Composition of Lower Kittanning Coal, in American Chemical Society: p. 41–52, doi:10.1021/bk-1986-0301.ch003.
- Roberts, E. M., 2007, Facies architecture and depositional environments of the Upper Cretaceous Kaiparowits Formation, southern Utah: *Sedimentary Geology*, v. 197, no. 3–4, p. 207–233, doi:10.1016/j.sedgeo.2006.10.001.
- Ruffel, A., and R. Worden, 2000, Palaeoclimate analysis using spectral gamma-ray data from Aptian (Cretaceous) of southern England and southern France: *Palaeogeography, Palaeoclimatology, Palaeoecology*, v. 155, p. 18.
- Runtunuwu, E., and H. Pawitan, 2008, Hydrometeorological monitoring network of Java Island and hydrologic characteristics of the major river basins: *Bulletin of the Terrestrial Environment Research Center University of Tsukuba*, v. 8, no. Supplement 2, p. 55–64.
- Rust, B. R., 1978, A classification of alluvial channel systems: *Canadian Society of Petroleum Geologists*, v. 5, p. 187–198.
- Rust, B. R., and M. R. Gibling, 1990, Braidplain Evolution in the Pennsylvanian South Bar Formation, Sydney Basin, Nova Scotia, Canada: *SEPM Journal of Sedimentary Research*, v. Vol. 60, no. I, p. 59–72, doi:10.1306/212F9110-2B24-11D7-8648000102C1865D.
- Saez, A, Cabrera, L, Jensen, A, Chong, G., 1999, Late Neogene lacustrine record and palaeogeography in the Quillagua – Llamara basin , Central Andean fore-arc (northern Chile): *Palaeogeography, Palaeoclimatology, Palaeoecology*, v. 151, p. 5–37, doi:10.1016/S0031-0182(99)00013-9.

- Sáez, A., M. Inglès, L. Cabrera, and A. de las Heras, 2003, Tectonic–palaeoenvironmental forcing of clay-mineral assemblages in nonmarine settings: the Oligocene–Miocene As Pontes Basin (Spain): *Sedimentary Geology*, v. 159, no. 3–4, p. 305–324, doi:10.1016/S0037-0738(02)00333-0.
- Samuel, L., and Mudjito, 1975, A geological guide along the road between Cibadak-Pelabuanratu (south west Java): Geological Survey of Indonesia.
- Santra, M., R. J. Steel, C. Olariu, and M. L. Sweet, 2013, Stages of sedimentary prism development on a convergent margin-Eocene tye forearc basin, coast range, oregon, USA: *Global and Planetary Change*, v. 103, no. 1, p. 207–231, doi:10.1016/j.gloplacha.2012.11.006.
- Schiller, D. M., R. a Garrad, and L. Prasetyo, 1991, Eocene submarine fan sedimentation in southwest Java: Indonesian Petroleum Association, Proceedings 20th annual convention, Jakarta 1991, v. I, no. October 1991, p. 125–182.
- Schomacker, E. R., A. V. Kjemperud, J. P. Nystuen, and J. S. Jahren, 2010, Recognition and significance of sharp-based mouth-bar deposits in the Eocene Green River Formation, Uinta Basin, Utah: *Sedimentology*, v. 57, no. 4, p. 1069–1087, doi:10.1111/j.1365-3091.2009.01136.x.
- Schumm, S. A., 1968, Speculations Concerning Paleohydrologic Controls of Terrestrial Sedimentation: *Geological Society of America Bulletin*, v. 79, no. 11, p. 1573 LP-1588.
- Shanley, K. W., and P. J. McCabe, 1994, Perspectives on the Sequence Stratigraphy of Continental Strata: *AAPG Bulletin*, v. 78, no. 4, p. 544–568, doi:10.1306/BDFF9258-1718-11D7-8645000102C1865D.
- Shibata, K., and M. Ito, 2014, Relationships of bankfull channel width and discharge parameters for modern fluvial systems in the Japanese Islands: *Geomorphology*, v. 214, p. 97–113, doi:10.1016/j.geomorph.2014.03.022.
- Shibata, K., M. Ito, N. Nemoto, and S. O'Hara, 2010, Temporal variations in channel patterns and facies architecture in a gravelly fluvial system: The Paleogene Iwaki Formation on the Joban Coalfield, a forearc basin in Northeast Japan: *Island Arc*, v. 19, no. 3, p. 489–505, doi:10.1111/j.1440-1738.2010.00724.x.
- Simandjuntak, T. O., and A. J. Barber, 1996, Contrasting tectonic styles in the Neogene orogenic belts of Indonesia: Geological Society, London, Special Publications, v. 106, no. 1, p. 185–201, doi:10.1144/GSL.SP.1996.106.01.12.
- Singer, A., 1984, The paleoclimatic interpretation of clay minerals in sediments - a review: *Earth-Science Reviews*, v. 21, p. 251–293, doi:10.1016/0012-8252(84)90055-2.

- Sinha, R., E. M. Latrubesse, and G. C. Nanson, 2012, Quaternary fluvial systems of tropics: Major issues and status of research: *Palaeogeography, Palaeoclimatology, Palaeoecology*, v. 356–357, p. 1–15, doi:10.1016/j.palaeo.2012.07.024.
- Skelly, R. L., C. S. Bristow, and F. G. Ethridge, 2003, Architecture of channel-belt deposits in an aggrading shallow sandbed braided river: The lower Niobrara River, northeast Nebraska: *Sedimentary Geology*, v. 158, no. 3–4, p. 249–270, doi:10.1016/S0037-0738(02)00313-5.
- Soehaimi, A., 2008, Seismotektonik dan Potensi Kegempaan Wilayah Jawa: Indonesian Journal on Geoscience, v. 3, no. 4, p. 227–240, doi:10.17014/ijog.vol3no4.20085.
- Soeria-Atmadja, R., S. Suparka, C. Abdullah, D. Noeradi, and Sutanto, 1998, Magmatism in western Indonesia, the trapping of the Sumba Block and the gateways to the east of Sundaland: *Journal of Asian Earth Sciences*, v. 16, no. 1, p. 1–12, doi:10.1016/S0743-9547(97)00050-0.
- Soeria-Atmadja, R., and D. Noeradi, 2005, Distribution of early tertiary volcanic rocks in south Sumatra and west Java: The Island Arc, v. 14, no. 4, p. 679–686, doi:10.1111/j.1440-1738.2005.00476.x.
- Stewart, D. J., 1981, A meander-belt sandstone of the Lower Cretaceous of Southern England: *Sedimentology*, v. 28, no. 1, p. 1–20, doi:10.1111/j.1365-3091.1981.tb01658.x.
- Suttner, L. J., and P. K. Dutta, 1986, Alluvial sandstone composition and paleoclimate, I. Framework mineralogy: *Journal of Sedimentary Petrology*, v. 56, no. 1975, p. 329–345, doi:10.1306/212F8909-2B24-11D7-8648000102C1865D.
- Syvitski, J. P. M., S. Cohen, A. J. Kettner, and G. R. Brakenridge, 2014, How important and different are tropical rivers? - An overview: *Geomorphology*, v. 227, p. 5–17, doi:10.1016/j.geomorph.2014.02.029.
- Tan, K. H., 2008, Soils in the Humid Tropics and Monsoon Region of Indonesia: Boca Raton, CRC Press, 557 p.
- Tānavsuu-Milkeviciene, K., and J. Frederick Sarg, 2012, Evolution of an organic-rich lake basin - stratigraphy, climate and tectonics: Piceance creek basin, eocene green river formation: *Sedimentology*, v. 59, no. 6, p. 1735–1768, doi:10.1111/j.1365-3091.2012.01324.x.
- Thomas, J. V., B. Parkash, and R. Mohindra, 2002, Lithofacies and palaeosol analysis of the Middle and Upper Siwalik Groups (Plio-Pleistocene), Haripur-Kolar section, Himachal Pradesh, India: *Sedimentary Geology*, v. 150, no. 3–4, p. 343–366, doi:10.1016/S0037-0738(01)00203-2.

- Tjia, H. D., 2013, Morphostructural Development of Gunungsewu Karst, Jawa Island: Indonesian Journal on Geoscience, v. 8, no. 2, p. 75–88, doi:10.17014/ijog.v8i2.157.
- Tooth, S., 2005, Splay Formation Along the Lower Reaches of Ephemeral Rivers on the Northern Plains of Arid Central Australia: Journal of Sedimentary Research, v. 75, no. 4, p. 636–649, doi:10.2110/jsr.2005.052.
- Turnbridge, I. P., 1984, Facies model for a sandy ephemeral stream and clay playa complex; the Middle Devonian Trentishoe Formation of North Devon, U.K.: Sedimentology, v. 31, no. 5, p. 697–715, doi:10.1111/j.1365-3091.1984.tb01231.x.
- Tye, R. S., and J. M. Coleman, 1989, Depositional processes and stratigraphy of fluvially dominated lacustrine deltas: Mississippi delta plain: Journal of Sedimentary Petrology, v. 59, no. 6, p. 973–996, doi:10.1306/212F90CA-2B24-11D7-8648000102C1865D.
- van Bemmelen, R. W., 1963, Volcanology and geology of ignimbrites in Indonesia, North Italy, and the U.S.A.: Bulletin Volcanologique, v. 25, no. 1, p. 151–173, doi:10.1007/BF02596548.
- van den Berg, J. H., 1995, Prediction of alluvial channel pattern of perennial rivers: Geomorphology, v. 12, no. 4, p. 259–279, doi:10.1016/0169-555X(95)00014-V.
- Van Der Neut, M., and P. G. Eriksson, 1999, Palaeohydrological Parameters of a Proterozoic Braided Fluvial System (Wilgerivier Formation, Waterberg Group, South Africa) Compared with a Phanerozoic Example: IAS Special Publications, v. 28, no. Fluvial Sedimentology VI, p. 381–392, doi:10.1002/9781444304213.ch27.
- Van Houten, F. B., 1973, Origin of red beds: A review-1961-1972: Annual Review Earth Planetary Science, v. 1, p. 39–61, doi:10.1146/annurev.ea.01.050173.000351.
- Waltham, D., 1994, Mathematics: A Simple Tool for Geologists: London, Chapman and Hall, 189 p.
- Warren Bell Hamilton, 1979, Tectonics of the Indonesian region: USGS Professional Paper 1078, doi:http://pubs.er.usgs.gov/publication/pp1078?mimetype=ris.
- Weltje, G. J., X. D. Meijer, and P. L. De Boer, 1998, Stratigraphic inversion of siliciclastic basin fills: a note on the distinction between supply signals resulting from tectonic and climatic forcing: Basin Research, v. 10, no. 1, p. 129–153, doi:10.1046/j.1365-2117.1998.00057.x.
- Whateley, M. K. G., and G. R. Jordan, 1989, Fan-delta-lacustrine sedimentation and coal development in the Tertiary Ombilin Basin, W Sumatra, Indonesia: Deltas: Sites and Traps for Fossil Fuels, v. 41, no. 1, p. 317–332, doi:10.1144/GSL.SP.1989.041.01.22.

- Wight, A., H. Friestad, I. Anderson, P. Wicaksono, and C. H. Reminton, 1997, Exploration history of the offshore Southeast Sumatra PSC, Java Sea, Indonesia: Geological Society, London, Special Publications, v. 126, no. 1, p. 121–142, doi:10.1144/GSL.SP.1997.126.01.10.
- Williams, G. P., 1988, Paleofluvial estimates from dimensions of former channels and meanders, *in* P. C. Baker, V.R., Kochel, R.C., Patton, ed., Flood Geomorphology: John Wiley & Sons, p. 321–334.
- Williams, G. P., 1984a, Paleohydrologic Equations for Rivers: Berlin, Heidelberg, Springer Berlin Heidelberg, 343–367 p., doi:10.1007/978-3-642-69759-3.
- Williams, G. P., 1986, River meanders and channel size: Journal of Hydrology, v. 88, no. 1–2, p. 147–164, doi:10.1016/0022-1694(86)90202-7.
- Williams, G. P., 1984b, Paleohydrological Methods and Some Examples from Swedish Fluvial Environments II. River Meanders: Geografiska Annaler. Series A, Physical Geography, v. 66, no. 1/2, p. 89, doi:10.2307/520941.
- Williams, G. P., 1978, Bank-full discharge of rivers: Water Resources Research, v. 14, no. 6, p. 1141–1154, doi:10.1029/WR014i006p01141.
- Witts, D., R. Hall, G. Nichols, and R. Morley, 2012, A new depositional and provenance model for the Tanjung Formation, Barito Basin, SE Kalimantan, Indonesia: Journal of Asian Earth Sciences, v. 56, p. 77–104, doi:10.1016/j.jseas.2012.04.022.
- Wohl, E., J. N. Kuzma, and N. E. Brown, 2004, Reach-scale channel geometry of a mountain river: Earth Surface Processes and Landforms, v. 29, no. 8, p. 969–981, doi:10.1002/esp.1078.
- Xu, J., 2004, Comparison of hydraulic geometry between sand- and gravel-bed rivers in relation to channel pattern discrimination: Earth Surface Processes and Landforms, v. 29, no. 5, p. 645–657, doi:10.1002/esp.1059.
- Young, R., W. E. Harmony, and T. Budiyo, 1995, The evolution of Oligo-Miocene fluvial sand-body geometries and the effect on hydrocarbon trapping; Widuri Field, West Java Sea: Sedimentary facies analysis; a tribute to the research and teaching of Harold G. Reading., v. 22, p. 355–380, doi:10.1002/9781444304091.ch15.

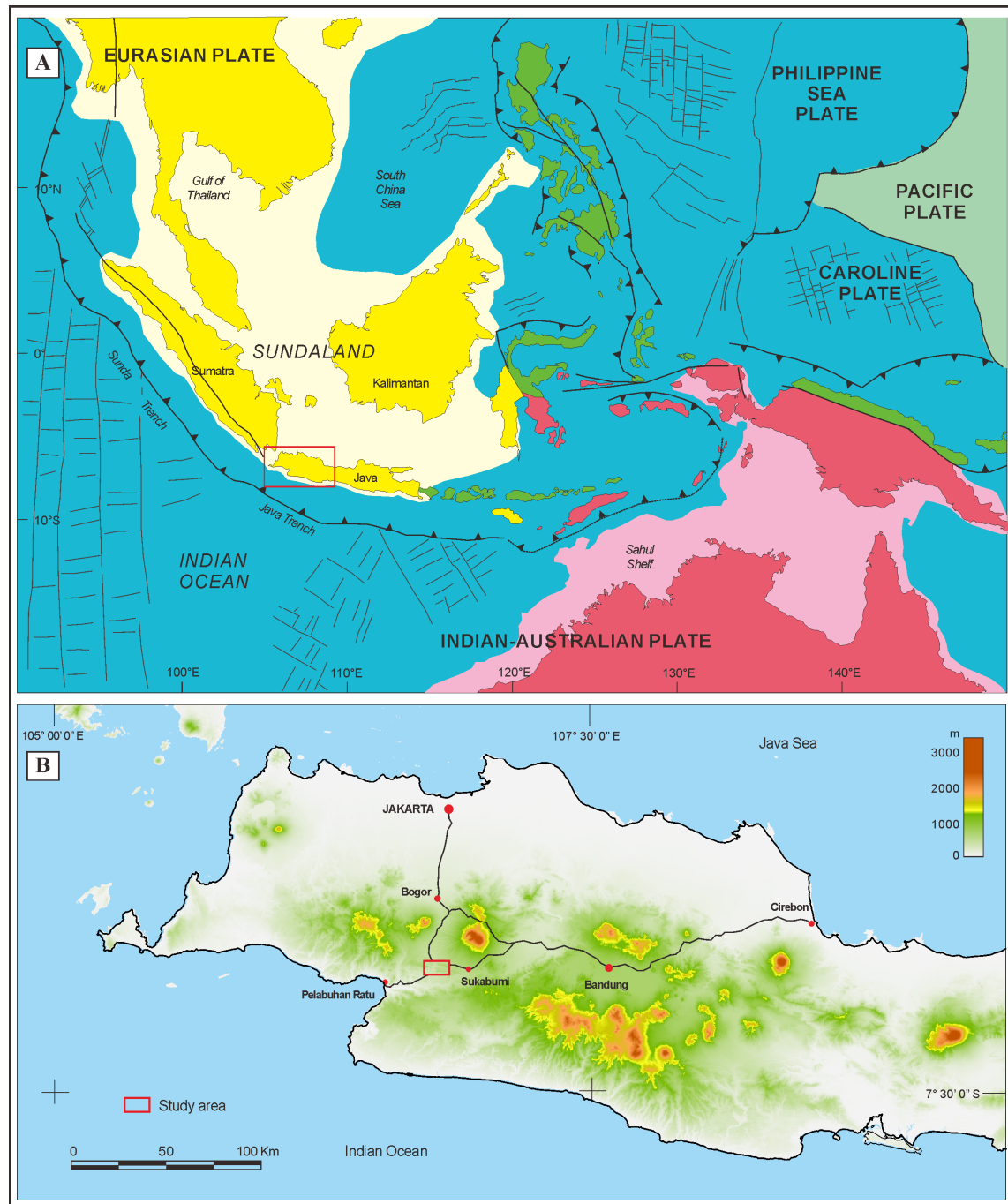


Fig. 1. (A) Present day plate-tectonic setting of Indonesian archipelago. The map was modified from Hall (1996; 2012). The study area is situated at the western part of Java Island, in the southern margin of the Sundaland. (B) Simplified geographical map of the West Java. The study area is located at the southwestern part of West Java, which is indicated by a red-coloured box.

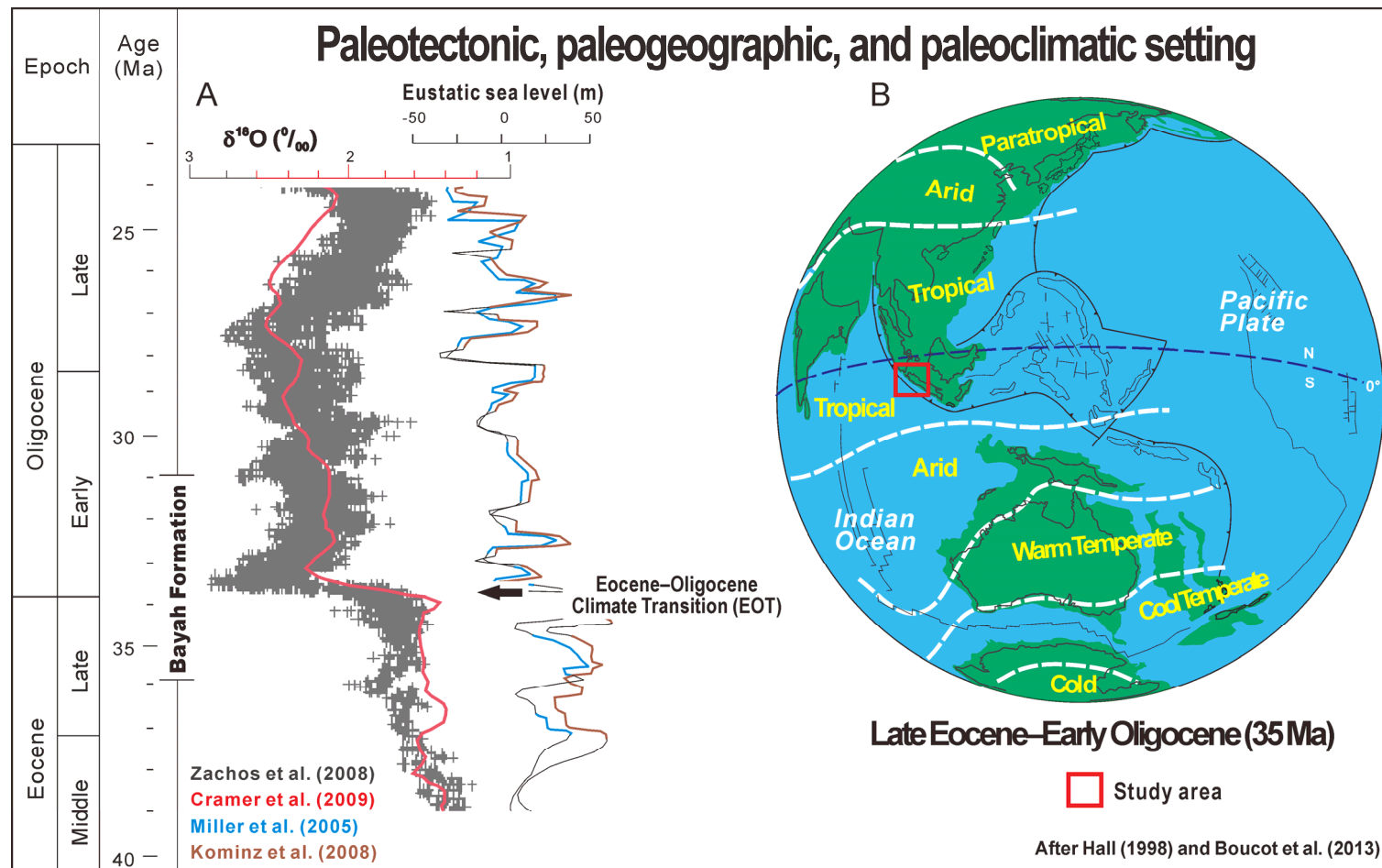


Fig. 2. (A) Global climatic changes based on oxygen-isotope records and eustatic sea-level curves (Miller et al., 2005; Kominz et al., 2008; Zachos et al., 2008; Cramer et al., 2009). (B) Regional tectonic and climatic settings of the Late Eocene–Early Oligocene for the SE Asian continental margin. Modified from Hall (1998) and Boucot et al. (2013).

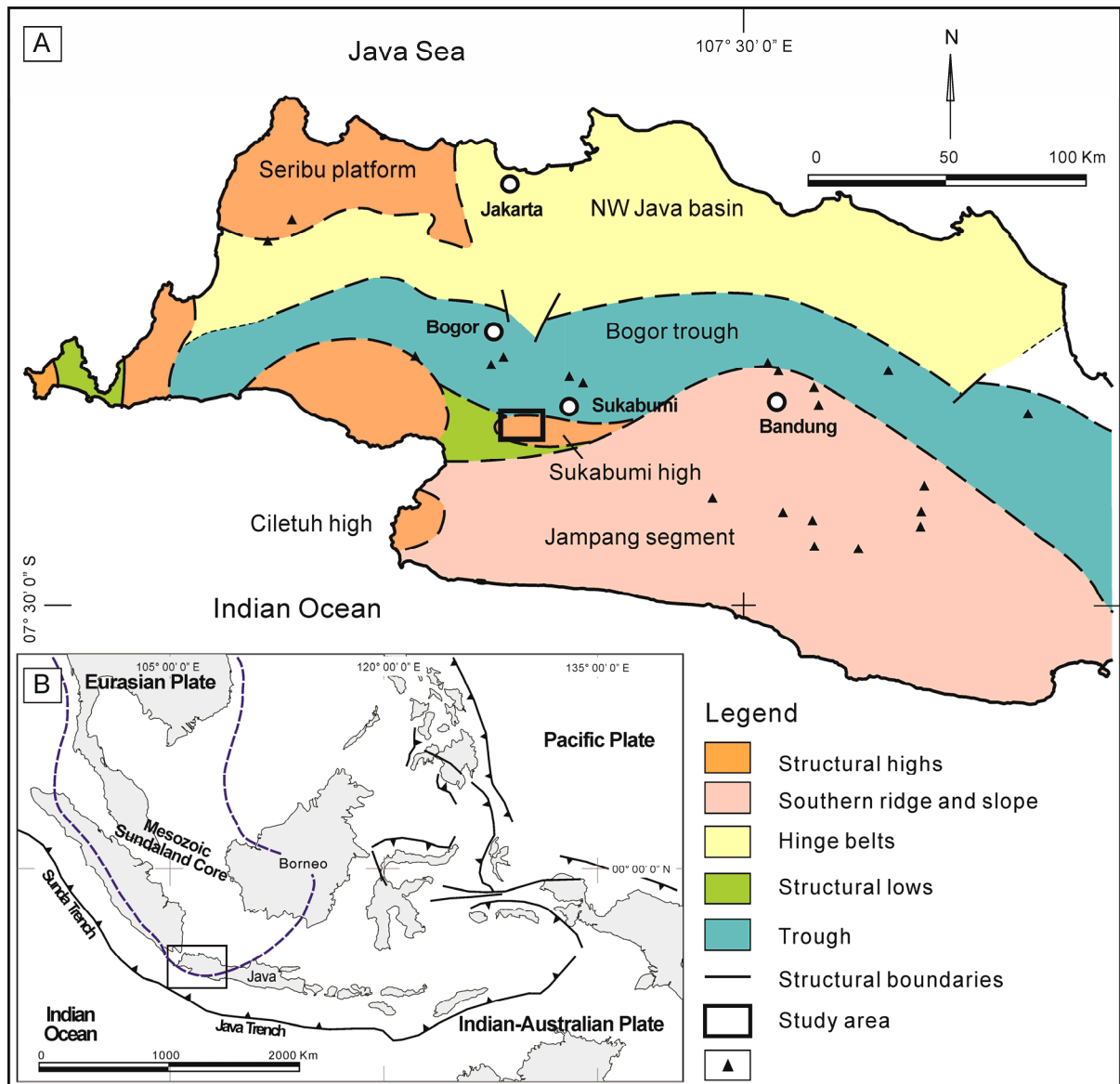


Fig. 3. Simplified map of morphotectonic units of the Western part of Java island (modified from Baumann et al., 1973). These units are defined based on the presence of high relief morphology and depressions, which correspond to structural high and low, respectively. The study area is indicated by black-colour rectangle, and situated in the Sukabumi high morphotectonic unit.

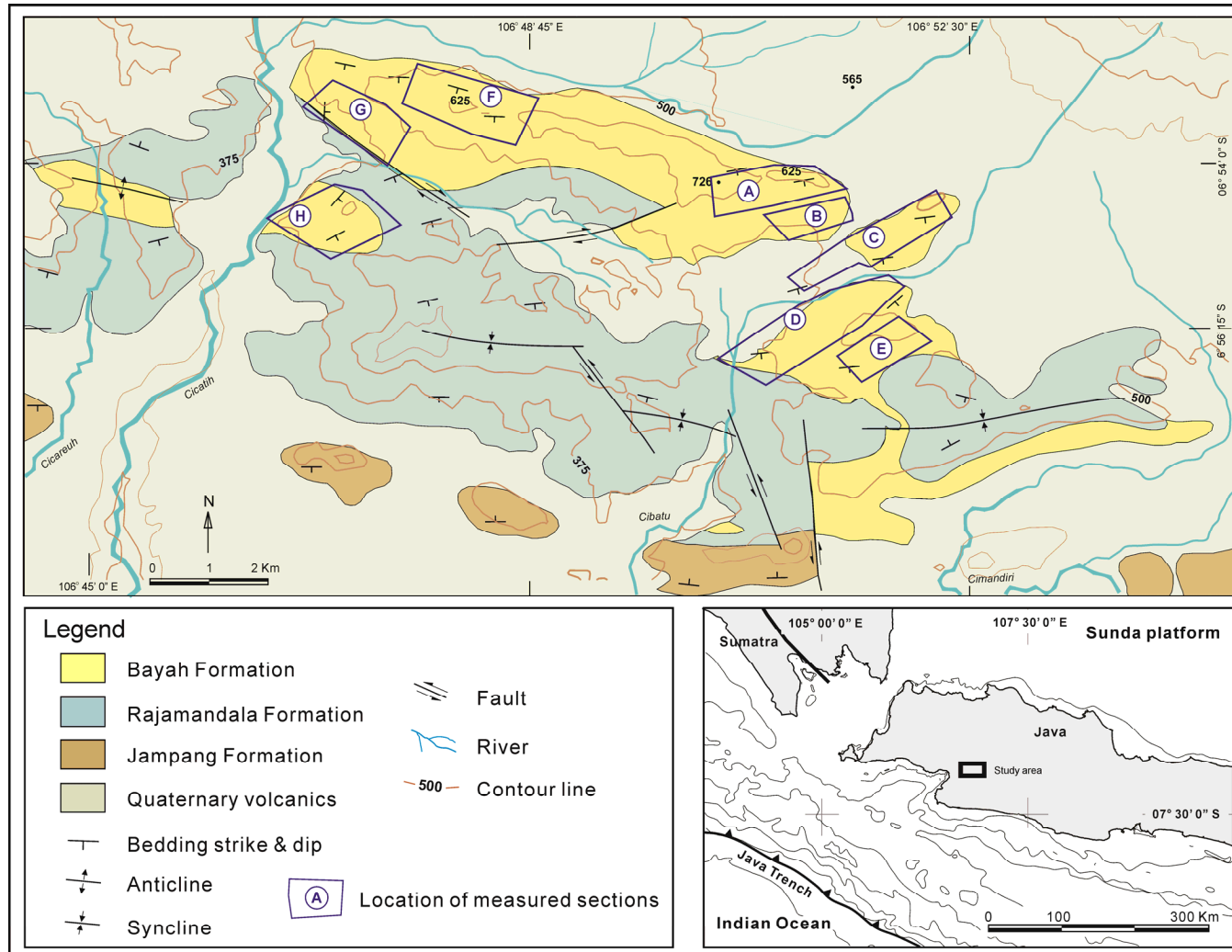


Fig. 4. Geological map of the study area in the Sukabumi high morphotectonic unit. Modified from Effendi et al. (1989). This map shows the distribution of the Bayah Formation in the Sukabumi high. Outcrops of the Bayah Formation extends along 19 km from the northwest to southeast, forming a homoclinal ridge structure dipping to the south.

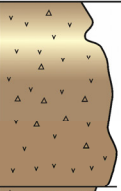
Epoch	Formation	Lithology	Palaeontology and Palynology	Approximate age
QUATERNARY	Quaternary volcanics			
MIOCENE	E	Jampang Fm.	Deep marine	
	L	Rajamandala Fm.	4) <i>Heterostegina borneensis</i> <i>Miogypsinoides dehaarti</i> (Te 1-4/P22)	$\pm 23 \sim 26$ Ma
OLIGOCENE		(Batuasih marl)	3) <i>Globorotalia opima opima</i> (P19) nannoplankton zone (CP 18)	$\pm 28 \sim 31$ Ma
	E	Bayah Fm.	2) Pasir Bongkok suite (Early Oligocene): <i>Florschuetzia trilobata</i> <i>Verrumonoletes usmensis</i> <i>Monocolpites medius</i>	$\pm 31 \sim 33.9$ Ma
EOCENE	L		1) Gunung Walat suite (Late Eocene): <i>Meyeripollis nayarkotensis</i> <i>Proxapertites operculatus</i> <i>Palmaepollenites kutchensis</i>	$\pm 33.9 \sim 37.5$ Ma

Fig. 5. Generalized stratigraphic column of the study area in the Sukabumi high (adapted from Adinegoro, 1973; Samuel and Mudjito, 1975; Effendi et al., 1989; Morgenroth et al., 2007; Hendrizan et al., 2012; Morley, 2012).

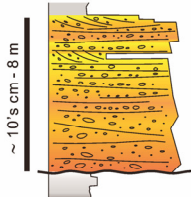
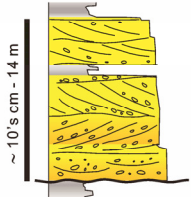
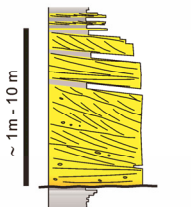
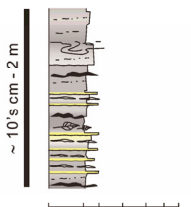
Log Type	Lithofacies Association	Description	Interpretation
	FA 1 Conglomerate deposits	Medium- to very thick-bedded (0.6–16 m thick) clast- and matrix-supported conglomerates and pebbly sandstones. Crude horizontal and trough cross-stratification and sharp-basal surfaces.	Coarse-grained, gravelly-channel-fill deposits at a distal portion of an alluvial-fan system. Gravelly longitudinal bar deposits.
	FA 2 Conglomeratic sandstone deposits	Medium- to very thick-bedded (0.7–14 m thick), medium- to coarse-grained sandstones with sharp- and erosional bases, trough cross-stratification, and downcurrent-dipping foresets. Intercalations of muddy deposits (5–20 cm thick) are locally observed.	Conglomeratic sandstone channel-fill deposits. Downstream migration and aggradation of coarse-grained bar deposits.
	FA 3 Sandstone-dominated deposits	Medium- to very thick-bedded (0.8–12 m thick) medium- to fine-grained sandstones with inclined-accretion surfaces and trough cross-stratification. Sharp and erosional base and fining-upward pattern of more than 1 m thick, which fine gradationally upward to muddy deposits of FA 4 or FA 5. Thin-bedded carbonaceous mudstones (10–40 cm thick) are locally intercalated within this sandstone-dominated deposits.	Sandstone-dominated channel-fill deposits, represented by lateral accretion of point-bar deposits, and in local association with fine-grained deposition from suspended loads during intervals of lateral migration of point bars.
	FA 4 Interbedded carbonaceous mudstones with laminated mudstones and siltstones	Interbedded dark-grey mudstones with parallel-arranged carbonaceous fragments, thin lignites (0.5–3 cm thick), and ripple-laminated siltstones. Soft-sediment deformation structures are locally observed.	Mud-filled abandoned-channel deposits. Fine-grained deposition from suspended loads during intervals of channel shifting process and channel-belt avulsion.

Fig. 6. Summary of the facies associations (FA1–FA4) recognized in the Bayah Formation.

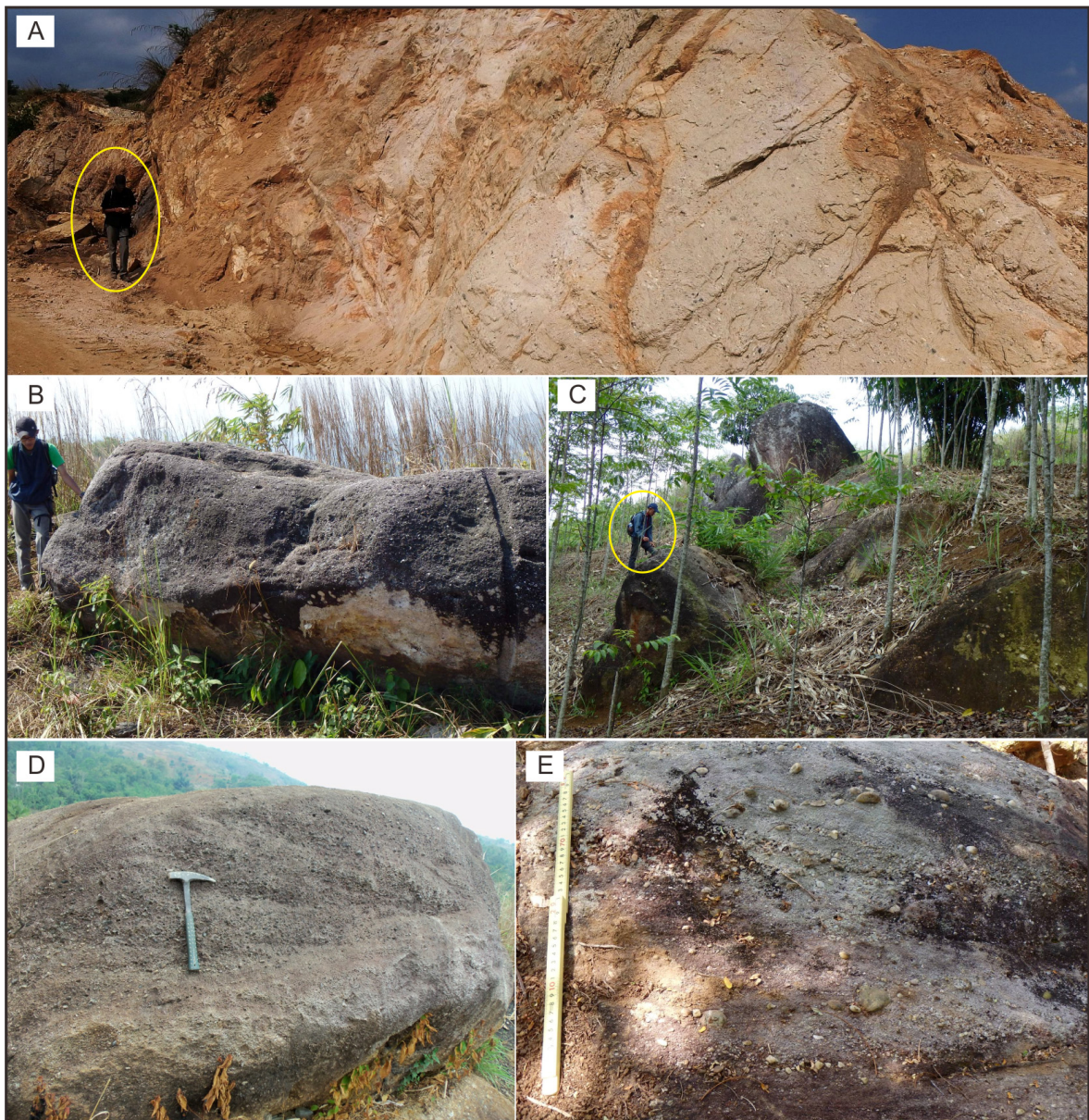


Fig. 7. (A–C) Outcrop photographs of conglomerates (FA1). Person with yellow circle for scale. (D–E) Close-up photographs of FA1, showing crude foreset bedding (D) and cross-stratified conglomerates (E).

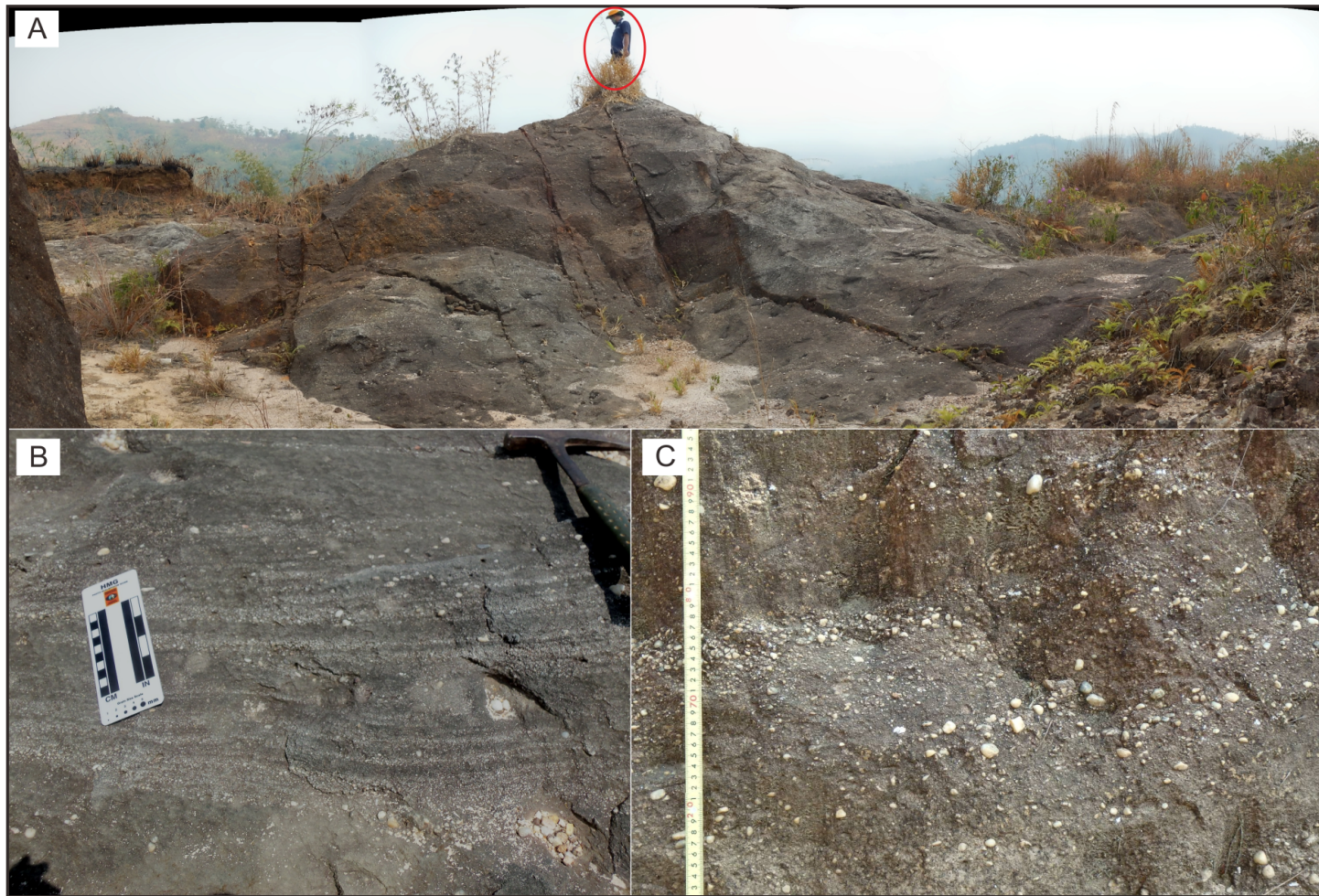


Fig. 8. (A) Outcrop photograph of the conglomeratic sandstones (FA2). Person with red circle for scale. (B–C) Close-up photographs of FA2, showing crudely graded stratification (B) and poorly bedded conglomeratic sandstones (C).

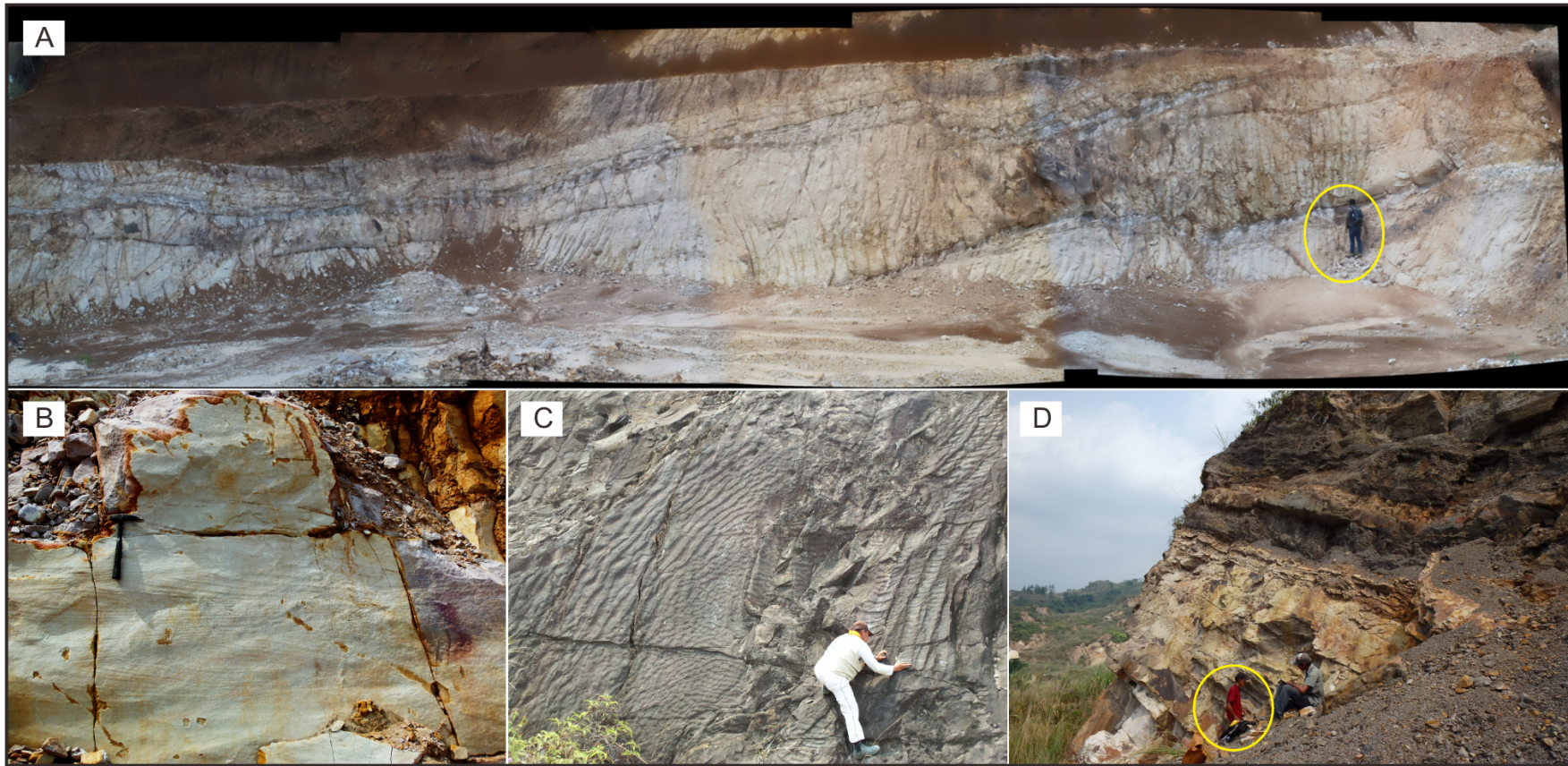


Fig. 9. Outcrop photograph of sandstone-dominated deposits (FA3). Person with yellow circle for scale guide. (B) Close-up photograph of FA3, showing distinct trough cross-stratification. Hammer for scale. (C–D) Current ripples on the top of bedding surfaces the FA3 deposits (C) and a fining-upward pattern to the overlying mudstones (D).

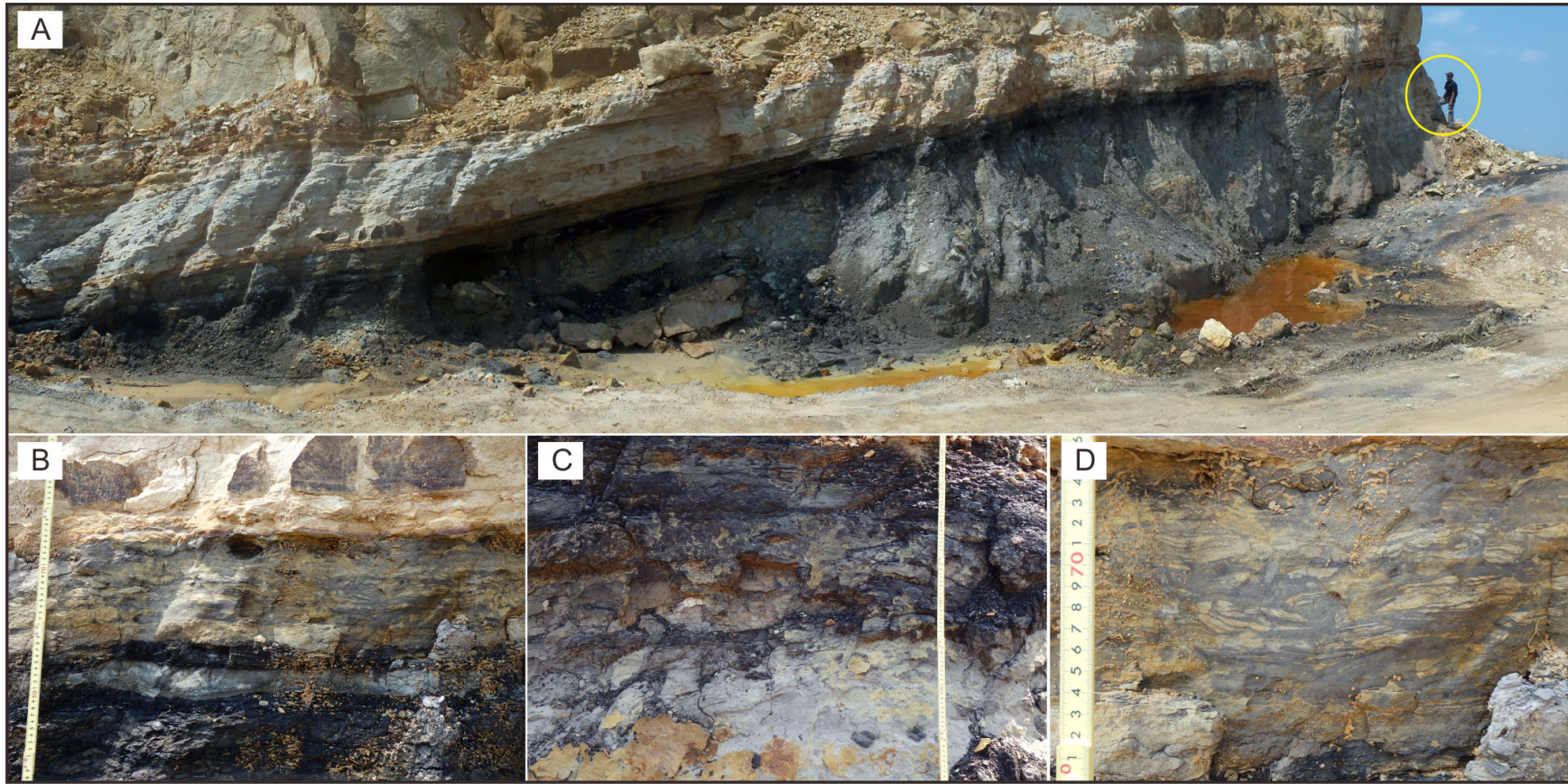


Fig. 10. (A) Outcrop photograph of the interbedded carbonaceous mudstones with laminated mudstones and siltstones (FA4). Person with yellow circle for scale. (B–D) Close-up photographs of FA4, showing current ripple-laminated siltstones (B and D), carbonaceous fragments (C), and soft-sediment deformation structures (D).

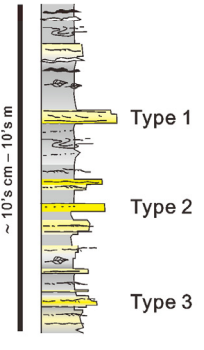
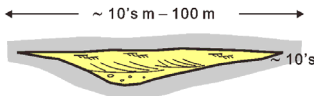
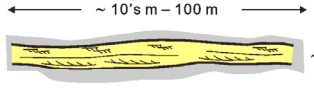
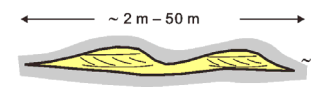
Log type	Lithofacies association	Description	Interpretation
	<div>FA 5</div> <p>Carbonaceous mudstones with thin lignite traces and thin sandstone intercalations (sandstone type 1 – type 3)</p>	Interbedded dark-grey carbonaceous mudstones, siltstones, kaolinite mudstones, lignite traces and thin sandstones intercalations (sandstone-beds type1–type3). Laterally extensive, up to a 10's meter-thick deposits. Current-ripple cross-lamination and faint laminations with local association of soft-sediment deformation structures. Coarsening-upward patterns are commonly observed (0.4–1 m thick).	Muddy flood-plain deposits formed in a floodplain in response to flood events with carbonaceous-rich sediments accumulated in swamp-floodplain environment. Flood incursion from a distance channels. Intercalated thin sandstone beds represent a flood-induced sandy deposits.
Sandstone-bed types in FA 5			
Shape	Description	Interpretation	
<p>Type 1</p> 	Thin-bedded sandstones with basal scours which have lenticular shape. Fine- to medium-grained sandstones are dominant with occasional intercalations of pebbles, which an overall fining-upward pattern.	Fill of small-scale channels on a floodplain environments during flood stages.	
<p>Type 2</p> 	Sheet-like sandstone bodies with locally scoured bases, encased in dark-grey carbonaceous mudstones. Internally plane-parallel and trough cross-stratification and current-ripple cross-lamination are dominant.	Crevasse-splay deposits due to breaching of levees during flood stages.	
<p>Type 3</p> 	Thin-bedded sandstones with current-ripple cross-laminations and small trough cross-stratification. Medium-grained sand. The sandstone beds commonly show undulated, sharp-based bedding contact.	Deposition and migration of small-scale bedforms by waning flows from overfilled channels of an active streams in low-relief overbank areas.	

Fig. 11. Summary of the facies associations (FA5) recognized in the Bayah Formation.

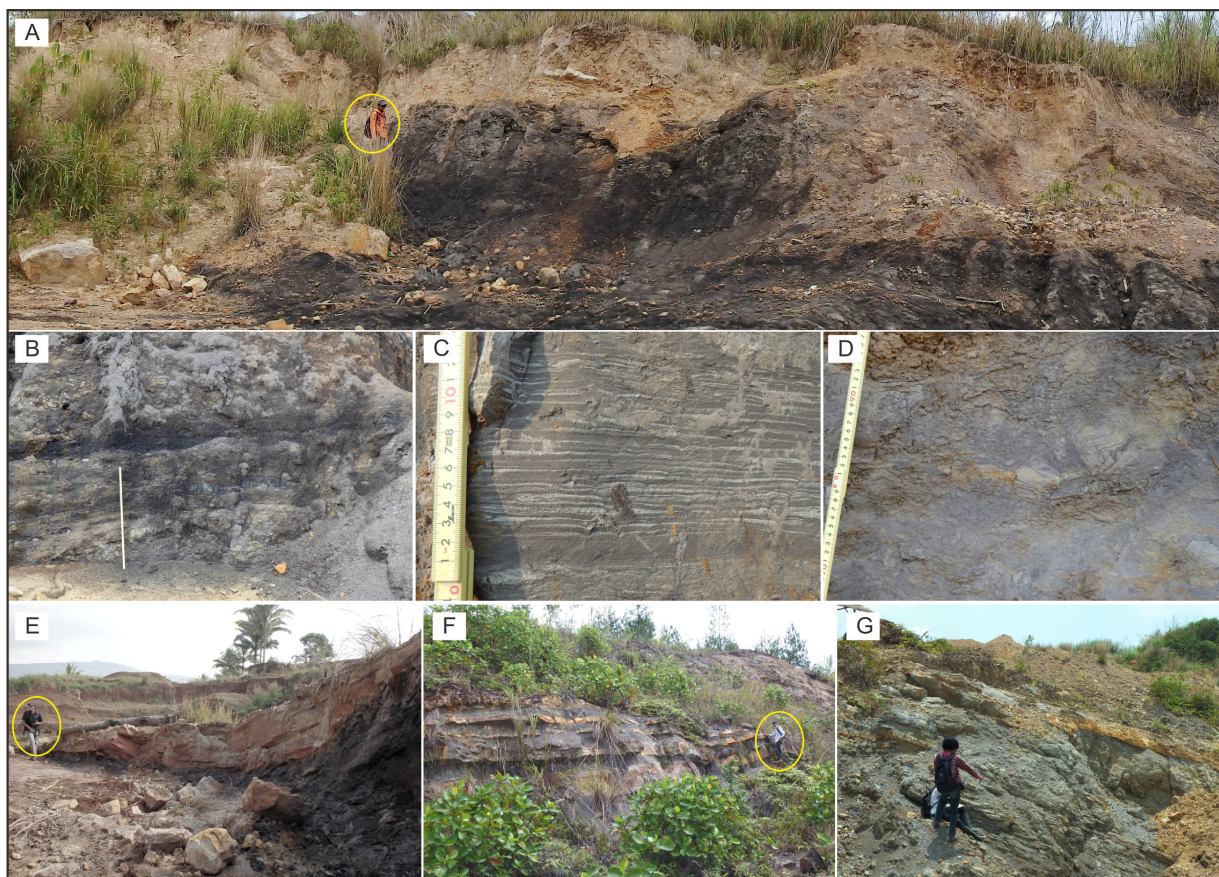


Fig. 12. (A) Outcrop photograph of carbonaceous mudstones with thin lignite layers and thin sandstone intercalations (FA5). Person with yellow circle for scale. (B–D) Close-up photographs of FA5. (E–G) Intercalated sandstone bed types in FA5. Person with yellow circle for scale.

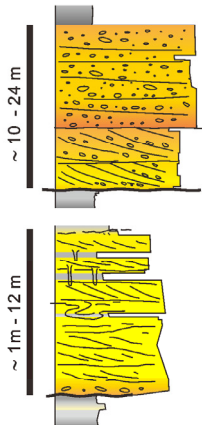
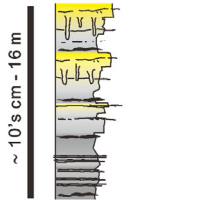
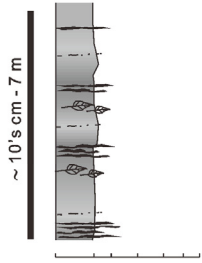
Log Type	Lithofacies Association	Description	Interpretation
	<p>FA6</p> <p>Crudely stratified gravelly sandstones and bioturbated sandstones with soft-sediment deformation</p>	<p>Sharp-based, laterally extensive sandstones and gravelly-sandstones with downstream-inclined stratification and thin mudstone intercalations. Vertical burrows and large-scale load structures are locally developed.</p>	<p>Gravelly sandstones and sandstones of a proximal delta-front mouth-bar deposits in response to high sediment discharges from a river channels into a standing water.</p>
	<p>FA 7</p> <p>Sandy siltstones interbedded with carbonaceous mudstones</p>	<p>Organic matter-rich layers and faintly-laminated rhytmites intercalated in massive mudstones and bioturbated sandy-siltstones showing coarsening-upward patterns.</p>	<p>Distal delta-front deposits formed in a lacustrine environment.</p>
	<p>FA 8</p> <p>Interbedded dark-coloured organic-rich mudstones with plant fragments</p>	<p>Combination of thick and laterally-extensive organic-rich mudstones with papery parting and carbonaceous mudstones with minor lamination. Freshwater-lacustrine algae (<i>Pediastrum</i> spp.) are present.</p>	<p>Lacustrine deposits in an oxygen-depleted condition below a thermocline. Fine-grained sediments were supplied from a delta system</p>

Fig. 13. Summary of the facies associations (FA6–FA8) recognized in the Bayah Formation.

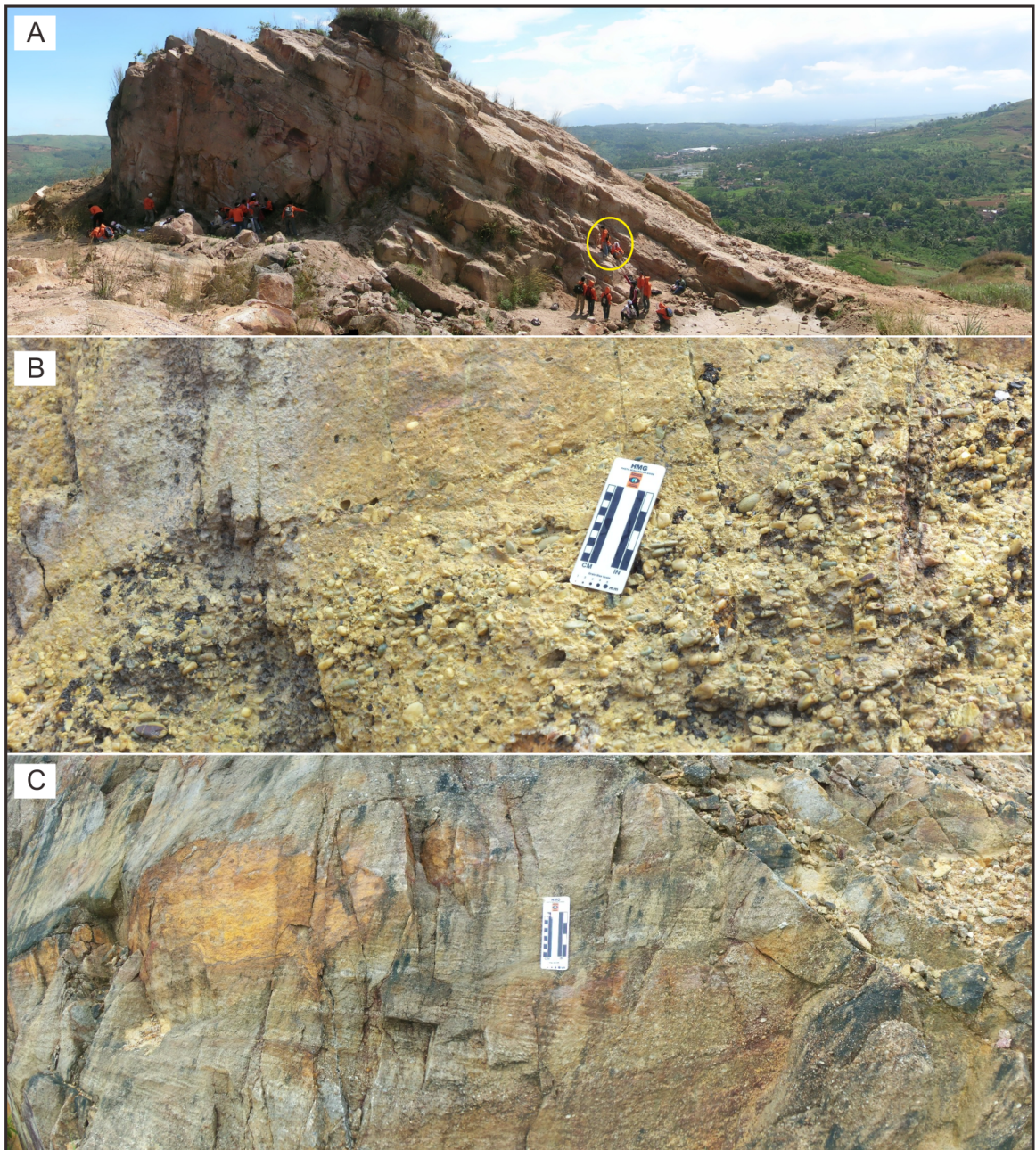


Fig. 14. (A) Outcrop photograph of crudely stratified gravelly sandstones and bioturbated sandstones with soft-sediment deformation (FA6). Person with yellow circle for scale. (B–C) Close-up photographs of FA6, showing conglomerates and gravelly sandstone with foreset bedding.

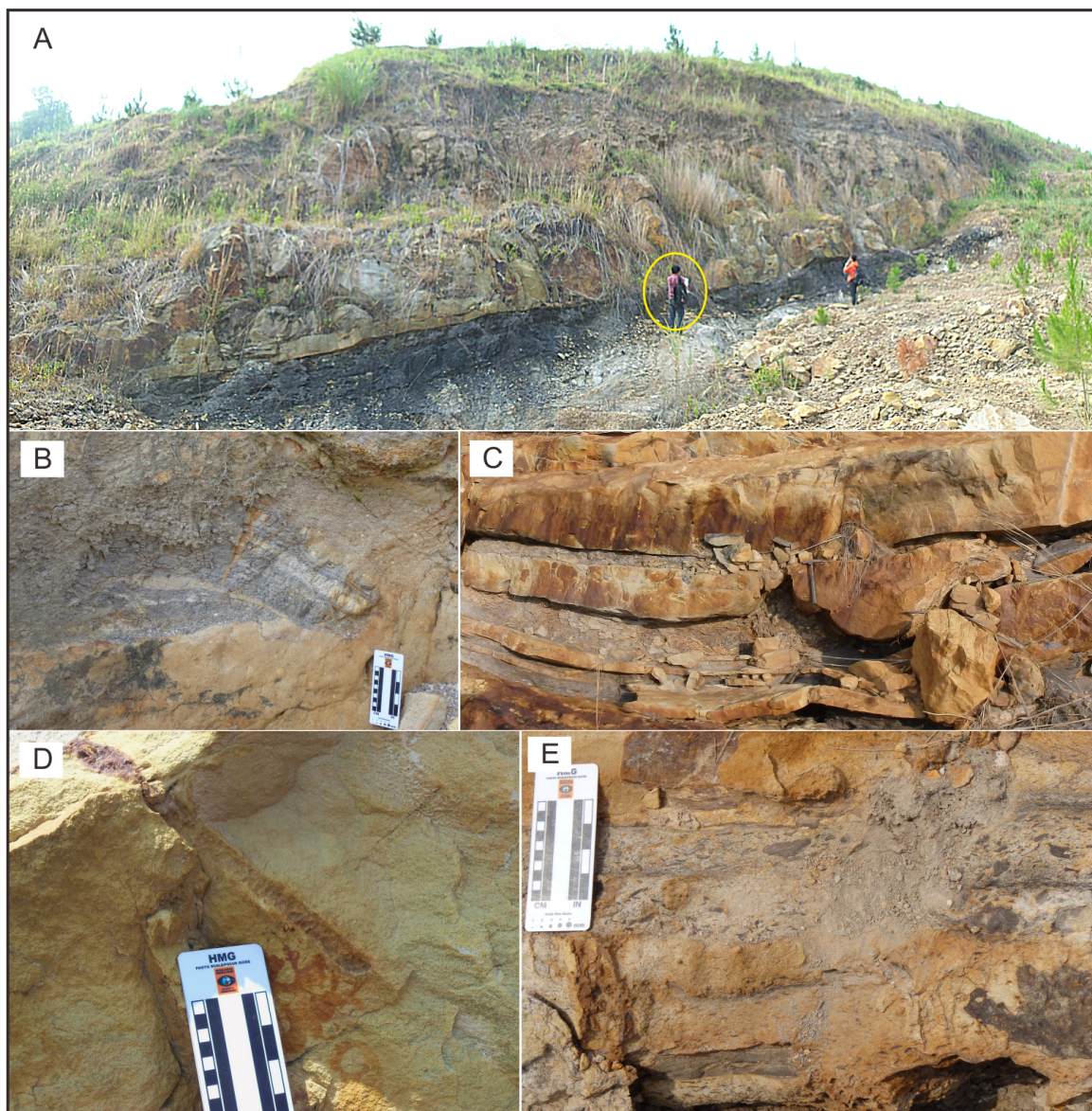


Fig. 15. (A) Outcrop photograph of crudely stratified gravelly sandstones and bioturbated sandstones with soft-sediment deformation (FA6). Person with yellow circle for scale. (B–E) Close-up photographs of FA6, showing soft-sediment deformation (B and E), load structures (C), and bioturbation (D).

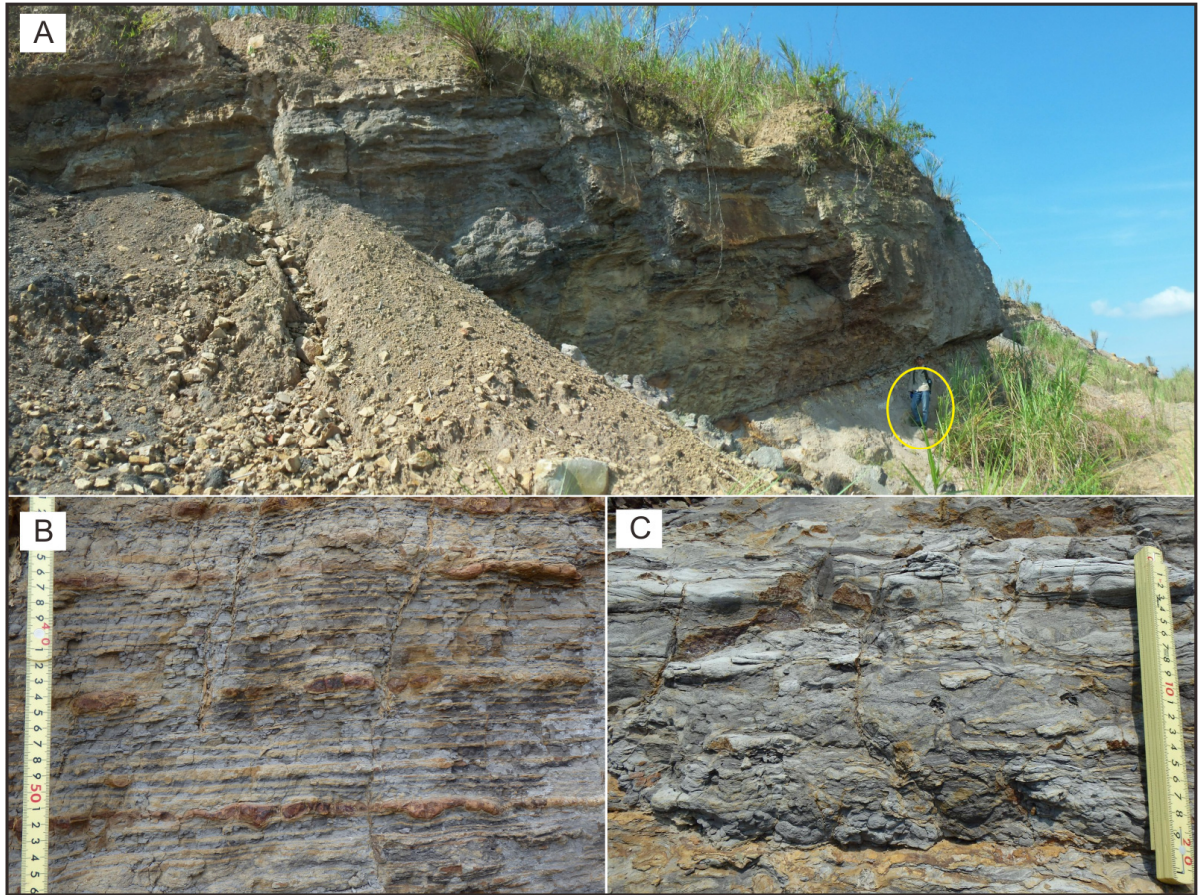


Fig. 16. (A) Outcrop photograph of sandy-siltstones interbedded with carbonaceous mudstones facies association (FA7). Person with yellow circle for scale. (B) Close-up photograph of FA7, shows rhythmically interlaminated sandy siltstones and mudstones. (C) Close-up photograph of FA7, shows intensely bioturbated mudstones.

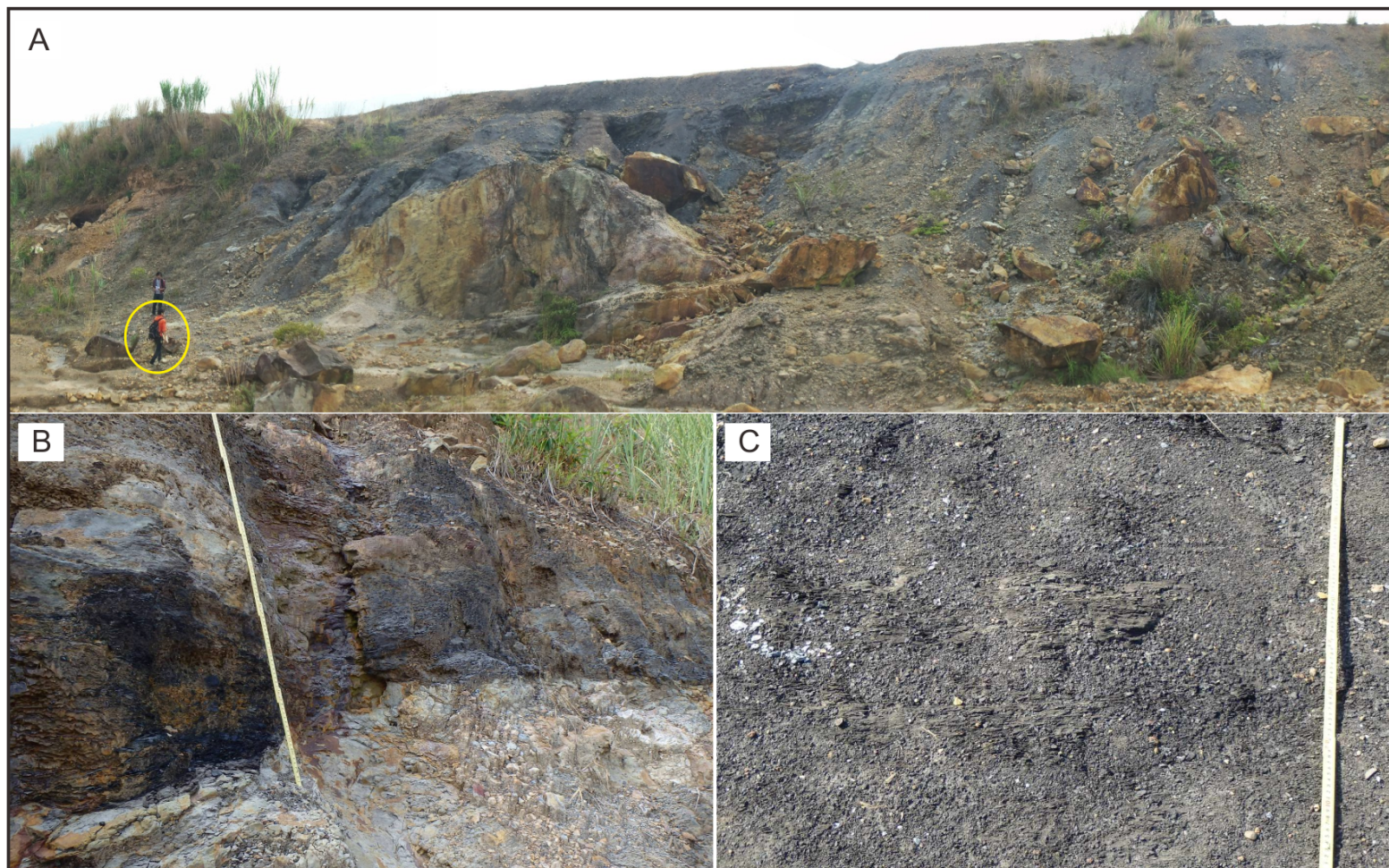


Fig. 17. (A) Outcrop photograph of interbedded dark-coloured, organic-rich mudstones with plant fragments facies (FA8). Person with yellow circle for scale. (B) Close-up photograph of FA8, showing black-coloured, plate-like laminated organic rich mudstones. (C) Close-up photograph of FA8, showing carbonaceous mudstones with papery parting.

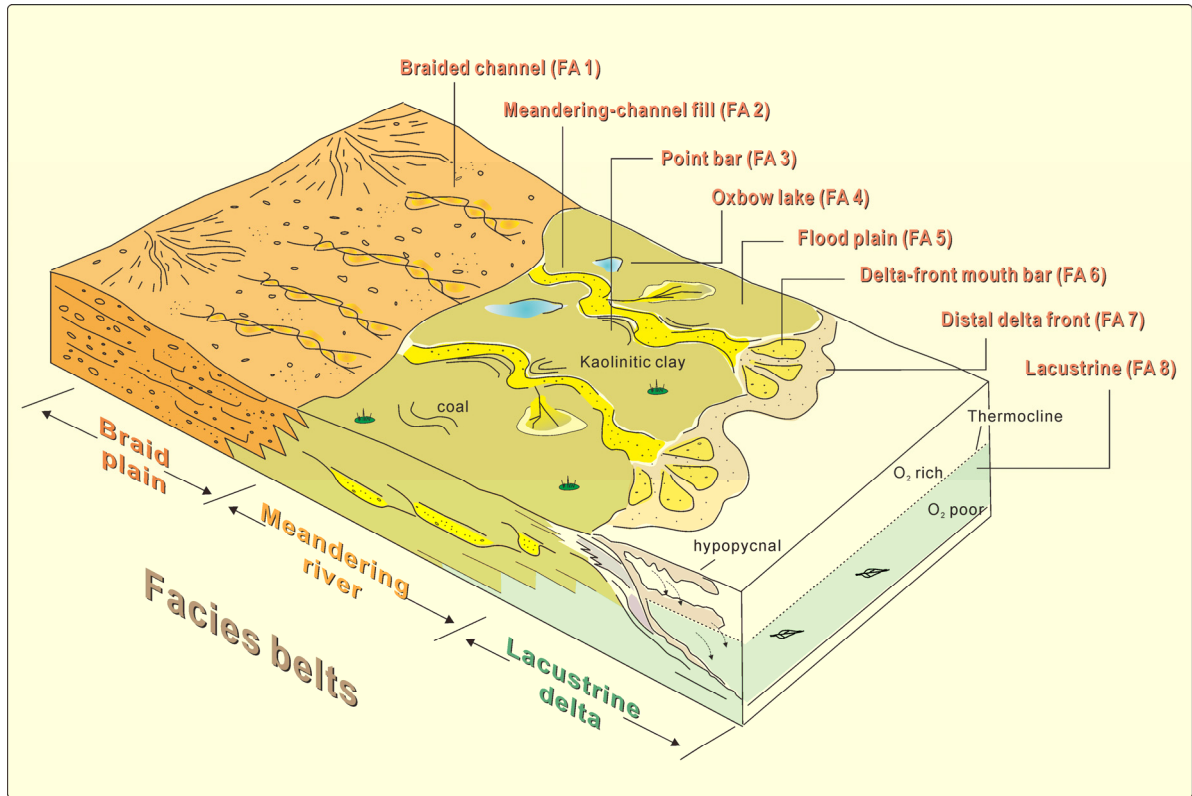


Fig. 18. Schematic diagram illustrating a generalized model of nonmarine depositional system and facies belts in the Bayah Formation in the study area. Relationships between facies associations and facies belts are shown in this diagram.

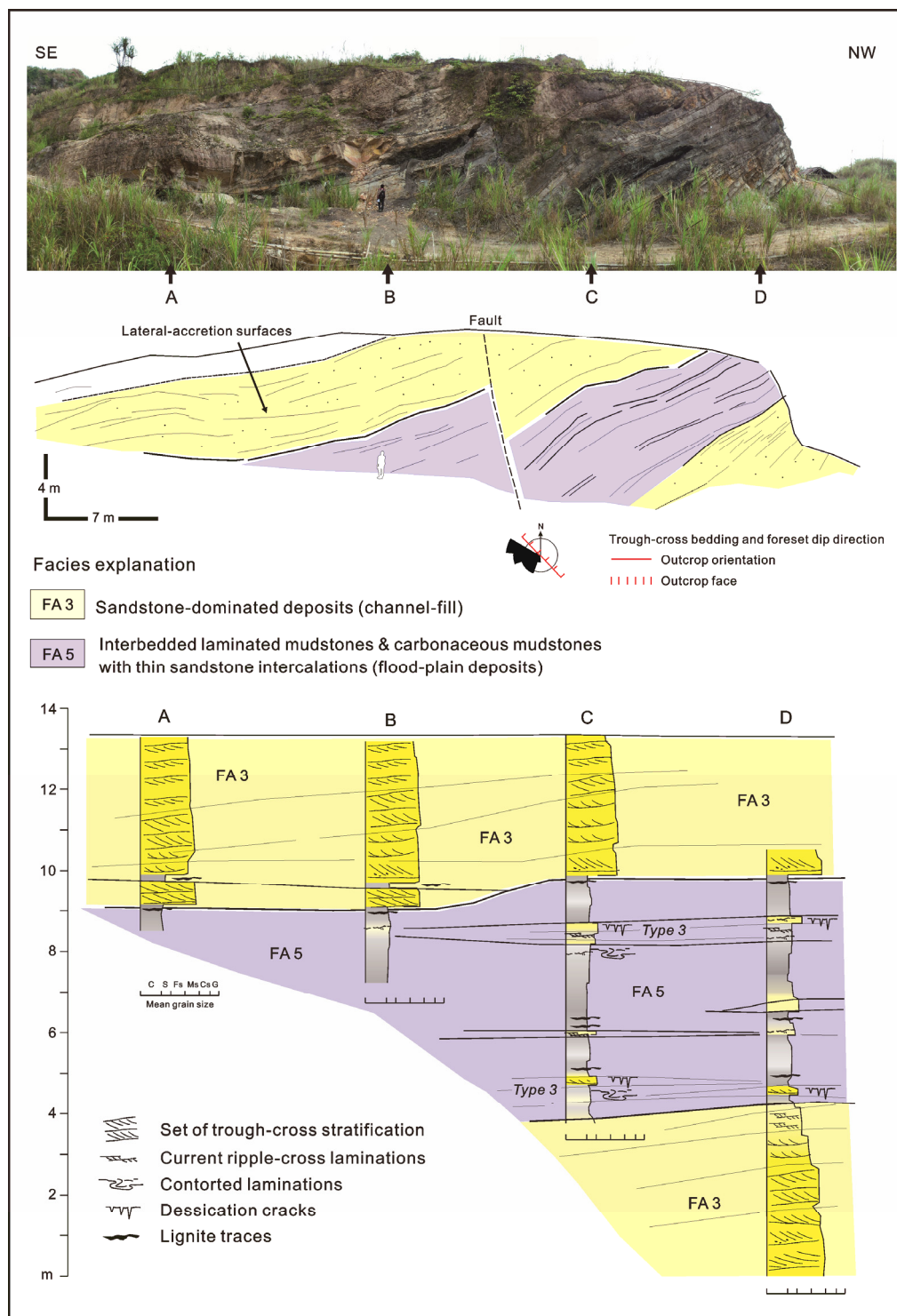


Fig. 19. Diagram composed of photo panel, interpreted outcrop panel, and log section, which show geometry and stratigraphic relationship of facies associations. The outcrop section represents field relationship between FA3 and FA5. Thick FA5 is encased in FA3. Inclined bedding represents lateral accretion of bar deposits characterizing FA3. Thin type 3 sandstone intercalations present in this FA5.

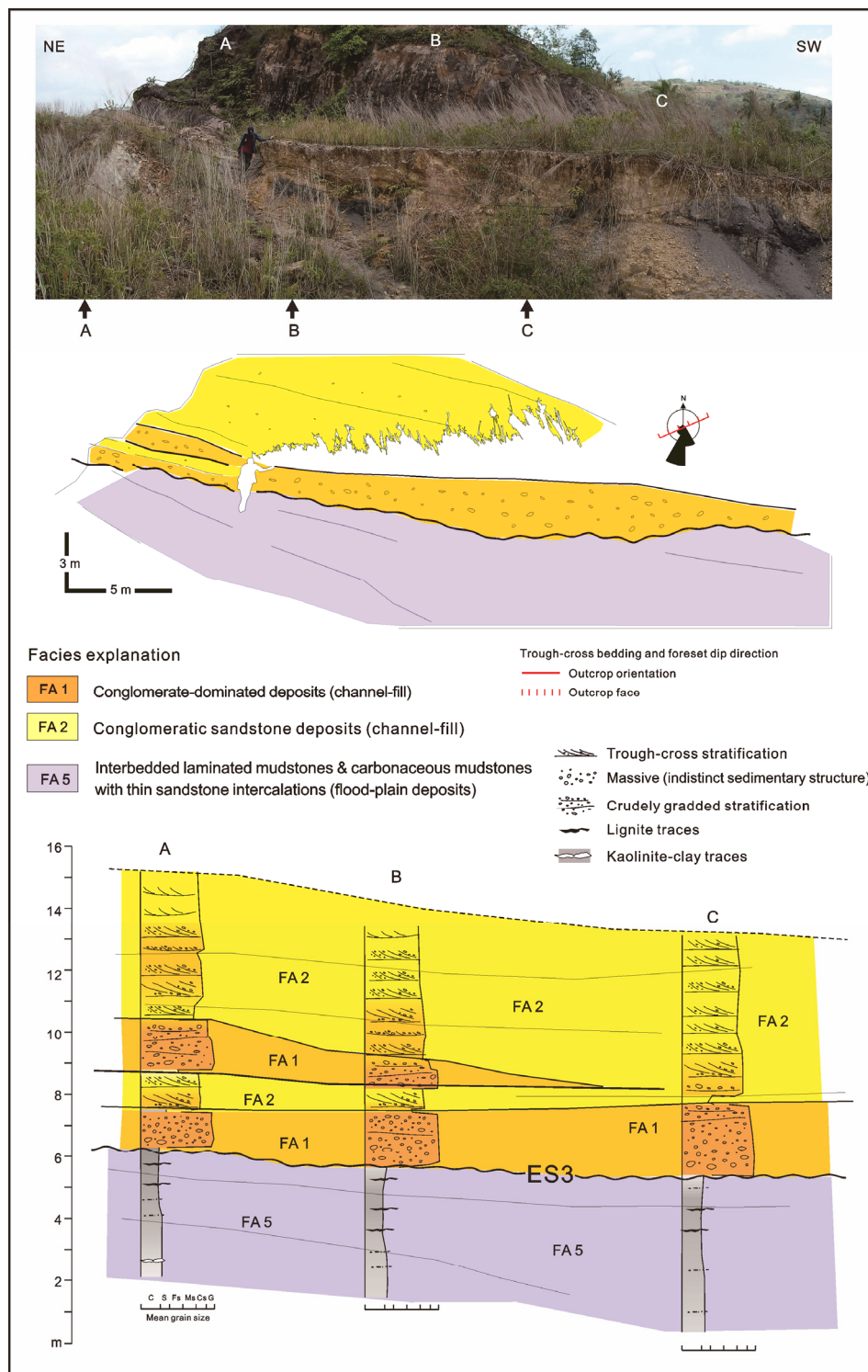


Fig. 20. Diagram composed of photo panel, interpreted outcrop panel, and log section, which show geometry and stratigraphic relationship of facies associations. The outcrop section shows the field relationships between FA1, FA2, and FA5. Distinct erosional surfaces that mark the base of intervals in the base of FA1, which incised into FA5 mudstones.

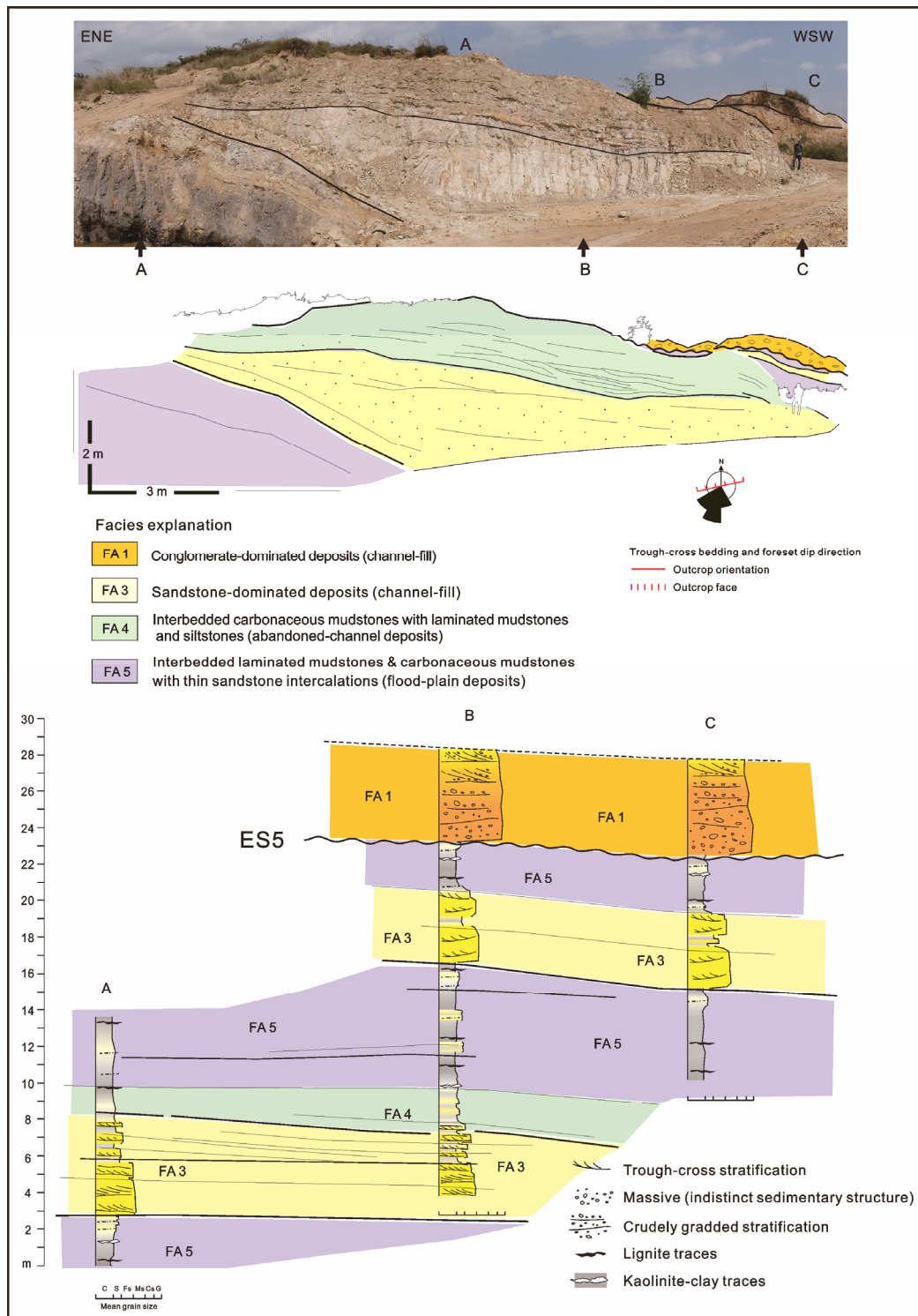


Fig. 21. Diagram composed of photo panel, interpreted outcrop panel, and log section, which show geometry and stratigraphic relationship of facies associations. The outcrop section represents field relationships between FA1, FA3, FA4, and FA5. Fining-upward sandstone deposits of FA3 in the lower part were underlain by mudstone of FA4, and fine upward into FA5 mudstone of floodplain deposits.

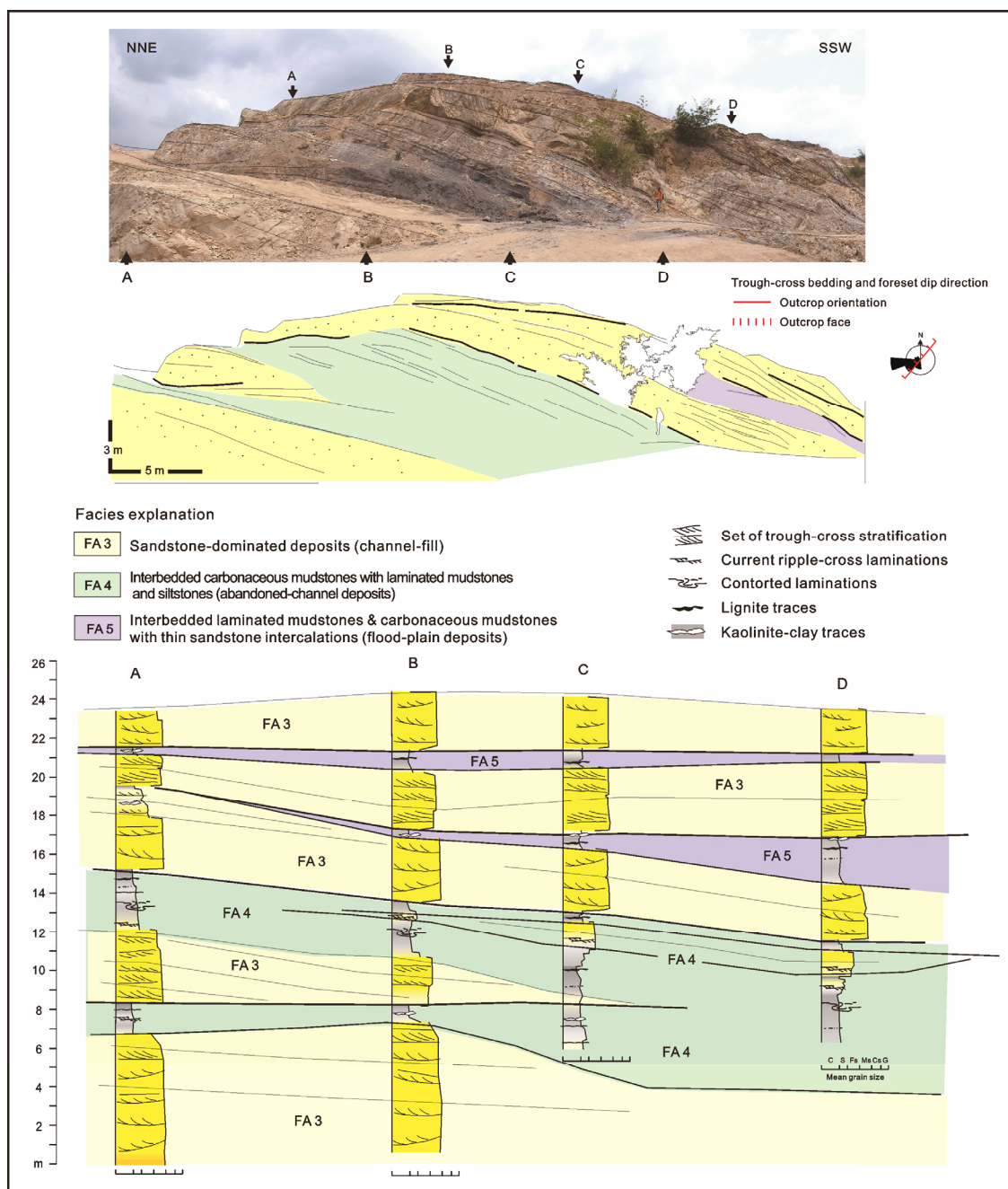


Fig. 22. Diagram composed of photo panel, interpreted outcrop panel, and log section, which show geometry and stratigraphic relationship of facies associations. The outcrop section represents field relationships between FA3, FA4, and FA5. The lateral-offset stacking between the lower FA3 package and the upper FA3 package are characterized by the presence of transitional deposits that consists of interbedded laterally accreted deposits of FA4 mudstones.

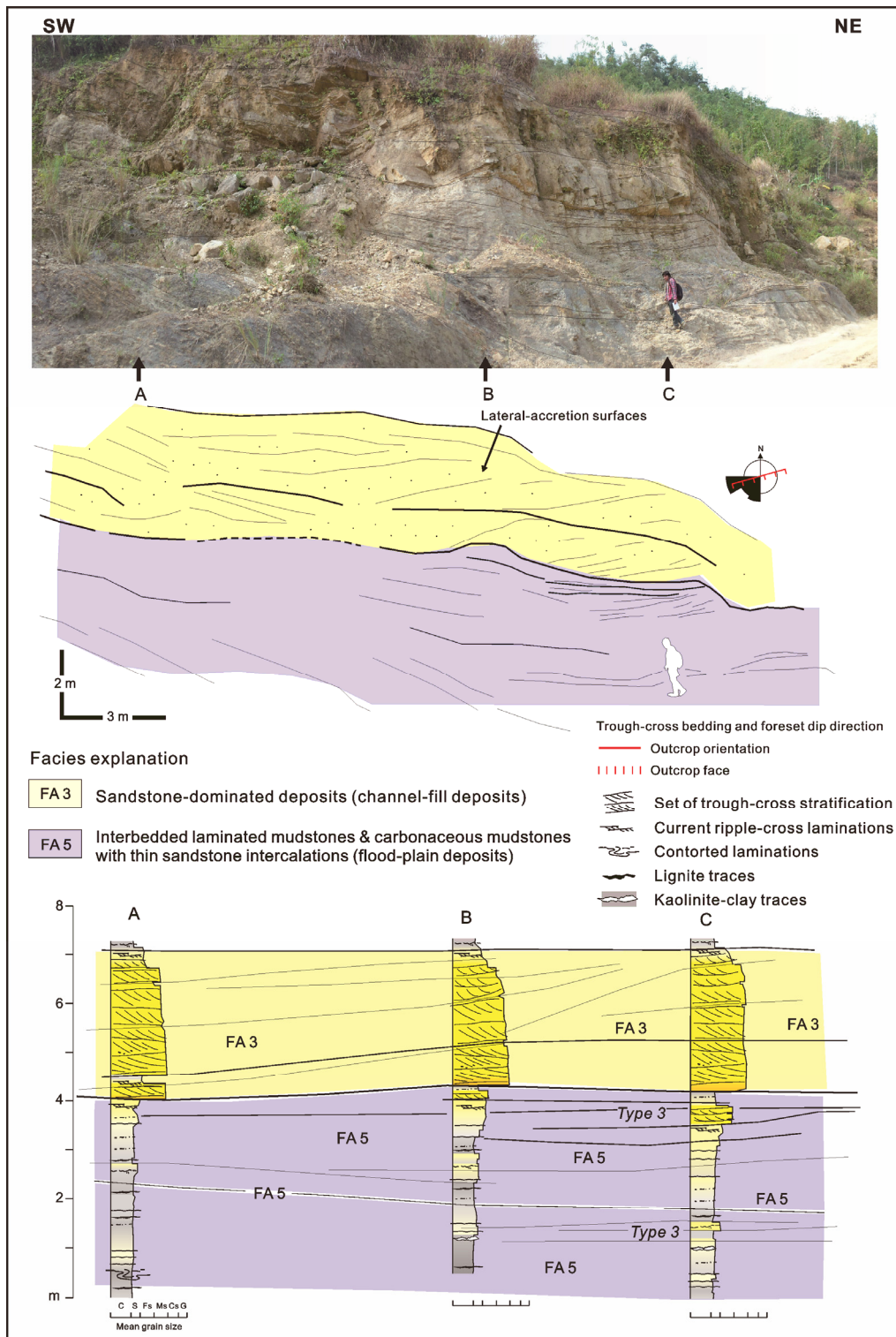


Fig. 23. Diagram composed of photo panel, interpreted outcrop panel, and log section, which show geometry and stratigraphic relationship of facies associations. The outcrop section represents field relationships between FA3 and FA5. The log section shows coarsening-upward mudstone-dominated deposits of FA5 in the lower part and change upward into the laterally accreted deposits in the FA5 sandstones.

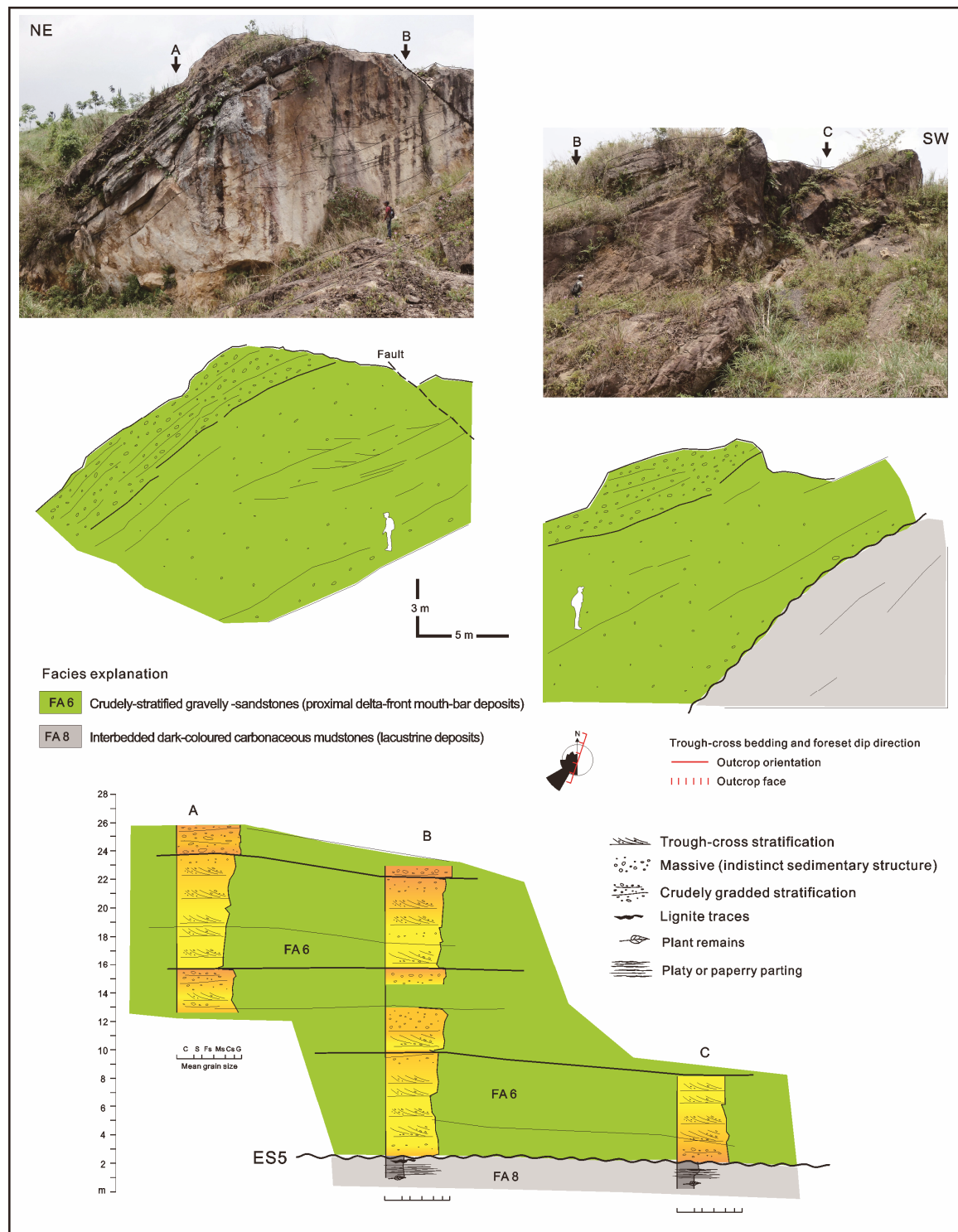


Fig. 25. Diagram composed of photo panel, interpreted outcrop panel, and log section, which show geometry and stratigraphic relationship of facies associations. The outcrop section represents vertically stacked relationships between FA6 in the lower part, which incised into the underlying FA8 mudstones.

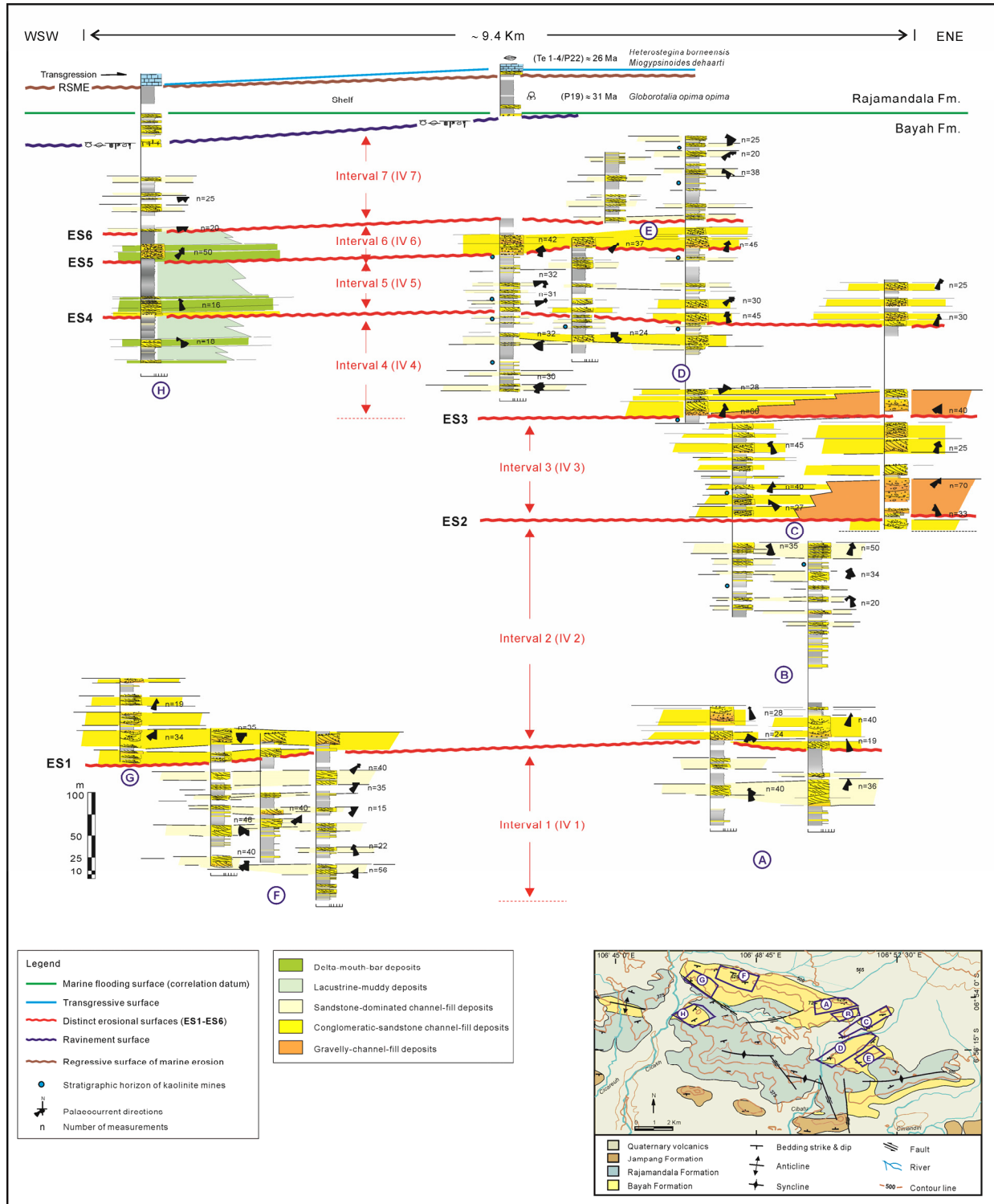


Fig. 26. Stratigraphic correlation of the fluvial–lacustrine–delta succession of the Bayah Formation. The succession is divided into 7 intervals (IV1–IV7 in ascending order) based on mapping of 6 distinct erosional surfaces (ESs) (i.e., ES1 to ES6 in ascending order). These erosional surfaces are defined in the base of channel-fill or mouth-bar deposits, which are coarser than those developed beneath each erosional surface. Inset map in the lower right shows locations of measured sections.

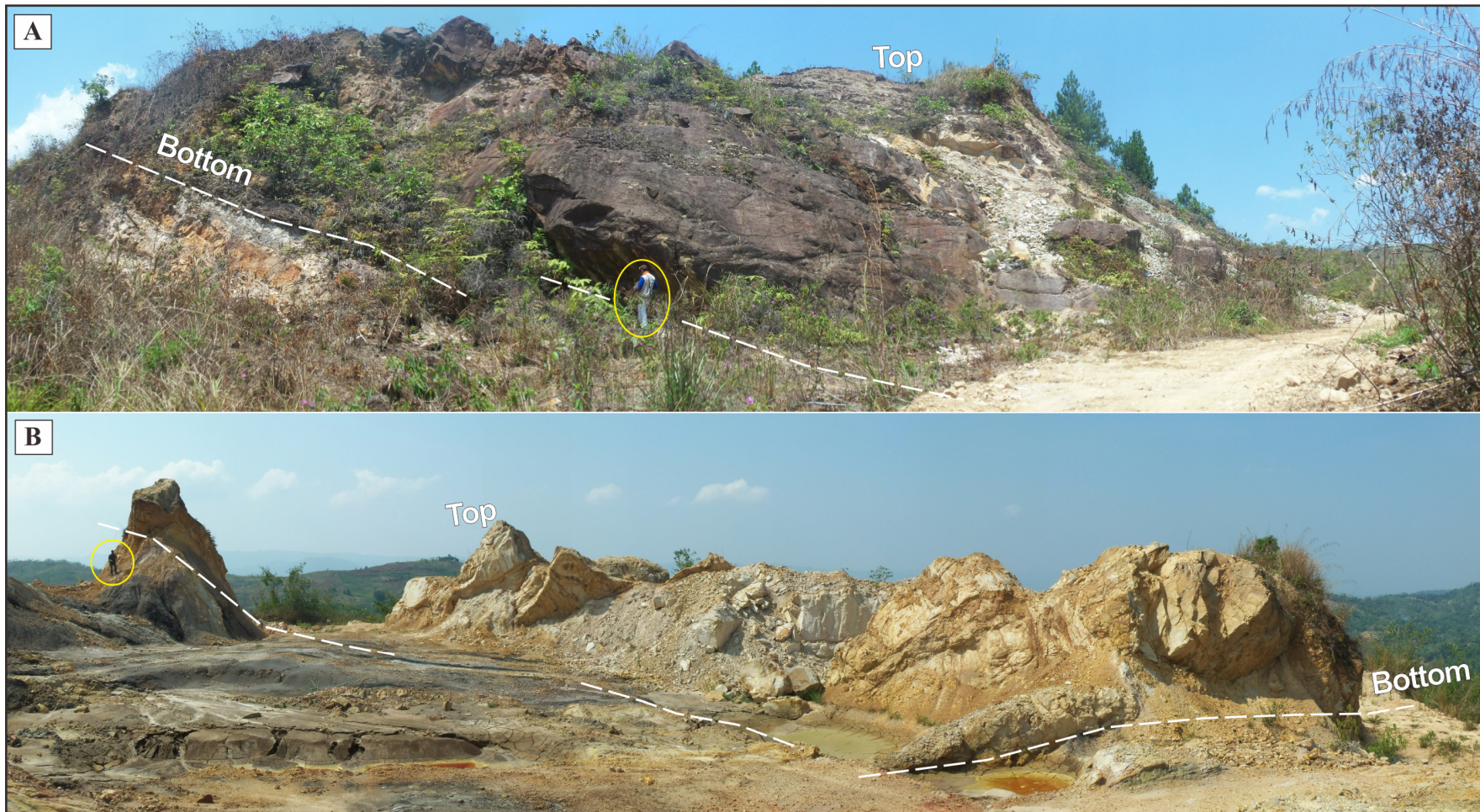


Fig. 27. (A–B) Example of distinct erosional surfaces at the base of the intervals (ES1 and ES5). These erosional surfaces are defined in the base of channel-fill deposits (FA2 and FA1), which are coarser than those developed beneath each erosional surface.

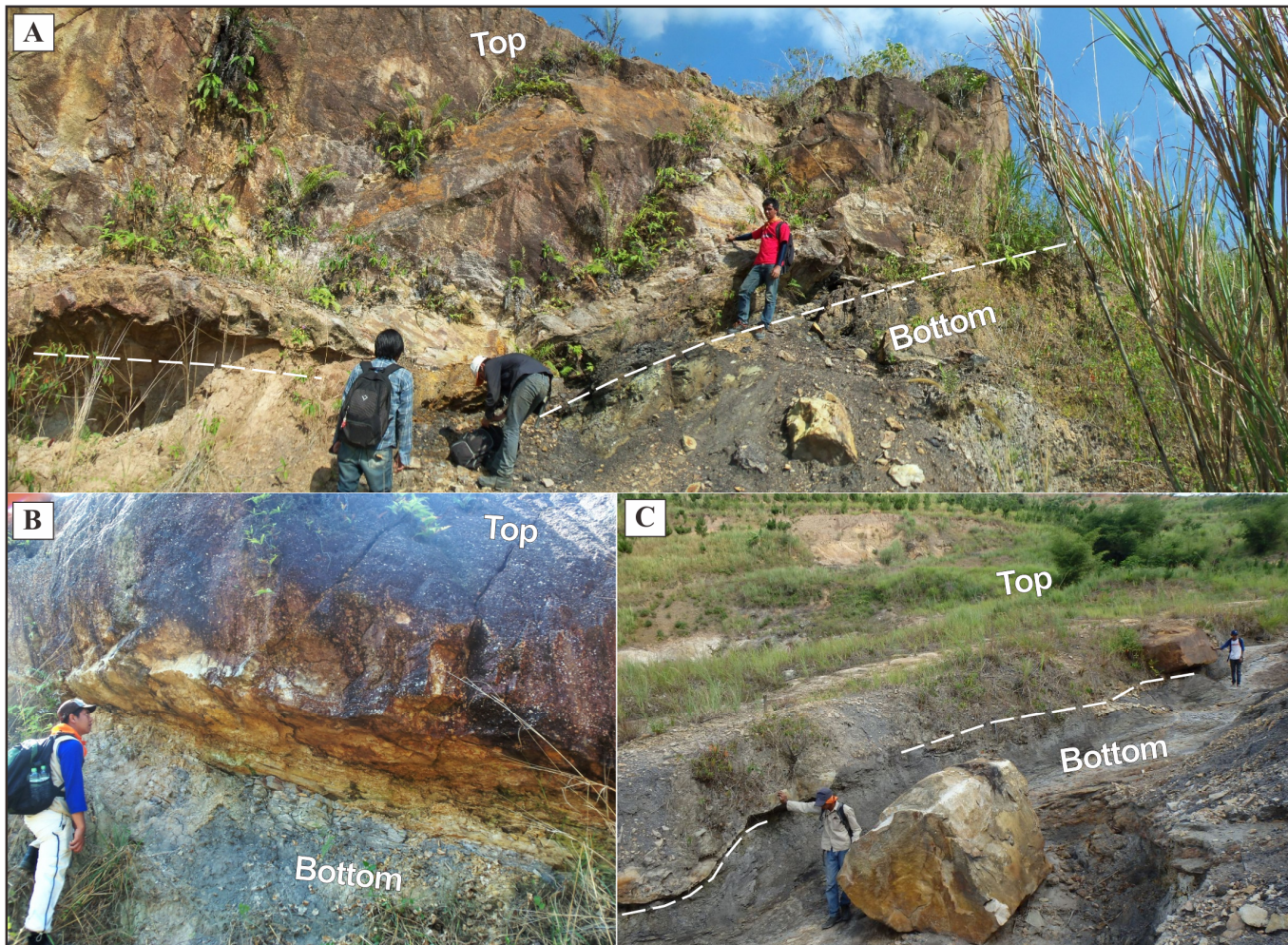


Fig. 28. (A–C) Example of distinct erosional surfaces at the base of the intervals (ES5, ES3, and ES4). In addition to the presence of coarse-grained facies, which developed above the mudstone facies, the distinct erosional surfaces are also characterized by distinct scouring surfaces (A and C).

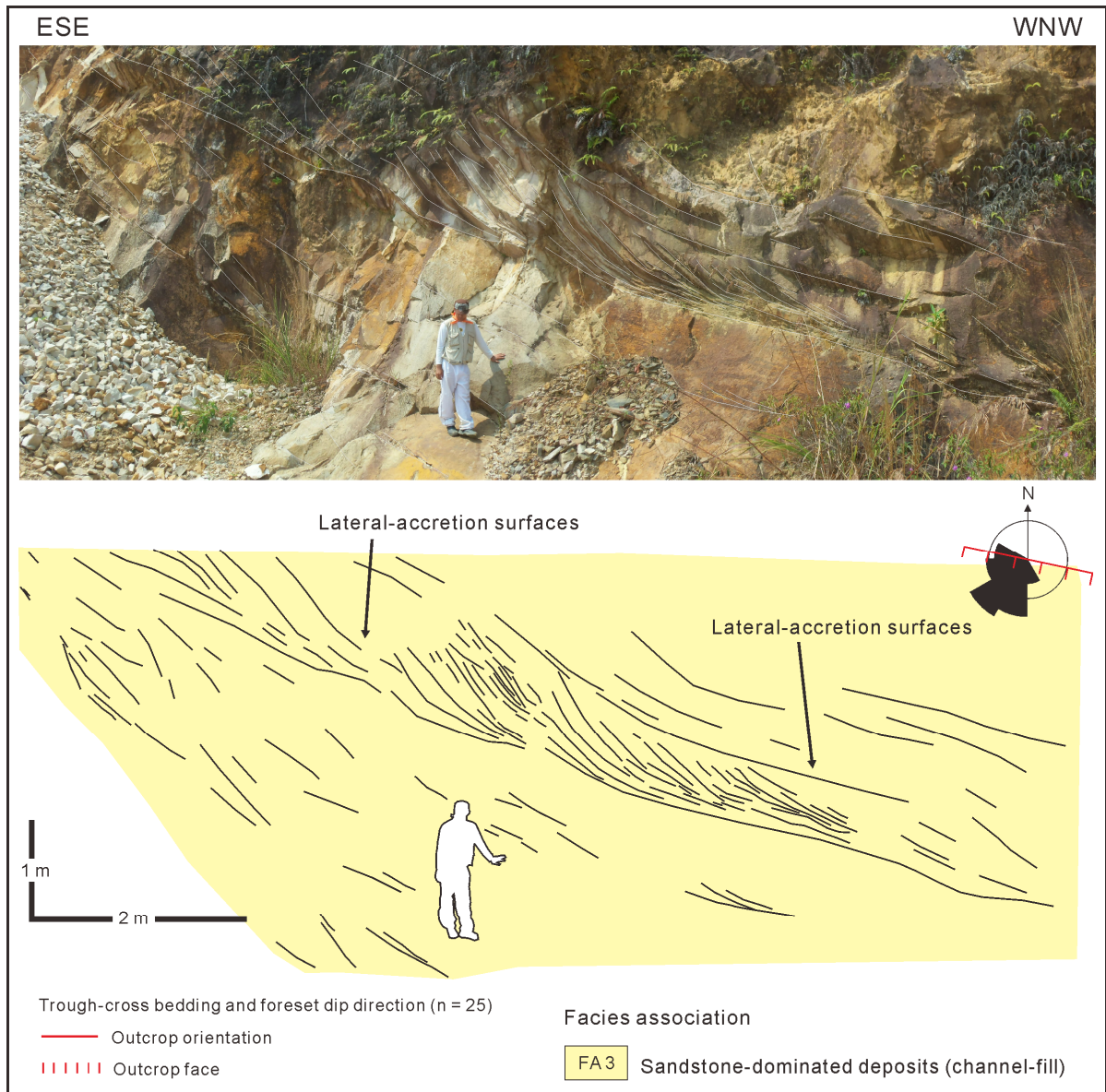


Fig. 29. Interpreted outcrop panel showing larger-scale inclined stratifications, which consist of smaller-scale laterally accreted deposits. These deposits are commonly associated with FA3 and show both tabular and lenticular external geometry. This outcrop is situated within the interval 1 (IV1).

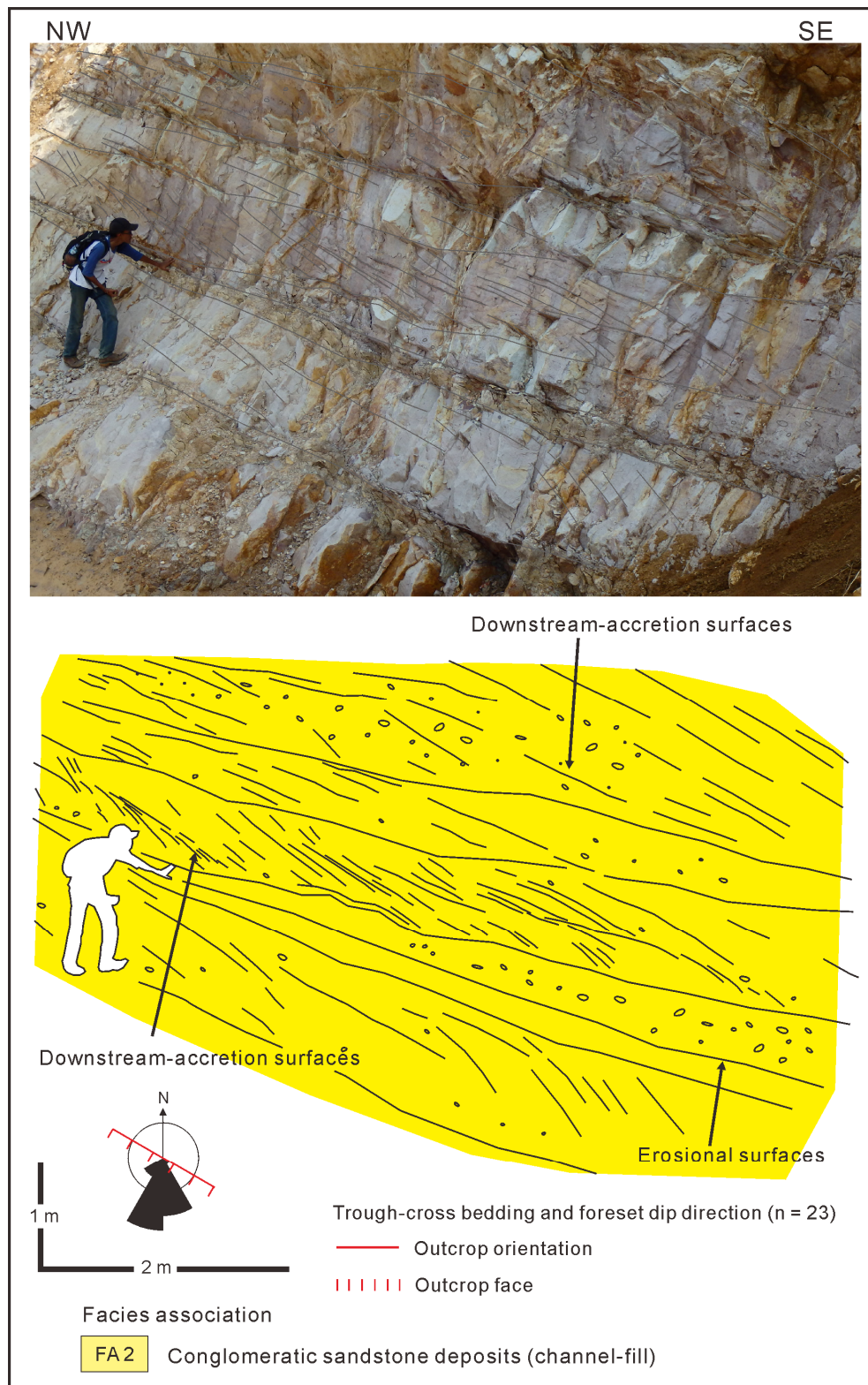


Fig. 30. Interpreted outcrop panel showing composite sets of cross-stratification, which represent downstream-accreted deposits. These deposits are associated with FA2 and show tabular geometry. This type of deposits is common in the lower part of the interval 2 (IV2).

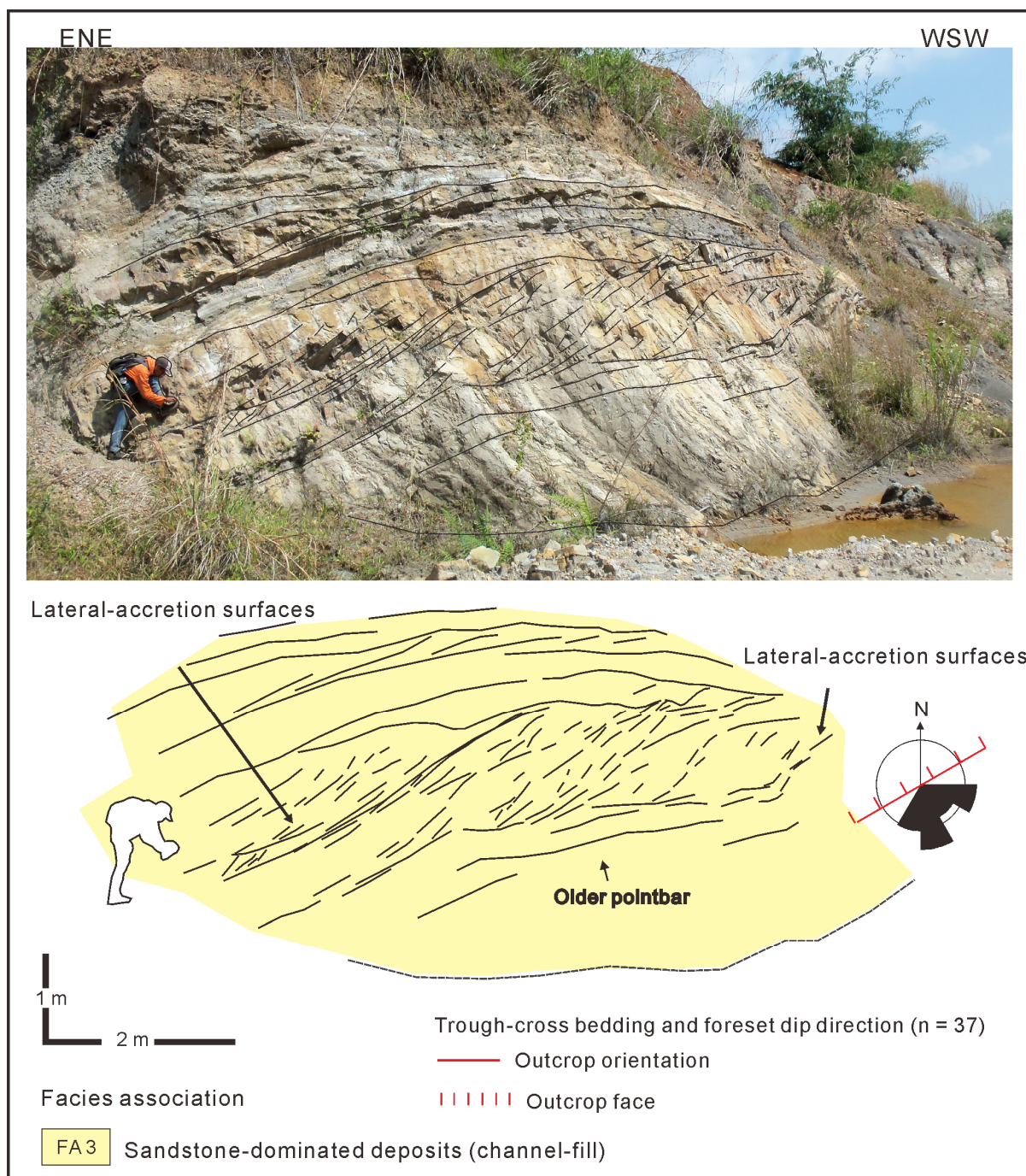


Fig. 31. Interpreted outcrop panel showing large-scale inclined stratifications, which consist of smaller-scale laterally accreted deposits. These deposits are associated with FA3 and show lenticular geometry. These laterally accreted sandstones are interbedded with mudstones in the upper part. This type of deposits is common in the upper part of the interval 2 (IV2).

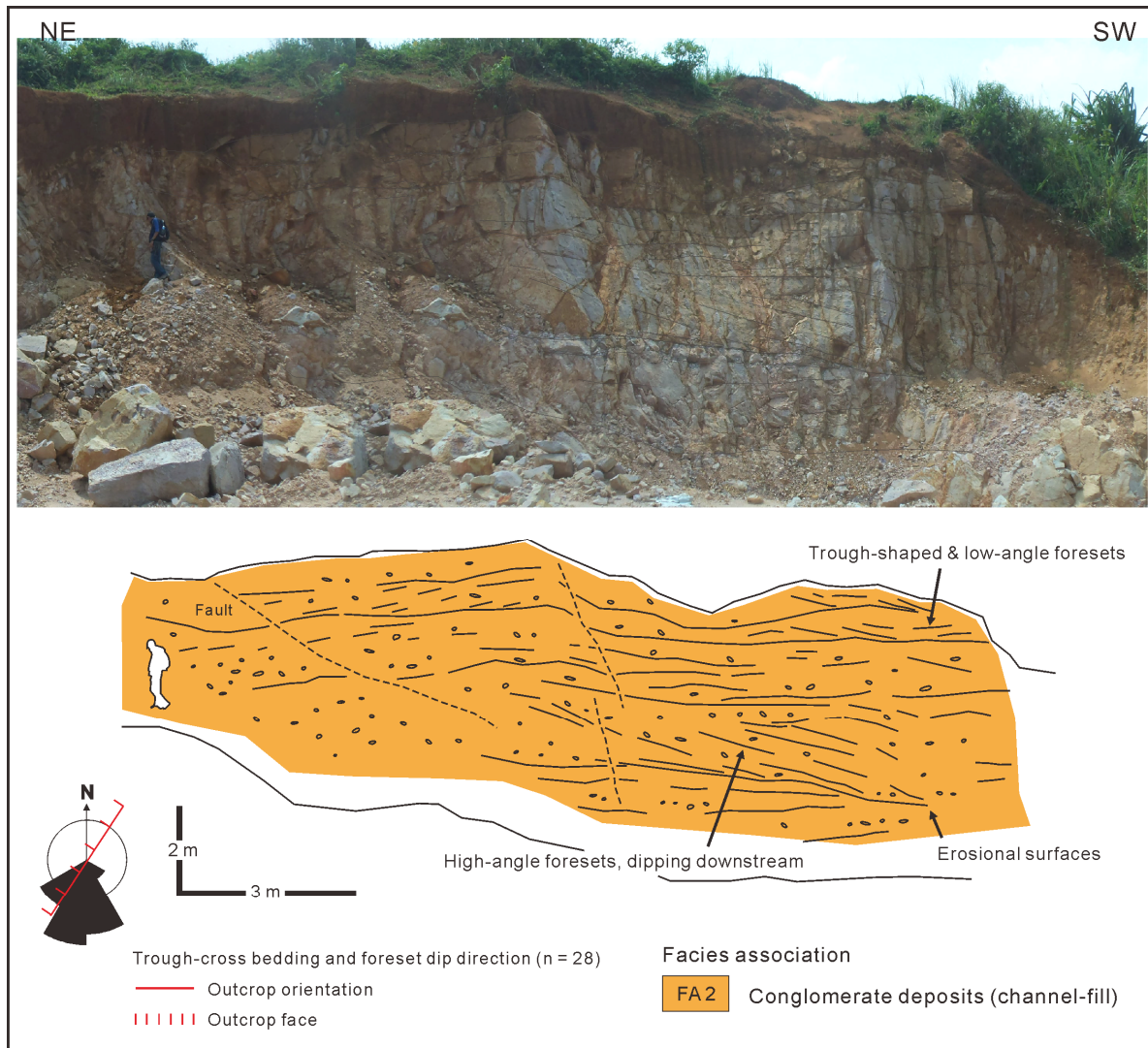


Fig. 32. Interpreted outcrop panel showing thick high-angled foreset cross-stratifications that represent downstream-accreted deposits. These deposits are associated with FA1 and show sheet-like, and tabular geometry. This type of deposits is common in the interval 3 (IV3).

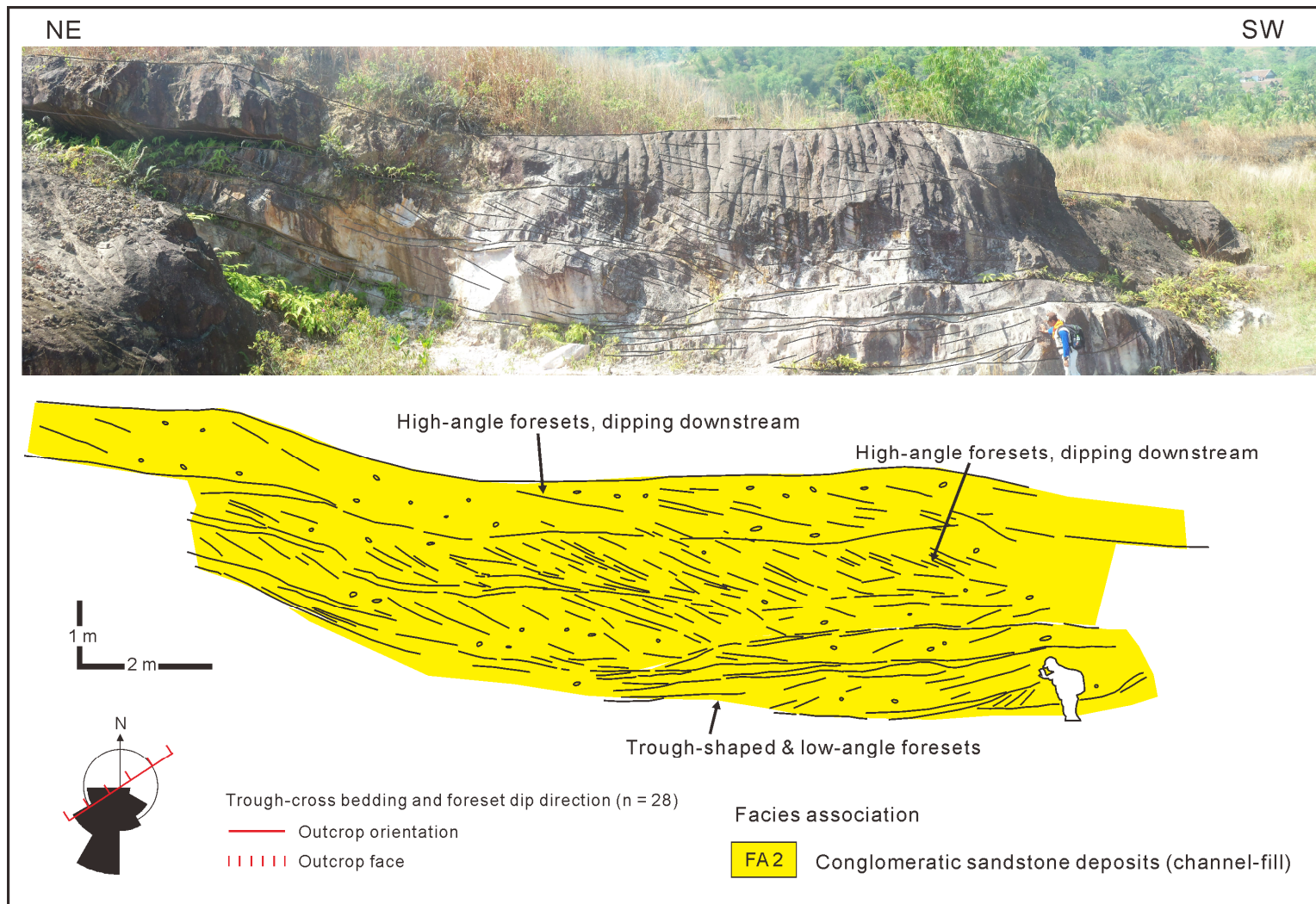


Fig. 33. Interpreted outcrop panel showing composite sets of cross-stratification, which represents downstream-accreted deposits. These deposits are associated with FA2 and show tabular geometry. This type of deposits is common in the interval 4 (IV4).

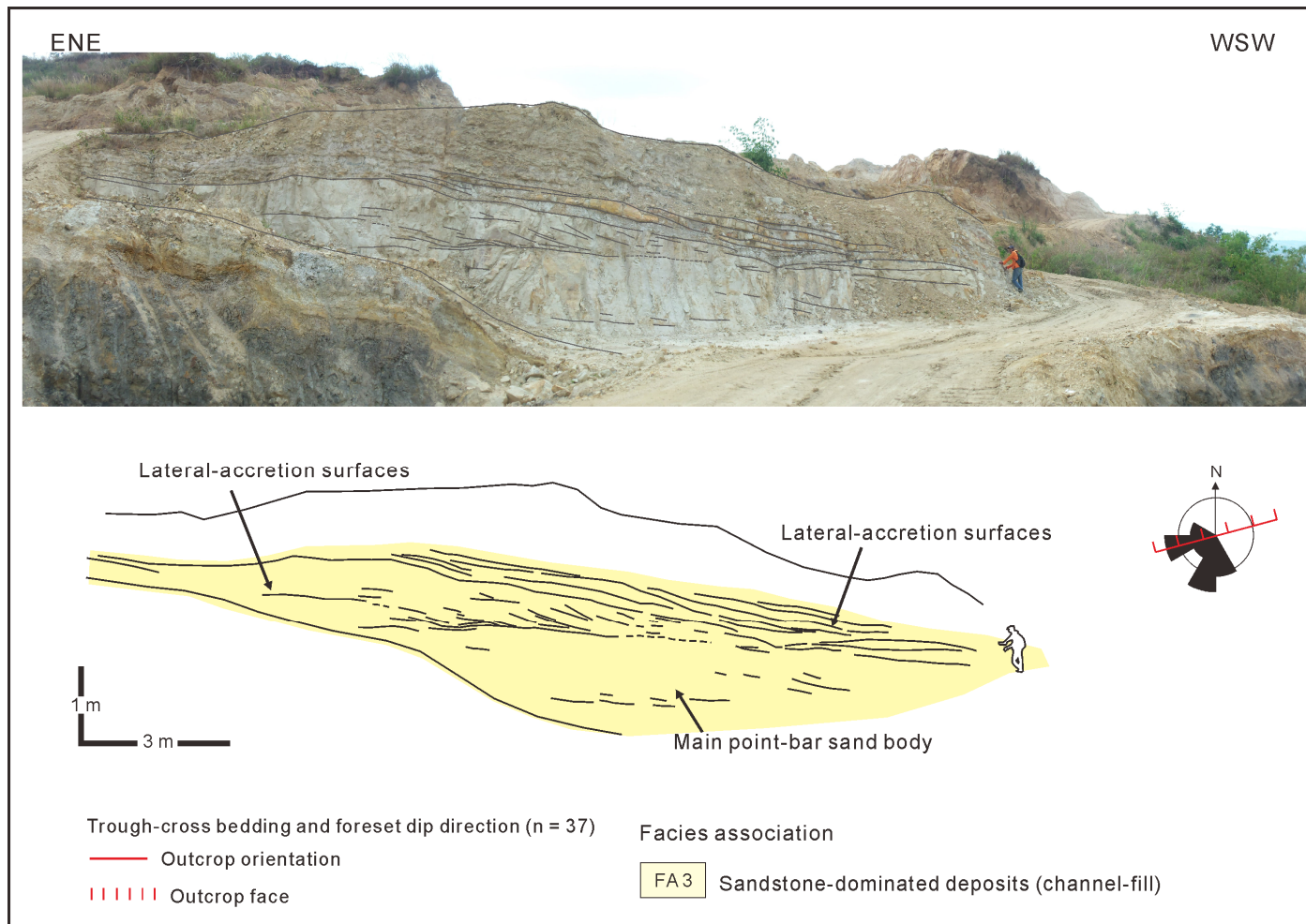


Fig. 34. Interpreted outcrop panel showing large-scale inclined stratifications in the lower part and composite sets of cross-stratification, which represents laterally accreted deposits. These deposits are associated with FA3 and show lenticular geometry. These laterally accreted sandstones are interbedded with mudstones in the upper part. This type of deposits is common in the interval 5 (IV5).

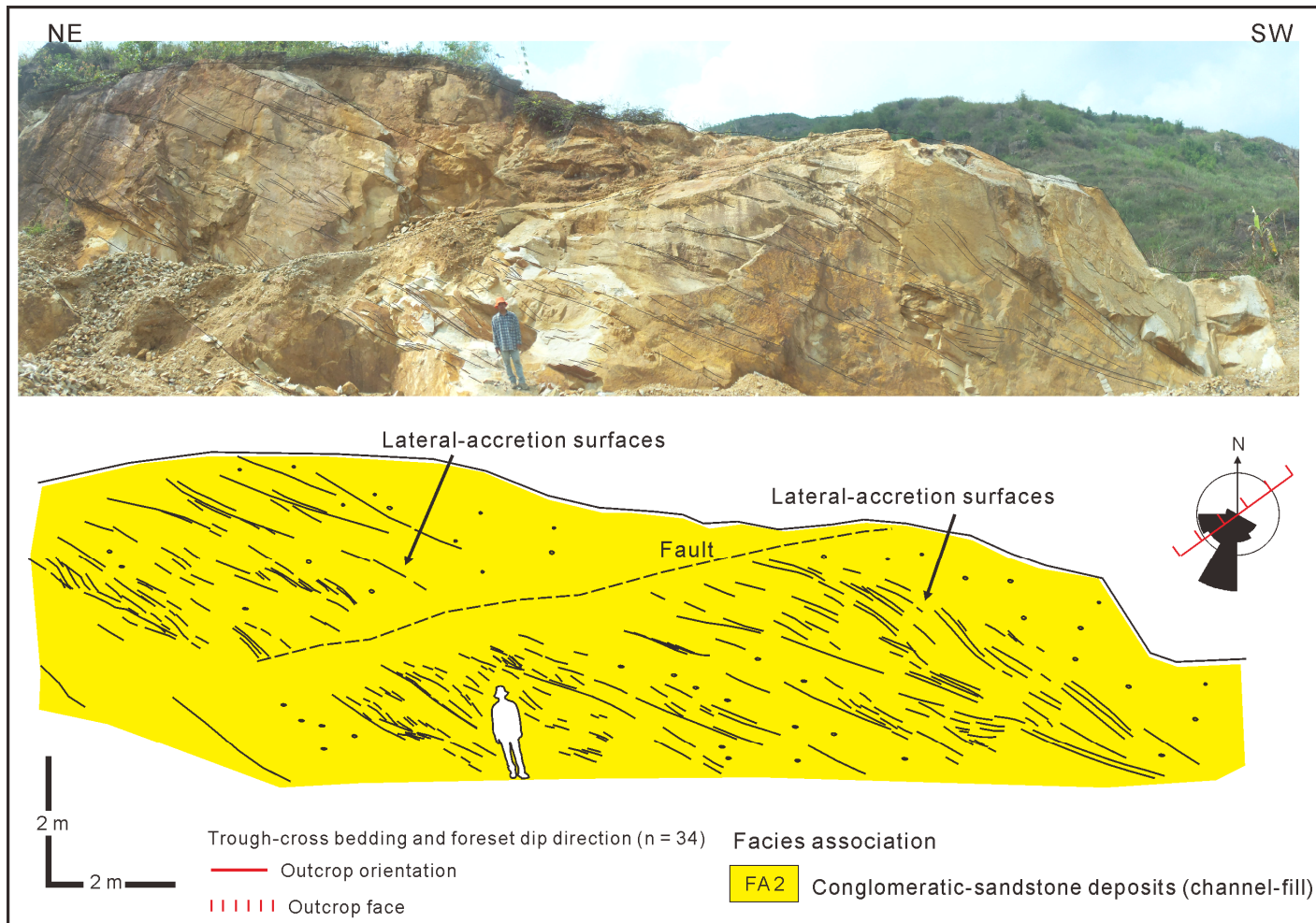


Fig. 35. Interpreted outcrop panel showing large-scale inclined stratifications, which consist of smaller-scale laterally accreted deposits. These deposits are associated with FA2 and show tabular geometry. This type of deposits is common in the upper part of the interval 6 (IV6).

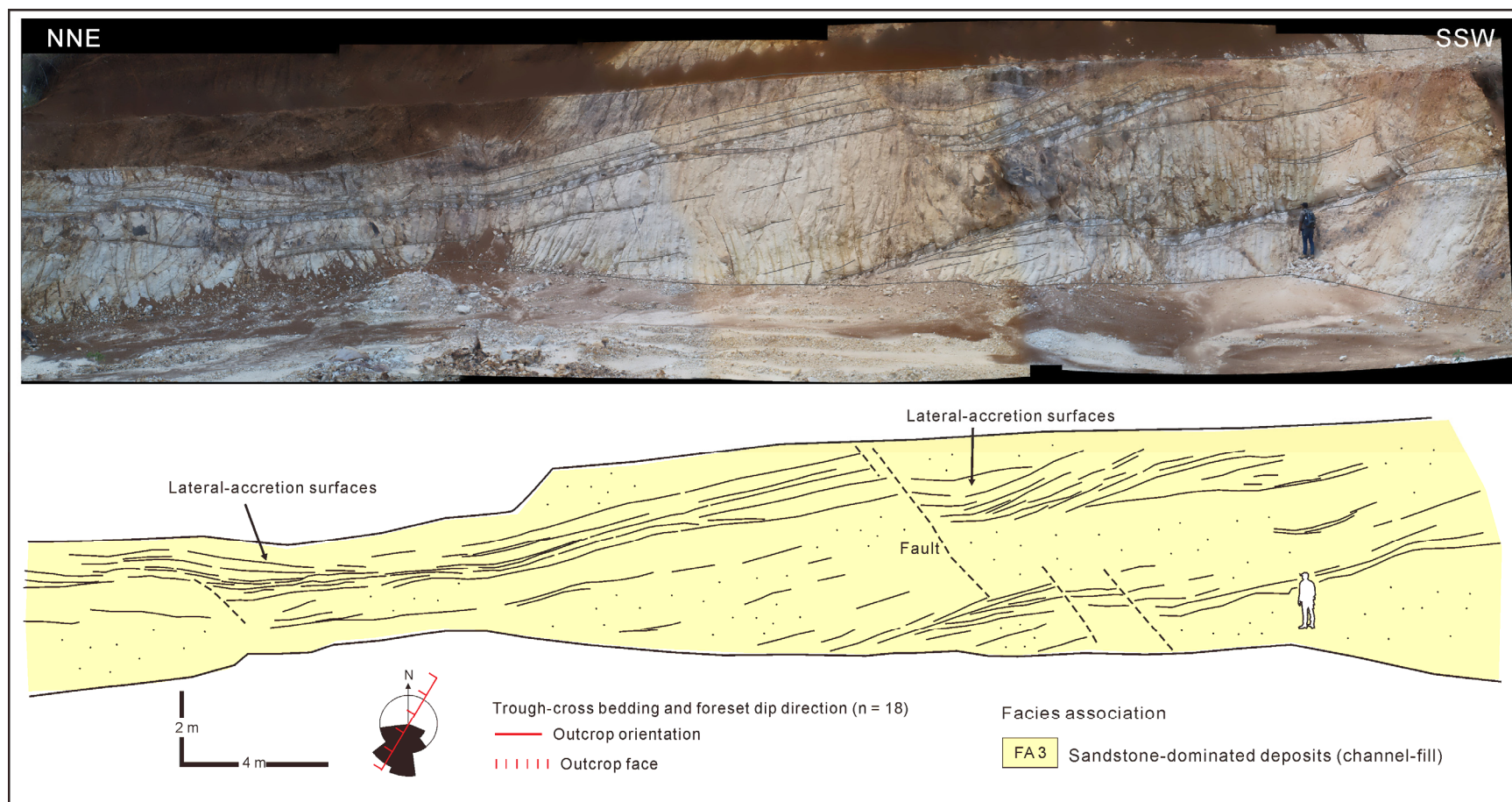


Fig. 36. Interpreted outcrop panel showing large-scale inclined stratifications, which consist of smaller-scale laterally accreted deposits. These deposits are associated with FA3 and show tabular and lenticular geometry. The laterally accreted sandstones are interbedded with mudstones in the upper part. This type of deposits is common in the interval 7 (IV7).

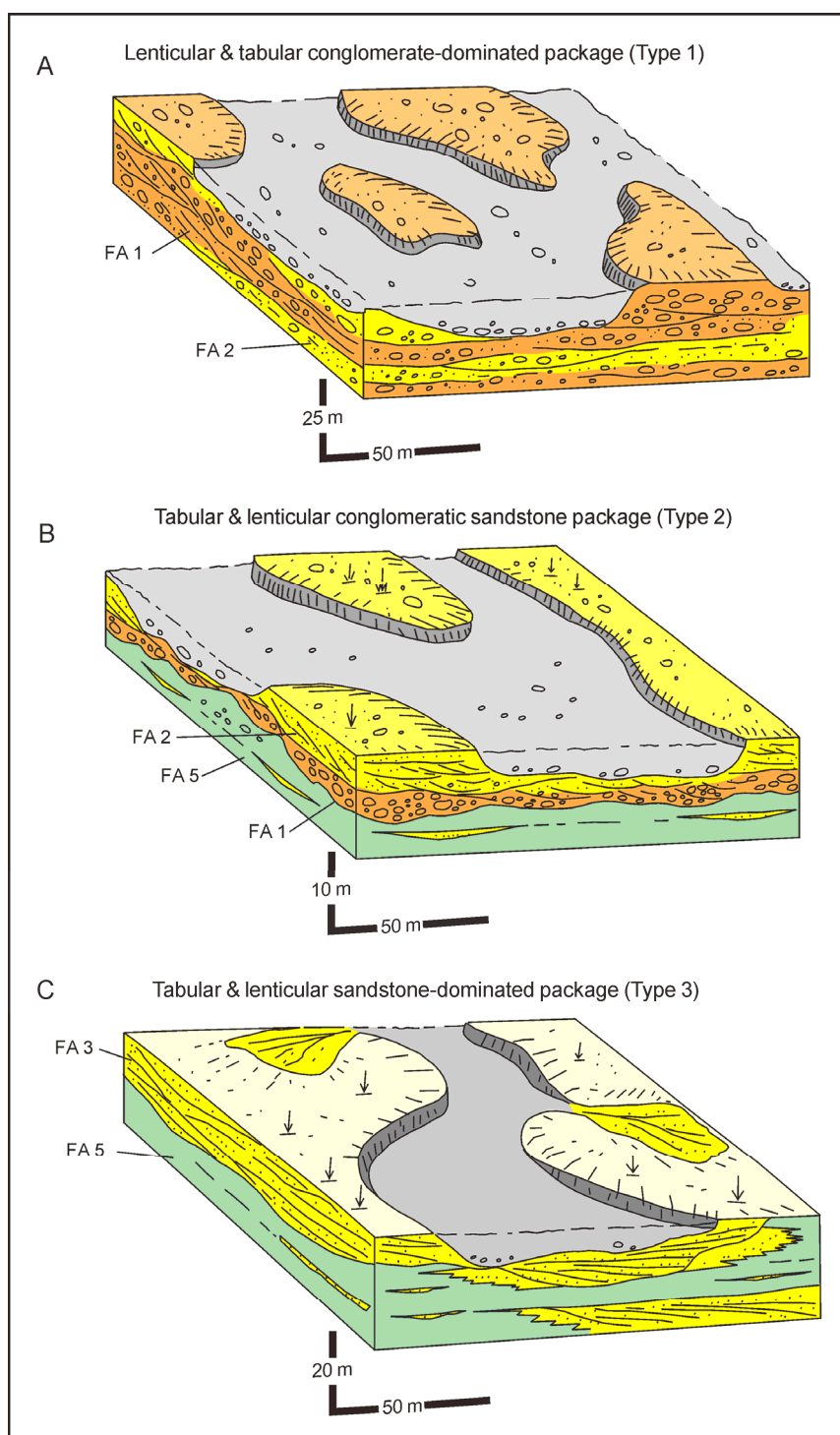


Fig. 37. Schematic block diagram illustrating three types of distinct geometry and style of channel-fill deposits of the Bayah Formation fluvial succession. (A) Lenticular and tabular conglomerate-dominated packages (Type 1 channel-fill deposits). (B) Tabular and lenticular conglomeratic-sandstone packages (Type 2 channel-fill deposits). (C) Tabular and lenticular sandstone-dominated packages (Type 3 channel-fill deposits).

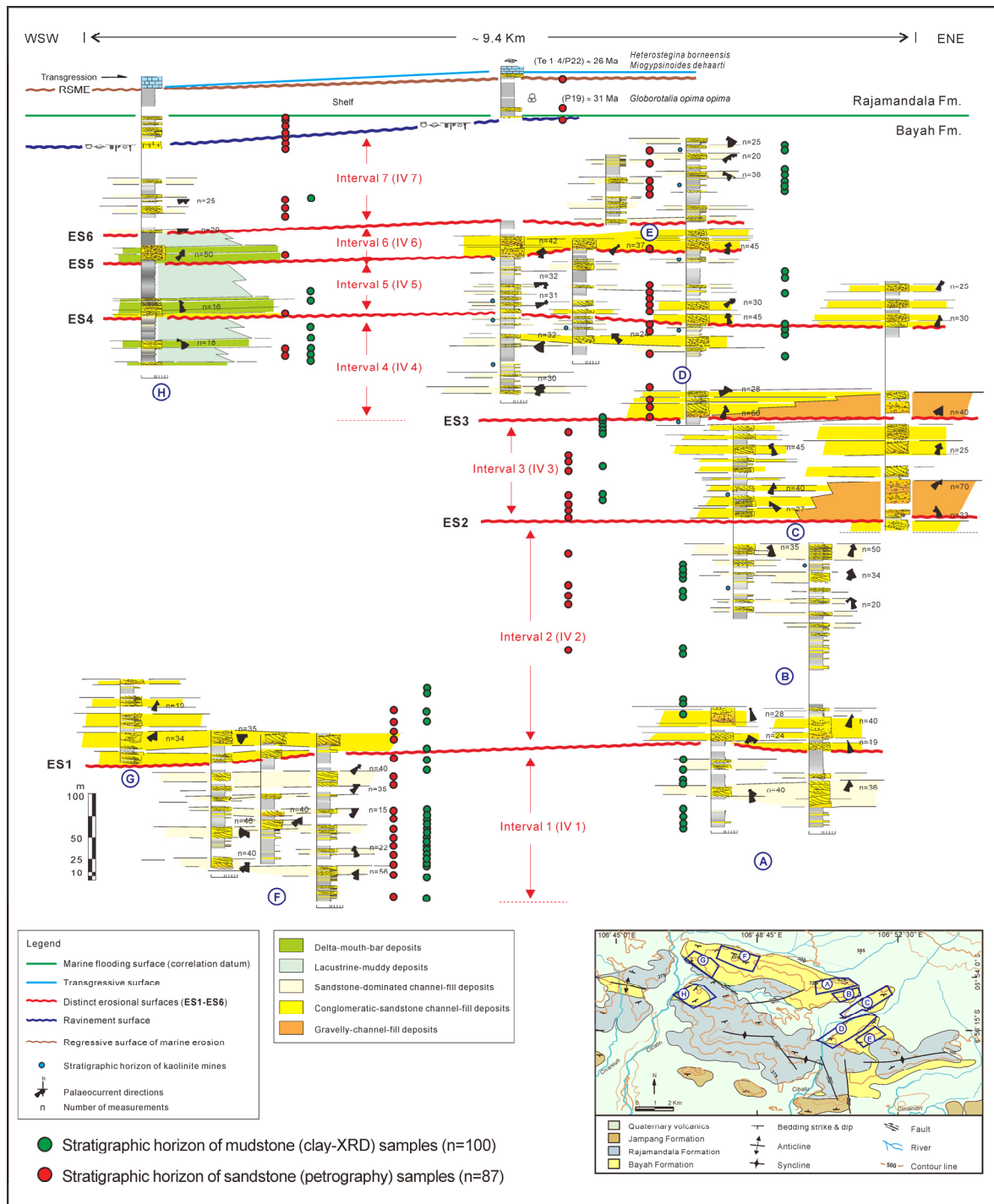


Fig. 38. Stratigraphic positions of rock-samples for laboratory examination. Stratigraphic horizons of mudstone samples for XRD measurement are represented by green-coloured circles, and those of sandstone samples for petrographic examination are represented by red-coloured circles.

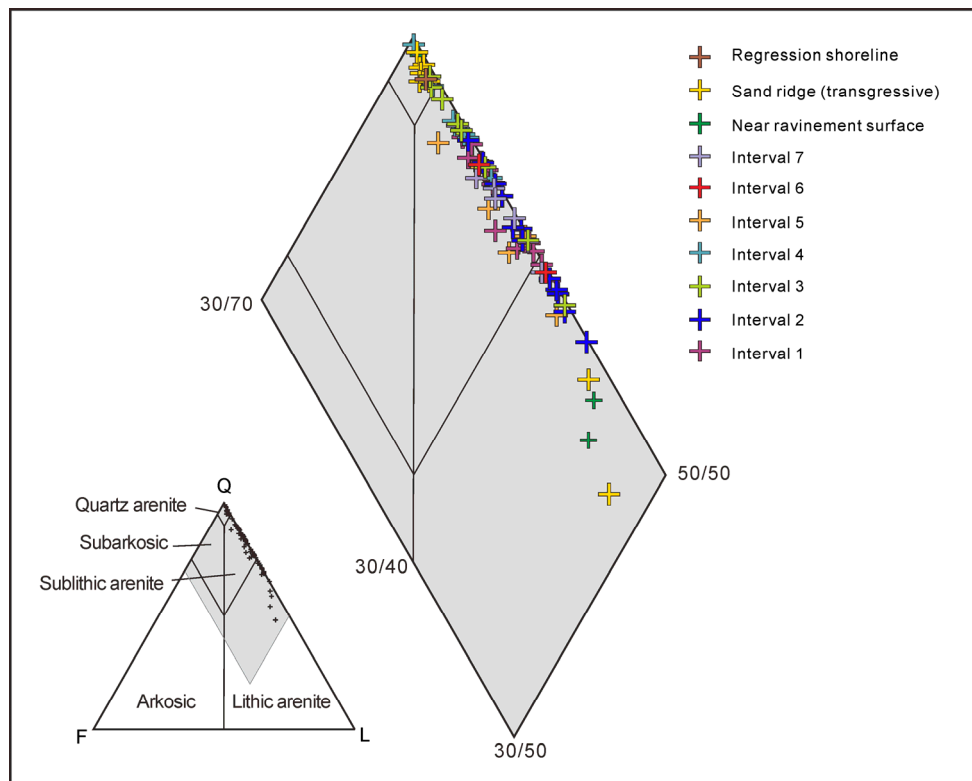


Fig. 39. Ternary sandstone classification diagram (Pettijohn et al., 1987) based on quartz grains (Q), feldspar grains (F) and rock fragments (L). The grey-shade area was enlarged to show the sample subdivision into three compositional types i.e. (1) quartz-arenite sandstones, (2) sublithic-arenite sandstones and (3) lithic-arenite sandstones.

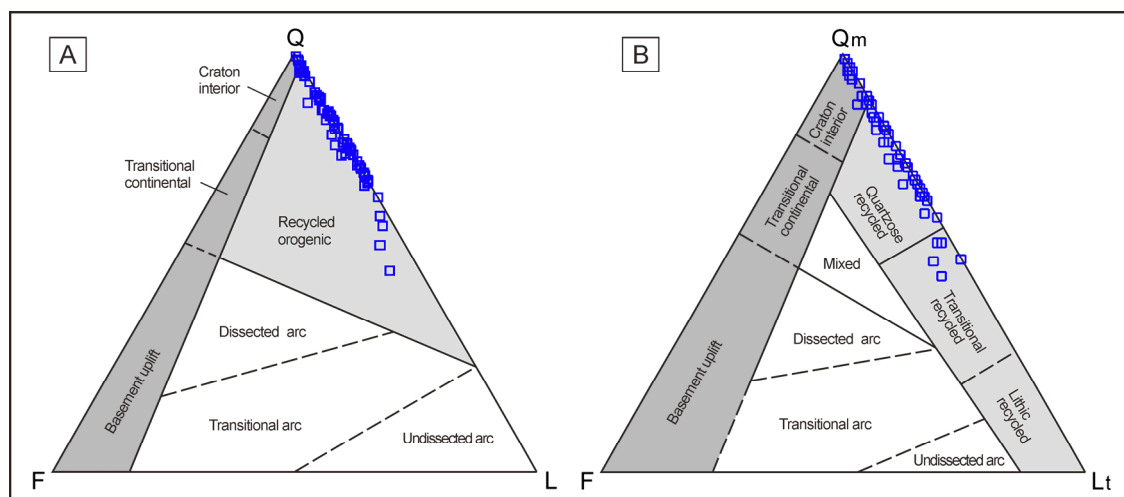


Fig. 40. Ternary sandstone plots to infer provenance types (Dickinson et al., 1983). (A) Plot based on total quartz (Q = monocrystalline quartz + polycrystalline quartz), feldspar (F = K-feldspar + plagioclase) and rock fragment (L). (B) Plot based on quartz monocrystalline (Qm), Feldspar (F = K-feldspar + plagioclase), and total rock fragment (Lt = rock fragment + quartz polycrystalline).

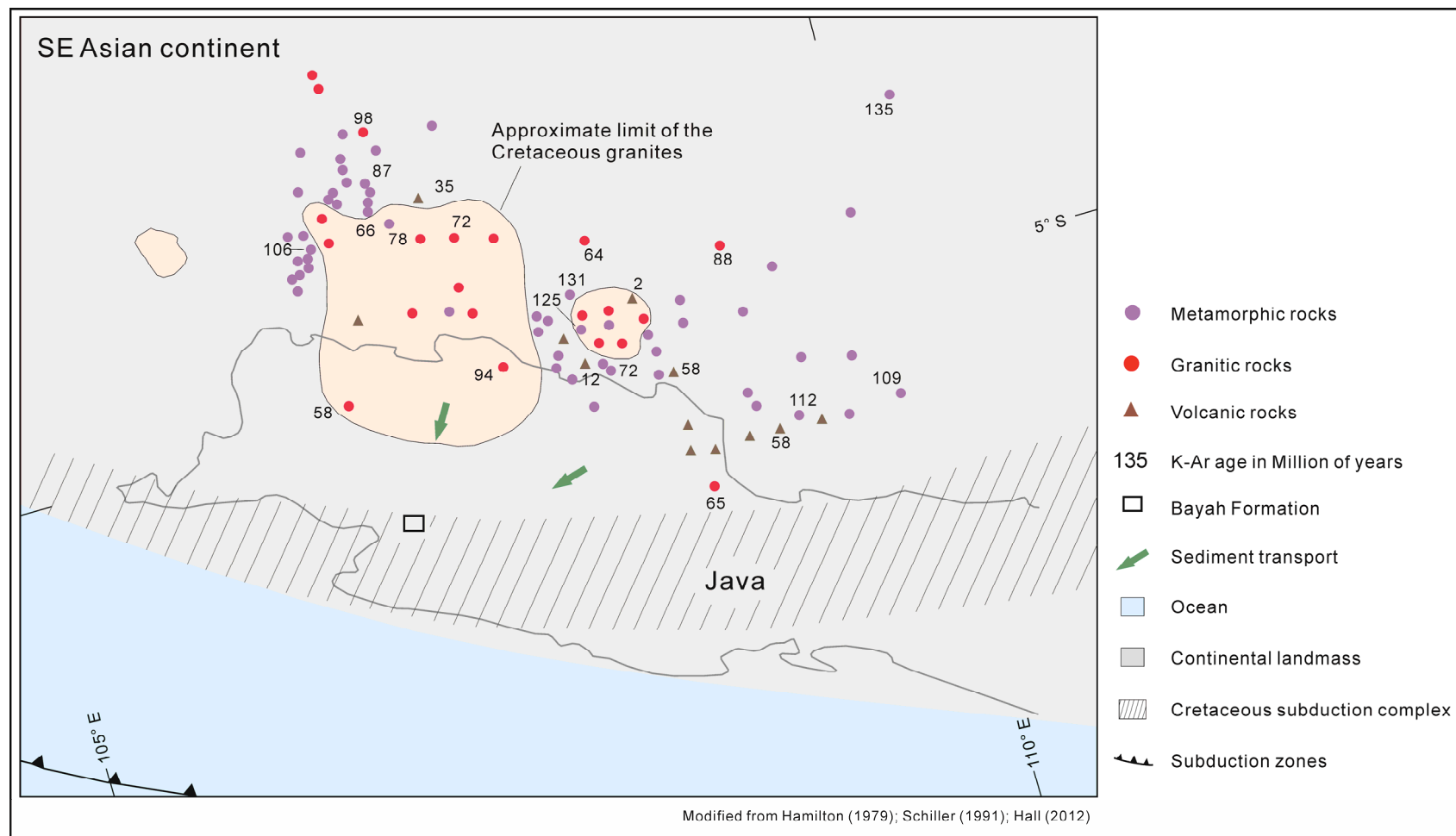


Fig. 41. Map of the Mesozoic basement rocks in the Northwest Java basin and adjacent areas (modified from Hamilton, 1979; Schiller et al., 1991; Hall, 2012). Study area is indicated with a small black-coloured rectangle. The Mesozoic basement rocks consist primarily of granitoid, metamorphic, and volcanic rocks.

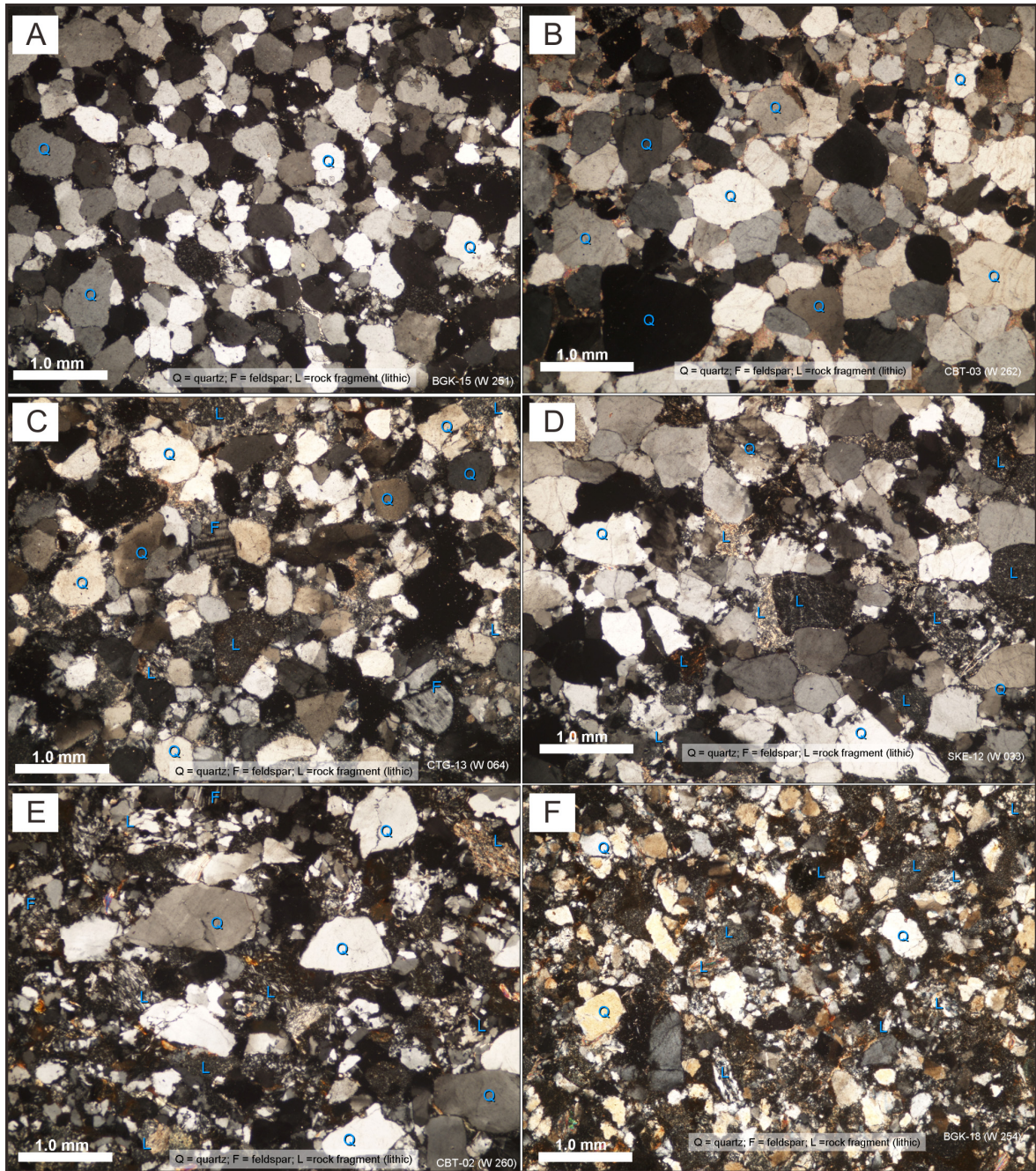


Fig. 42. Microscopic photographs representing examples of typical sandstone groups of the Bayah Formation according to the ternary classification. (A) and (B) indicate quartz-arenite sandstones ($Q_{97}F_0L_3$ and $Q_{96}F_1L_4$ respectively). (C) and (D) indicate sublithic-arenite sandstones ($Q_{86}F_1L_{13}$ and $Q_{71}F_1L_{29}$ respectively). (E) and (F) indicate lithic-arenite sandstones ($Q_{54}F_5L_{41}$ and $Q_{61}F_2L_{37}$ respectively).

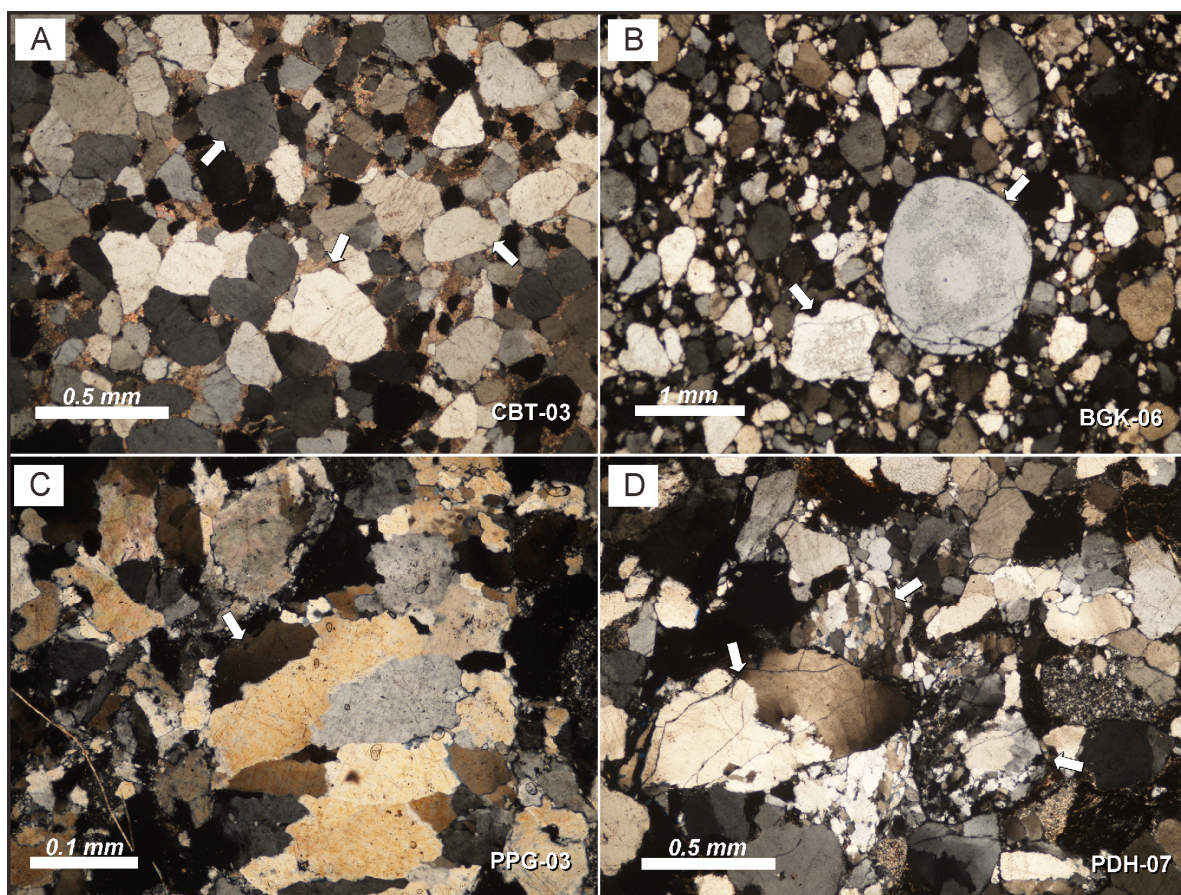


Fig. 43. Microscopic photographs representing examples of quartz-framework grains of the Bayah Formation sandstones. (A) and (B) show various petrographic aspects of monocrystalline quartz (Qm), indicated by white arrows. (A) and (B) show various petrographic aspects of polycrystalline quartz (Qp), indicated by white arrows.

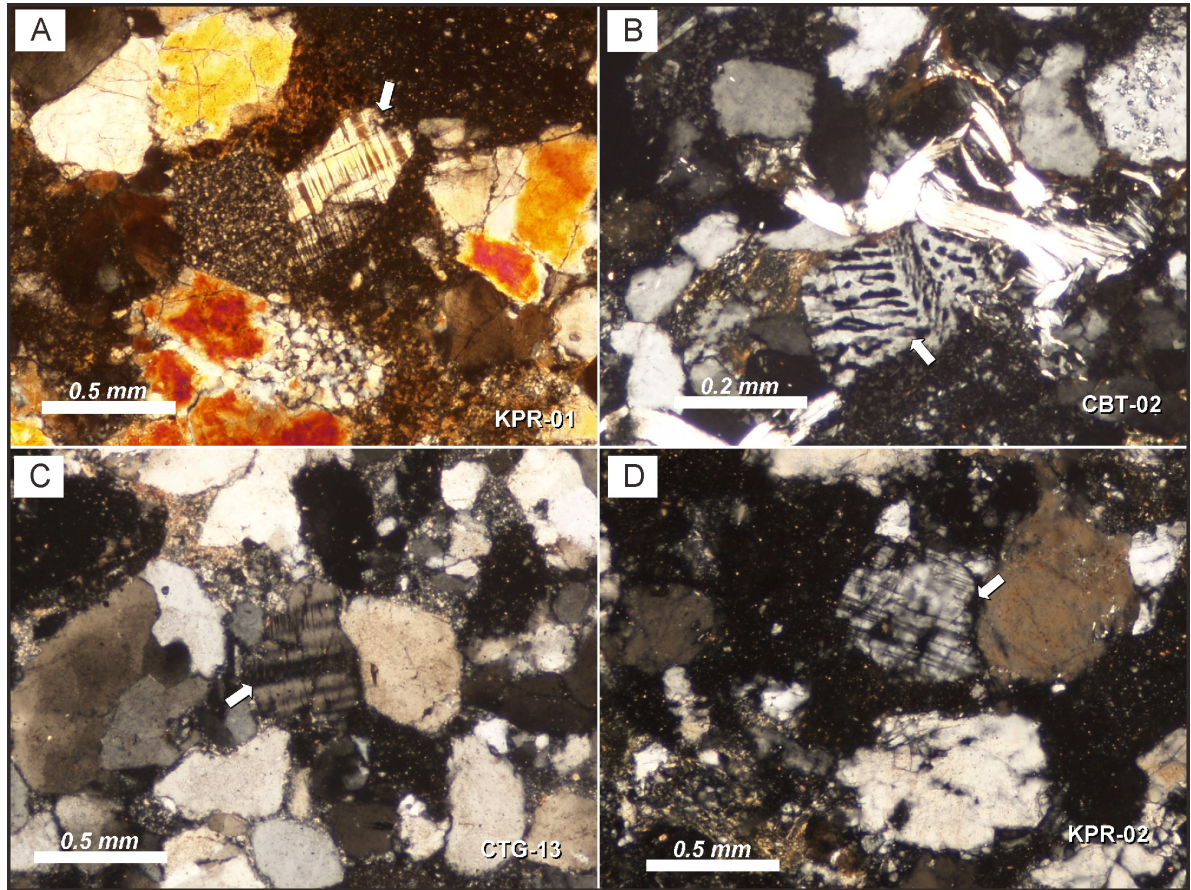


Fig. 44. Microscopic photographs representing various petrographic aspects of feldspar-framework grains observed in the Bayah Formation sandstones. (A) Grid twinning of microcline feldspar, indicated by white arrows. (B) myrmekitic texture of K-feldspar, indicated by white arrows. (C) and (D) polysynthetic twinning of plagioclase, indicated by white arrows.

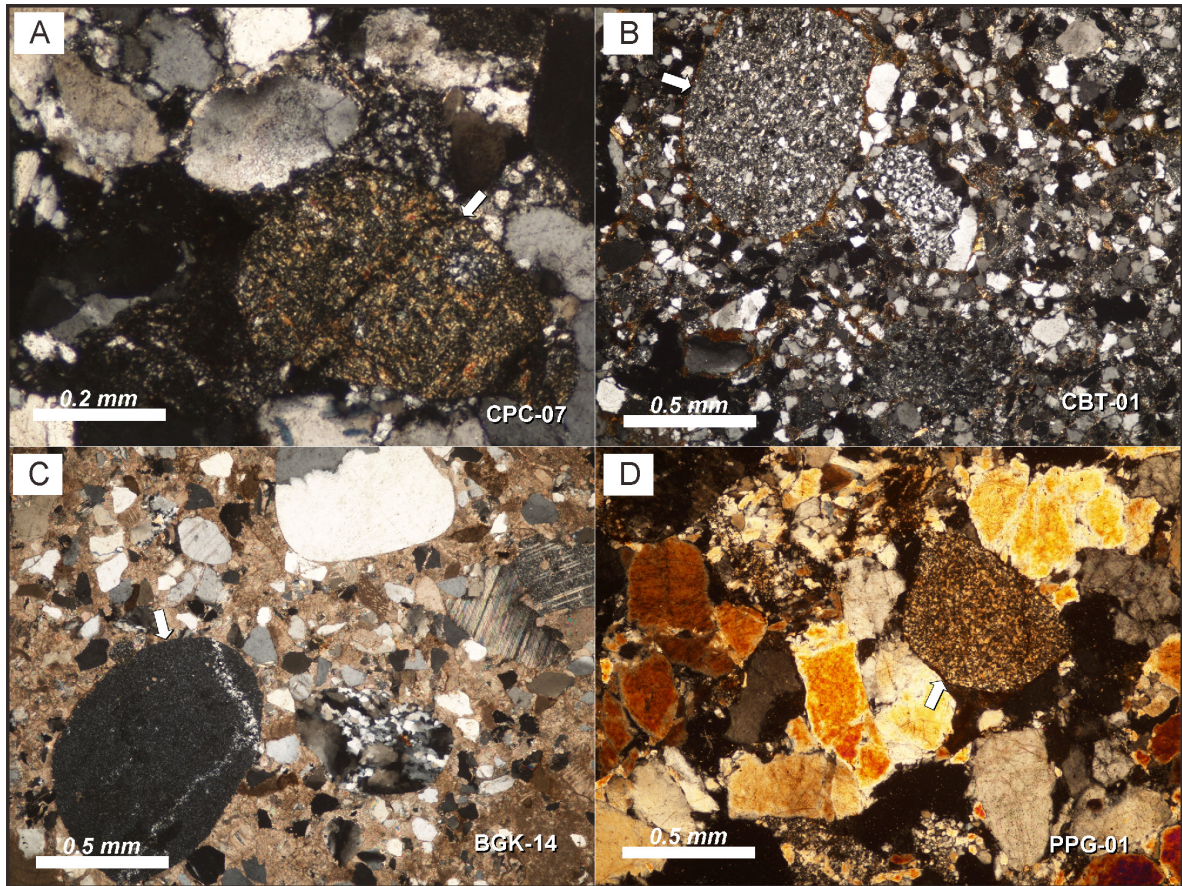


Fig. 45. Microscopic photographs representing various classes of sedimentary rock fragments (Ls) observed in the Bayah Formation sandstones. (A) and (B) graywacke fragments, indicated by white arrows. (C) and (D) cryptocrystalline-siliceous rock and chert fragments respectively, indicated by white arrows.

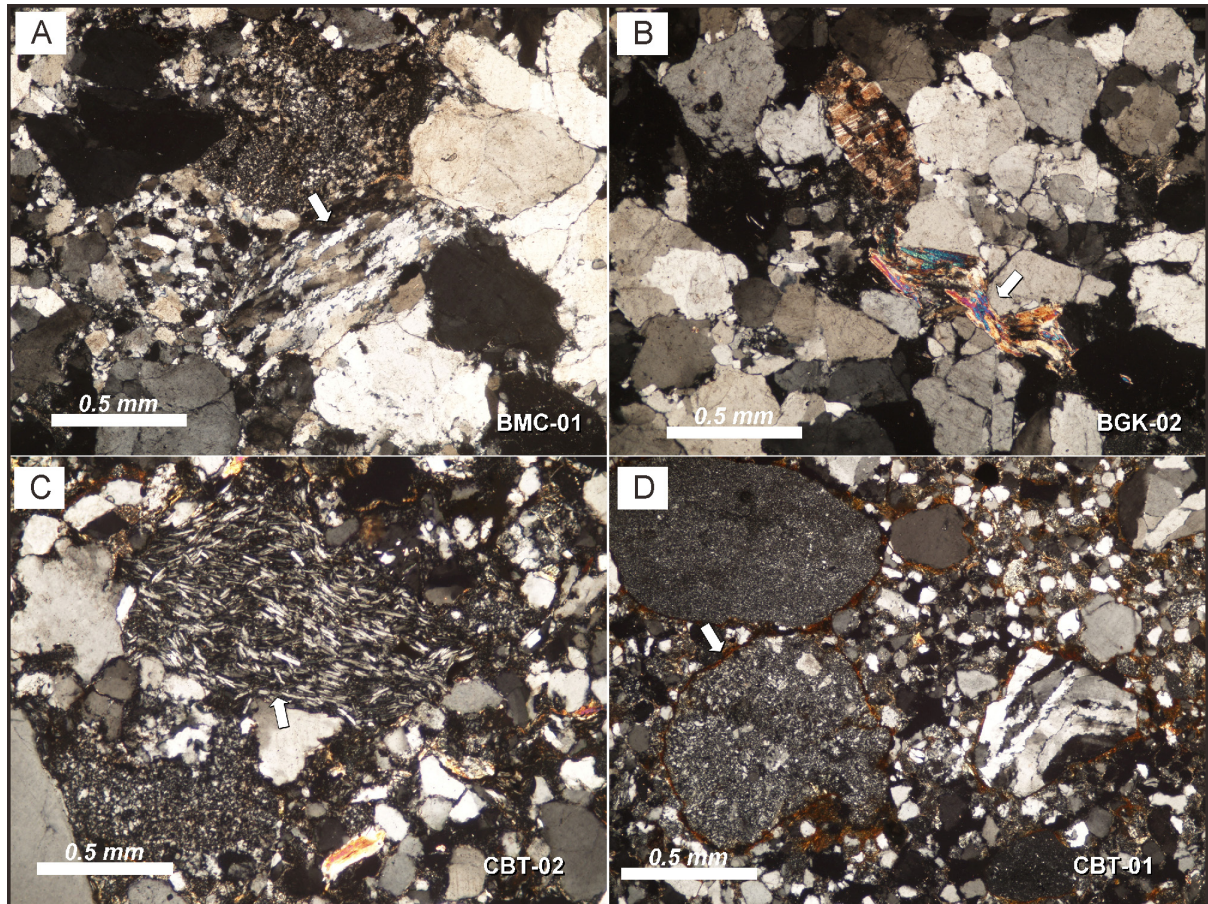


Fig. 46. Microscopic photographs representing various classes of metamorphic rock fragments (Lm) and volcanic rock fragments (Lv) observed in the Bayah Formation sandstones. (A) and (B) quartzite and mica-schist fragments respectively, indicated by white arrows. (C) and (D) trachytic and rhyolitic volcanic-rock fragments respectively, indicated by white arrows.

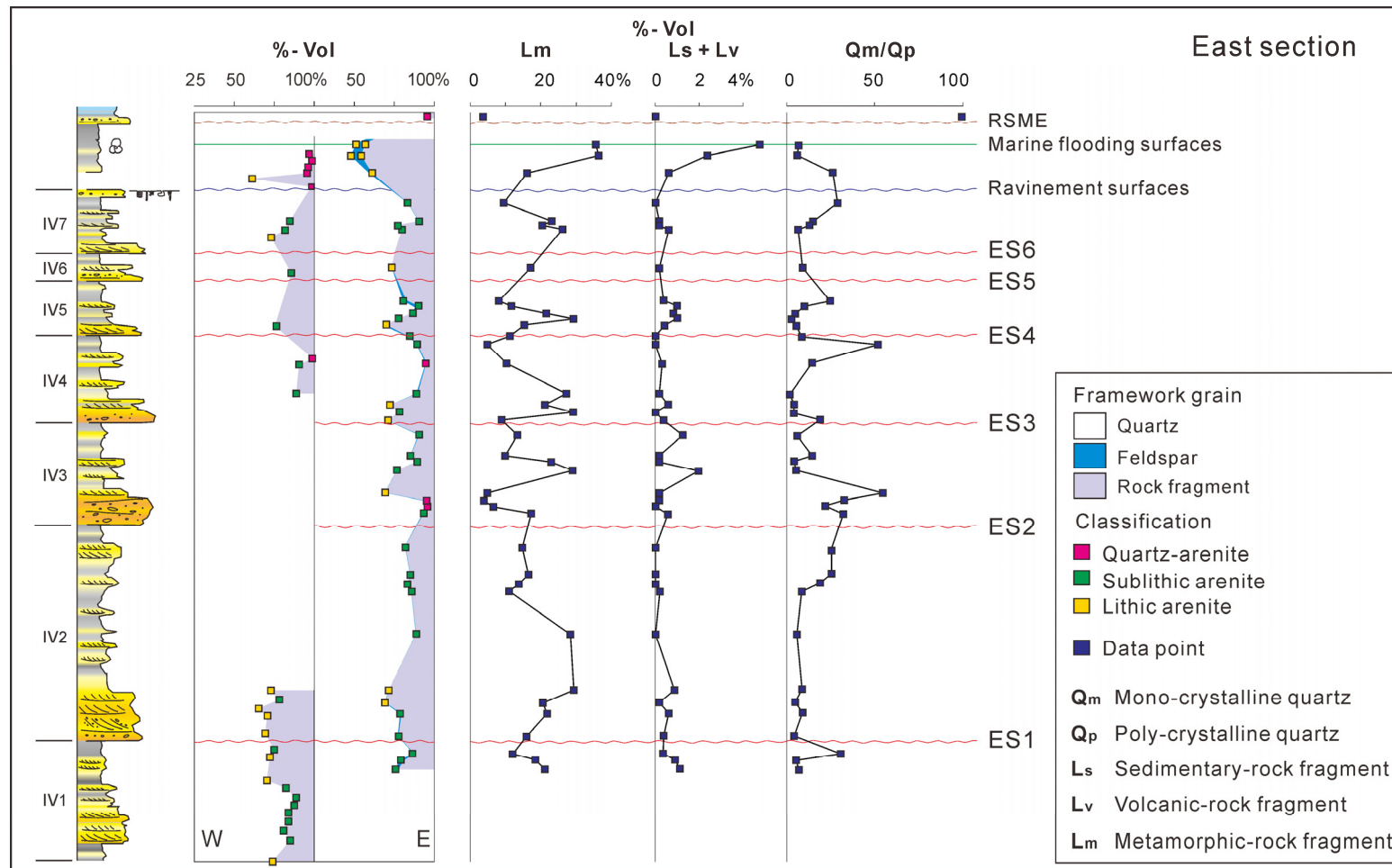


Fig. 47. Temporal variation in framework composition of sandstones for the eastern sections (locations A, B, C, D, and E are indicated in Fig. 4).

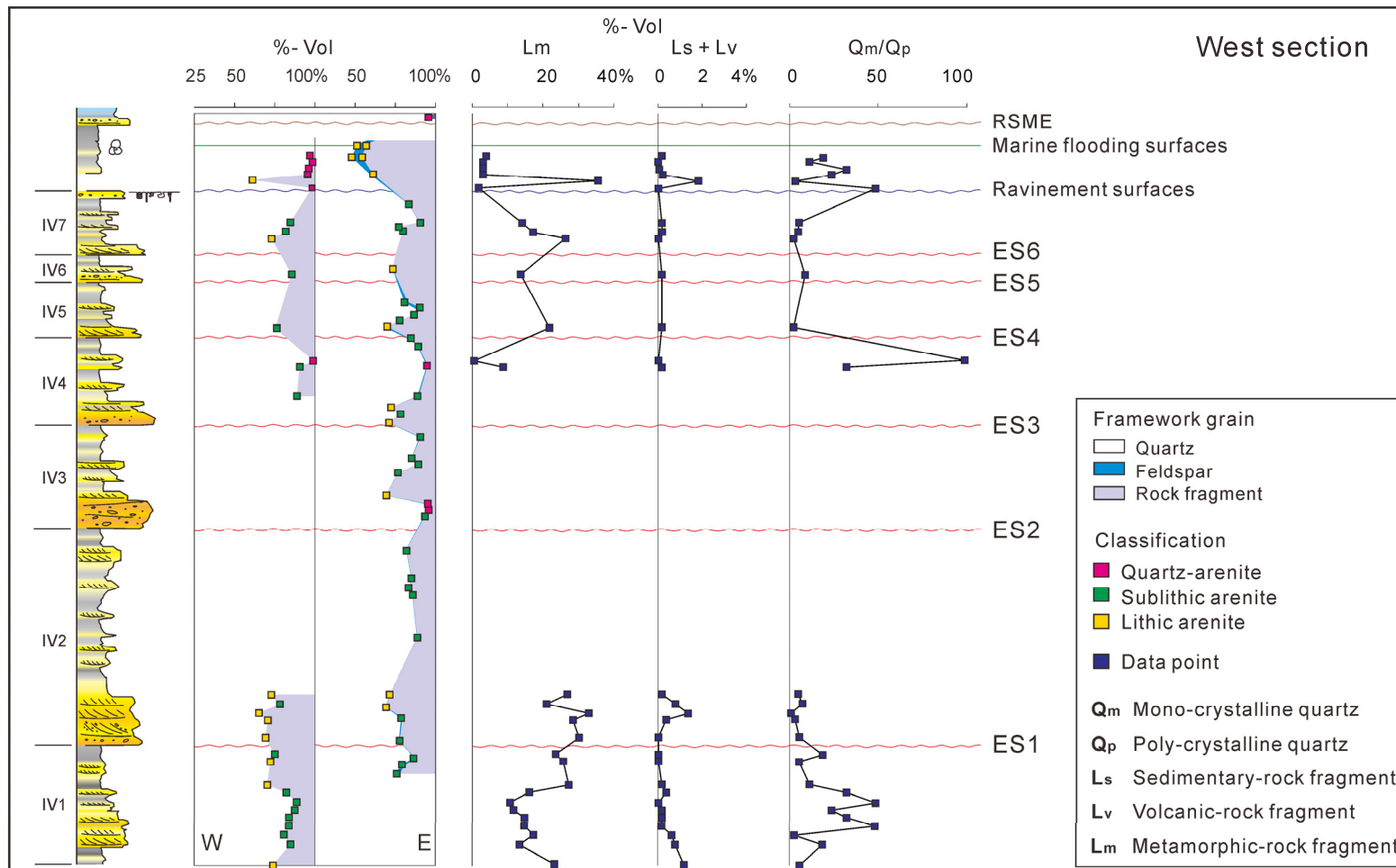


Fig. 48. Temporal variation in framework composition of sandstones for the western sections (locations F, G, and H are indicated in Fig. 4).

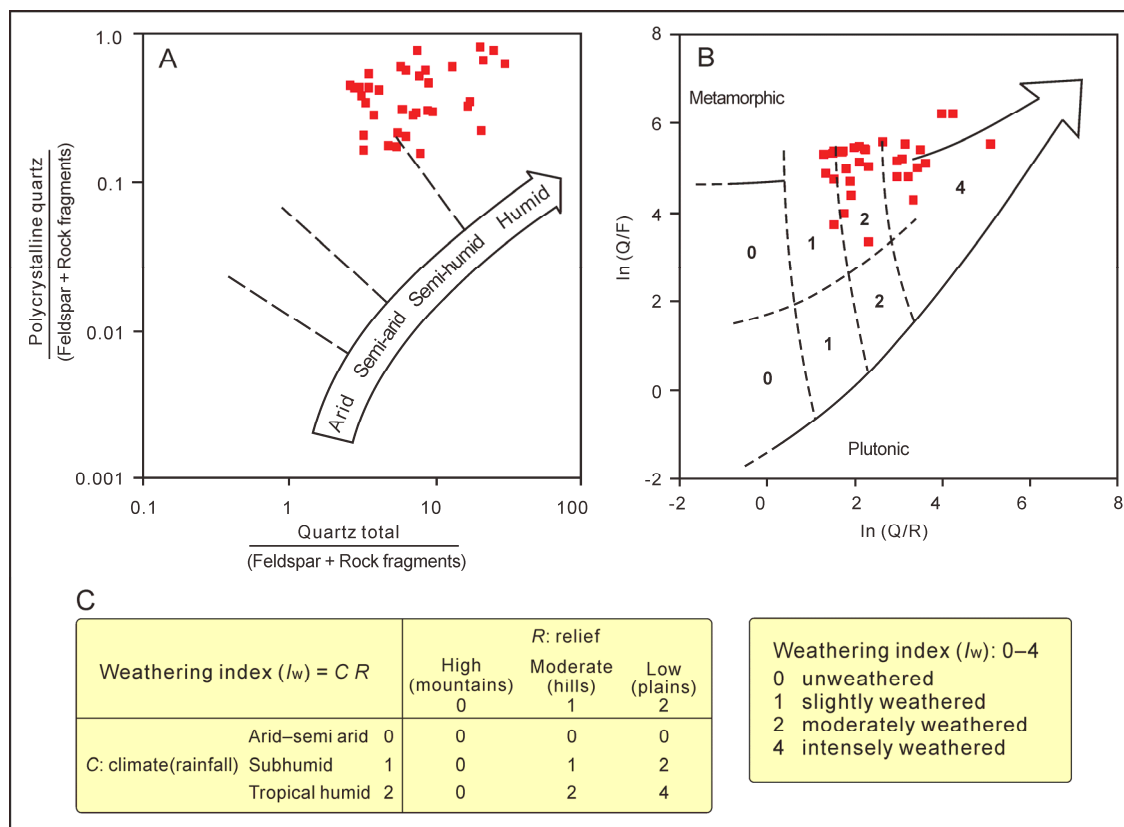


Fig. 49. (A) Bivariant log-plot of the Bayah Formation's sandstones to discriminate compositional maturity based on grain types ratios which are the most sensitive to climatic control (Suttner and Dutta, 1986). (B) Logratio plot between grain types to indicate the importance of weathering according to Weltje et al. (1998). (C) Weathering-index factors are defined in terms of climate and physiographic parameters.

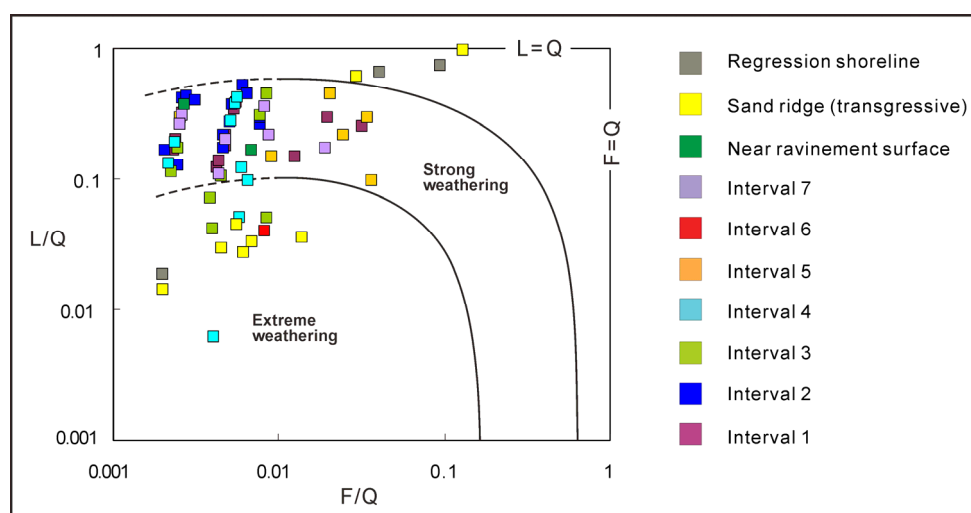


Fig. 50. Log-plot between rock fragment–quartz ratio (L/Q) and feldspar–quartz ratio (F/Q) according to Garzanti et al. (2013). The diagram can be used to evaluate the relative importance of climate on detrital mode by estimating the substantial loss of feldspar and rock fragments during weathering of the parent-rock lithology in source areas.

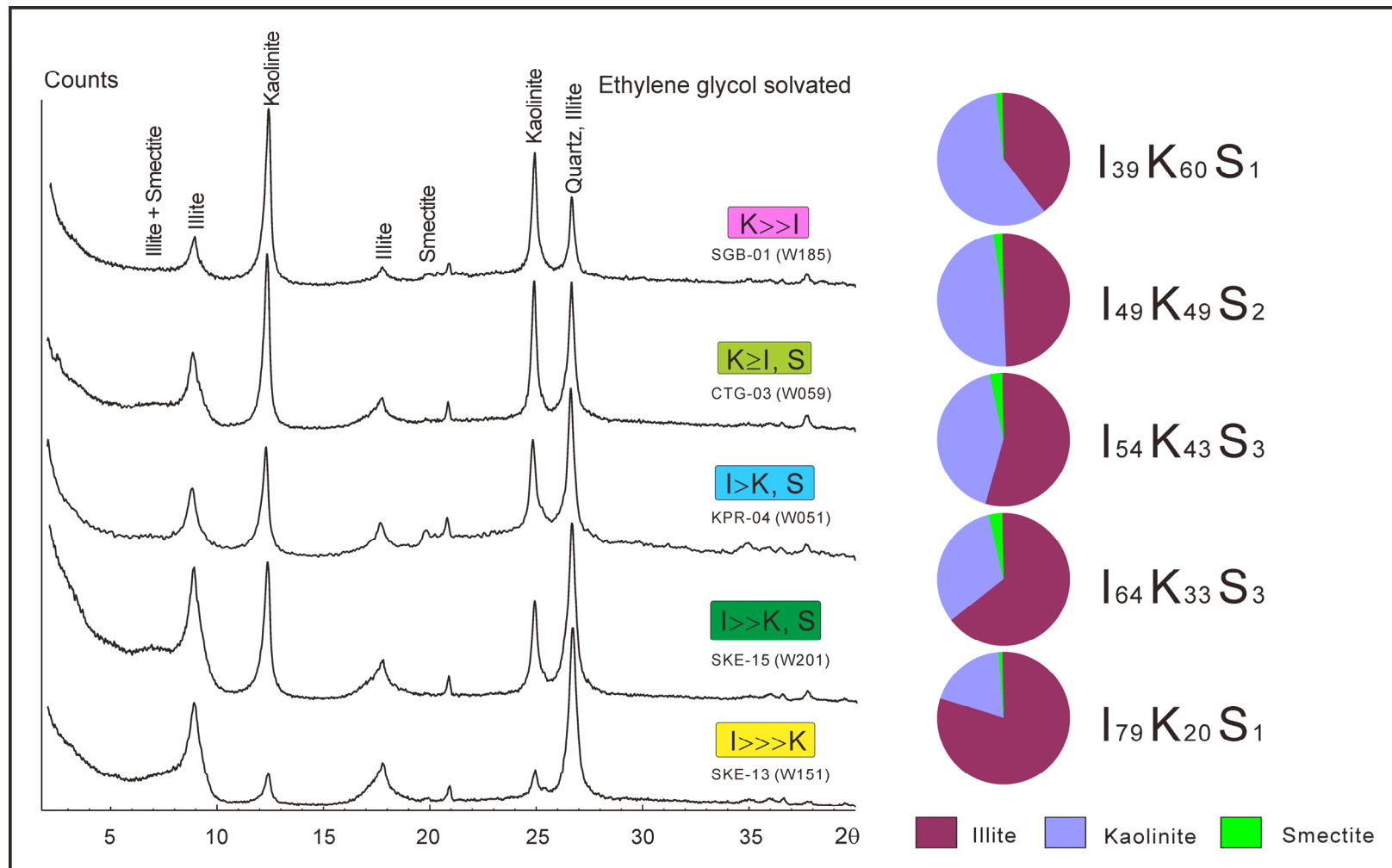


Fig. 51. Five X-ray diffractograms of mudstone samples of the Bayah Formation. The diffractogram patterns represent five groups of the clay mineral assemblages. This is reflected by the variation in the estimated volume percentages between illite, kaolinite, and smectite. Gradual changes in illite and kaolinite in each group are indicated by pie diagrams.

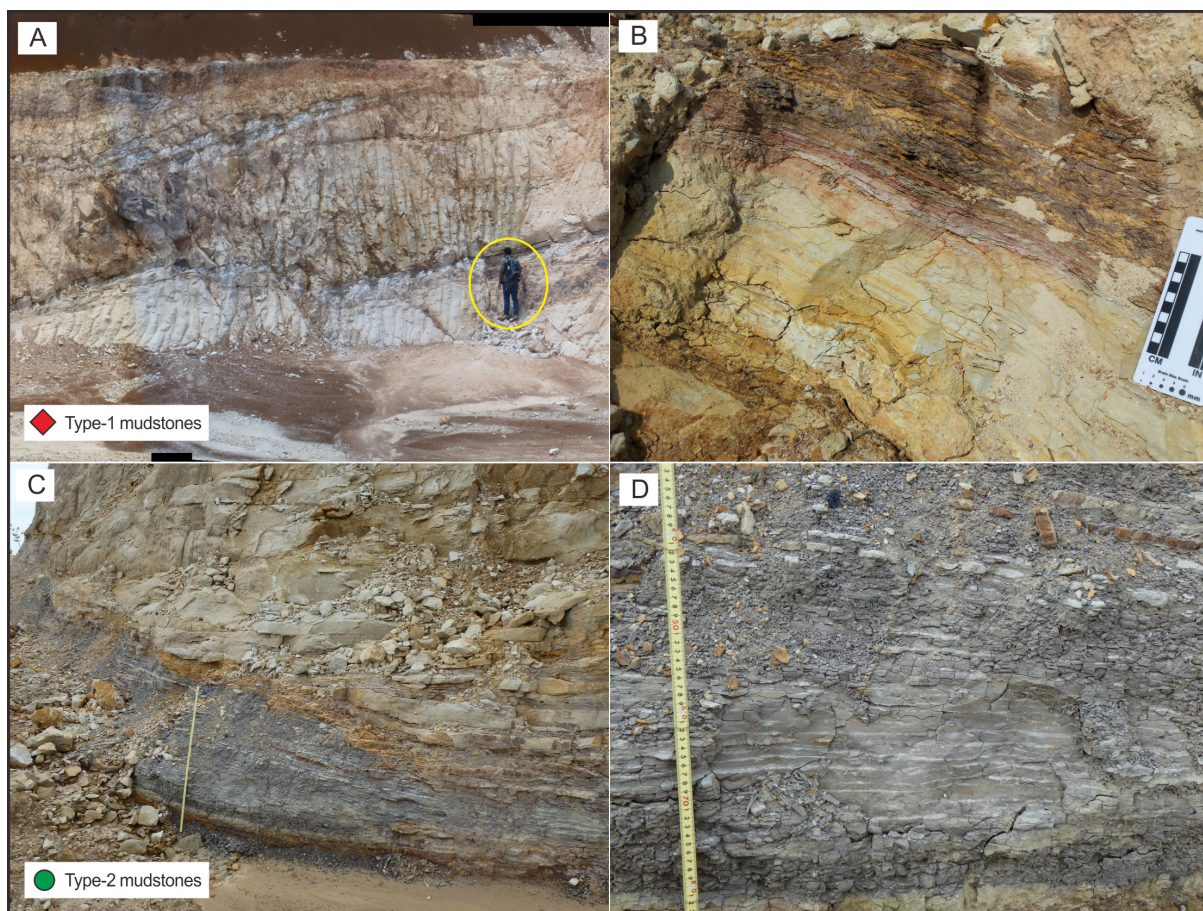


Fig. 52. Mudstone samples for XRD measurement were taken from four predominant types of mudstones of the Bayah Formation. (A) Type 1 mudstones, characterized by thin-bedded, structureless mudstones with white–purplish colours and rootlets. (B) Close-up photo of the Type 1 mudstones. (C) Type 2 mudstones, characterized by greyish-laminated mudstones with thin sandstone intercalations. (D) Close-up photo of the Type 2 mudstones.

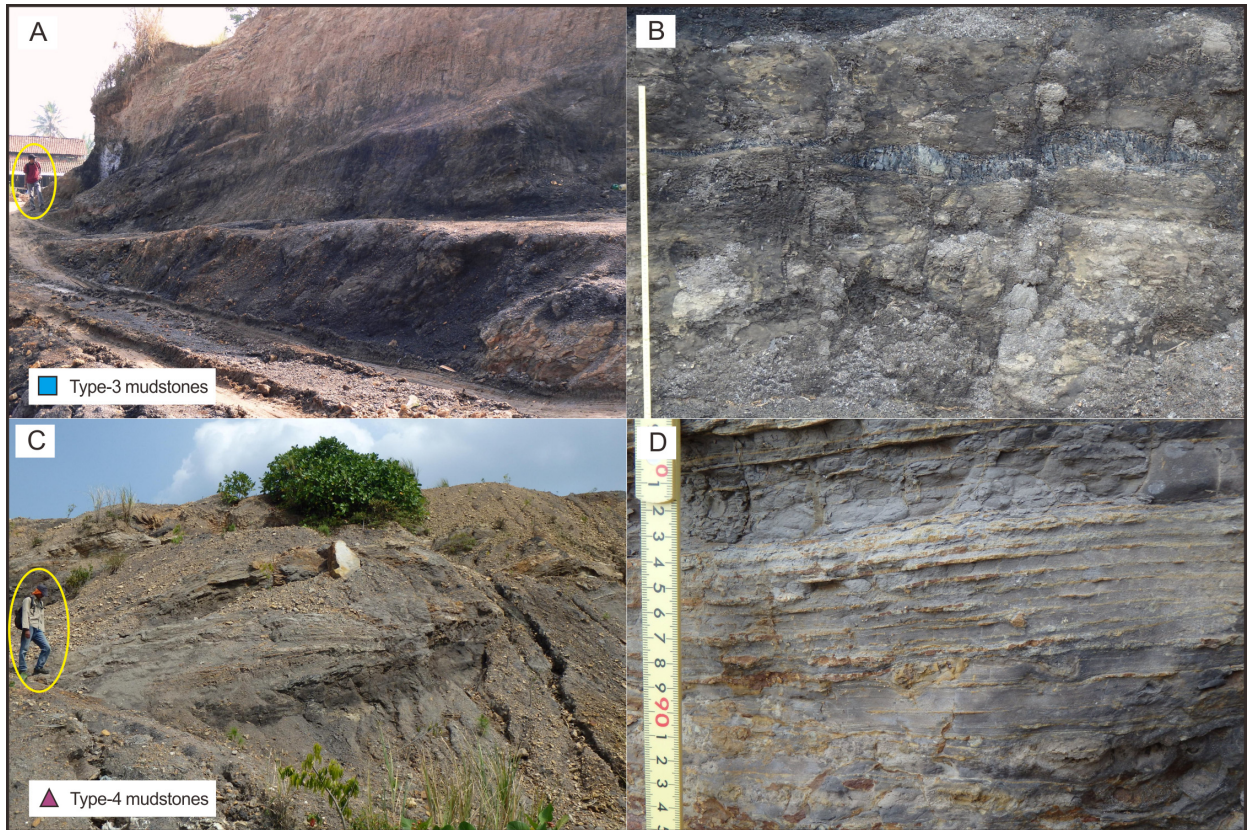


Fig. 53. (*continued*). (A) Type 3 mudstones, consist of greyish–black, structureless mudstones with minor lignite and plant remains. (B) Close-up photo of the Type 3 mudstones. (C) Type 4 mudstones, consist of rhythmite-bioturbated mudstones with concretions and plant remains. (D) Close-up photo of the Type 4 mudstones.

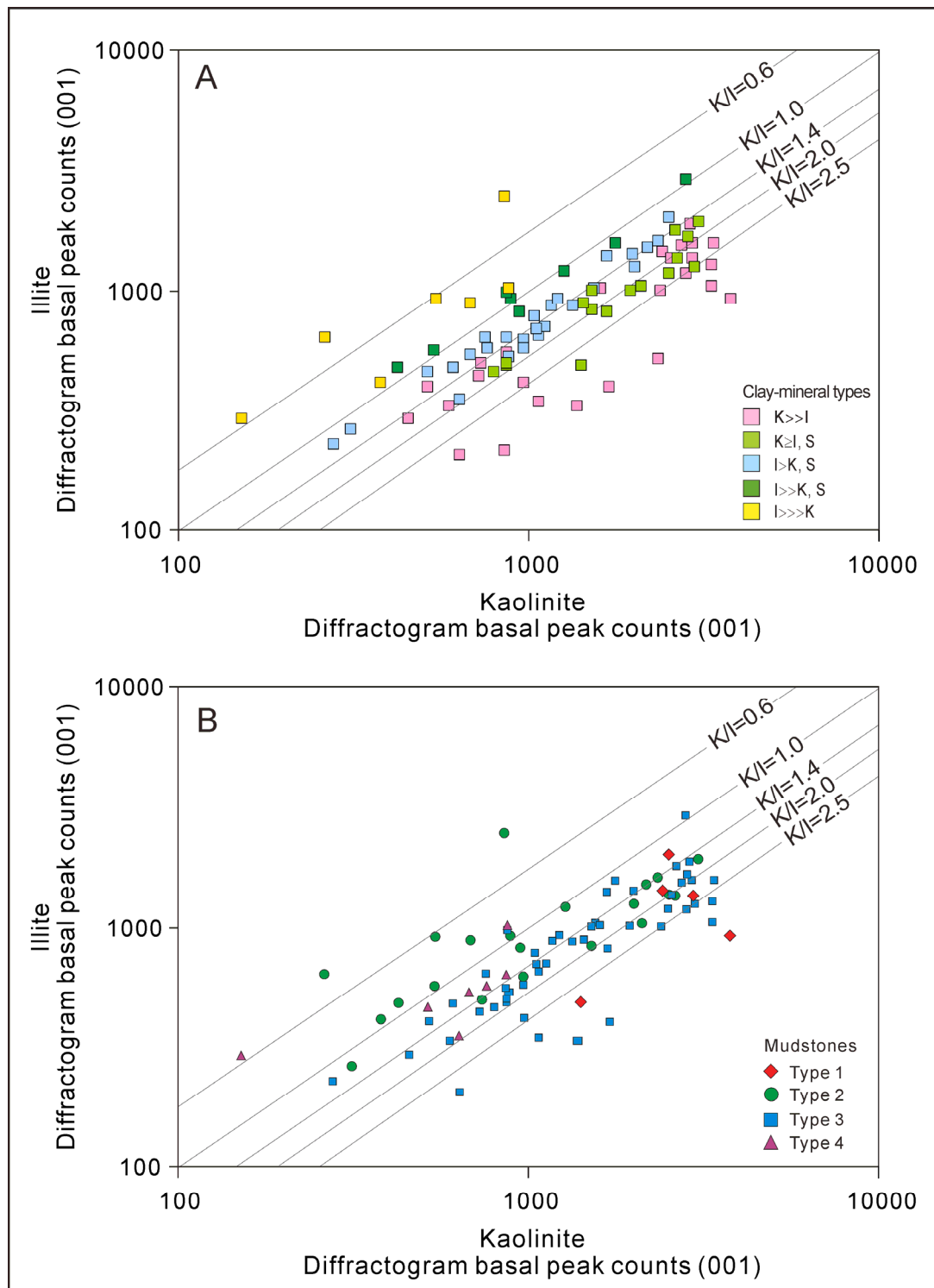


Fig. 54. (A) Log-plot of peak-area counts between kaolinite and illite for five clay mineral groups. Each mineral group is distributed nearly parallel to the kaolinite–illite ratio lines. (B) Log-plot of peak-area counts between kaolinite and illite for four different types of mudstone deposits. Two predominant types of mudstone deposits (Types 2 and 3) are distributed nearly parallel to the kaolinite–illite ratio lines.

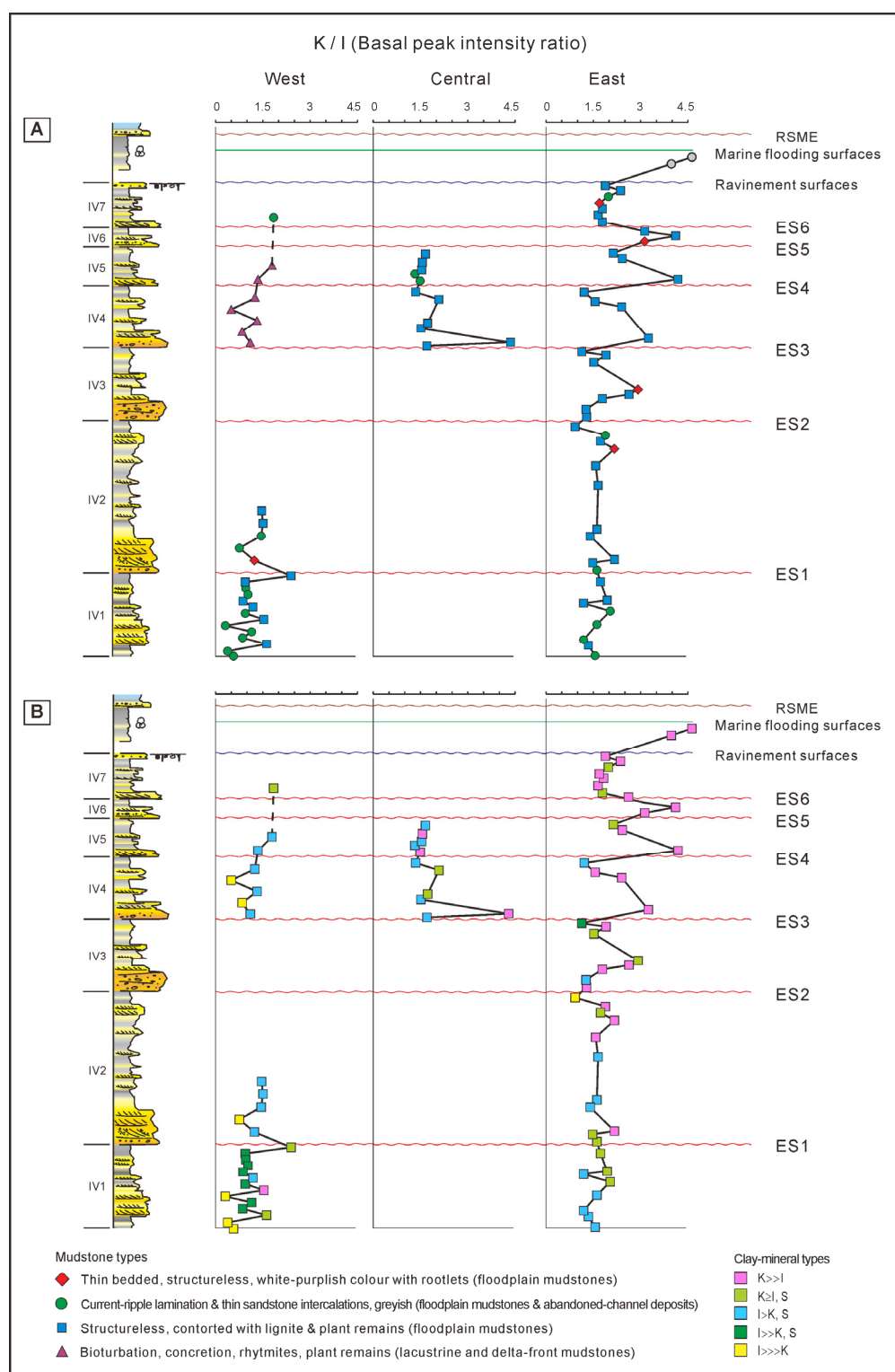


Fig. 55. (A) Temporal and spatial variation in kaolinite–illite ratios for mudstone types of the Bayah Formation. (B) Temporal and spatial variation in kaolinite–illite ratios for clay mineral groups of the Bayah Formation (western sections refer to locations F, G, and H; central sections refer to location D; eastern sections refer to locations A, B, C, D, E in Fig. 4).

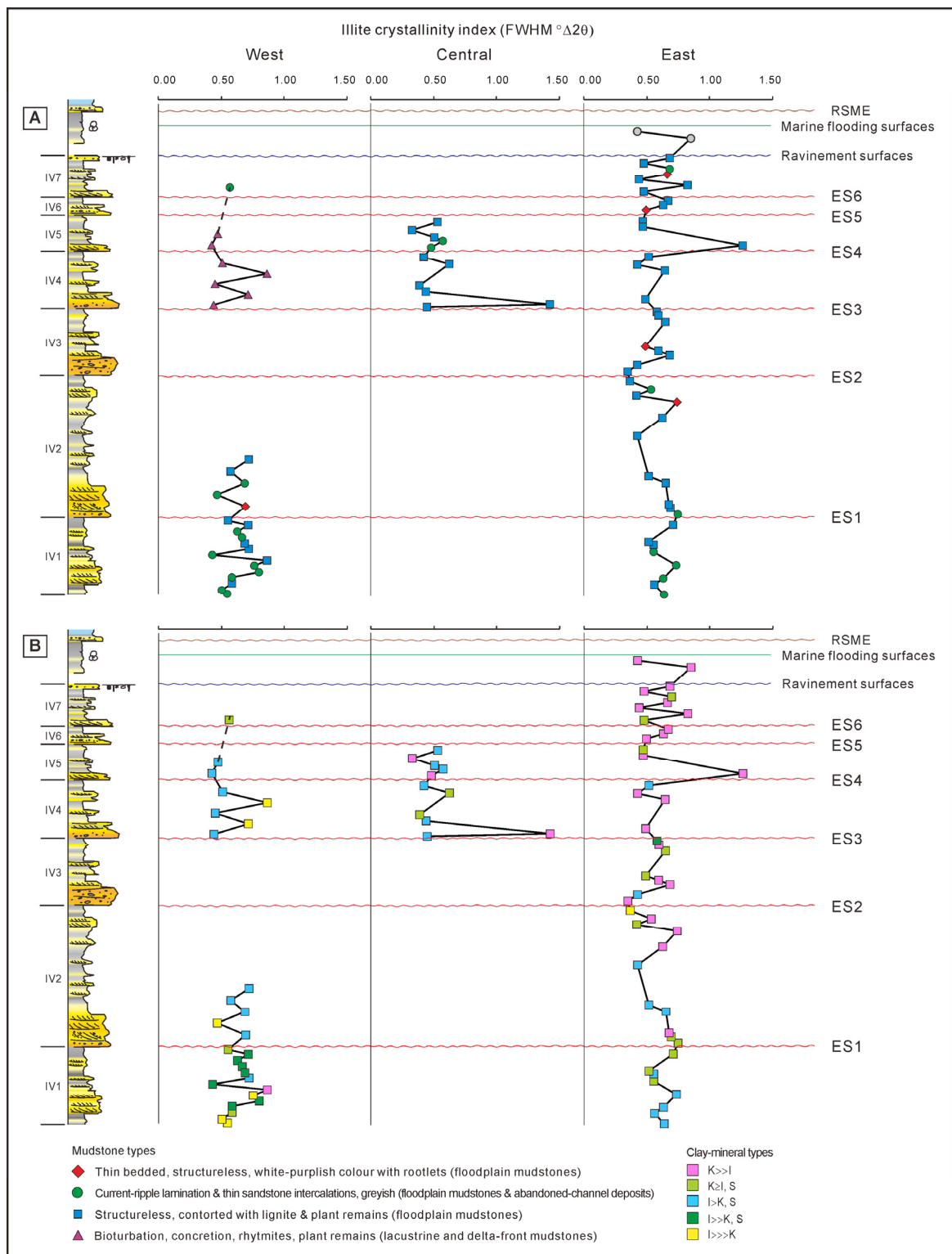


Fig. 56. (A) Temporal and spatial variation in the illite crystallinity index for mudstone types of the Bayah Formation. (B) Temporal and spatial variation in the illite crystallinity index for clay mineral groups of the Bayah Formation.

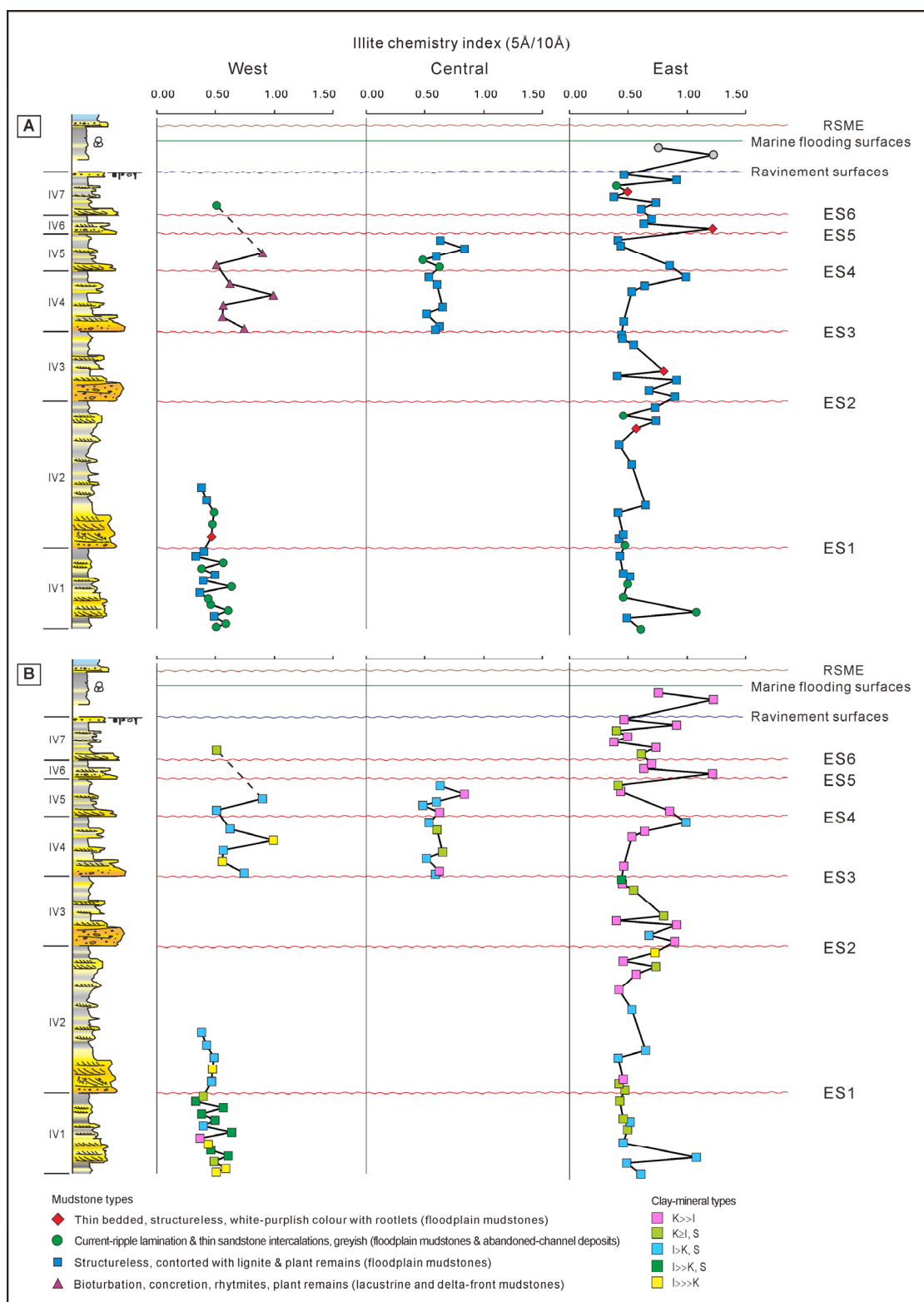


Fig. 57. (A) Temporal and spatial variation in the illite chemistry index for mudstone types of the Bayah Formation. (B) Temporal and spatial variation in the illite chemistry index for clay mineral groups of the Bayah Formation.

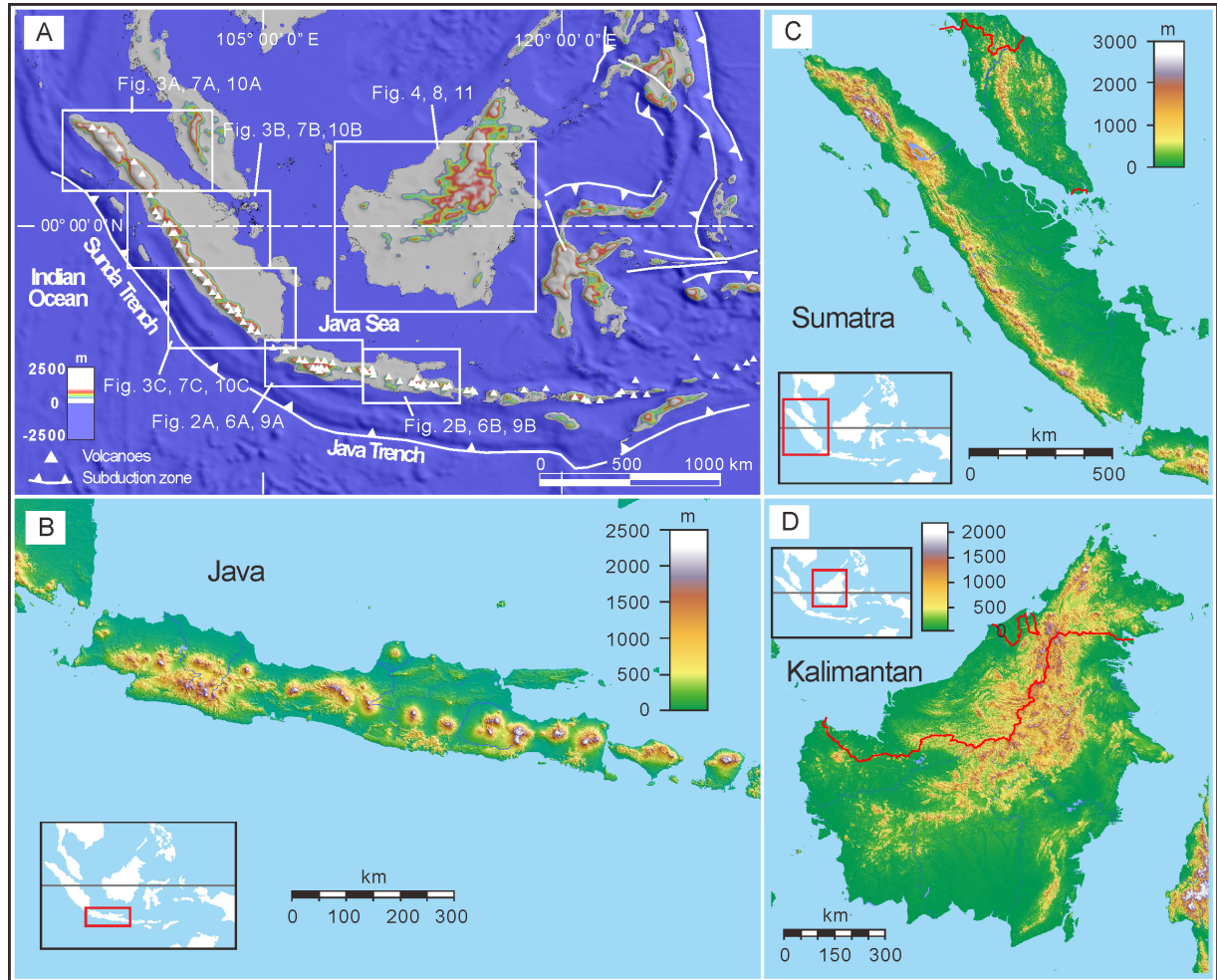


Fig. 58. Maps showing the tectonic and geomorphological setting of the Indonesian islands. (A) A plate-tectonic framework of the Indonesian islands. Simplified from Hall (1997). Rectangles show locations used for the collection of hydrological and geomorphological data. (B) Geomorphological features of Java. (C) Geomorphological features of Sumatra. (D) Geomorphological features of Kalimantan. Figures B, C and D are simplified from wikimedia.org (2007), and inset maps show the locations of the islands in the Indonesian archipelago.

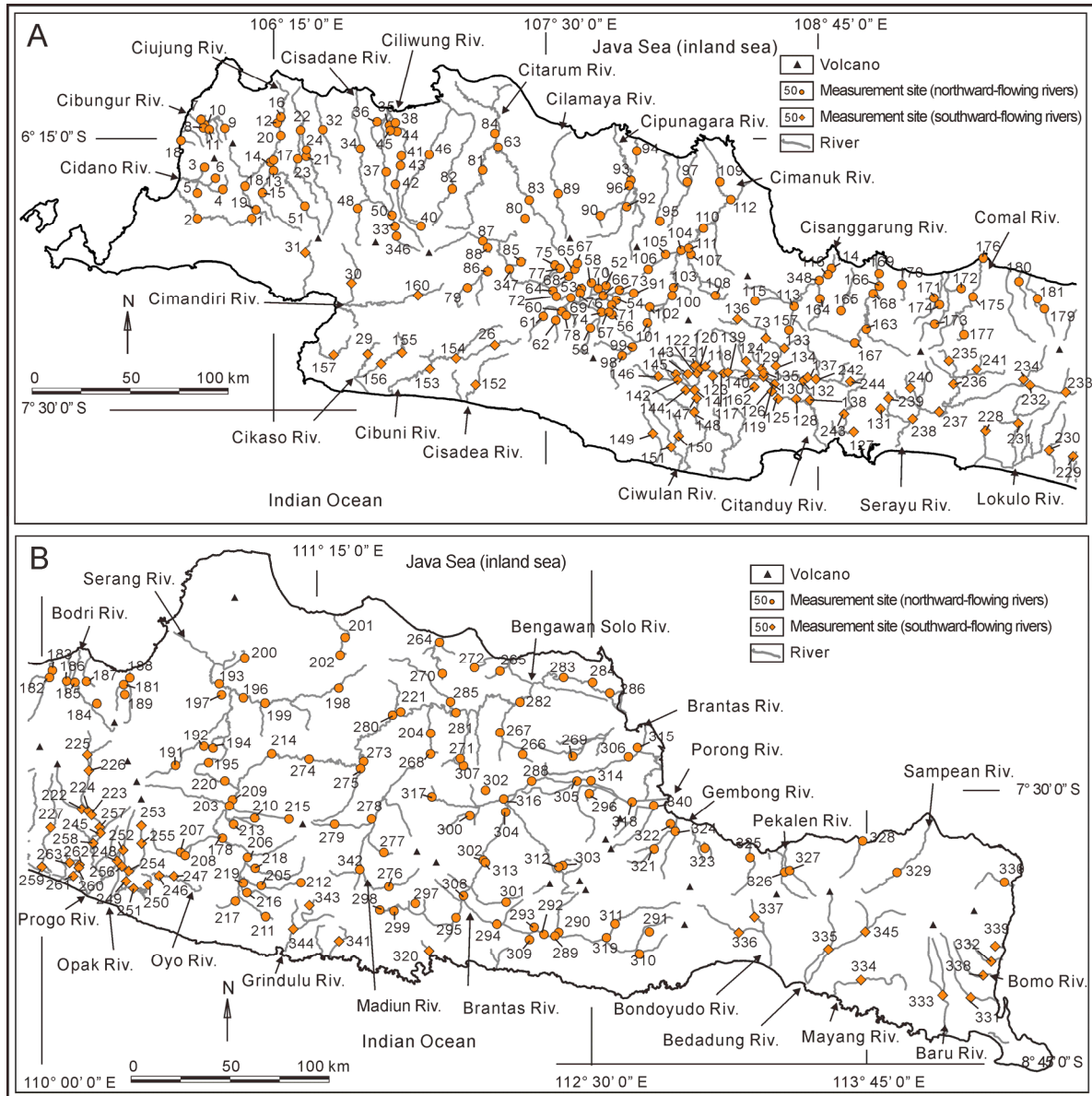


Fig. 59. Locations of measurement sites for discharges in Java. Site numbers are listed in Table 1.

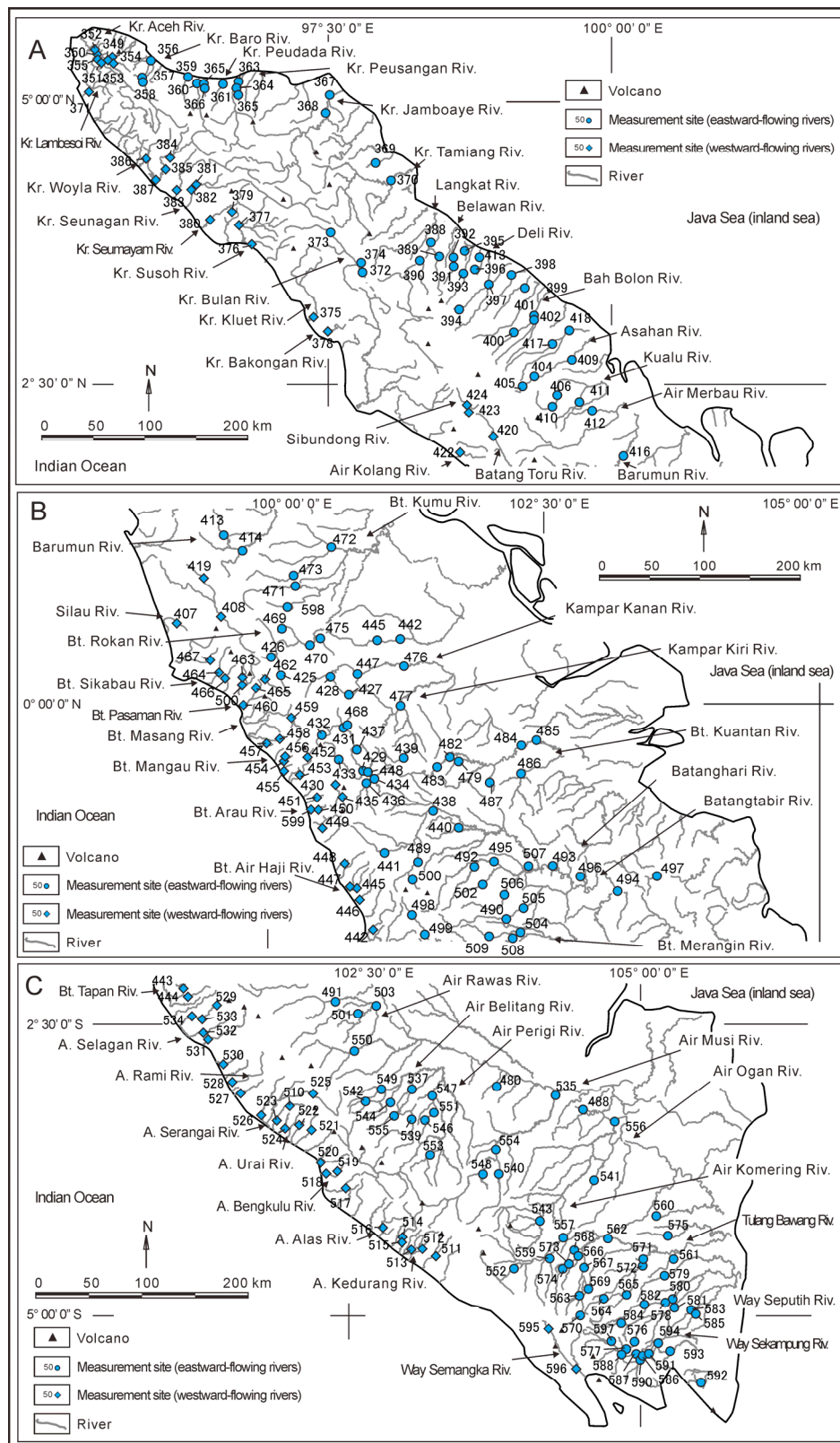


Fig. 60. Locations of measurement sites for discharges in Sumatra. Site numbers are listed in Table 1.

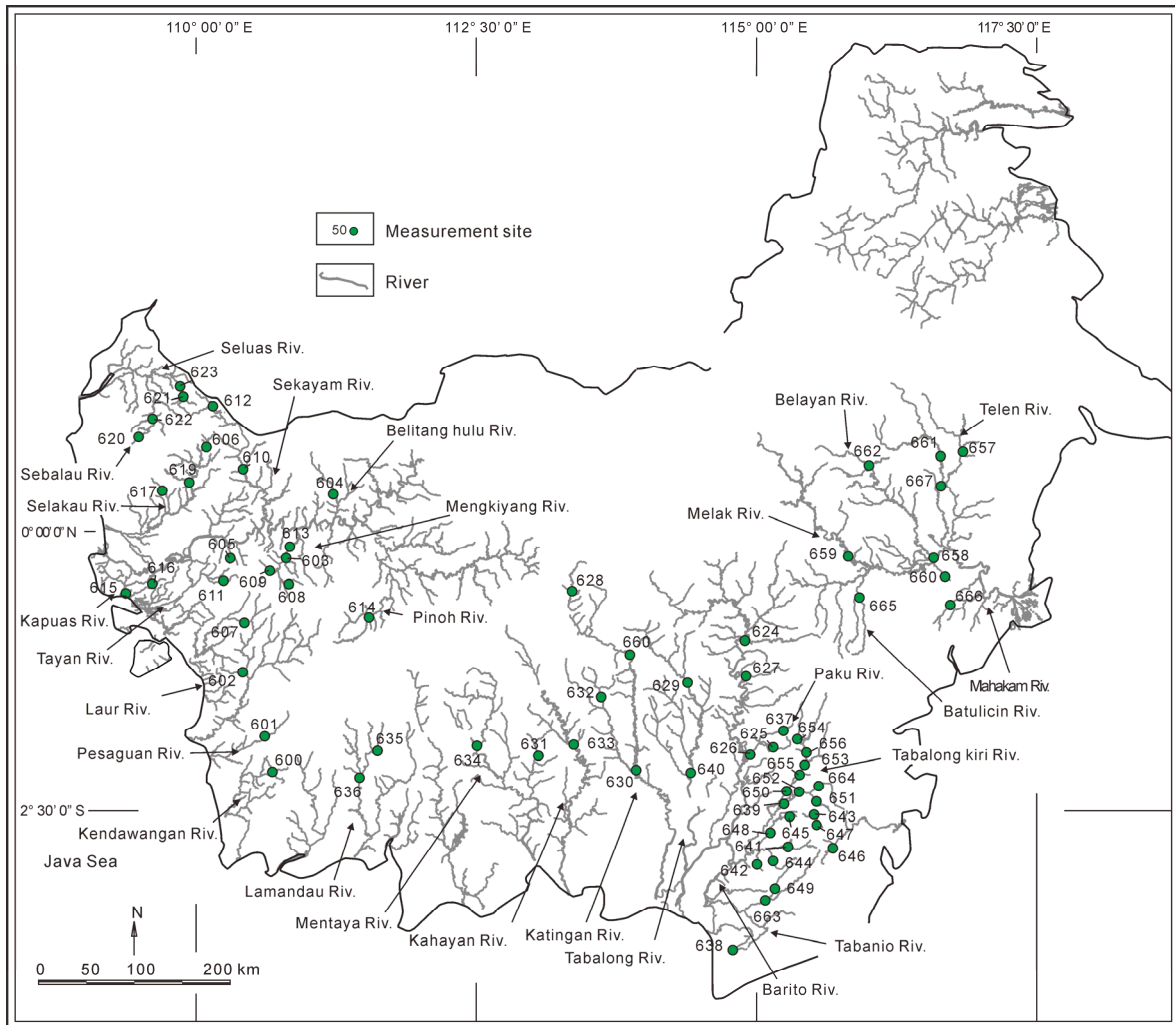


Fig. 61. Locations of measurement sites for discharges in Kalimantan. Site numbers are listed in Table 1.

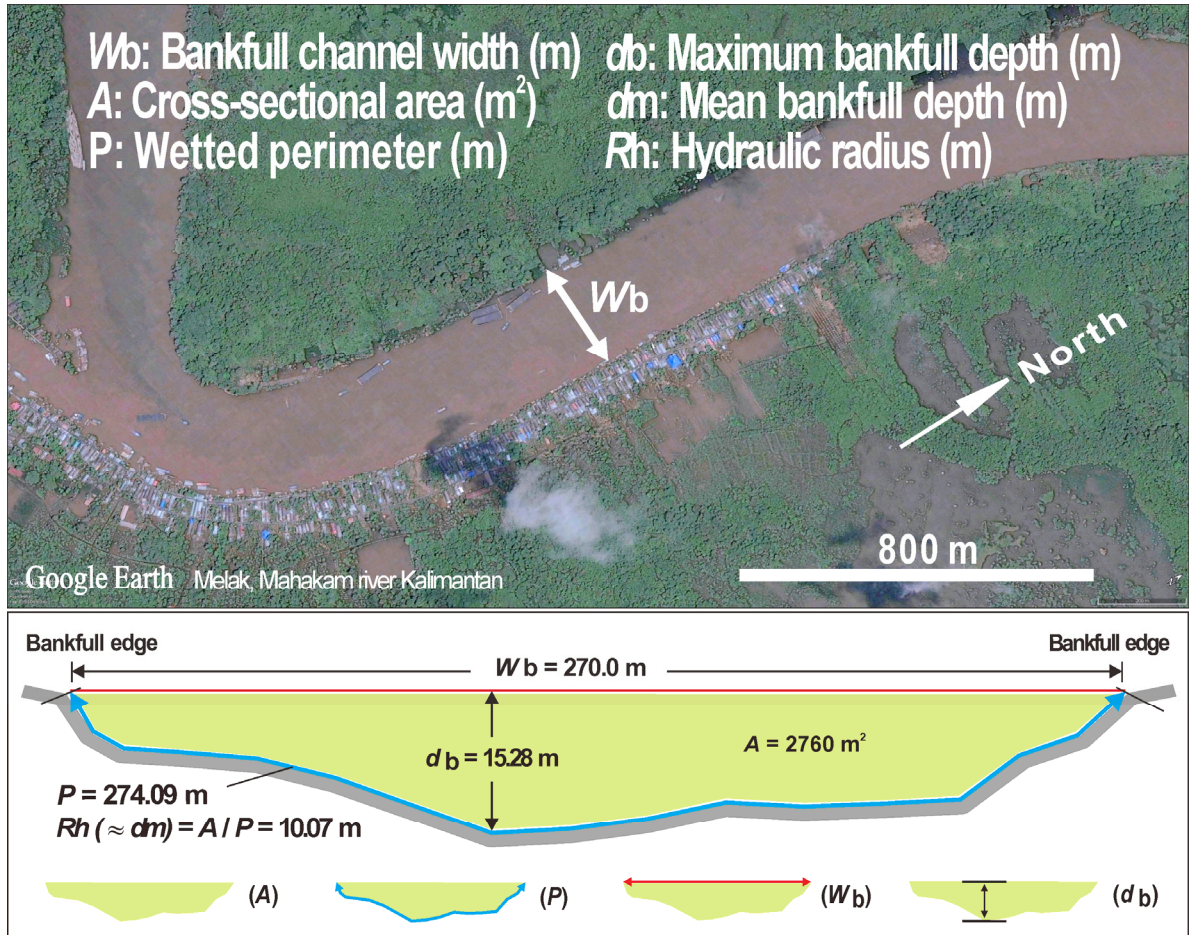


Fig. 62. (A) An example of the measurement of a bankfull channel width (W_b) from an aerial photograph Mahakam River in Melak, Kalimantan (site 641 in Table 1) (Google Earth). (B) An example of the cross-sectional geometry of a river channel in the middle reaches of the Mahakam River at Melak, Kalimantan (site 641 in Table 1), illustrating definition of cross-sectional parameters. See Table 4 for list of symbols.

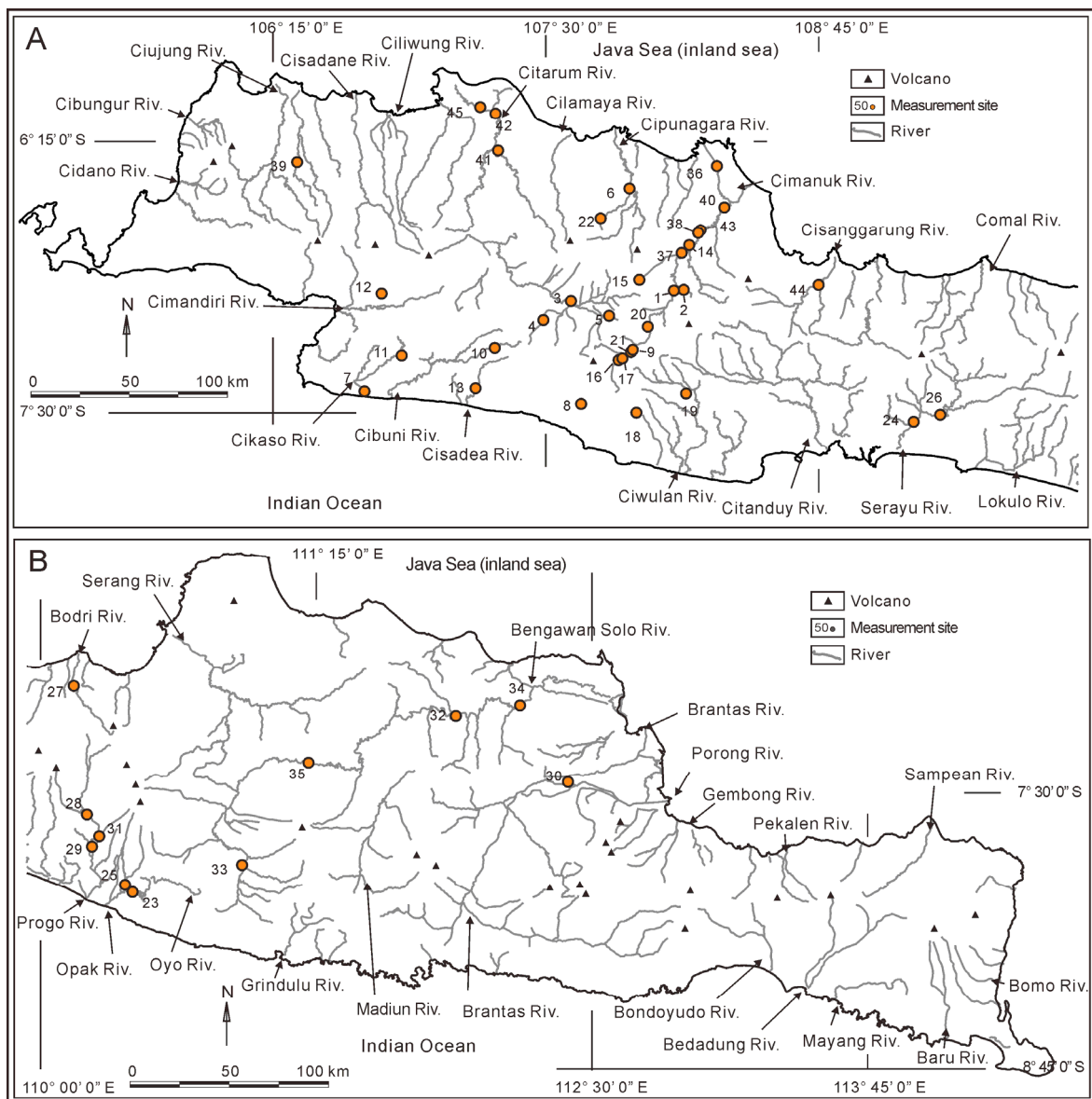


Fig. 63. Locations of measurement sites for cross-sectional geometry of fluvial channels in Java. Site numbers are listed in Table 2.

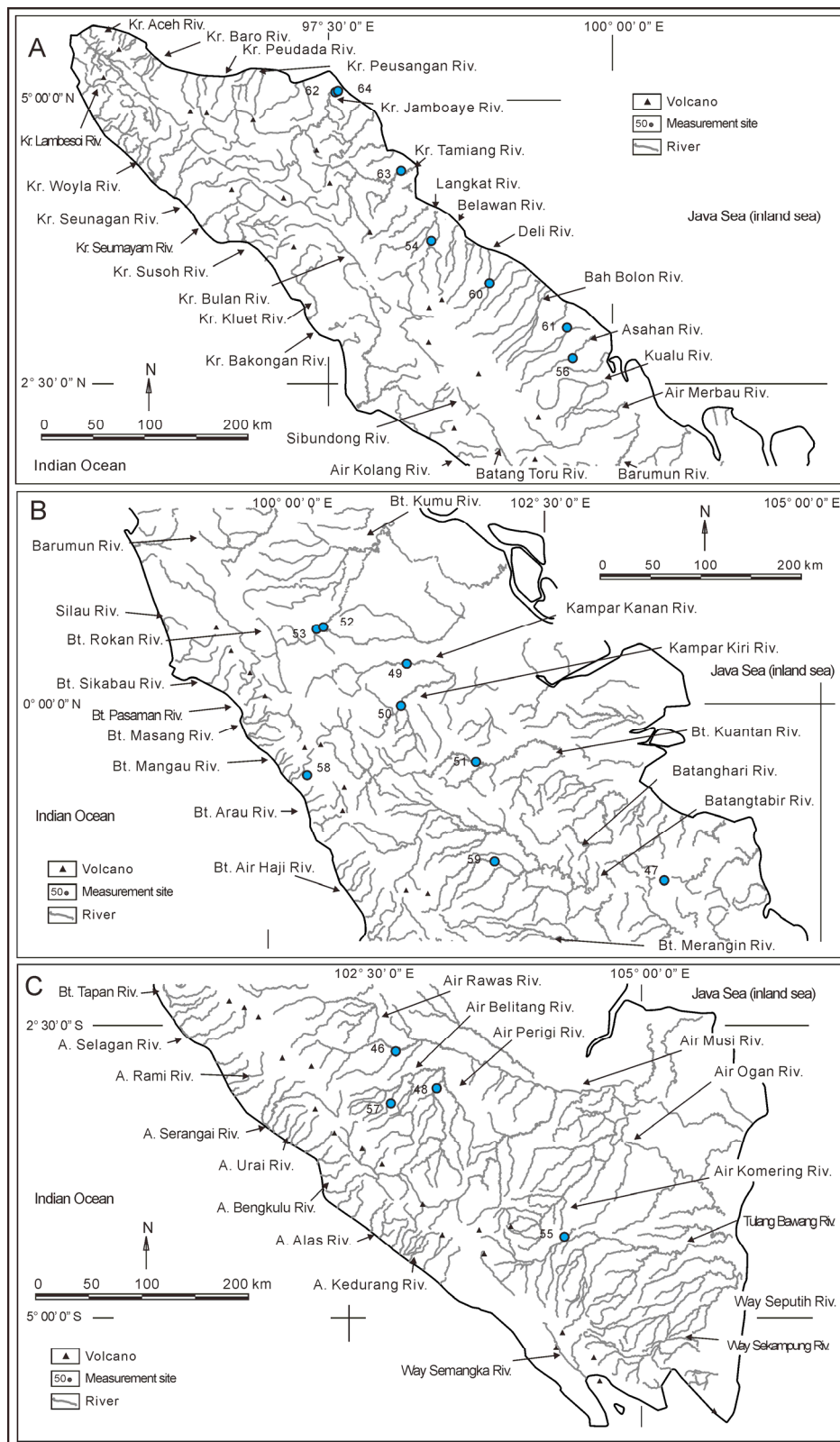


Fig. 64. Locations of measurement sites for cross-sectional geometry of fluvial channels in Sumatra. Site numbers are listed in Table 2.

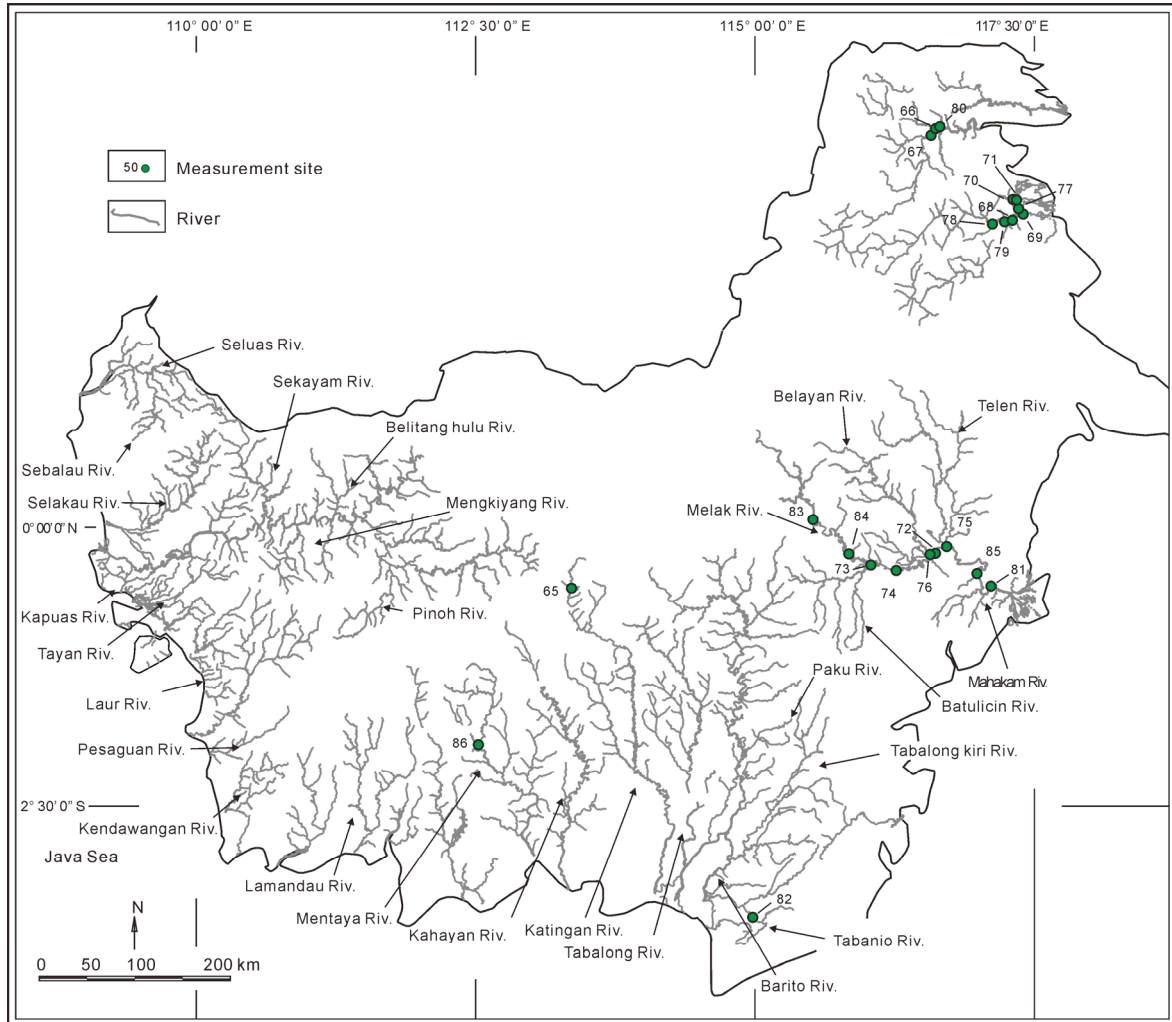


Fig. 65. Locations of measurement sites for cross-sectional geometry of fluvial channels in Kalimantan. Site numbers are listed in Table 2.

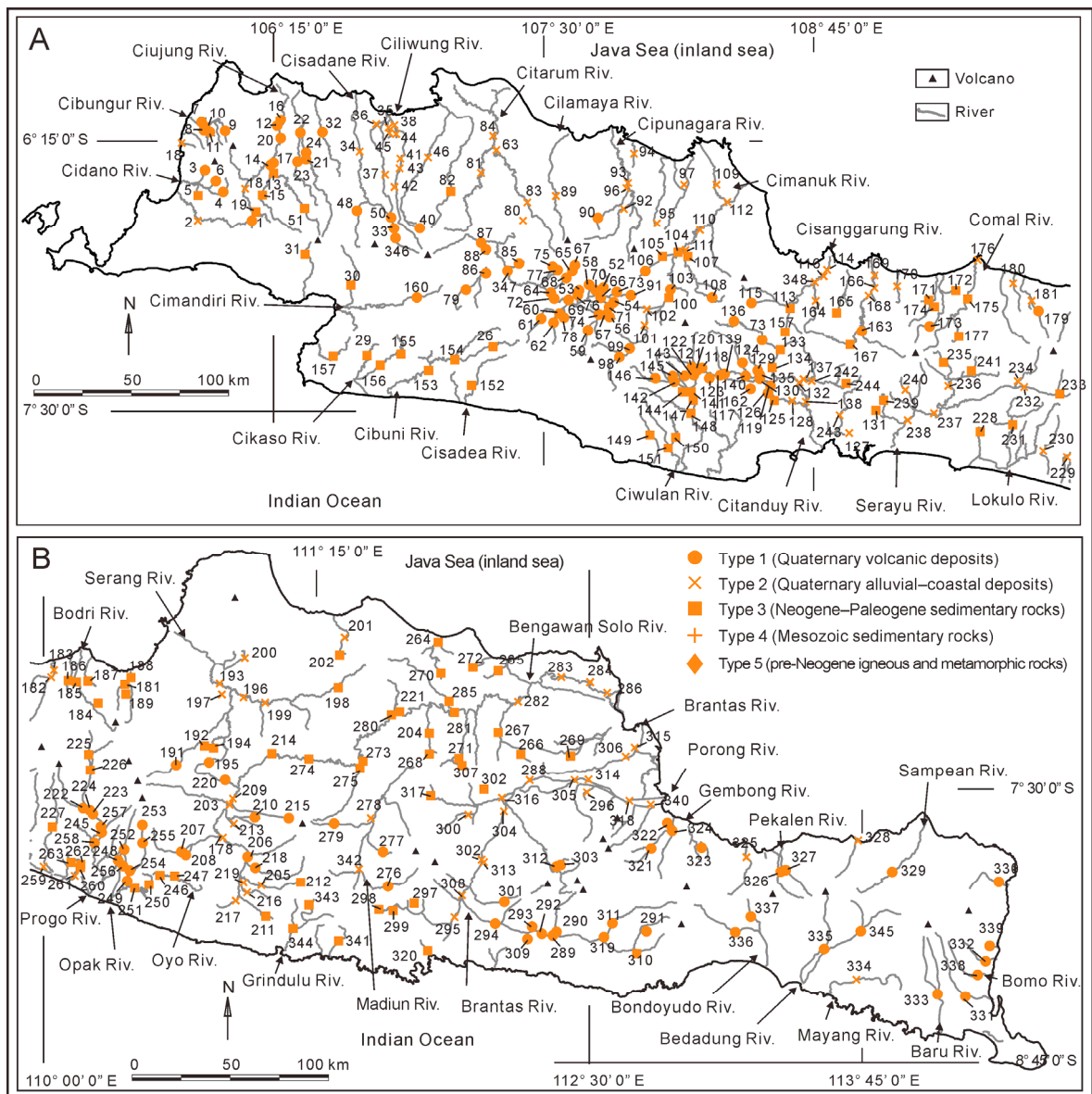


Fig. 66. River bed and bank materials at the measurement sites for discharges in Java. Site numbers are listed in Table 1.

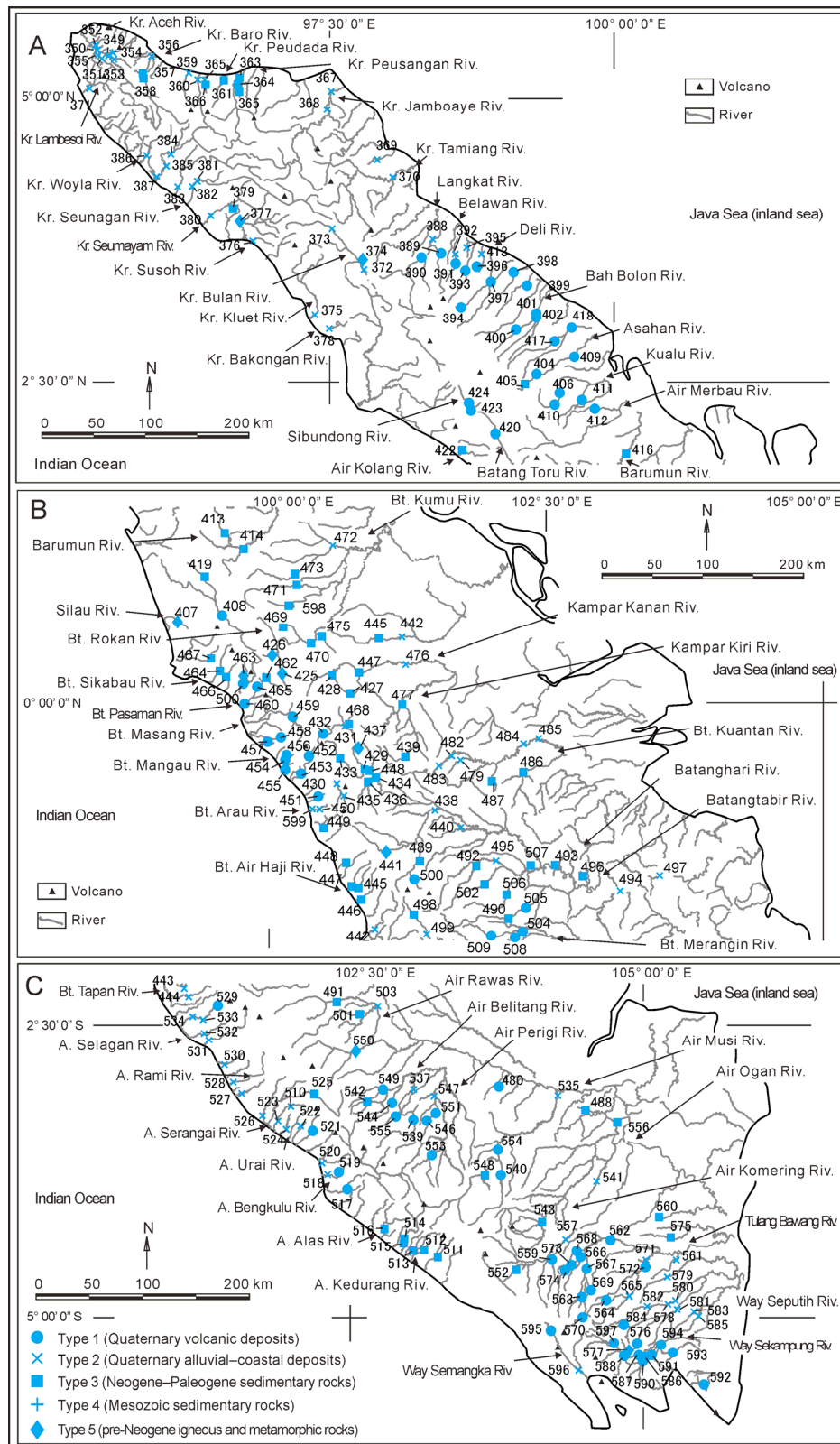


Fig. 67. River bed and bank materials at the measurement sites for discharges in Sumatra. Site numbers are listed in Table 1.

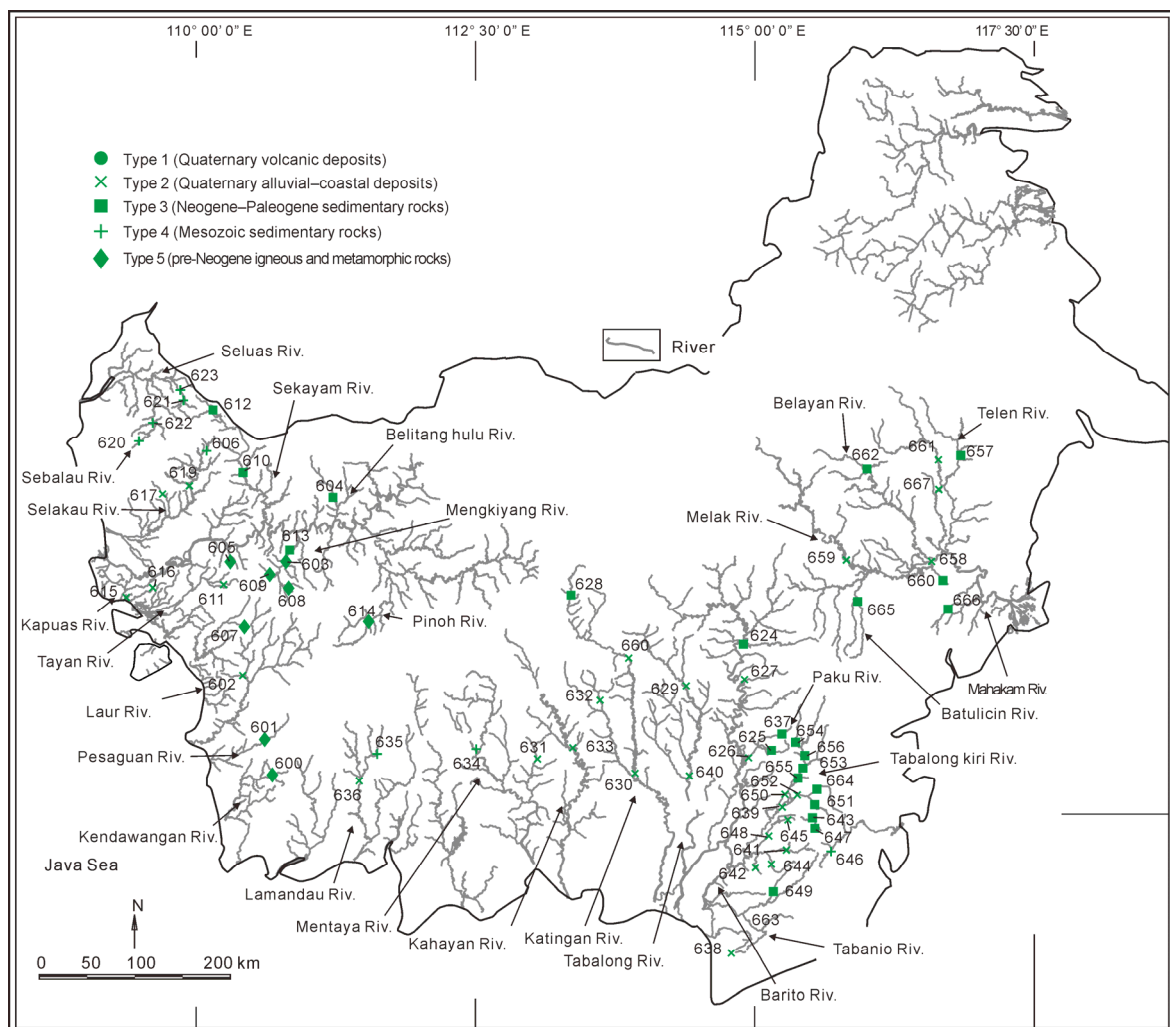


Fig. 68. River bed and bank materials at the measurement sites for discharges in Kalimantan. Site numbers are listed in Table 1.

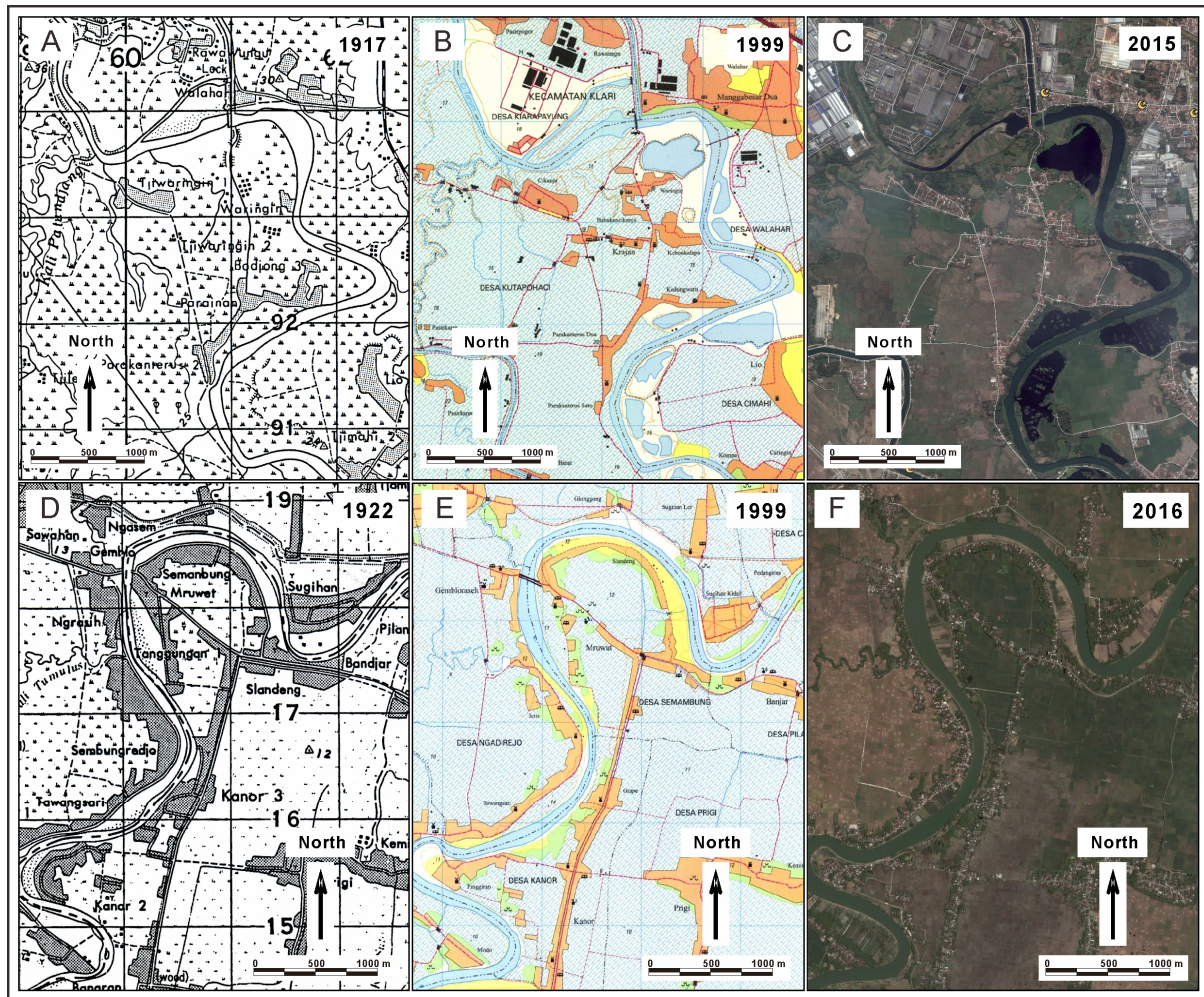


Fig. 69. An example of the comparison of river morphology using topographic maps and satellite images from the early 20th century, the end of 20th century, and the present to evaluate the degree of engineering modification of fluvial systems. The Citarum River at Tanjungpura is shown in (A) 1917, (B) 1999, and (C) 2015 (site 63 in Fig. 2 and Table 1). Map A is from the 1:50,000 Topografische Dienst. Batavia, surveyed from 1908 to 1917, and reprinted by the U.S. Army Map Service. Map B is from the 1:25,000 Indonesian Agency for Geospatial Information topographic map, surveyed in 1999 and map C is from a Google Earth's aerial photograph. The Bengawan Solo River at Bojonegoro is shown in (D) 1922, (E) 1999, and (F) 2016 (site 271 in Fig. 2 and Table 1). Map D is from the 1:50,000 Topografische Dienst. Batavia, surveyed in 1922, and reprinted by U.S. Army Map Service. Map E is from the 1:25,000 Indonesian Agency for Geospatial Information topographic map, surveyed in 1997, and map F is from a Google Earth's aerial photograph.

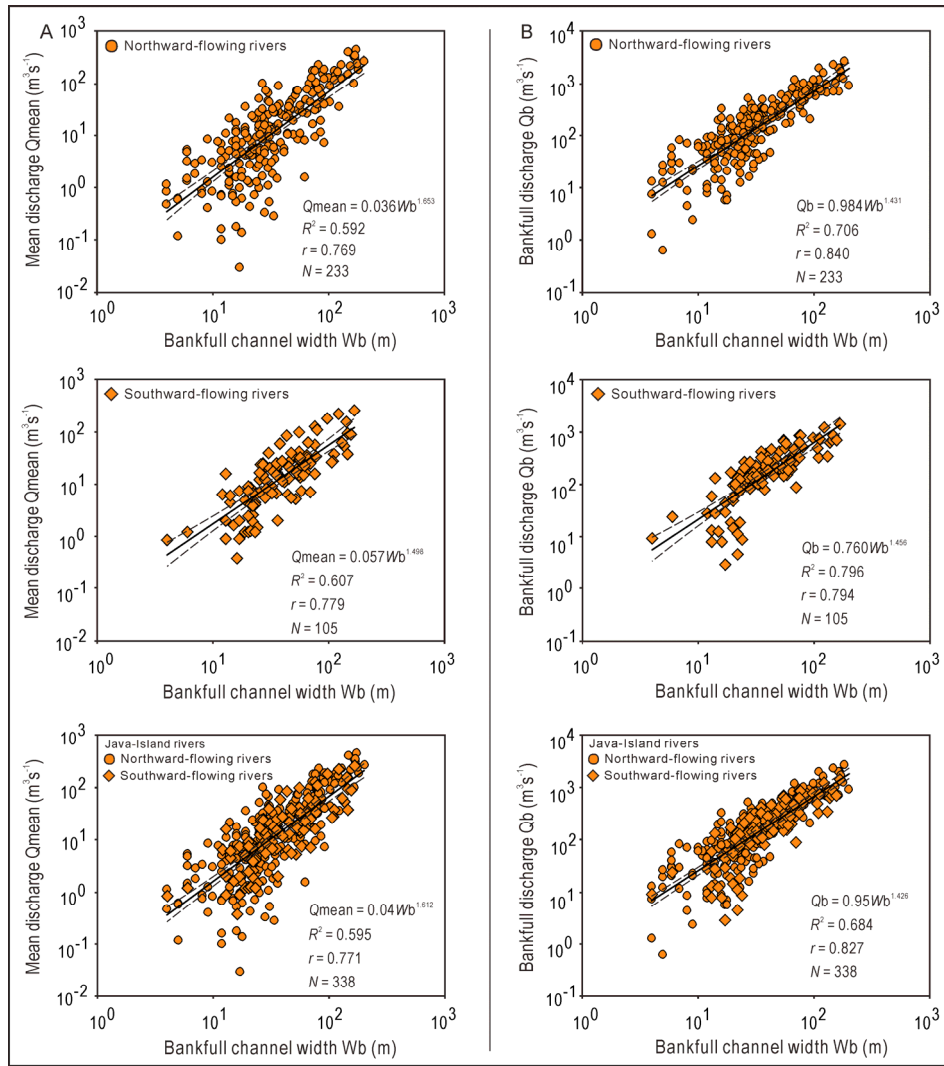


Fig. 70. (A) Relationships between bankfull channel width (W_b) and mean discharge (Q_{mean}) and (B) between W_b and the bankfull discharge (Q_b) for northward-flowing and southward-flowing rivers in Java and for all rivers in Java.

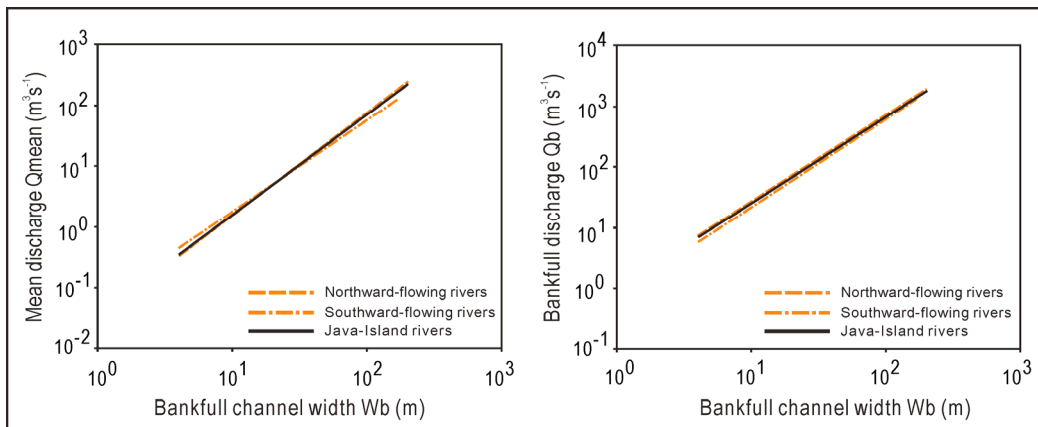


Fig. 71. Comparison of the regression lines for northward-flowing and southward-flowing rivers, and for all rivers in Java. Data are shown in Fig. 70.

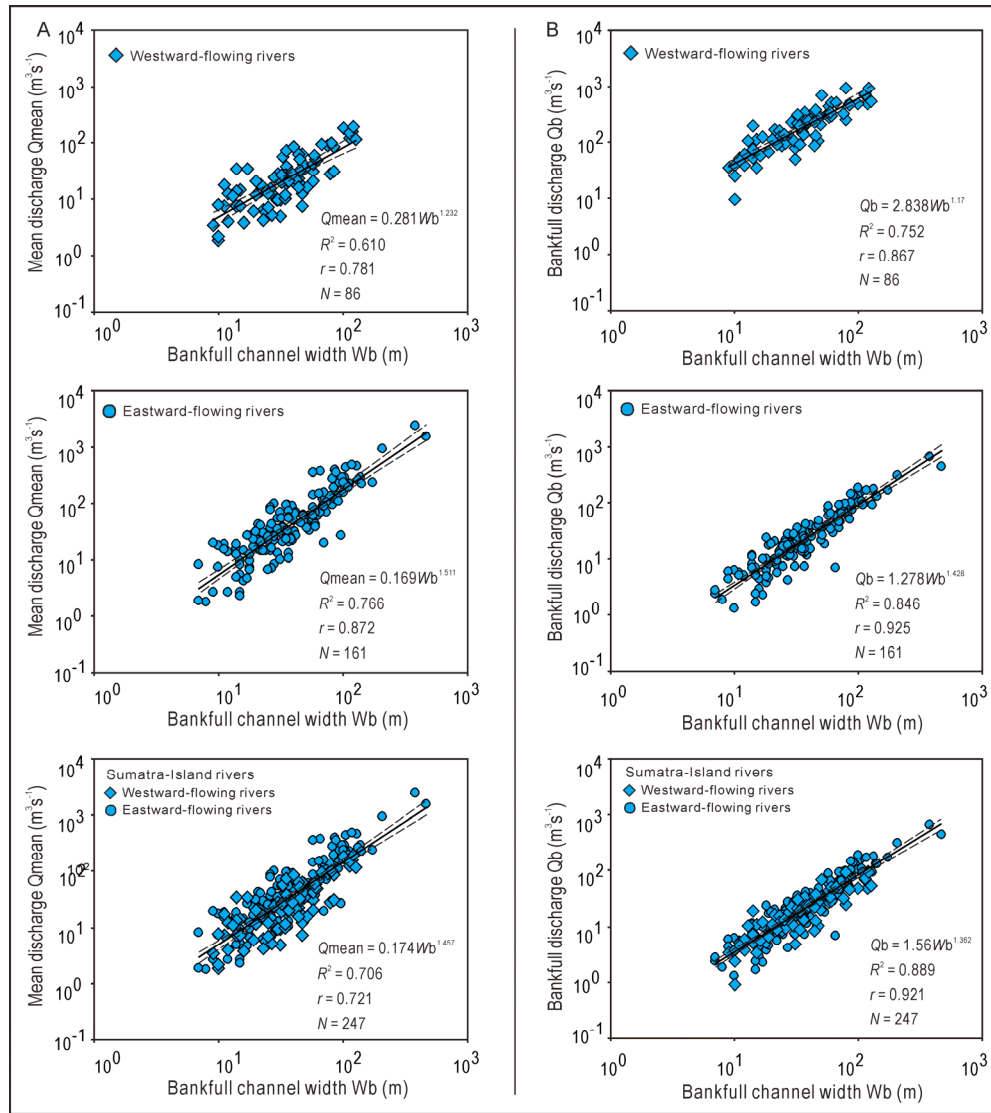


Fig. 72. Relationships between W_b and Q_{mean} (A) and between W_b and Q_b (B) for westward-flowing and eastward-flowing rivers in Sumatra, and for all rivers in Sumatra.

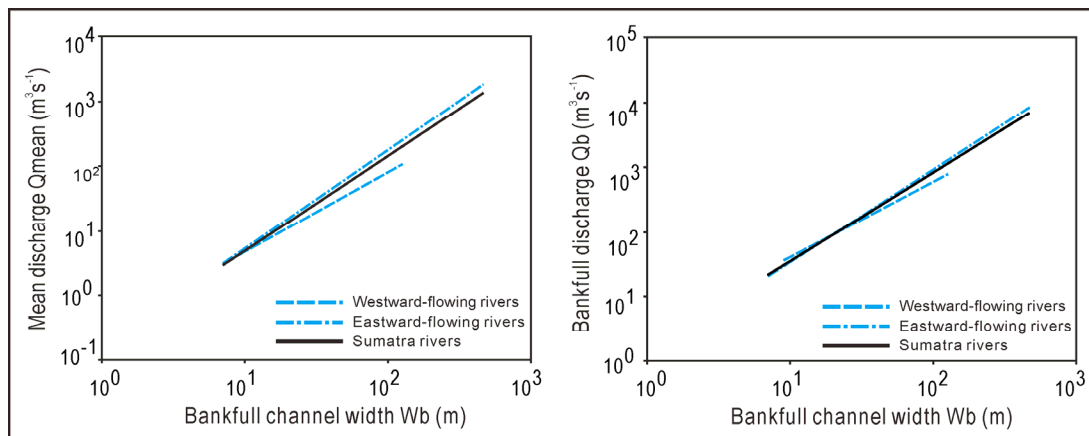


Fig. 73. Comparison of the regression lines for westward-flowing and eastward-flowing rivers, and all rivers in Sumatra. Data are shown in Fig. 72.

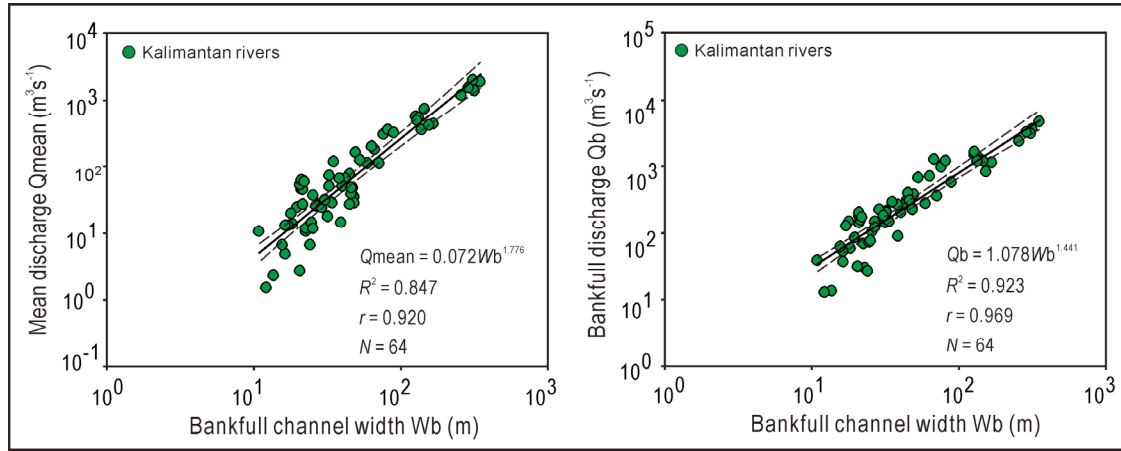


Fig. 74 Relationships between W_b and Q_{mean} , and W_b and Q_b for all rivers in Kalimantan.

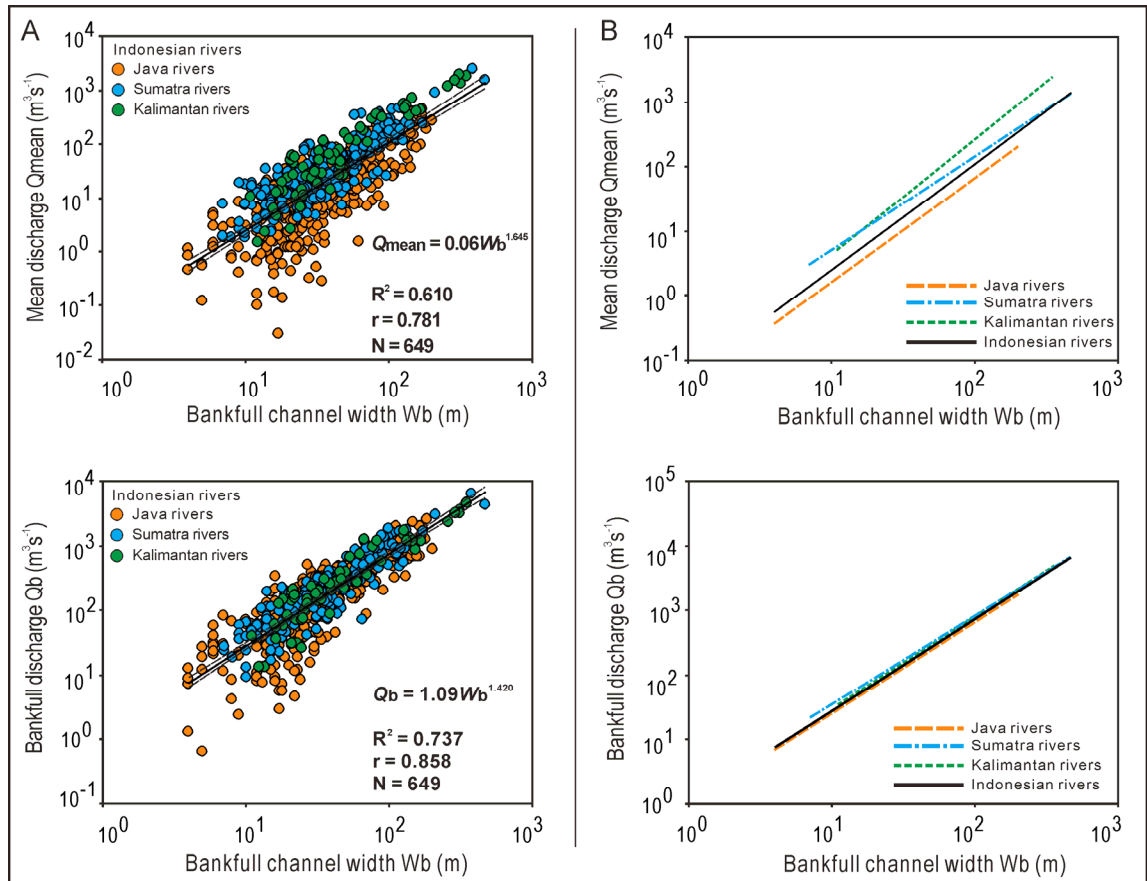


Fig. 75 (A) Relationships between W_b and Q_{mean} , and W_b and Q_b for all rivers in Java, Sumatra, and Kalimantan. (B) Comparisons of the regression lines for hydrological data given in A.

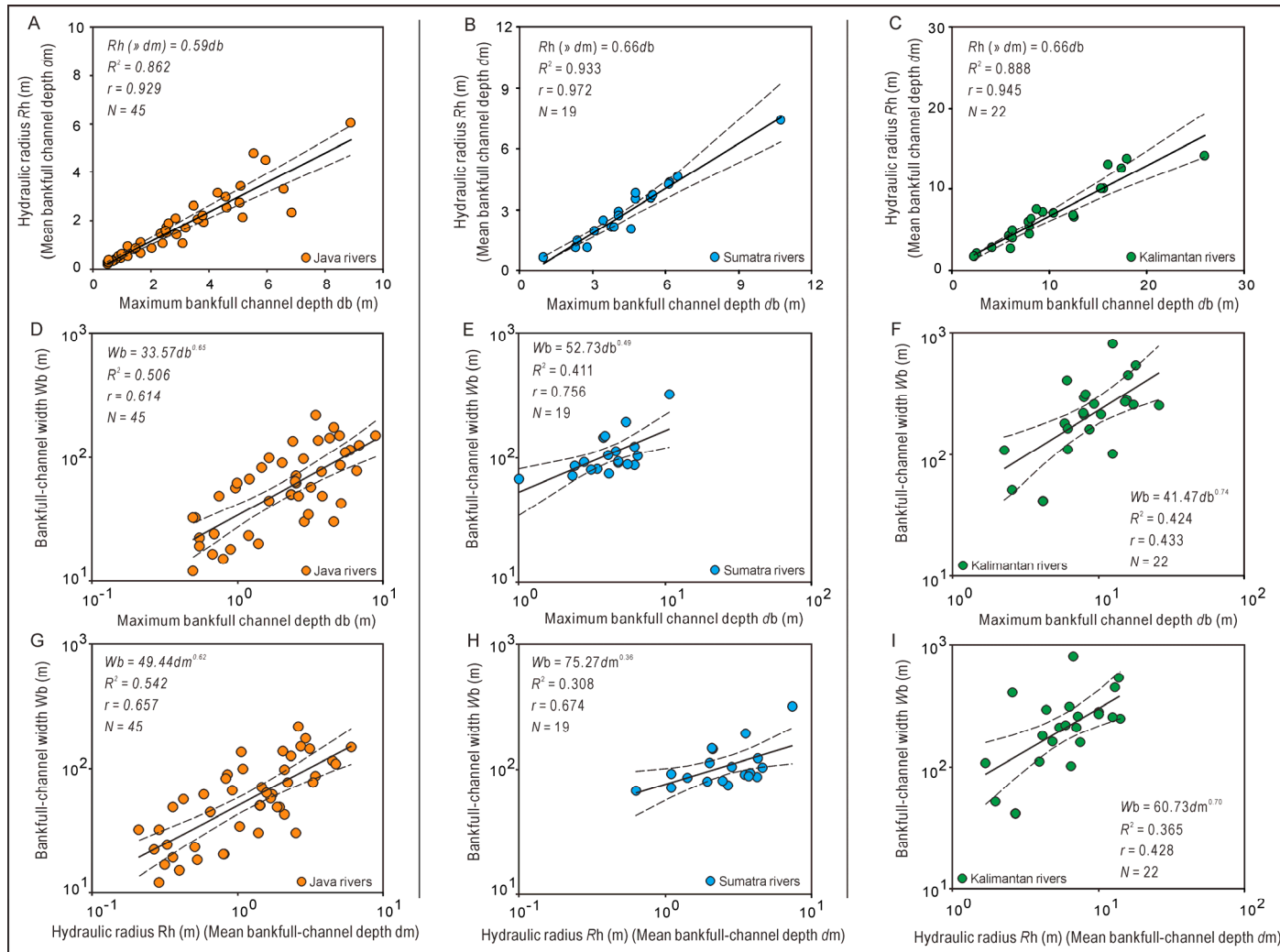


Fig. 76. Relationship between mean bankfull channel depth d_m and maximum bankfull channel depth (d_b) in (A) Java, (B) Sumatra, and (C) Kalimantan rivers. Relationship between W_b and the maximum bankfull channel depth (d_b) in (D) Java, in (E) Sumatra, and in (F) Kalimantan rivers. Relationship between W_b and d_m in (G) Java, in (H) Sumatra, and in (I) Kalimantan rivers.

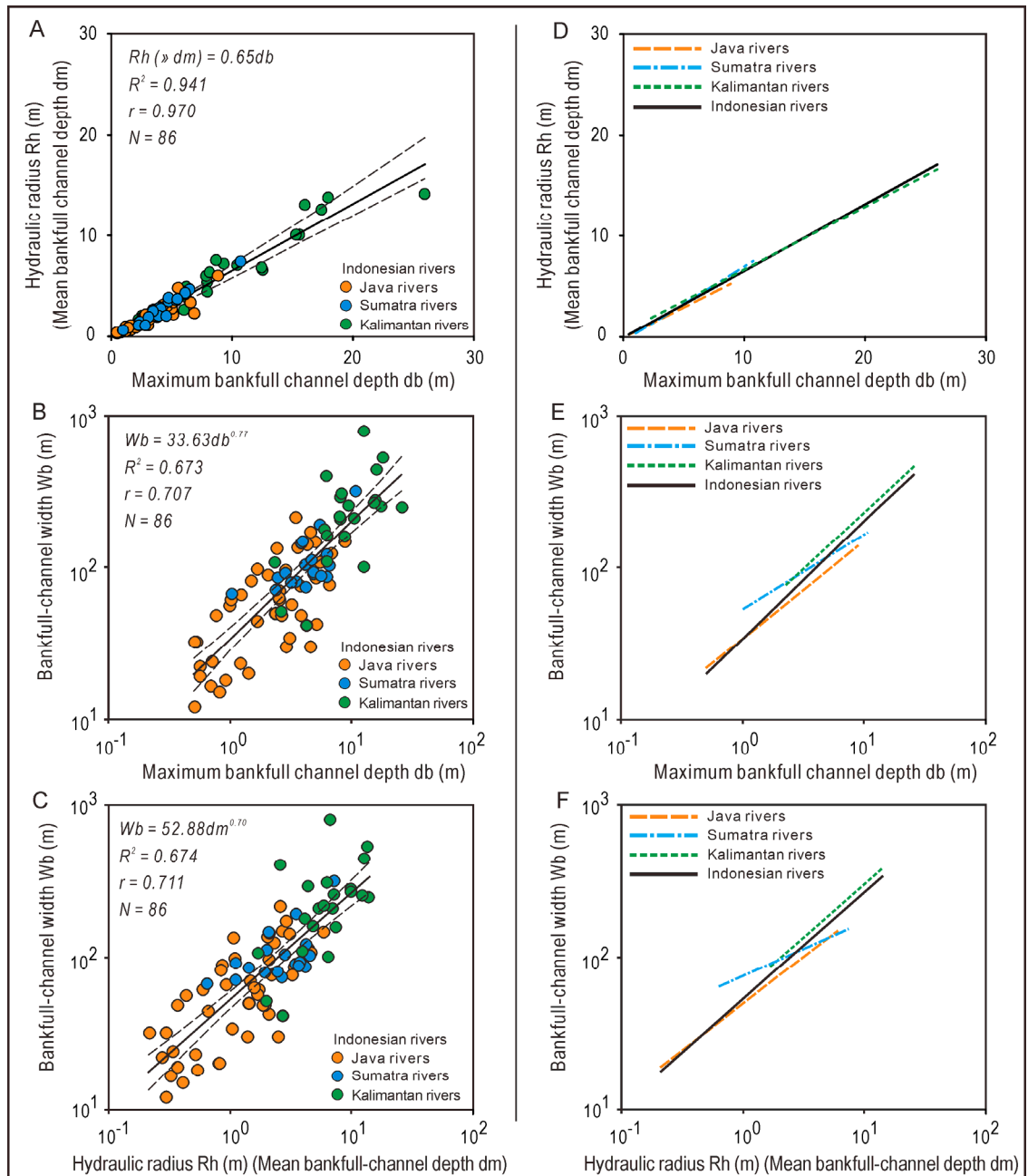


Fig. 77. (A–C) Empirical relationships between hydrological parameters in Indonesian rivers, and (D–F) comparison of regression lines for these relationships.

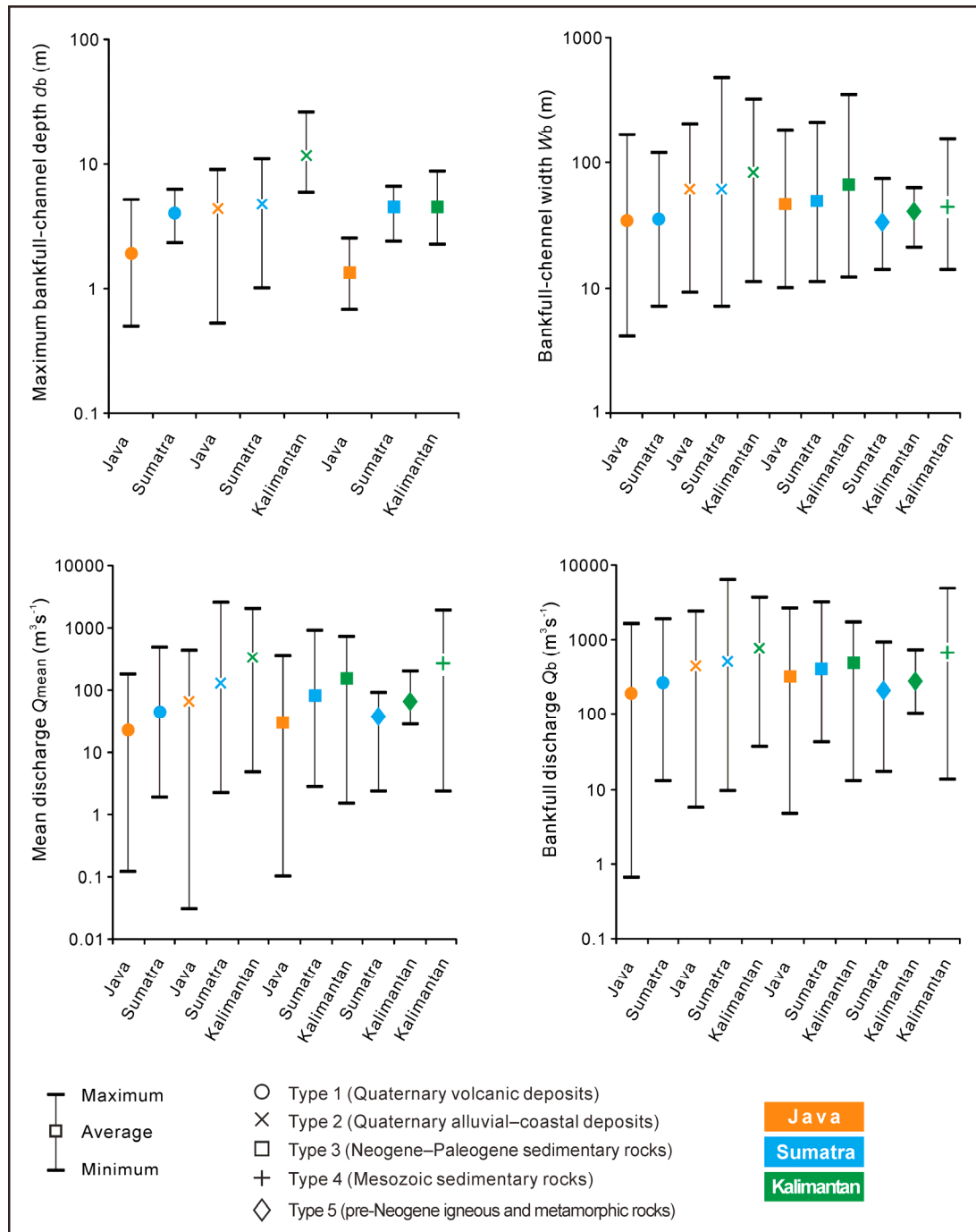


Fig. 78. Relationships between river bed and bank materials and d_b , W_b , Q_{mean} , and Q_b .

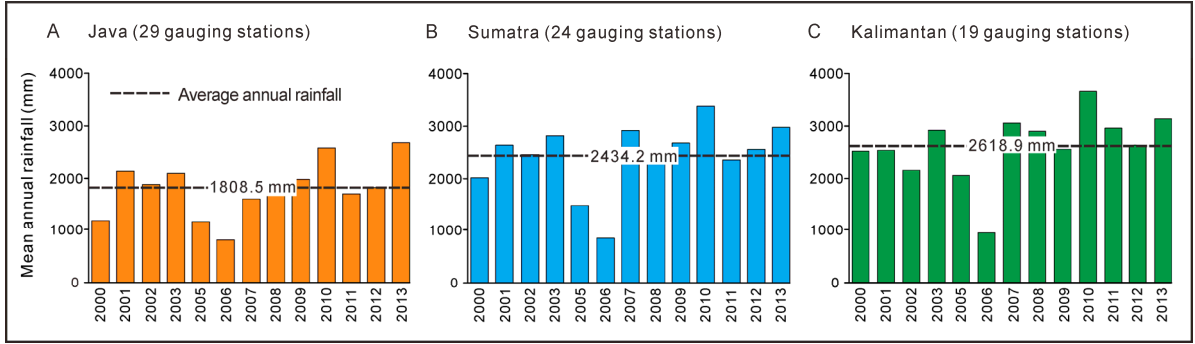


Fig. 79. Mean annual rainfall data from 2000 to 2013 in Java, Sumatra, and Kalimantan. Data are from Indonesia Central Bureau of Statistics (2015).

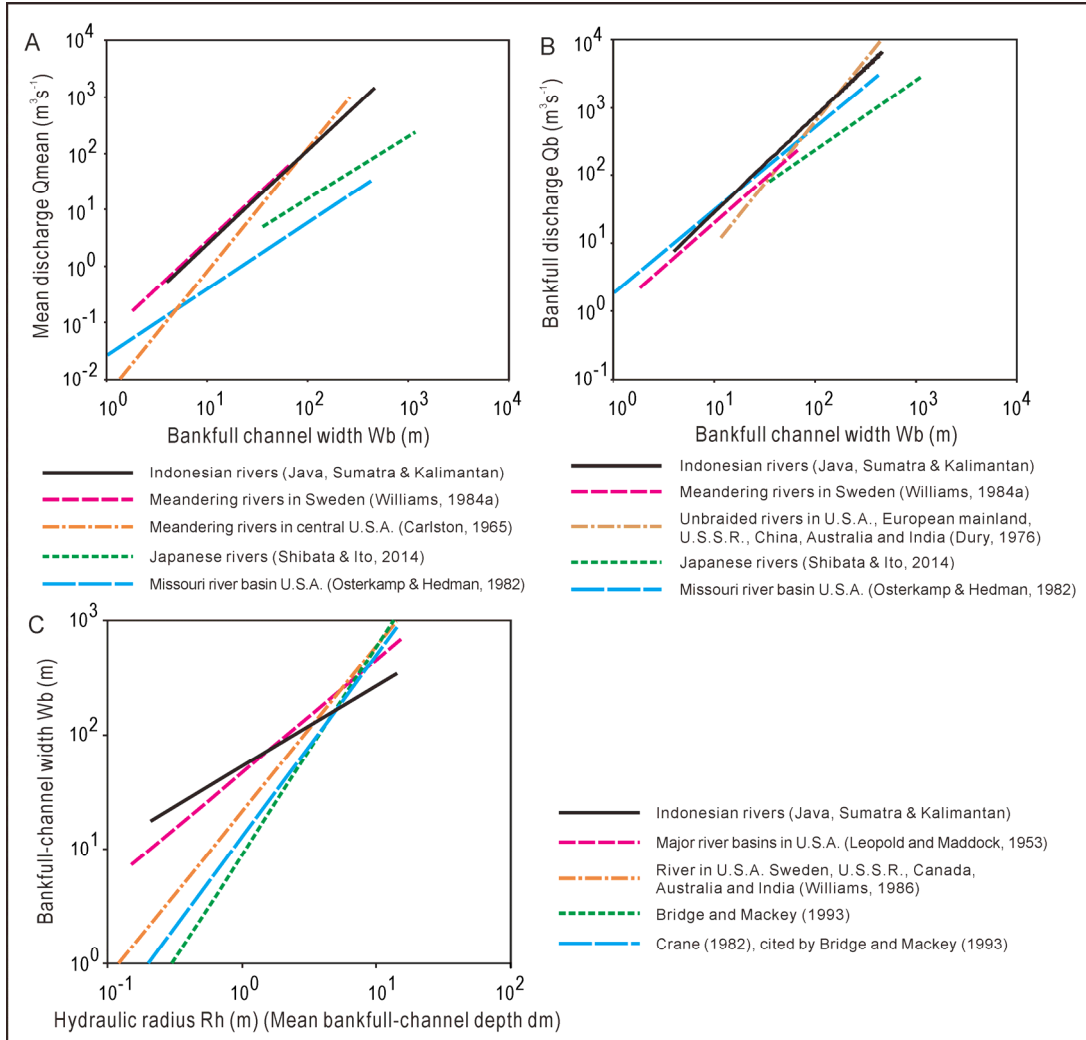


Fig. 80. Comparison of empirical relationships between hydrological parameters obtained from different regions for (A) Q_{mean} and W_b , (B) Q_b and W_b , and (C) W_b and d_m .

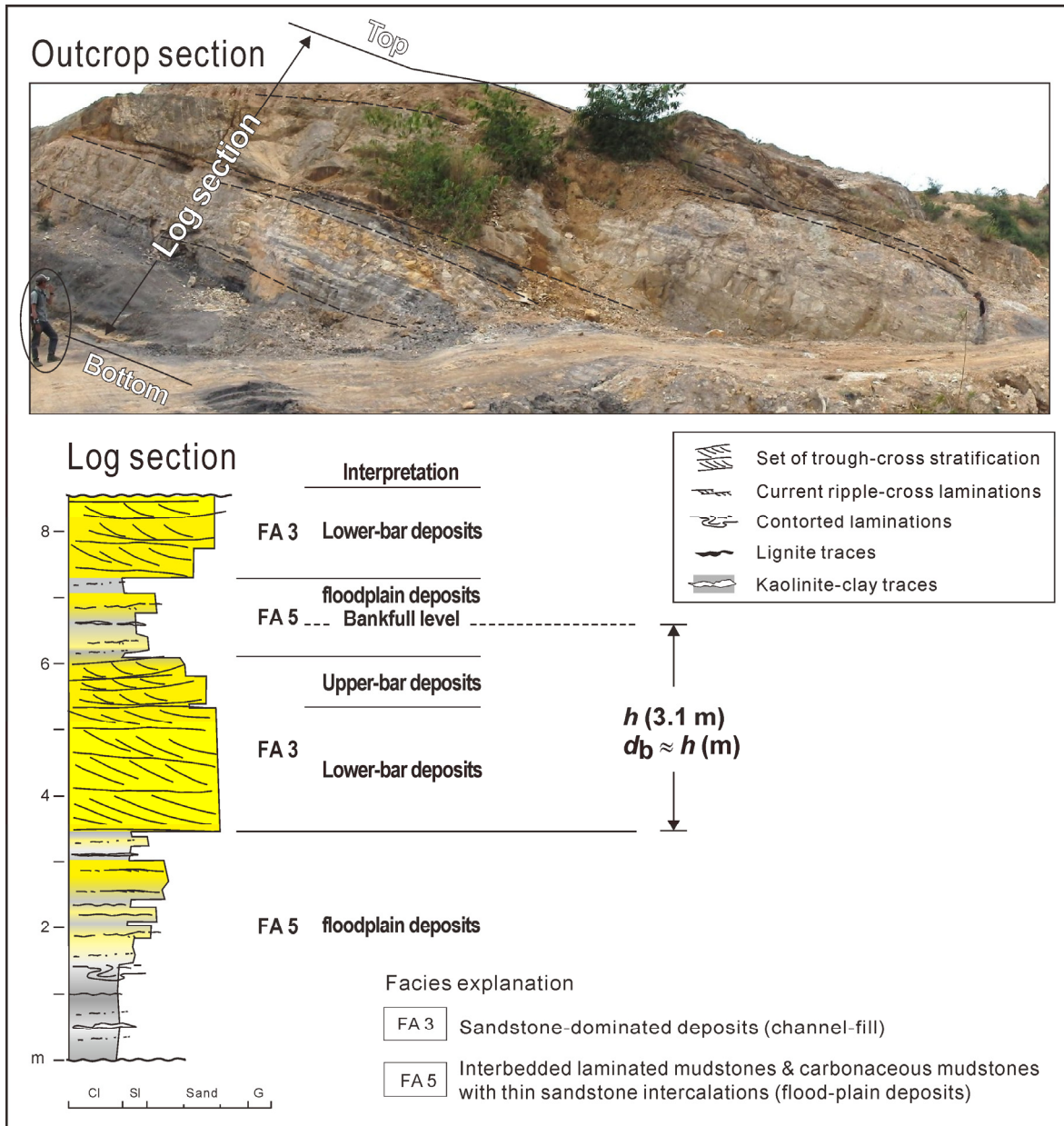


Fig. 81. Example-1 (IV 5) of log section measurement and interpretation of compound-bar thickness to estimate bankfull-channel depth. The interpreted maximum paleochannel depth associated with this channel-bar deposits was estimated at 3.1 m. Person with black circle give scale guide to the photograph.

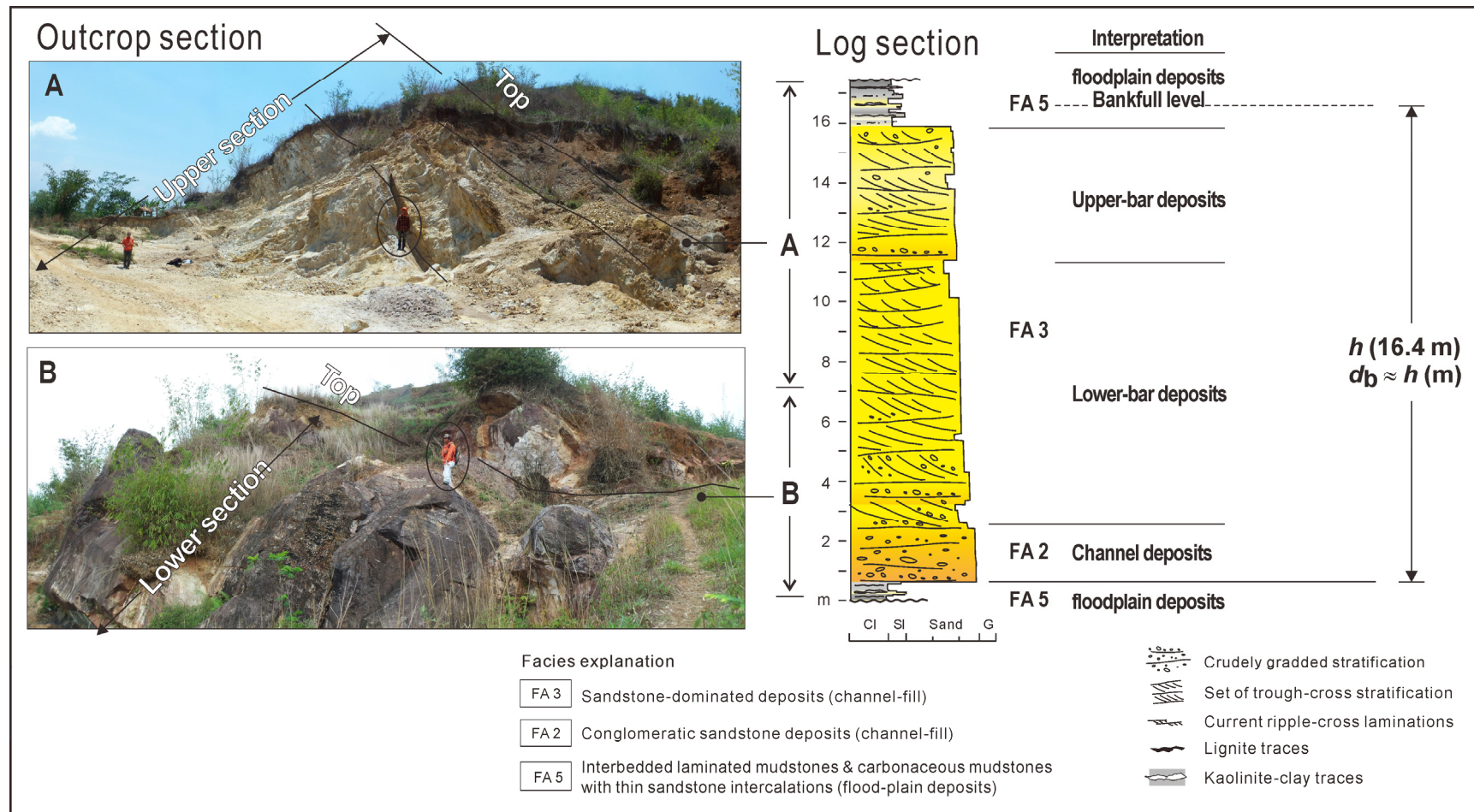


Fig. 82. Example-2 (IV 1) of log section measurement and interpretation of compound-bar thickness to estimate bankfull-channel depth at the. The interpreted maximum paleochannel depth associated with this channel-bar deposits was estimated at 16.4 m. Person with black circle give scale guide to the photograph.

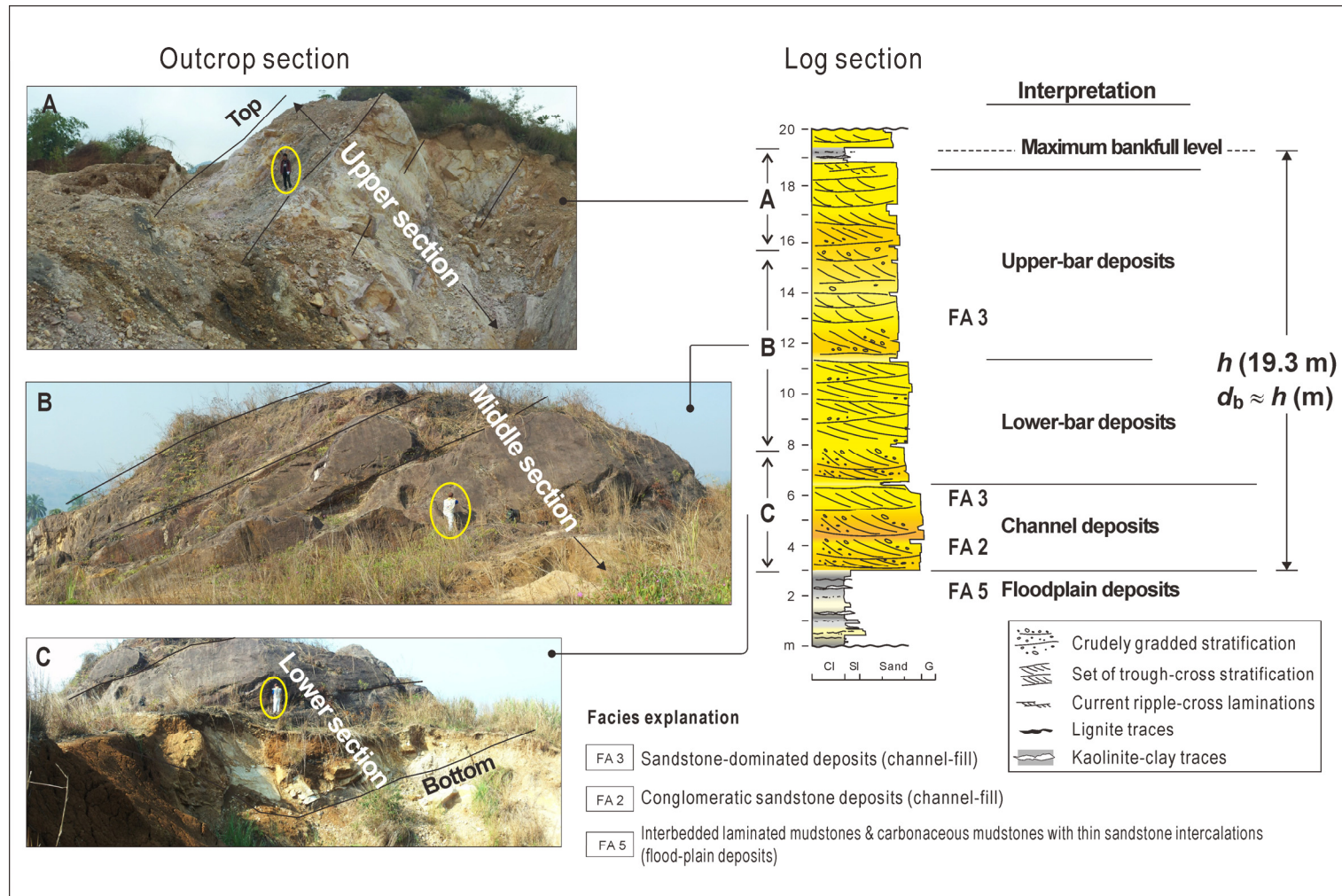


Fig. 83. Example-3 (IV 2) of log section measurement and interpretation of compound-bar thickness to estimate bankfull-channel depth at the. The interpreted maximum paleochannel depth associated with this channel-bar deposits was estimated at 19.3 m. Person with black circle give scale guide to the photograph.

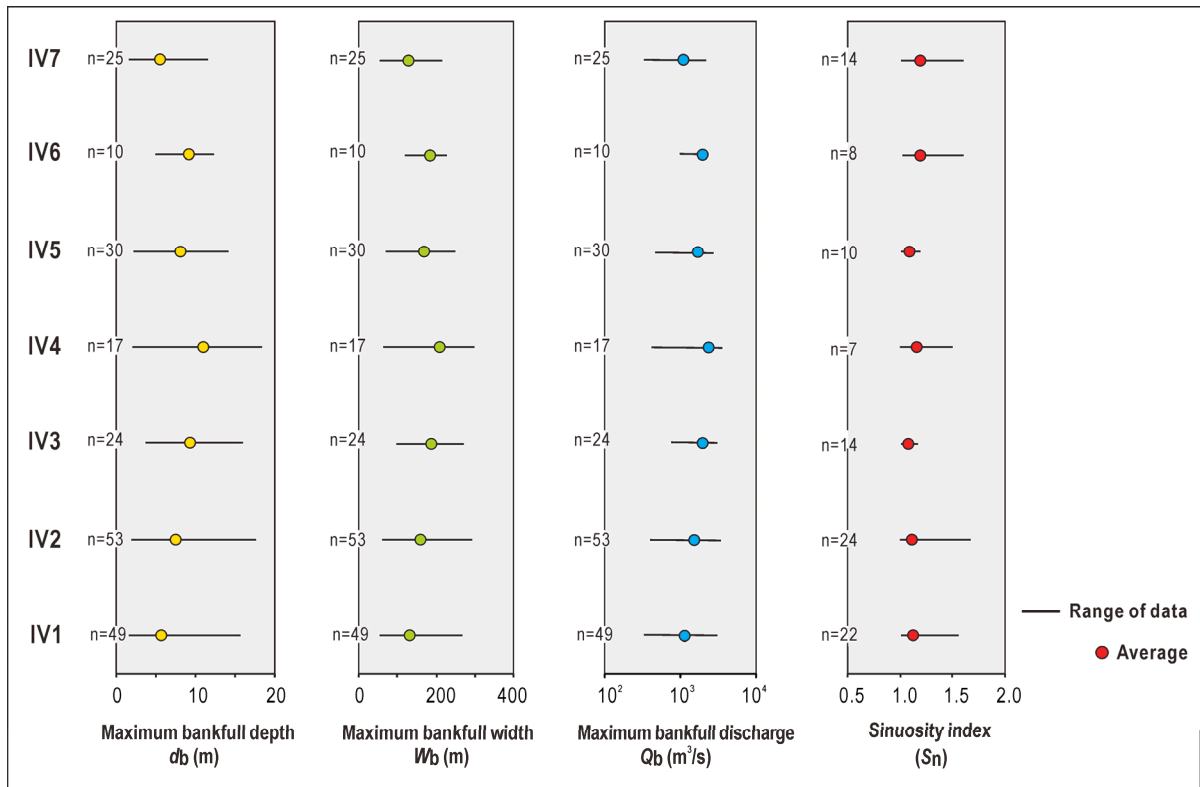


Fig. 84. Result of the paleochannel dimension and paleodischarge reconstruction using data from the fluvial succession of the Bayah Formation.

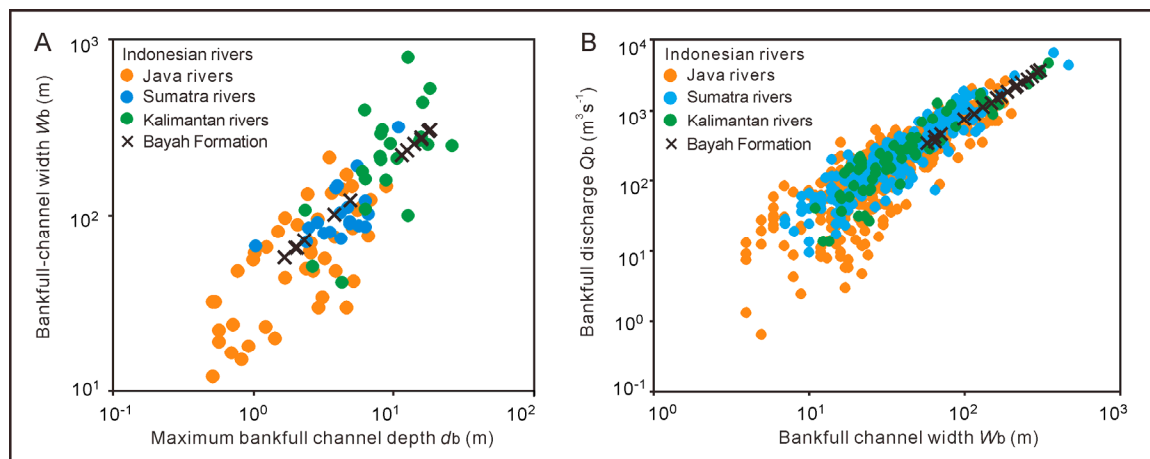


Fig. 85. Diagram indicating relationships between paleohydrological features of the Indonesian modern river and the reconstructed paleohydrological features of the Bayah Formation.

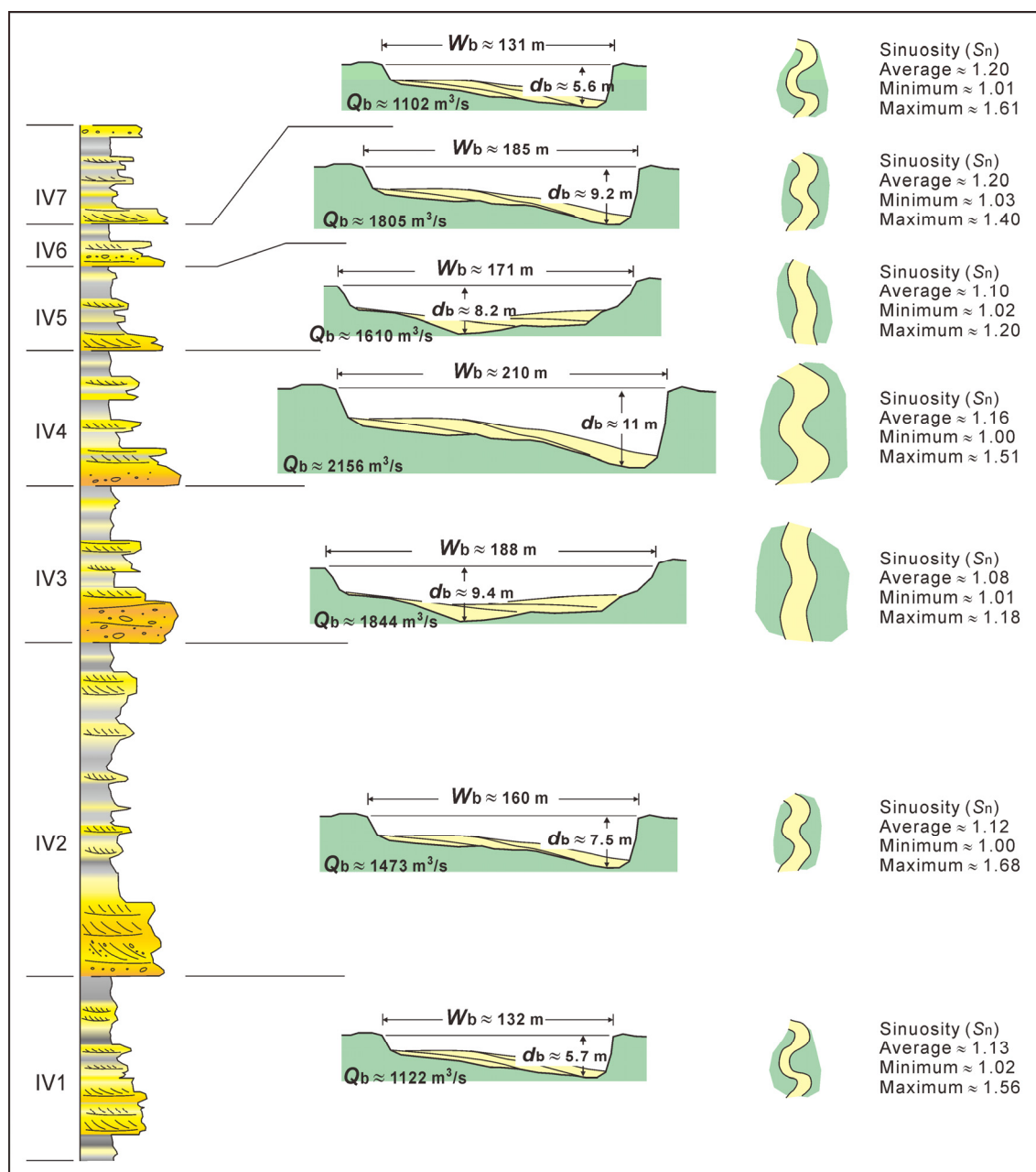


Fig. 86. Schematic illustration of temporal variation in paleohydrological parameters of the Bayah Formation. Each schematic channel dimension represents average paleohydrological parameter values of the intervals (IV1–IV7). Illustrations of paleochannel cross-section and plan-view sinuosity were scaled according to the parameter values.

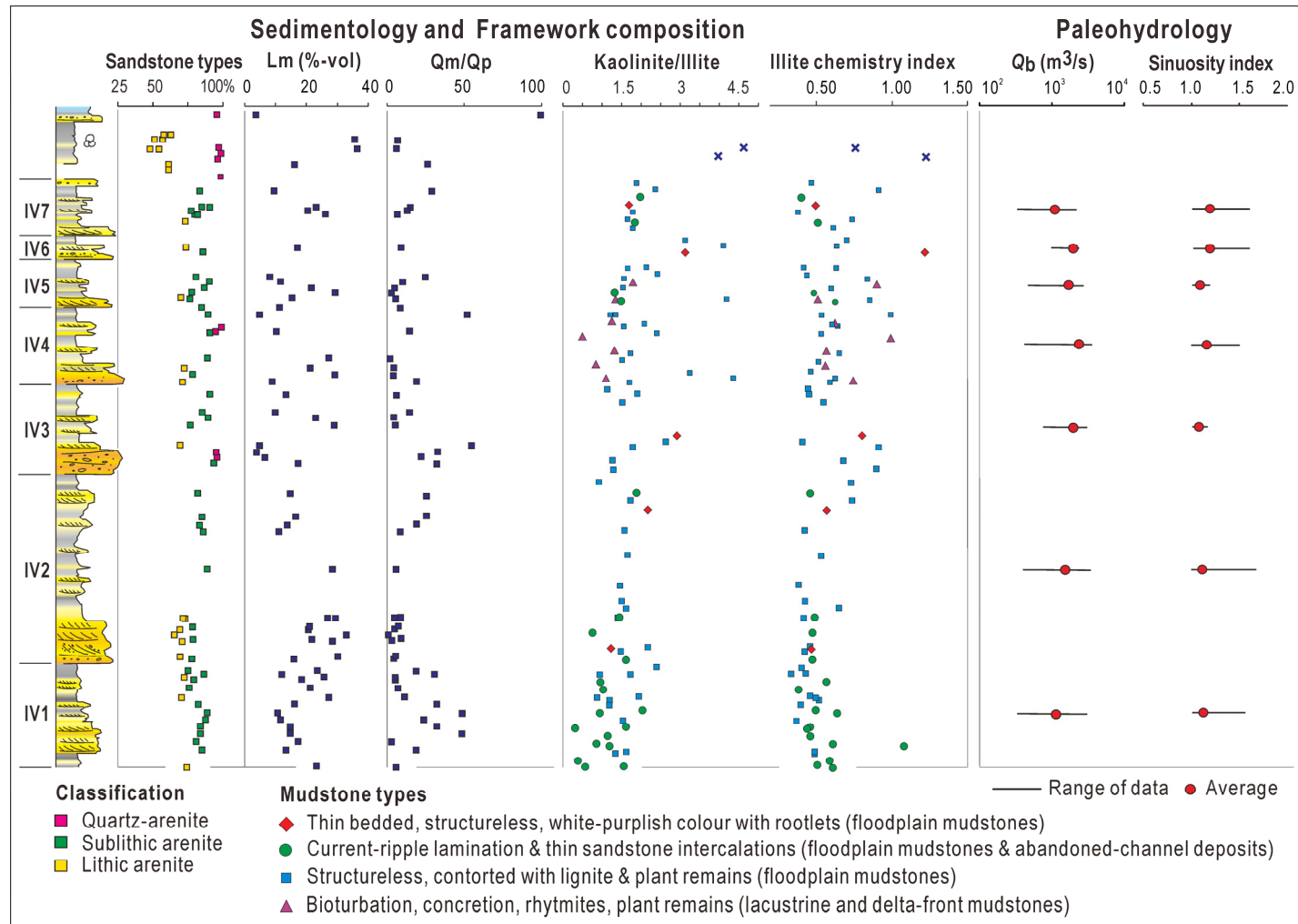


Fig. 87. A schematic summary diagram of temporal variations in framework composition of sandstones, clay mineral composition, and paleohydrological features of the Bayah Formation fluvial-lacustrine-delta succession in relation to its component intervals (IV1–IV7). See Fig. 26 for the definition of the intervals.

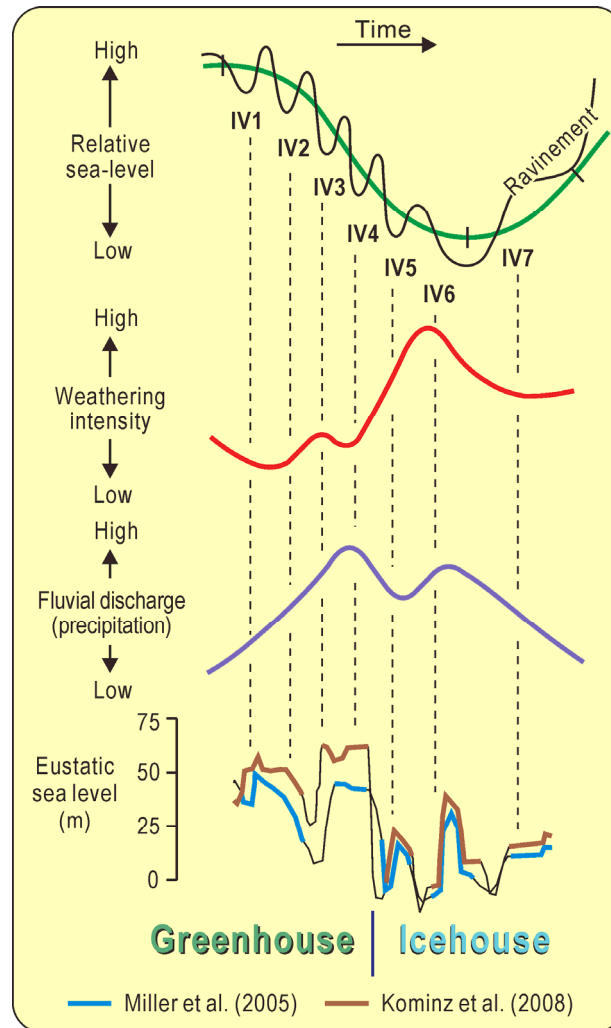


Fig. 88. The relationships between relative changes in sea level, intensity of weathering, and precipitation for the development of the Bayah Formation fluvial–lacustrine–delta succession in a convergent margin setting influenced by a low-latitude tropical climatic condition during a transitional period from greenhouse to icehouse stages at the Eocene–Oligocene time. IV1–IV7 denote component intervals of the formation defined in Fig. 26.

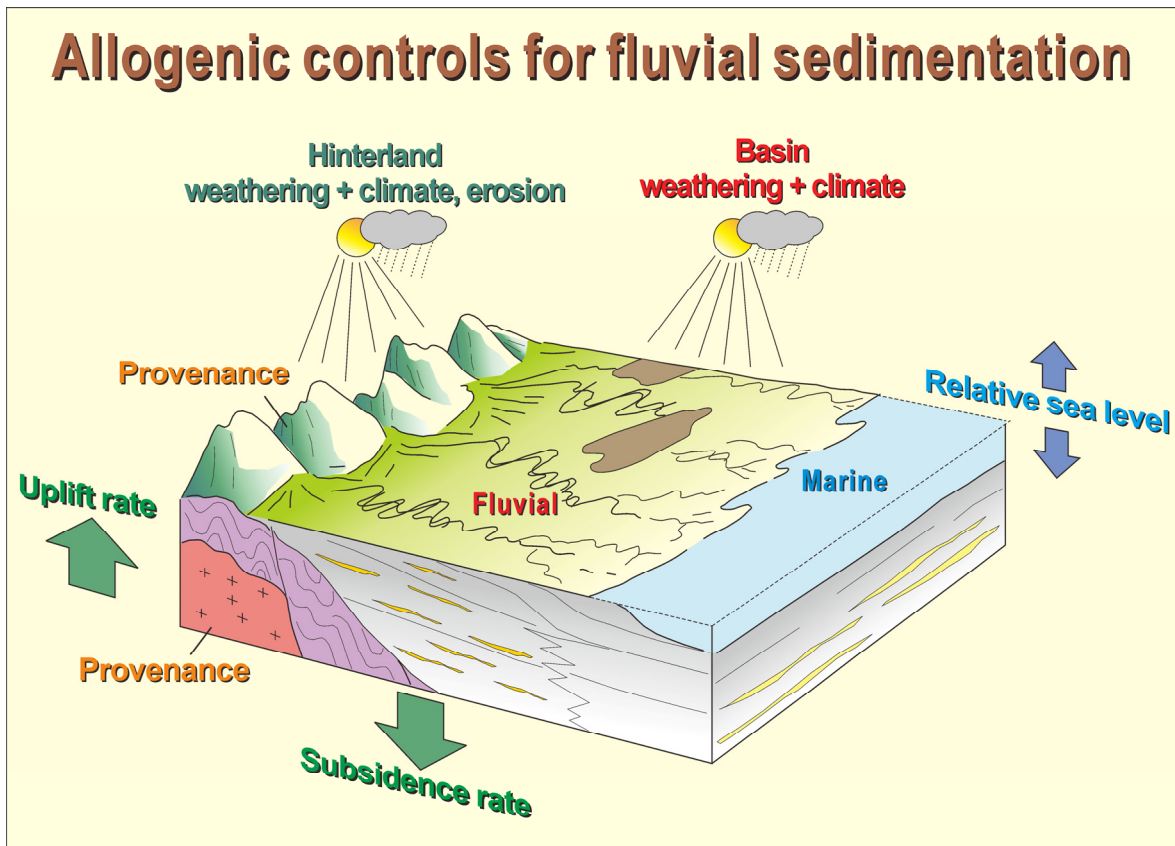


Fig. 89. Summary diagram illustrating the interaction of external factors that control spatial and temporal variations in channel-fill deposits, fluvial styles, and framework composition of the Bayah Formation. Fluctuation in the rate of subsidence, changes in rainfall seasonality, and relative sea level seem to have been the most significant factors of allogenic controls for the development of the Bayah Formation.

Table 1. Hydrological data from river channels in the Indonesian islands. The numbers correspond to the site numbers in Figs. 59, 60, and 61.

No.	River system	River	Site name	W_b (m)	Q_{mean} (m^3s^{-1})	Q_b (m^3s^{-1})	Observation year (Q_{mean})
1	Ciliman	Ciliman	Leuwikopo	20	9.35	84.68	1986–2009
2	Ciliman	Ciliman	Munjul	40	24.28	118.95	1986–2009
3	Cibungur	Cisata	Pasir Sereh	19	4.06	47.60	1986–2009
4	Cibungur	Cilemer	Cipadung	21	4.14	28.56	1977–1993
5	Cibungur	Cimoyan	Pasir Gadung	13	3.97	54.83	1990–2009
6	Cibungur	Cikadueun	Cibogo	12	2.44	91.08	1990–2009
7	Cidano	Cidano	Peusar	31	10.99	44.57	1993–2009
8	Cibama	Cibama	Kalumpang	17	2.90	62.12	1990–1993
9	Cidano	Cidanghiang	Cibitung	9	0.41	2.36	1991–2009
10	Cidano	Cibojong	Tambakan	7	2.89	11.45	1991–2009
11	Cidano	Cikalumpang	Panggilingan	8	0.87	4.30	1991–2009
12	Cibanten	Cibanten	Pabuaran	18	1.97	20.05	1993–2007
13	Ciujung	Ciberang	Sabagi	30	25.16	211.65	1987–2009
14	Ciujung	Ciberang	Jembatan Keong	35	28.93	349.81	1995–2009
15	Ciujung	Cisimet	Leuwidamar	36	15.83	132.57	1992–2009
16	Ciujung	Ciujung	Kragilan	76	93.59	818.88	1986–2009
17	Ciujung	Ciujung	Rangkasbitung	86	79.90	728.81	1986–2009
18	Ciujung	Ciujung	Cileuleus	28	18.95	138.44	1993–2009
19	Ciujung	Ciujung hulu	Bojongmanik	22	7.29	44.55	1994–2009
20	Ciujung	Ciujung	Kedung Cinde	75	96.68	462.00	1997–2009
21	Cidurian	Cidurian	Kopomaja	25	19.57	190.74	1986–2003
22	Cidurian	Cidurian	Parigi	37	28.22	250.26	1986–2009
23	Ciujung	Cibeureum	Neglasari	12	6.88	62.20	1987–2009
24	Cidurian	Cidurian	Ranca Sumur	14	21.52	85.17	1992–2009
25	Cibuni	Cibuni	Cibungur	55	96.34	682.66	1986–2005
26	Cibuni	Cibuni	Palatar	27	19.27	163.00	1991–2005
27	Cikaso	Cikaso	Parungseah	55	41.61	647.70	1992–2005
28	Cikaso	Cikaso	Leuwipanjang	35	19.13	178.32	1991–2005
29	Cikaso	Cikaso	Cipawarang	27	24.80	125.00	1987–1994
30	Cimandiri	Citarik	Pajagan	25	12.56	98.04	1993–2005
31	Cibareno	Cibareno	Ciawi	35	24.59	190.48	1990–2005
32	Cimanceuri	S. Cimanceuri	Kutruk (Balaraja)	16	17.31	118.11	1992–2006
33	Cisadane	Cisadane	Genteng	19	14.02	85.29	1991–2008
34	Cisadane	Cisadane	Babakan	30	64.55	273.82	1994–2008
35	Kali Angke	Kali Grogol	Pal Merah	17	0.98	5.68	1992–2008
36	Kali Angke	Kali Angke	Rawabuaya	23	4.29	18.64	1990–2009
37	Kali Angke	Kali Pasanggarahan	Sawangan	14	1.77	27.85	1992–2009
38	Kali Angke	Kali Pasanggarahan	Kebon Jeruk	37	16.02	38.10	1989–2009
39	Ciliwung	Ciliwung	Katulampa	55	8.21	317.71	1990–2009
40	Ciliwung	Ciesek	Palumbon	8	0.75	8.40	1986–1993
41	Ciliwung	Ciliwung	Ratujaya	36	11.73	230.39	1991–2007
42	Ciliwung	Ciliwung	Kampung Kelapa	25	13.19	223.17	1990–2007
43	Ciliwung	Ciliwung	Sugutamu	19	35.64	150.56	1987–2007
44	Ciliwung	Kali Krukut	Bendungan Hilir	11	7.65	48.83	1991–2009
45	Kali Sunter	Kali Sunter	Cipinang Muara	9	8.55	22.17	1992–2009
46	Kali Bekasi	Sungai Bekasi	Pondok Mitra	35	27.38	207.28	2005–2010
47	Cikarang	Cikarang	Cikarang	32	14.19	149.01	1986–2004
48	Cisadane	Cianten	Sodong	50	19.32	276.23	1991–2000
49	Cisadane	Cisadane	Batubeulah	166	96.62	696.23	1986–2008
50	Cisadane	Cisadane	Legokmuncang	31	14.77	144.25	1986–2009
51	Ciujung	Ciberang	Cileuksa	32	6.36	121.00	1929–1934
52	Citarum	Cikeruh	Cikuda	12	0.72	42.94	1986–2009
53	Citarum	Cibodas	Jatisari	9	1.24	20.46	1986–1990
54	Citarum	Cijalupang	Peundeuy	5	0.59	19.43	1986–2009
55	Citarum	Cikeruh	Babakan Bandung	6	1.29	30.90	1986–1995
56	Citarum	Cirasea	Cengkrong	6	3.10	29.09	1987–2009
57	Citarum	Cirasea	Andir	7	2.92	29.94	1986–1992
58	Citarum	Cipanjal	Kepuh	5	0.60	27.10	1986–2009
59	Citarum	Citarum	Cibangoak	6	5.20	40.30	1986–1992
60	Citarum	Cisangkuy	Kamasan	16	17.02	139.21	1986–2009
61	Citarum	Ciwidey	Cukanggenteng	11	7.50	59.50	1996–2009
62	Citarum	Cisangkuy	Pataruman	6	4.70	58.22	2005–2009

Table 1. (continued)

No.	River system	River	Site name	W_b (m)	Q_{mean} (m ³ s ⁻¹)	Q_b (m ³ s ⁻¹)	Observation year (Q_{mean})
63	Citarum	Citarum	Tanjungpura	73	173.50	941.80	1960–1979
64	Citarum	Citarum	Nanjung	29	72.99	397.43	1986–2009
65	Citarum	Cikapundung	Maribaya	8	3.40	68.65	1986–2009
66	Citarum	Cikapundung	Pasirluyu (bypass)	18	4.68	67.82	1989–1994
67	Citarum	Cigulung	Maribaya	7	1.83	82.97	1986–2009
68	Citarum	Cikapundung	Gandok	10	3.05	70.36	1986–2009
69	Citarum	Citarum	Dayeuhkolot	37	88.60	322.45	1986–2009
70	Citarum	Cidurian	Sukapada	5	0.57	12.12	1986–2009
71	Citarum	Citarik	Rancakemit	16	12.56	72.78	1986–2000
72	Citarum	Citarum	Mahmud	49	49.38	230.90	1986–2009
73	Citarum	Citarik	Cangkuang	6	1.49	20.64	1998–2008
74	Citarum	Citarum	Majalaya	19	11.93	133.28	1986–2009
75	Citarum	Cimahi	Cicakung	4	0.84	7.26	1996–2009
76	Citarum	Cibeureum	Sukajadi	4	1.12	12.91	1986–1992
77	Citarum	Cibereum	Cihideung	4	0.47	1.29	1998–2009
78	Citarum	Cikondang	Cihaur	22	5.54	52.73	1986–1992
79	Citarum	Cilalawi	Cilalawi	16	4.31	86.09	2006–2010
80	Citarum	Cibeet	Weir hulu	55	30.25	371.82	1986–1992
81	Citarum	Cipamingkis	Dayeuh	62	8.08	174.43	1986–1995
82	Citarum	Cimeta	Bepak	21	2.76	64.75	1993–2009
83	Citarum	Cisokan	Mangled	27	22.56	245.43	1991–2009
84	Citarum	Cikundul	Cikerta	20	8.84	120.56	1999–2009
85	Citarum	Cibalagung	Leuwigarut	24	2.38	79.34	1991–2009
86	Cilamaya	Cilamaya	Cipeundeuy	25	15.29	215.96	1986–2009
87	Ciasem	Ciasem	Curug ageung	12	4.99	34.93	1990–2009
88	Citarum	Cibeuying	Tanjungwangi	5	0.12	0.64	1991–1996
89	Cipunegara	Cipunegara	Sumur Barang	45	30.42	273.93	1970–1981
90	Cipunegara	Cipunegara	Salam Darma	52	59.86	253.89	1969–1977
91	Kali Sewo	Kali Sewo	Sewo Harjo	22	4.11	24.83	1970–1979
92	Cipanas	Cipanas	Cikamurang	26	5.42	228.06	1994–2009
93	Cipunagara	Cipunagara	Kiarapayung	53	71.39	585.43	1980–2009
94	Cipanas	Cipanas	Cibereng	13	11.03	96.59	1970–1979
95	Cimanuk	Cimanuk	Bojongloa	18	7.23	80.66	1986–2009
96	Cimanuk	Cimanuk	Leuwidaun	24	21.55	193.15	1986–2009
97	Cimanuk	Cimanuk	Cipasang	30	46.95	225.15	1986–1997
98	Cimanuk	Cimanuk	Leuwigoong	34	27.42	209.79	1986–2009
99	Cimanuk	Cipancar	Cibedug	14	1.87	21.62	1986–1992
100	Cimanuk	Cimanuk	Wado	47	42.16	308.45	1986–2009
101	Cimanuk	Cimanuk	Tomo	82	77.18	486.70	1986–2009
102	Cimanuk	Cipeles	Warung Peti	23	21.02	141.47	1986–1992
103	Cimanuk	Cipeles	Sukatali	29	13.04	326.40	1993–1998
104	Cimanuk	Cilutung	Dam Kamun	80	77.79	592.34	1988–2009
105	Cimanuk	Cilutung	Bantar Merak	66	25.61	690.35	1988–1998
106	Cimanuk	Cimanuk	Jatibarang	89	146.12	709.00	1970–1977
107	Cimanuk	Cimanuk	Monjot	104	89.84	821.59	1988–2009
108	Cimanuk	Cikeruh	Jatiwangi	92	7.19	842.71	1988–2009
109	Cimanuk	Cimanuk	Kertasemaya	112	137.41	1146.64	1988–2009
110	Cisanggarung	Cisanggarung	Baok	83	78.47	534.35	2006–2010
111	Cisanggarung	Cisanggarung	Jembatan Losari	68	99.70	1139.96	1999–2007
112	Cisanggarung	Cisanggarung	Cibinuang	22	5.64	63.25	2006–2010
113	Cisanggarung	Cisanggarung	Pasuruan	48	31.93	406.10	1988–1994
114	Citanduy	Citanduy	Cirahong	38	60.63	389.32	1986–2008
115	Citanduy	Citanduy	Leuwitonjong	26	23.86	190.32	1970–2001
116	Citanduy	Citanduy	Pataruman	75	123.98	853.52	1986–2009
117	Citanduy	Ciloseh	Cinehel	21	8.90	62.25	1986–1990
118	Citanduy	Ciloseh	Sukaratu	22	2.62	121.14	1986–2009
119	Citanduy	Cimulu	Argasari	6	1.21	23.46	1986–1990
120	Citanduy	Cikalang	Cibitung	26	15.97	172.95	1986–1992
121	Citanduy	Cimuntur	Banaruka	27	24.26	110.75	1995–2008
122	Citanduy	Ciseel	Cilisung	32	9.04	185.14	1987–2009
123	Citanduy	Ciseel	Binangun	37	14.79	232.10	1990–2009
124	Citanduy	Cimeneng	Stinggil	14	4.60	132.39	2006–2010
125	Citanduy	Ciseel	Ciawitali	31	19.98	229.87	1993–2001
126	Citanduy	Cimuntur	Cibeka	13	15.78	60.50	2005–2009

Table 1. (continued)

No.	River system	River	Site name	W_b (m)	Q_{mean} (m ³ s ⁻¹)	Q_b (m ³ s ⁻¹)	Observation year (Q_{mean})
127	Citanduy	Barokeh	Sawangan	19	5.05	174.51	2005–2010
128	Citanduy	Citanduy	Cikawung	98	180.41	773.02	1993–1999
129	Citanduy	Cijolang	Cikadu	50	31.63	419.01	1986–2008
130	Citanduy	Cijolang	Bebedahan	65	35.24	367.79	1993–1999
131	Citanduy	Cimuntur	Karangmulyan	43	85.66	463.83	1981–1986
132	Citanduy	Cijolang	Cibali	4	0.87	9.00	1997–2009
133	Citanduy	Cikawung	Cukangleuleus	47	38.76	306.06	1995–1999
134	Citanduy	Citanduy	Karangsari	142	157.06	704.57	1986–2009
135	Citanduy	Ciliung	Tenjolaya	12	6.51	27.55	1993–1999
136	Citanduy	Cileueur	Bojong (Bunar)	36	23.18	150.45	1995–2009
137	Cimedang	Cimedang	Leuwibudah	58	7.39	150.76	1990–2009
138	Ciwulan	Ciwulan	Mangunreja	65	32.18	335.88	1986–2009
139	Ciwulan	Cikunir	Cipawitra	13	1.96	13.31	1986–2009
140	Ciwulan	Cikunir	Asta	33	17.34	101.98	1987–2009
141	Ciwulan	Cimerah	Sukaherang	14	6.16	27.92	1991–1997
142	Ciwulan	Cikunten	Dangur	20	9.23	96.13	1986–1997
143	Ciwulan	Ciwulan	Sukaraja	111	38.31	726.01	1986–2009
144	Ciwulan	Ciwulan	Sodong	137	53.89	614.99	2003–2009
145	Cipatujah	Cipalu	Bojongsari	21	4.00	90.10	1986–2007
146	Cilangla	Cilangla	Leuwineukteuk	56	28.64	482.74	1986–2008
147	Cilangla	Cijalu	Ciawitali	44	6.34	231.26	1986–2009
148	Cisadea	Cisadea	Tenggek	37	14.63	79.71	1993–2009
149	Cibuni	Cibuni	Cibungur	80	106.53	509.28	1986–2009
150	Cibuni	Cibuni	Palatar	109	27.37	320.15	1991–2009
151	Cikaso	Cikaso	Parungseah	77	34.59	845.30	1992–2009
152	Ciletuh	Ciletuh	Cipiring	35	6.72	131.01	1988–2009
153	Cimandiri	Cicatih	Kebon randu	57	28.68	220.27	1981–1986
154	Cimandiri	Cimandiri	Tegaldatar	53	19.39	193.78	1986–2009
155	Cimandiri	Cimandiri	Leuwilisung	52	5.31	189.95	1993–2009
156	Cimandiri	Citarik	Pajagan	28	12.13	83.01	1993–2009
157	Pemali	Pemali	Notog	64	47.37	241.79	1992–2009
158	Cisanggarung	Cijangkelok	Cibendung	45	24.97	126.40	1992–2009
159	Kabuyutan	Kali Kabuyutan	Kertasari	30	1.10	23.01	1992–2009
160	Pemali	Pemali	Kedung Tukang	38	39.90	324.68	1981–1988
161	Pemali	Pemali	Bantar Kawung	60	27.10	576.15	1992–2009
162	Pemali	Pemali	Rengas Pendawa	36	34.69	497.33	1992–2009
163	Pemali	Pemali	Brebes	90	40.62	910.67	1992–2009
164	Kali Gung	Kali Gung	Pesayangan	77	9.35	316.91	1992–2009
165	Kali Rambut	Kali Rambut	Cipero	24	5.55	29.28	1992–2009
166	Kali Waluh	Waluh	Sungapan	30	6.09	69.60	1992–2009
167	Comal	Comal	Kecepit	32	12.37	80.18	1986–2009
168	Comal	Genteng	Kaliwadas	25	26.80	147.13	1996–2009
169	Comal	Comal	Sukowati	104	43.30	560.60	1993–2006
170	Comal	Comal	Jatijero	80	31.75	567.63	1994–2009
171	Comal	Lumeneng	Watukumpul	35	3.55	79.88	1990–2009
172	Kupang	Kupang	Pagarukir	26	5.57	87.18	1986–2009
173	Kupang	Kali Pekalongan	Kuripan Kidul	30	12.63	168.44	1992–2009
174	Sambong	Sambong	Kedungdowo	25	9.43	105.91	1992–2009
175	Kuto	Kuto	Kutosari	124	35.67	712.06	1975–1979
176	Kuto	Kuto	Karanganom	74	16.55	418.23	1992–2009
177	Glagah	Glagah	Kedung Sari	14	4.94	62.08	1992–2006
178	Bodri	Bodri	Juwero	85	19.13	535.52	1986–2009
179	Belukar	Belukar	Sejomerto	27	4.34	119.65	1986–2009
180	Blorong	Blorong	Kedung Pucung	35	4.93	193.22	1986–2009
181	Garang	Garang	Pajangan	50	10.43	341.72	1986–2009
182	Garang	Garang	Patemon	16	11.21	332.75	1992–2000
183	Garang	Kreo	Kalipancur	15	7.61	192.93	1993–2009
184	Serang	Serang	Muncar	21	4.51	84.90	1986–2009
185	Serang	Serang	Guwo	62	1.58	419.00	1993–1998
186	Serang	Serang	Tongpait	79	98.76	556.36	1986–1990
187	Serang	Laban	Jengglong	34	5.93	235.89	1993–1999
188	Serang	Giren	Giren	18	0.60	7.16	1994–2000
189	Lusi	Lusi	Menduran	31	42.39	331.30	1986–1991
190	Serang	Lusi	Kunduran	27	31.28	208.25	1986–1991

Table 1. (continued)

No.	River system	River	Site name	W_b (m)	Q_{mean} (m ³ s ⁻¹)	Q_b (m ³ s ⁻¹)	Observation year (Q_{mean})
191	Serang	Lusi	Banjarrejo	16	8.13	220.95	1994–2000
192	Serang	Lusi	Tawangharjo	70	43.04	719.70	1995–1999
193	Juana	Logung	Kedung Mojo	21	1.19	44.59	1990–2009
194	Sulang	Sulang	Sulang	15	0.75	67.64	1988–2008
195	Sulang	Besek	Tlogo	12	0.16	10.88	1992–2009
196	Bengawan Solo	Bengawan Solo	Kedung Areng	77	30.50	376.33	1969–2000
197	Bengawan Solo	Gondang	Stren	26	4.50	37.86	1999–2007
198	Bengawan Solo	Tirtomoyo	Sulingi	44	10.87	476.81	1992–2006
199	Bengawan Solo	Bengawan Solo	Jurang Gempal	87	59.82	762.72	2000–2008
200	Bengawan Solo	Dengkeng	Paseban	39	7.35	192.39	1990–2009
201	Bengawan Solo	Bengawan Solo	Jurug	74	67.26	554.91	1992–2009
202	Bengawan Solo	Goseng	Ngunut	34	0.28	35.00	1993–2000
203	Bengawan Solo	Plawatan	Donorejo	18	0.14	37.66	1993–2001
204	Bengawan Solo	Wungu	Pakisbaru	12	0.10	7.89	1993–2001
205	Bengawan Solo	Ngunut II	Kuwon	17	0.03	31.57	1993–2000
206	Bengawan Solo	Padas	Grasak	10	0.82	60.25	1993–2000
207	Bengawan Solo	Tapan	Tapan	16	0.18	9.24	1993–2000
208	Bengawan Solo	Temon	Duwet Lor	25	0.99	200.91	1993–2000
209	Bengawan Solo	Alang	Kedungpadas	21	0.43	121.98	1993–2000
210	Bengawan Solo	Keduang	Ngadipiro	42	5.45	119.88	1993–2009
211	Bengawan Solo	Wuryantoro	Tiken	31	0.53	166.04	1993–2001
212	Bengawan Solo	Cemoro	Ngrukun	23	5.21	225.26	1990–2009
213	Bengawan Solo	Bengawan Solo	Balun	183	186.91	2611.33	2006–2010
214	Progo	Tangsi	Susukan	24	6.81	176.41	1986–2009
215	Progo	Elo	Mendut	45	25.94	251.03	1986–2009
216	Progo	Progo	Borobudur	144	36.70	688.29	1986–2009
217	Progo	Progo	Kranggan II	57	13.90	281.00	1986–2009
218	Progo	Progo	Badran	55	15.26	148.59	1992–2009
219	Bogowonto	Bogowonto	Pungangan	45	21.49	153.73	1999–2009
220	Kali Jali	Kali Jali	Winong	25	7.23	269.59	1986–2009
221	Padegolan	Padegolan	Pajengkolan	35	15.07	412.14	2000–2007
222	Lokulo	Lokulo	Kali Gending	70	24.75	279.37	1990–2009
223	Serayu	Serayu	Banjarnegara	75	55.87	629.70	1986–2009
224	Serayu	Begaluh	Krasak	27	14.95	131.85	1992–2009
225	Serayu	Merawu	Clangap	64	17.05	202.38	1990–2009
226	Serayu	Klawing	Dagan	17	7.46	43.89	1992–2009
227	Serayu	Klawing	Slinga	146	93.42	836.85	1993–2009
228	Serayu	Serayu	Banyumas	121	214.45	1197.91	1986–2009
229	Serayu	Serayu	Rawalo	168	253.94	1395.37	1986–2009
230	Serayu	Tajum	Tipar Kidul	75	15.53	331.50	1990–2009
231	Serayu	Banjaran	Kober	47	5.45	207.62	1992–2009
232	Serayu	Tambra	Karang Tengah	41	10.98	185.50	1980–1985
233	Citanduy	Cikawung	Cimei	30	39.21	169.33	1980–1988
234	Citanduy	Cikondang	Cibungur	19	1.24	18.75	1992–2007
235	Citanduy	Cikuya	Surusunda	16	0.38	8.08	1992–2007
236	Kali Progo	Progo	Duwet	67	62.61	469.17	1970–2006
237	Kali Oyo	Oyo	Bunder	29	8.07	141.02	1982–2006
238	Kali Opak	Kedung Keris	Kedung Keris	22	1.92	4.67	1992–1998
239	Kali Opak	Winongo	Padokan	20	2.43	47.78	1993–2006
240	Kali Opak	Opak	Karangsemut	45	13.11	147.31	1980–2003
241	Kali Opak	Oyo	Dogongan	35	25.29	333.32	1972–1977
242	Kali Opak	Oyo	Kedungmiri	53	16.59	205.86	1976–1988
243	Kali Opak	Code	Pogung	20	1.22	14.23	1992–2009
244	Kali Opak	Opak	Pulo	24	1.47	8.59	1992–2009
245	Kali Opak	Tambakbayan	Seturan	17	0.88	2.91	2001–2009
246	Kali Opak	Gajahwong	Papringan	15	1.60	12.34	1994–2009
247	Kali Opak	Code	Kaloran	17	1.98	29.04	1994–2005
248	Kali Progo	Progo	Kali Bawang	130	63.19	342.73	1993–2009
249	Kali Progo	Progo	Bantar	156	89.10	685.80	1973–2002
250	Kali Serang	Progo	Sapon	40	28.25	286.50	1992–1998
251	Kali Serang	Serang	Durungan	28	5.50	264.01	1971–2004
252	Kali Serang	Serang	Bendungan	32	6.80	146.34	1978–2002
253	Kali Serang	Serang	Pengasih	36	2.04	109.80	1992–2004
254	Kali Serang	Ngrancah	Sermo	13	0.91	7.80	1986–1994

Table 1. (continued)

No.	River system	River	Site name	W_b (m)	Q_{mean} (m ³ s ⁻¹)	Q_b (m ³ s ⁻¹)	Observation year (Q_{mean})
255	Kali Prumpung	Prumpung	Belikanget	12	0.66	9.55	1988–2006
256	Kali Klero	Klero	Genaharjo	14	1.05	13.96	1993–2008
257	Bengawan Solo	Cawak	Kedung Lerep	16	1.52	47.26	1992–2008
258	Bengawan Solo	Kerjo	Pejok	20	1.31	152.18	2000–2008
259	Bengawan Solo	Kali Gandong	Setren	12	3.29	43.02	1993–2008
260	Kali Lamong	Lamong	Simoanggrok	16	6.23	76.00	1989–2001
261	Kali Nglirip	Nglirip	Singgahan	14	2.35	35.05	1993–2008
262	Bengawan Solo	Pacal	Senganten	28	0.33	46.00	1993–2009
263	Kali Gembul	Gembul	Merakurak	24	1.26	39.74	1992–2006
264	Bengawan Solo	Bengawan Solo	Napel	112	172.80	1965.70	1971–2009
265	Bengawan Solo	Bengawan Solo	Kauman	100	126.25	1185.40	1974–2008
266	Bengawan Solo	Kali Madiun	Ngawi	65	77.45	813.61	1975–2009
267	Bengawan Solo	Kali Keang	Ponorogo	42	4.82	45.65	1992–2009
268	Bengawan Solo	Kali Madiun	Nambangan	57	37.68	481.40	1974–2009
269	Bengawan Solo	Kali Gandong	Kebo Agung	27	8.22	114.40	1992–2009
270	Bengawan Solo	Bengawan Solo	Cepu	170	308.55	1906.95	1972–2009
271	Bengawan Solo	Bengawan Solo	Bojonegoro	165	340.34	1945.21	1971–2009
272	Bengawan Solo	Bengawan Solo	Babat	172	440.78	1656.71	1971–2009
273	Bengawan Solo	Bengawan Solo	Karang Geneng	170	346.10	1272.39	2004–2009
274	Bengawan Solo	Bengawan Solo	Karang Binangun	178	238.83	1120.85	2003–2009
275	Bengawan Solo	Kali Kening	Selogabus	25	26.23	194.93	2006–2010
276	Bengawan Solo	Bengawan Solo	Sembayat	147	387.54	1950.03	2006–2010
277	Kali Brantas	Kali Brantas	Kertosono	82	222.96	994.16	1993–2006
278	Kali Brantas	Kali Brantas	Ploso	154	210.50	1008.03	1993–2006
279	Kali Brantas	Kali Brantas	Sutami Dam	82	75.60	271.05	1986–1993
280	Kali Brantas	Kali Brantas	Wlingi (waduk)	27	99.77	506.83	1986–1993
281	Kali Brantas	K. Sumberampel	Baros	22	23.14	124.98	1991–2009
282	Kali Brantas	Kali Brantas	Kaulon	79	105.25	444.00	1971–1975
283	Kali Brantas	Kali Brantas	Papringan	92	121.98	617.60	1971–1975
284	Kali Brantas	Kali Brantas	Pundensari	76	171.65	635.33	1974–2009
285	Kali Brantas	Kali Ngrowo	Kali Turi	31	9.38	44.77	1971–1979
286	Kali Brantas	Kali Bangsal	Kedung Uneng	18	1.54	5.78	1977–2009
287	Kali Brantas	Kali Bagong	Temon	25	2.75	108.11	1976–2009
288	Kali Brantas	Kali Keser	Keser	24	9.34	74.42	1993–2009
289	Kali Brantas	Kali Duren	Trenggalek	16	0.53	13.78	1991–2009
290	Kali Brantas	Kali Kedung Suko	Nganjuk	26	4.91	56.97	1986–1994
291	Kali Brantas	Kali Lahar	Bacem	23	0.71	12.24	1992–2009
292	Kali Brantas	Kali Brantas	Mojovento (Kediri)	91	183.26	588.68	1975–2009
293	Kali Brantas	Kali Sayang	Jabon	15	0.69	22.65	1987–2009
294	Kali Brantas	Kali Brantas	Kertosono	128	223.15	934.28	1974–2009
295	Kali Brantas	Kali Brantas	Mojokerto	202	268.22	880.26	1974–2009
296	Kali Brantas	Kali Surabaya	Tawang Sari	54	72.73	350.53	1992–2009
297	Bengawan Solo	Kali Gangseng	Sugiharas	27	1.59	89.03	1993–2003
298	Kali Brantas	Kali Brantas	Jeli	71	129.74	587.31	1993–2001
299	Kali Brantas	Kali Brantas	Lodoyo (Waduk)	130	124.12	667.17	1993–2000
300	Kali Brantas	Kali Brantas	Sengguruh	80	40.08	609.60	1994–2000
301	Kali Brantas	Kali Brantas	Gadang	33	31.14	164.07	1993–2001
302	Kali Brantas	Kali Konto	Selorejo	85	11.16	700.00	1994–2009
303	Kali Brantas	Kali Brantas	Mrican	149	147.52	685.75	1993–2000
304	Kali Brantas	Kali Brantas	New Lengkong	116	145.49	692.14	1994–2000
305	Kali Brantas	Kali Brantas	Gunung Sari	92	40.15	206.10	1995–2000
306	Kali Brantas	Kali Widas	Lengkong widas	45	34.90	357.42	1993–2001
307	Kali Brantas	Kali Widas	Bening (waduk)	14	1.24	29.83	1996–2000
308	Kali Brantas	Kali Porong	Porong	114	115.11	778.77	1994–2001
309	Kali Brantas	Kali Lesti	Tawang Rejani	57	10.73	165.02	1994–2001
310	Kali Brantas	Kali Ngasinan	Parit raya Bendo	60	15.24	186.58	1994–2001
311	Kali Welang	Kali Welang	Purwodadi	26	3.44	54.22	1992–2009
312	Kali Welang	Kali Welang	Pohjethak	28	5.33	145.25	2006–2010
313	Kali Rejoso	Kali Rejoso	Winongan	27	12.83	75.22	1991–2009
314	Kali Gembong	Kali Gembong	Warung Dowo	33	1.77	214.45	2006–2010
315	Kali Kramat	Kali Kramat	Probolinggo	29	3.02	91.68	1992–2009
316	Kali Pekalen	Kali Pekalen	Condong	26	10.50	55.32	1975–2009
317	Kali Pekalen	Kali Rondoningo	Jurang Jero	28	4.53	15.85	1991–2009
318	Kali Deluwang	Kali Deluwang	Demung (Besuki)	36	1.48	145.39	1992–2009

Table 1. (continued)

No.	River system	River	Site name	W_b (m)	Q_{mean} (m ³ s ⁻¹)	Q_b (m ³ s ⁻¹)	Observation year (Q_{mean})
319	Kali Sampean	Kali Sampean	Masabit	44	10.30	216.51	1975–2001
320	Kali Bajumati	Kali Bajulmati	Bajulmati	30	2.34	27.34	1992–2001
321	Kali Setail	Kali Setail	Keradenan	22	6.64	129.85	1992–2009
322	Kali Tambong	Kali Tambong	Pakistaji	23	4.44	76.87	1992–2002
323	Kali Baru	Kali Baru	Karandoro	62	22.11	279.91	1974–2009
324	Kali Mayang	Kali Sanen	Sanenrejo	40	11.54	187.07	1976–2009
325	Kali Bedadaung	Kali Bedadung	Rawatamtu	57	32.05	597.59	1991–2009
326	Kali Asem	Kali Asem	Sentul	20	7.43	57.26	1977–2009
327	Kali Bondoyudo	Kali Bondoyudo	Wonorejo	25	16.59	203.61	1974–2009
328	Kali Bomo	Kali Bomo Bawah	Rogojampi	23	3.97	123.46	2000–2009
329	Kali Bomo	Kali Bomo Atas	Parijati (Srono)	21	1.26	100.84	1996–2009
330	Kali Kadalpang	Kali Kadalpang	Bendung Kejen	32	2.99	44.85	1998–2009
331	Kali Lorok	Kali Lorok	Wonodadi	70	7.12	87.57	1992–2008
332	Kali Madiun	Kali Slahung	Sumoroto	28	15.67	165.70	2000–2006
333	Kali Grindulu	Kali Kedungpring	Nawangan	23	1.21	18.82	1993–2009
334	Kali Grindulu	Kali Grindulu	Gunung Sari	107	26.13	490.32	1975–2009
335	Kali Mayang	Kali Mayang	Pakusari	22	3.84	11.55	1996–2010
336	Cisadane	Cisadane	Maseng	19	11.01	202.04	1915–1940
337	Citarum	Citarum	Cipetir (Palumbon)	120	165.15	1586.67	1922–1980
338	Cisanggarung	Cisanggarung	Cilengkrang	43	22.81	293.40	1973–1977
339	Kr. Aceh	Kr. Aceh	Kp. Seulimeun	21	18.66	166.25	1972–2007
340	Kr. Aceh	Kr. Aceh	Kp. Darang	79	28.12	245.23	1977–2008
341	Kr. Aceh	Kr. Keumireun	Siron	47	7.40	105.85	1981–2008
342	Kr. Aceh	Kr. Aceh	Pasi	58	30.88	275.55	1981–2008
343	Kr. Aceh	Kr. Aceh	Lampisang Tunong	45	18.53	129.58	1981–1997
344	Kr. Boga	Kr. Boga	Kp Boga	23	6.53	156.89	1992–2008
345	Kr. Aceh	Kr. Jreue	Kp. Jreue	31	4.85	49.55	1992–2008
346	Kr. Baro	Kr. Baro	Klibeut	28	8.11	121.06	1973–1982
347	Kr. Baro	Kr. Baro	Kemala dalam	30	12.56	145.00	1973–1977
348	Kr. Baro	Kr. Baro	Kp. Geuni Puni	37	13.25	72.96	1980–1997
349	Kr. Peudada	Kr. Peudada	Menasang Lawang	54	33.02	178.95	1991–2008
350	Kr. Peusangan	Kr. Peusangan	Beukah	65	72.29	406.75	1979–1997
351	Kr. Peusangan	Kr. Peusangan	Simp. Jaya	83	93.81	556.36	1984–1997
352	Kr. Peusangan	Kr. Sempo	Sempo	37	10.55	74.68	1991–2008
353	Kr. Mane	Kr. Mane	Lhok Kuyun	39	24.25	112.82	1981–1996
354	Kr. Mane	Kr. Tuan	Lhok Joek	18	7.28	66.78	1981–2006
355	Kr. Jambo Aye	Kr. Jambo Aye	Lhok Nibong	86	190.63	816.16	1972–1997
356	Kr. Jambo Aye	Kr. Jambo Aye	Rampah	84	121.20	749.84	1975–1980
357	Kr. Tamiang	Kr. Tamiang	Kuala Simpang	102	287.48	1158.67	1975–1996
358	Kr. Lambesoi	Kr. Lambesoi	Sango	85	30.81	492.65	1993–1997
359	Kr. Bulan	Lawe Bulan	Kutacane	9	3.50	35.63	1975–1979
360	Kr. Gimpang	Lawe Alas	Gempang	35	25.87	151.83	1973–1977
361	Kr. Alas	Lawe Alas	Suka Rimbun	33	57.79	260.73	1979–1996
362	Kr. Kluet	Kr. Kluet	Gn. Puding	119	154.25	483.33	1981–1987
363	Kr. Susoh	Kr. Susoh	Kota Tinggi	44	22.61	87.89	1985–1997
364	Kr. Bah Barot	Kr. Bah Barot	Kp. P. Cermin	75	87.39	326.72	1992–1996
365	Kr. Seumayam	Kr. Seumayam	Seumayam	27	7.18	42.26	1985–1997
366	Kr. Tripa	Kr. Tripa	G. Kong	100	200.73	549.23	1980–1997
367	Kr. Seunagan	Kr. Seunagan	Driengguru	49	32.05	159.23	1982–1997
368	Kr. Seunagan	Kr. Seunagan	P. Udeng/Kulu	35	73.36	234.68	1980–1994
369	Kr. Meureubo	Kr. Meureubo	Meunasah Rayek	113	121.05	704.54	1984–1989
370	Kr. Woyla U/S	Kr. Woyla U/S	M. Tutut	126	115.89	543.42	1991–1996
371	Kr. Woyla	Kr. Woyla D/S	Kuala Bhee	113	147.20	734.36	1983–1996
372	Kr. Teunom	Kr. Teunom	Tui Kareng	121	194.50	919.25	1991–1996
373	Kr. Sabe	Kr. Sabe	Panggong	48	41.82	285.68	1981–1996
374	S. Langkat	S. Wampu	Stabat	112	224.33	950.58	1975–2011
375	S. Bingai	S. Bingei	Kp Pahlawan	36	23.32	263.80	1992–2011
376	S. Wampu	S. Mencirim	Binjai	70	19.28	348.23	1992–2001
377	S. Belawan	S. Belawan	Asam Kumbang	26	14.11	214.55	1973–2011
378	S. Belawan	S. Belawan	Kp. Lalang	21	14.96	98.70	1980–2011
379	S. Deli	S. Deli	Helvetia	14	15.79	79.44	1980–2011
380	S. Deli	S. Deli	Simeme	15	9.54	69.64	1972–2011
381	S. Percut	S. Percut	Tembung	18	9.77	64.37	1990–2011
382	S. Blumai	S. Blumai	Tanjung Morawa	19	16.82	172.75	1972–1987

Table 1. (continued)

No.	River system	River	Site name	W_b (m)	Q_{mean} (m ³ s ⁻¹)	Q_b (m ³ s ⁻¹)	Observation year (Q_{mean})
383	S. Ular	S. Ular	Pulau Tagor	50	52.11	214.73	1972–2011
384	A. Blutu	S. Blutu	Pekan Selasa	10	7.33	12.94	1992–2011
385	A. Padang	S. Padang	Tebing Tinggi	40	49.20	153.81	1976–2011
386	Bah Bolon	Bah Bolon	Batu Gajah	37	20.22	130.41	1972–2011
387	Bah Bolon	Bah Bolon	Nagori Bandar	38	23.53	202.93	1968–2011
388	Bah Bolon	Bah Tongguran	Tembaan	52	59.49	344.59	1982–2011
389	S. Serdang	S. Serdang	Serdang	32	33.09	229.98	1991–2009
390	S. Asahan	S. Asahan	Porsea	28	96.64	142.40	1966–1979
391	S. Asahan	S. Asahan	Siruar	36	95.73	165.73	1966–1979
392	S. Asahan	S. Asahan	Simorea	39	88.57	190.07	1966–1979
393	S. Asahan	S. Silau	Buntupane	30	52.93	109.58	1993–2009
394	S. Asahan	S. Silau	Kisaran Naga	63	60.93	283.39	1972–2009
395	S. Asahan	S. Asahan	Pulau Raja	58	141.15	361.79	1977–2006
396	S. Kualu	S. Kualuh	Pulau Dogom	42	70.13	365.00	1982–2998
397	S. Kualu	A. Natas	Bdr. Durian	21	40.89	205.51	1984–2010
398	S. Bilah	A. Merbau	Simpang Ampat	24	14.31	155.77	1991–2011
399	S. Barumun	Bt. Pane	Lubuk Sipelanduk	33	27.60	192.92	1973–1997
400	S. Barumun	Bt. Pane	Gunung Tua	41	31.17	383.24	1977–1993
401	S. Barumun	S. Barumun	Binanga	68	119.00	610.23	1975–1984
402	S. Barumun	Bt. Barumun	Kuta Pinang	82	274.95	645.03	1978–2011
403	Bt. Natal	Bt. Natal	Rantau Sore	30	28.14	219.66	1991–2011
404	Bt. Gadis	Bt. Gadis	Perbangunan	45	30.77	367.00	1973–1989
405	Bt. Gadis	Bt. Angkola	Air Libung	35	18.19	141.10	1974–2011
406	Bt. Toru	Aek Sigeon	Pasar Sironggit	15	14.24	112.25	1982–2011
407	Bt. Toru	Batang Toru	Hapesong Baru	85	85.10	456.71	1977–2011
408	A. Kolang	A. Kolang	Kp. Kolang	58	41.24	332.16	1991–2011
409	A. Sibundong	A. Sibundong	Dolok Sanggul	12	4.14	38.85	1991–2011
410	A. Silang	A. Silang	Marade	14	7.58	52.60	1983–2010
411	Bt. Rokan	Bt. Sumpur	Batu Bertindih	33	20.13	163.88	1978–2010
412	Bt. Rokan	Bt. Sontang	Ulu Sontang	14	18.81	113.50	1996–2010
413	Batang Kampar	Batang Mahat	Pkl. Kotobaru	51	35.09	259.90	2006–2010
414	Bt. Rokan	Bt. Lampasi	Batu Hampar	12	2.69	48.45	1996–2004
415	Bt. Kuantan	Bt. Ombilin	Tanjung Ampalu	56	48.98	381.82	1977–2010
416	Bt. Kuantan	Bt. Sumani	Bandar Padang	39	20.80	217.59	1977–2010
417	Bt. Kuantan	Bt. Sinamar	Taram	46	43.35	371.29	1979–2010
418	Bt. Kuantan	Bt. Agam	Padang Tarab	14	12.52	111.45	1984–2010
419	Bt. Kuantan	Bt. Selo	Saruaso	15	5.60	57.76	1982–2010
420	Bt. Kuantan	Bt. Sukam	Muara Batu	97	26.61	1343.19	1996–2010
421	Bt. Kuantan	Bt. Lembang	Kt Baru/ B. Kudo	24	5.74	87.54	1996–2010
422	Batang Kuantan	Bt. Pelangki	Dusun Tuo	42	26.74	248.62	1997–2010
423	Bt. Kuantan	Bt. Sumpu Malalo	Sumpu Malalo	18	9.61	37.12	2006–2010
424	Bt. Hari	Bt. Hari	Sungai Dareh	173	238.93	1644.95	1976–2009
425	Bt. Hari	Bt. Sangkir	Sampu	33	38.35	294.51	1979–2010
426	Bt. Hari	Bt. Siat	Koto Baru	25	25.88	171.01	1982–2010
427	Bt. Hari	Bt. Suliti	Sungai Ipuh	16	4.16	29.69	1995–2004
428	Bt. Tapan	Bt. Indrapura	Air Batu	35	37.04	263.49	1980–2010
429	Bt. Tapan	Bt. Tapan	Lubuk Begalung	47	12.67	304.83	1992–2001
430	Bt. Tapan	Bt. Lunang	Lunang	51	16.29	689.83	1993–2009
431	Bt. Air Haji	Bt. Air Haji	Danau	43	26.57	307.06	1978–2009
432	Air Gadang	Bt. Pelepah	Tj Masjid	36	20.15	139.21	1978–2009
433	Bt. Kambang	Bt. Lengayang	Koto Baru	45	32.27	245.65	1996–2001
434	Bt. Surantih	Bt. Suratih	Ganting	28	11.41	122.01	1993–2009
435	Bt. Tarusan	Bt. Tarusan	Kayu Gadang	42	21.42	265.03	1985–2009
436	Bt. Arau	Bt. Arau	Lubuk Sari	27	5.14	119.72	1982–2009
437	Bt. Air Dingin	Bt. Air Dingin	L. Minturun	29	9.60	225.96	1978–2009
438	Bt. Anai	Bt. Anai	Kandang Ampat	15	7.59	34.81	1988–2009
439	Bt. Tapakis	Bt. Tapakis	Kota Gadis	10	1.86	39.00	1995–1999
440	Bt. Mangau	Bt. Mangau	Kurai Taji	32	19.84	213.89	1985–2009
441	Bt. Pariaman	Bt. Pariaman	Jati Mudik	14	13.98	73.73	1995–2009
442	Bt. Atokan	A. Naras	Durian Dangka	25	7.14	127.54	1985–2009
443	Bt. Atokan	Bt. Kalulukutan	Batu Ampa	23	4.30	110.65	1995–2009
444	Bt. Simamar	Bt. Antokan	Siguhung	26	15.23	96.60	2005–2009
445	Bt. Masang	Bt. Masang	Sipisang	28	23.86	122.91	1975–2008
446	Bt. Masang	Bt. Patimah	Kapundung	58	20.44	439.60	2004–2009

Table 1. (continued)

No.	River system	River	Site name	W_b (m)	Q_{mean} (m ³ s ⁻¹)	Q_b (m ³ s ⁻¹)	Observation year (Q_{mean})
447	Bt. Pasaman	Bt. Pasaman	A Gadang	80	100.43	919.21	1981–2001
448	Bt. Pasaman	Bt. Tongar	Lb. Panjang	23	16.18	121.31	2004–2009
449	Bt. Pasaman	Bt. Kenaikan	Muara Kiawai	22	17.70	92.17	1982–2009
450	Bt. Sikabau	Bt. Sikabau	Ujung gading	35	26.31	255.66	1982–2005
451	Bt. Pasaman	Bt. Tongar	Lb. Toreh	34	26.79	182.06	1987–2008
452	Bt. Sikilang	Bt. Sikilang	Sei Aur	37	20.11	340.39	1974–2009
453	Batang Gadis	Bt. Batahan	Silaping	38	29.76	242.14	1974–2005
454	S. Rokan	Bt. Lubuk	Pasar Tangun	48	62.84	378.66	1981–2010
455	S. Rokan	Bt. Rokan Kiri	L. Bendahara	90	135.89	752.48	1975–2010
456	S. Rokan	Bt. Lubuk	Ujung Gurap	65	372.92	71.09	1983–2010
457	S. Rokan	Bt. Sosa	Dalu Dalu	38	62.01	292.82	1983–1992
458	S. Rokan	Bt. Kumu	Tj Medan	26	85.64	160.11	1981–1991
459	S. Rokan	Bt. Kumu	Kotabangun	27	23.43	111.08	1983–2010
460	S. Siak	Bt. Tapungkiri	Pantai Cermin	31	68.78	192.39	1980–2010
461	S. Siak	S. Tandun	Tandun	71	74.24	453.60	1980–2010
462	S. Kampar	S. Kampar Kanan	D. Bingkuang	105	219.06	1546.15	1977–2010
463	S. Kampar	Bt. Kampar kiri	Lipat Kain	85	194.77	915.01	1979–2010
464	S. Kampar	Bt. Lipai	Kebun Durian	28	36.40	172.20	2004–2010
465	S. Kampar	Bt. Sangingi	Kota Baru	58	50.16	374.74	1980–2010
466	S. Kampar	Bt. Kampar Kanan	Muara Mahat	100	156.58	1344.08	1988–1992
467	S. Kampar	Kampar Kanan	Muara Takus	72	121.63	914.00	1983–1991
468	Bt. Kuantan	Bt. Kuantan	Lb. Ambacang	95	230.03	1253.93	1988–2009
469	Bt. Kuantan	Bt. Kuantan	Bandar Alai	99	291.62	1024.40	1988–2009
470	Bt. Kuantan	Bt. Kuantan	Batu Gajah	106	428.72	1073.00	1988–2009
471	Bt. Kuantan	Bt. Kuantan	P. Berhala	138	289.41	1280.54	1988–2009
472	Bt. Kuantan	S. Cinahu	Pejangki	29	32.04	255.65	1988–2009
473	S. Gangsal	S. Gangsal	Lisul	38	24.12	134.18	1988–2009
474	Batanghari	Bt. Hari	Sei Dareh	132	255.55	1732.53	1988–2009
475	Batanghari	Batang Sangir	Sampu	30	31.19	252.48	1988–2009
476	Batanghari	Bt. Tabir	M. Jernih	60	41.88	335.51	1988–2009
477	Batanghari	Bt. Tembesi	Muara Inum	87	382.22	994.60	1988–2009
478	Batanghari	Bt. Ule	Lb. Tapus	34	27.24	258.20	1988–2009
479	Batanghari	Batang Hari	Muara Kilis	209	906.85	3068.52	1984–2009
480	Batanghari	Batang Hari	Muara Tembesi	466	1559.48	4385.64	1984–2009
481	Batanghari	Bt. Tebo	Air Gemuruh	85	119.26	496.38	1980–2009
482	Batanghari	Bt. Kumpeh	Pematang Bidaro	26	35.59	117.89	1987–2009
483	Batanghari	Bt. Hari	Duren	380	2447.27	6393.62	1979–2009
484	Batanghari	Sei Ulak	Ulakderas	35	94.17	137.39	1983–2009
485	Batanghari	Bt. Merao	Debai	22	39.09	75.67	1980–2009
486	Batanghari	Bt. Sangkir	Tanah Kampung	19	17.09	46.61	1983–2009
487	Batanghari	Bt. Asai	Dusun Benso	73	68.16	741.11	1983–2009
488	Batanghari	Bt. Bungo	Rantau Pandan	28	21.55	116.29	1983–2009
489	Batanghari	Bt. Singkut	Rantau Tenang	25	21.92	73.67	1983–2009
490	Batanghari	Bt. Merangin	Bangko	100	240.02	1851.87	1983–2009
491	Batanghari	Bt. Tabir	Rantau Panjang	65	69.22	560.32	1983–2009
492	Batanghari	Bt. Pelepat	Rantau Kelayang	32	31.97	201.05	1983–2009
493	Batanghari	Bt. Alai	Tirtakencana	11	18.85	56.91	1983–2009
494	Batanghari	Bt. Mesumai	Sei Manau	31	9.97	73.97	1983–2009
495	Batanghari	Bt. Merangin	Pulau Rengas	92	106.89	1346.33	1983–2009
496	A. Musi Kejalo	A. Musi Kejalo	Cawang Lama	10	2.21	9.35	1980–2010
497	A. P.Guci	A. Padang Guci	Bungin Tambun	31	9.60	79.23	1980–2010
498	A. Kedurang	A. Kedurang	Batu Ampar	30	9.73	105.34	1980–2010
499	A. Nipis	A. Bangkenang	Sukarami	20	11.64	112.05	1980–2010
500	A. Manas	A. Mana	Bandar Agung	61	49.14	292.48	1980–2010
501	A. Maras	A. Maras	Maras Hulu	16	3.93	57.20	1980–2010
502	A. Alas	A. Alas	Rantau Panjang	60	50.42	517.42	1980–2010
503	A. Nelas	A. Nelas	Lubuk Puding	34	10.31	192.57	1980–2010
504	A. Bengkulu	A. Bengkulu	Tb. Trujan	39	28.33	230.64	1980–2010
505	A. Bengkulu	A. Bengkulu	Kancing	11	7.56	51.28	1980–2010
506	A. Lemau	A. Lemau	Paku Haji	12	12.39	59.60	1980–2010
507	A. Lais	A. Lais	Kuro Tidur	10	7.69	24.22	1980–2010
508	A. Bintunan	A. Bintunan	Lubuk Banyau	34	11.99	93.63	1980–2010
509	A. Serangai	A. Serangai	Paninjau	13	11.39	106.86	1980–2010
510	A. Urai	A. Urai	Urai Hulu / Ketahun	19	6.12	65.92	1980–2010

Table 1. (continued)

No.	River system	River	Site name	W_b (m)	Q_{mean} (m ³ s ⁻¹)	Q_b (m ³ s ⁻¹)	Observation year (Q_{mean})
511	A. Ketahun	A. Ketahun	Tunggang	47	63.44	284.18	1980–2010
512	A. Lelangi	A. Lelangi	Lubuk Mindai	20	20.52	114.32	1980–2010
513	A. Rami	A. Rami	Pulau	25	12.43	136.94	1980–2010
514	A. Ipuh	A. Ipuh	Sibak Muko (Muko)	67	92.03	511.41	1980–2010
515	A. Teramang	A. Bantal	Pondok Baru	44	62.38	355.39	1980–2010
516	A. Teramang	A. Teramang	Trunggung	32	27.00	313.91	1980–2010
517	A. Dikit	A. Dikit	Saribulan	59	59.56	346.54	1980–2010
518	A. Selagan	A. Selagan	Tras Trujam	14	34.84	196.81	1980–2010
519	A. Majunto	A. Majunto	Lalang Luas	17	34.63	125.78	1980–2010
520	A. Majunto	A. Majunto Hilir	Lubuk Pinang	45	50.51	370.20	1980–2010
521	A. Musi	S. Lematang	S. Rotan	58	354.49	758.14	1992–2007
522	A. Musi	S. Klingi	Lubuk Rumbai	60	70.56	565.67	2004–2009
523	A. Musi	A. Megang	Megang Sakti	16	14.15	44.42	1985–1999
524	A. Musi	A. Musi	Mambang	88	355.97	1414.69	1973–1999
525	A. Musi	A. Beliti	Rantau ringin	58	60.34	573.79	1974–2009
526	A. Musi	A. Enim	Dusun Lingga	69	88.87	597.33	1977–1985
527	A. Musi	A. Komeriing	Minanga	78	136.92	949.33	2004–2009
528	A. Musi	A. Belitang	Tirtanadi	18	12.40	48.91	1978–2008
529	A. Musi	A. Lengkayap	Bt. Putih	58	82.98	848.92	1980–2009
530	A. Musi	A. Malus	Tj Raya	14	4.87	69.72	1982–2009
531	A. Musi	A. Rawas	Muara Rupit	142	227.91	1271.59	1981–1992
532	A. Musi	A. Temelat	Ciptodadi	17	4.63	22.52	1981–1997
533	A. Musi	A. Perigi	Darmabakti	15	2.74	24.21	1981–1997
534	A. Musi	A. Lematang	Lebakbudi	74	106.16	626.29	1992–2009
535	A. Musi	A. Baal	Terawas	33	27.79	239.21	1981–1999
536	A. Musi	A. Rawas	Pulau Kidak	70	91.50	905.38	1991–1999
537	A. Musi	A. Kungku	Ciptodadi	15	8.35	50.90	1993–1999
538	A. Musi	W. Selabung	Kt. Agung	19	27.54	88.66	1993–2009
539	A. Musi	A. Pang	Ulak Badung	35	24.38	318.80	1991–1999
540	A. Musi	A. Lematang	Pinang belarik	110	192.42	894.25	1990–2007
541	A. Musi	A. Kelingi	Ulak Surung	38	22.36	404.16	1992–2007
542	A. Musi	A. Ogan	Tj Raja	129	447.85	902.94	1993–2009
543	A. Musi	A. Komeriing	Martapura	70	156.49	442.01	1993–1999
544	A. Musi	S. Komeriing	Mangunjaya	41	64.75	150.67	1999–2007
545	W. Komeriing	W. Saka	Bunga Mayang	118	481.31	1645.01	1993–2003
546	W. Mesuji	W. Mesuji	Labuan Batin	37	74.34	244.55	1992–2008
547	W. Bujuk	W. T. Bawang	Bujuk Agung	25	6.87	130.31	1993–2001
548	W. T. Bawang	W. Umpu Kanan	Pakuan Ratu	64	145.93	571.73	1990–2009
549	W. T. Bawang	W. Umpu	Rantau Temiang	22	14.28	57.96	1985–2009
550	W. T. Bawang	W. Abung	Ogan Enam	19	23.51	89.61	1974–2009
551	W. T. Bawang	W. Rarem	Propal/ Kotabumi	27	41.60	272.81	1990–2008
552	W. T. Bawang	W. Tahmi	Tanjung Agung	33	36.71	238.75	1985–2009
553	W. T. Bawang	W. Umpu	Negeri Batin	36	31.75	240.24	1983–2009
554	W. T. Bawang	W. Girham	Rantau Jangkung	28	25.49	149.01	1992–2003
555	W. T. Bawang	W. Besay	Banjarmasin	23	28.70	131.79	1979–2009
556	W. T. Bawang	W. Besay	Petay (Sumberjaya)	21	21.60	91.13	1979–2003
557	W. T. Bawang	W. Umpu Kiri	Gunung Katun	26	75.00	194.83	1990–2006
558	W. T. Bawang	W. Besay	Sukajaya	22	20.98	92.86	1990–2009
559	W. T. Bawang	W. Giham	Filla Masin	10	17.81	64.31	1990–2003
560	W. T. Bawang	W. Giham	Air Ringkih	9	19.87	60.03	1991–2009
561	W. T. Bawang	W. Pedada	Banjar Agung	18	6.89	229.08	1995–2009
562	W. Seputih	W. Tatayan	Sindang Asri	8	1.84	18.40	1968–2008
563	W. Seputih	W. Waya	Banyuwangi	15	2.33	17.20	1968–2009
564	W. Seputih	W. Pangabuan	Terbanggi Besar	25	25.07	163.81	1990–2009
565	W. Seputih	W. Terusan	Gunung Batin	19	22.48	82.65	1990–2009
566	W. Seputih	W. Seputih	Buyut Udik	20	31.20	182.99	1978–2009
567	W. Seputih	W. Seputih	Segala Mider	7	8.07	23.55	1979–2009
568	W. Seputih	W. Pengabuan	Blambangan Pagar	18	12.58	101.28	1982–2005
569	W. Seputih	W. Raman	Raman Endra	12	13.95	51.32	1986–2008
570	W. Seputih	W. Pengabuan	Gedung Hatta	37	55.82	151.04	1990–2007
571	W. Seputih	Bt. Hari	Raman Fajar	11	14.90	51.55	1983–2009
572	W. Sekampung	W. Sekampung	Pujorahayu	32	53.29	341.18	1968–2009
573	W. Sekampung	W. Sekampung	Jurak	30	33.74	266.42	1968–2009
574	W. Sekampung	W. Sekampung	Kunyir	35	23.30	146.61	1968–2009

Table 1. (continued)

No.	River system	River	Site name	W_b (m)	Q_{mean} (m ³ s ⁻¹)	Q_b (m ³ s ⁻¹)	Observation year (Q_{mean})
575	W. Sekampung	Argo Guruh	Tigeneneng	37	55.20	221.51	1992–1999
576	W. Sekampung	W. Bulak	Dam Gatel (Weir)	23	14.22	119.75	1990–2009
577	W. Sekampung	W. Bulok	Bulokerto	27	15.79	168.56	1983–2009
578	W. Sekampung	W. Ketibung	Sidomulyo	7	1.93	28.41	1990–2001
579	W. Sekampung	W. Kandis	Tegal Lega / Trikora	9	2.67	44.36	1990–2009
580	W. Sekampung	W. Sekampung	Krisnowidodo	48	58.28	470.52	1996–2008
581	W. Semangka	W. Semangka	Liwa	11	17.47	48.55	1990–2006
582	W. Semangka	W. Semangka	Srikuncoro	40	84.83	235.60	1990–2006
583	W. Tl Bawang	W. Rarem	Pekurun	17	26.69	97.78	1980–2004
584	Batang Rokan	Batang Lubuk	Pengarayan	60	37.81	627.65	2001–2009
585	Batang Arau	Batang Arau	Kampung Baru	44	15.86	225.55	1982–1996
586	S. Pesaguan	S. Pesaguan	Tumbangtiti	26	37.24	103.88	1990–2004
587	S. Kapuas	S. Sekadau	Nanga Taman	49	35.94	236.10	1992–2010
588	S. Kapuas	S. Sengarit	Binjai	27	27.00	149.72	1992–2010
589	S. Kapuas	S. Landak	Serimbu	20	24.60	84.75	1991–1999
590	S. Kapuas	S. Sekayam	Balai Karangan	47	48.40	251.58	1991–1999
591	S. Kapuas	S. Mengkiyang	Balai Sebut	21	46.72	138.51	1992–2010
592	S. Kapuas	S. Mengkiyang	Balai Jeropet	45	77.50	302.52	1992–2010
593	S. Kapuas	S. Sekayam	Kembayan	67	178.27	1254.95	1993–2009
594	S. Kapuas	S. Tayan	Sosok	27	25.34	123.42	1995–2009
595	S. Sekayam	S. Ensabai	Beruak	18	13.48	57.02	1995–2010
596	S. Sekayam	S. Kayan	Mentunai	77	298.30	962.24	1992–2008
597	S. Sekayam	S. Pinoh	Kota baru	63	200.42	723.15	1995–2009
598	S. Mempawah	S. Menpawah	Karangan	18	19.61	145.34	1979–2008
599	S. Landak	S. Menyuke	Darit	22	46.43	186.24	1979–2008
600	S. Kapuas	S. Sengah	KerANJI Paidang	16	4.80	36.11	1983–2008
601	S. Selakau	S. Selakau	Seboteng	23	10.31	69.76	1996–2005
602	S. Landak	S. Landak	Monggo	82	356.59	1206.93	1992–2010
603	S. Sambas	S. Sebalau	Bengkayang	14	2.37	13.55	1991–2009
604	S. Sambas Besar	S. Seluas	Tadan	33	73.77	209.10	1990–2009
605	S. Sambas	S. Sambas Kecil	Ledo	33	49.71	202.58	1995–2006
606	S. Sambas	S. Kumba	Seluas	42	64.59	269.36	1984–2009
607	S. Barito	S. Barito	Muara Teweh	350	1870.57	4670.62	1978–2009
608	S. Barito	S. Paku	Tampa	23	11.69	30.26	1980–2001
609	S. Barito	S. Karau	Ampah	39	14.16	86.06	1993–2009
610	S. Barito	S. Montallat	Kandui	25	14.74	71.82	1993–2004
611	S. Kahayan	S. Manuhing	Tumbang Talaken	40	49.91	204.39	1993–2009
612	S. Kapus	S. Kapuas	Pujon	167	427.16	1159.46	1978–2009
613	S. Kahayan	S. Kahayan	Palangkaraya	257	1175.32	2370.59	1977–2006
614	S. Kahayan	S. Kahayan	Kuala Kurun	138	346.72	1302.55	1977–2008
615	S. Kahayan	S. Rungan	Tumbang Jutuh	71	108.27	361.11	1993–2006
616	S. Kahayan	S. Katingan	Kasongan	314	1366.67	3507.82	1995–2009
617	S. Mentaya	S. Mentaya	Kuala Kuayan	154	404.98	848.75	1990–2009
618	S. Lamandau	S. Arut	Pangkut	60	113.95	278.96	1993–2009
619	S. Lamandau	S. Lamandau	Nanga Bulik	128	563.72	1471.64	1993–2006
620	S. Karau	S. Awang	Hayaping	12	1.49	13.16	1996–2009
621	S. Barito	S. Tabanio	Bajuin	11	10.32	39.06	1993–1998
622	S. Barito	S. Negara	Amuntai	50	162.09	388.15	1993–2009
623	S. Barito	S. Tabalong	Tanjung	53	123.18	661.25	1993–1998
624	S. Barito	S. Amandit	Jambuhulu	29	24.85	230.06	1981–1998
625	S. Barito	S. Tapin	Linuh	17	13.30	126.90	1979–1997
626	S. Barito	S. Batu Alai	Batu Tangga	32	18.19	138.63	1980–1985
627	S. Barito	S. Tapin	Kuranji	25	11.44	75.44	1976–1998
628	S. Barito	S. Barabai	Kasarangan	16	12.96	53.29	1993–1998
629	S. Barito	S. Uya	Teratau	21	2.71	30.95	1980–1998
630	S. Barito	S. Barabai	Baruhbatung	16	6.61	62.04	1993–1998
631	S. Barito	S. Amandit	Lungau	22	26.54	152.76	1982–1998
632	S. Barito	S. Hanyar	Dusun Hanyar	49	29.37	213.28	1993–2001
633	S. Barito	S. Pitap	Bihara	24	6.72	26.79	1993–1998
634	S. Barito	S. Balangan	Lampihong	38	64.39	264.90	1993–1998
635	S. Barito	S. Tabalong Kiri	Mahe	47	38.90	310.60	1993–1998
636	S. Barito	S. Tabalong	Panaan	45	27.67	392.39	1991–1998
637	S. Barito	S. Tabalong	Batupulut	34	28.61	149.93	1993–1997
638	S. Barito	S. Ayu	Pasar Batulicin	21	12.11	124.12	1993–1998

Table 1. (continued)

No.	River system	River	Site name	W_b (m)	Q_{mean} (m ³ s ⁻¹)	Q_b (m ³ s ⁻¹)	Observation year (Q_{mean})
639	S. Mahakam	S. Telen	Keham	146	714.75	1170.40	1993–1997
640	S. Mahakam	S. Mahakam	K. Bangun	313	1973.47	3117.28	1996–2010
641	S. Mahakam	S. Melak	Melak	292	1555.32	3185.52	1992–2010
642	S. Mahakam	S. Kedang Kepala	Ancalong	133	537.45	1176.01	1991–2009
643	S. Mahakam	S. Klinjau	Longnah	89	321.70	564.12	1991–2009
644	S. Mahakam	S. Belayan	Tambang	129	471.43	1666.57	1992–2009
645	S. Barito	Riam Kiwa	Sei Langsat	46	48.25	312.68	1976–1998
646	S. Barito	S. Balangan	Balang Paringin	31	31.12	181.12	1980–1998
647	S. Barito	S. Batulicin	Karang Bintang	35	114.87	299.35	1995–2004
648	S. Barito	S. Cantung	Cantung	21	61.29	208.33	1979–2005
649	S. Barito	S. Kintap	Riam Adungan	22	58.92	171.47	1995–2004

Table 2. Cross-sectional data for river channels in the Indonesian islands. The numbers correspond to the site numbers in Figs. 63, 64, and 65.

No.	River system	River	Site name	P (m)	W_b (m)	A (m ²)	R_h ($\approx d_m$) (m)	d_b (m)
1	Cimanuk	Cimanuk	Wado	57.30	50.00	82.58	1.44	2.35
2	Cimanuk	Cialing	Pawenang	17.50	16.50	5.58	0.32	0.68
3	Citarum	Citarum	Dayeuhkolot	46.97	42.00	99.19	2.11	5.16
4	Citarum	Ciwidey	Cukanggenteng	21.17	20.00	17.08	0.81	1.40
5	Citarum	Citarum	Nanjung	32.62	30.00	82.12	2.52	4.63
6	Cipunagara	Cipunagara	Kiarapayung	49.37	48.00	95.98	1.94	3.82
7	Cikaso	Cikaso	Tanegan	33.95	32.00	6.98	0.21	0.52
8	Cimanuk	Cikandang	Pakenjeng	20.98	20.00	16.76	0.80	1.40
9	Cimanuk	Cimanuk	Jembatan Eretan	37.12	30.00	51.64	1.39	2.89
10	Cibuni	Cibuni	Palatar	49.58	44.00	32.34	0.65	1.65
11	Cikaso	Cikaso	Parungseah	56.90	48.00	20.50	0.36	0.75
12	Cimandiri	Cicatih	Cimanggu	42.32	34.00	43.90	1.04	3.10
13	Cisadea	Cisadea	Cikarang	65.51	56.00	28.00	0.43	0.98
14	Cimanuk	Cimanuk	Monjot	88.10	70.00	129.30	1.47	2.55
15	Cimanuk	Cihonje	Darmaraja	12.57	12.00	3.60	0.29	0.50
16	Cimanuk	Cimanuk	Bayongbong	17.03	15.00	6.75	0.40	0.80
17	Cimanuk	Cimanuk	Bojongloa	19.63	18.00	10.48	0.53	0.90
18	Cimanuk	Cikaengan	Singajaya	35.77	32.00	10.44	0.29	0.50
19	Ciwulan	Cikunir	Asta	28.00	24.00	9.27	0.33	0.70
20	Cimanuk	Cimanuk	Leuwigoong	24.43	23.00	12.58	0.51	1.20
21	Cimanuk	Cimanuk	Leuwidaun	23.72	22.00	6.42	0.27	0.55
22	Ciasem	Ciasem	Curug Agung	19.75	19.00	7.10	0.36	0.55
23	Kali Oyo	Kali Oyo	Kedungmiri	62.33	61.00	108.00	1.73	2.55
24	Serayu	Serayu	Rawalo	216.54	215.50	565.00	2.61	3.47
25	Kali Opak	Kali Opak	Karangsemut	61.22	61.00	36.00	0.59	1.00
26	Serayu	Serayu	Banyumas	127.30	125.00	296.00	2.33	6.87
27	Kali Bodri	Kali Bodri	Juwero	66.53	66.20	61.00	0.92	1.21
28	Kali Progo	Kali Progo	Borobudur	58.01	57.00	98.00	1.69	3.21
29	Kali Progo	Kali Progo	Bantar	134.83	134.00	143.00	1.06	2.40
30	Kali Brantas	Kali Brantas	Mojokerto	150.19	149.00	409.00	2.72	5.06
31	Kali Progo	Kali Progo	Duwet	47.27	48.20	89.00	1.88	2.63
32	Bengawan Solo	Bengawan Solo	Bojonegoro	173.71	172.00	514.00	2.96	4.59
33	Bengawan Solo	Bengawan Solo	Juranggempal	63.83	63.00	101.00	1.58	2.50
34	Bengawan Solo	Bengawan Solo	Babat	151.98	148.00	915.00	6.02	8.90
35	Bengawan Solo	Bengawan Solo	Kauman	88.21	86.00	302.00	3.42	5.11
36	Cimanuk	Cimanuk	Pamayahan	79.47	76.80	263.00	3.31	6.60
37	Cimanuk	Cimanuk	Tomo	89.13	89.00	77.00	0.86	2.05
38	Cimanuk	Cimanuk	Sindang Panongan	143.59	142.50	449.00	3.13	4.30
39	Ciujung	Ciujung	Rangkasbitung	98.42	98.00	108.00	1.10	1.65
40	Cimanuk	Cimanuk	Bondan	137.57	137.00	284.00	2.06	3.62
41	Citarum	Citarum	Tanjungpura	116.64	114.00	525.00	4.50	5.95
42	Citarum	Citarum	Pebayuran	97.58	97.00	205.00	2.10	2.86
43	Cimanuk	Cimanuk	Bendung Rentang	79.39	76.30	176.00	2.22	3.79
44	Cisanggarung	Cisanggarung	Babakan Losari	82.47	82.00	69.00	0.84	1.48
45	Citarum	Citarum	Teluk Kambulu	111.34	108.00	531.00	4.77	5.55
46	Rawas	Rawas	Muara Rupit	145.53	145.00	308.00	2.12	3.80
47	Batanghari	Batanghari	Sei Duren	322.07	320.00	2373.00	7.37	10.76
48	Musi	Musi	Desa Mambang	105.68	103.00	488.00	4.62	6.51
49	Kampar Kanan	Kampar Kanan	Danau Bingkuang	104.69	104.00	299.00	2.86	4.07
50	Kampar Kiri	Kampar Kiri	Lipat Kain	91.96	90.00	321.00	3.49	4.77
51	Batang Kuantan	Batang Kuantan	Pulau Berhalo	193.86	193.00	685.00	3.53	5.42
52	Rokan Kiri	Rokan Kiri	Lubuk Bendahara	86.41	86.00	123.00	1.42	2.41
53	Batang Kumu	Batang Kumu	Tanjung Medan	75.32	74.00	203.00	2.70	4.10
54	Wampu	Wampu	Stabat	125.30	122.00	540.00	4.31	6.19
55	Komering	Komering	Martapura	148.96	148.00	312.00	2.09	3.90
56	Asahan	Asahan	Pulau Raja	82.09	81.00	203.00	2.47	3.45
57	Lematang	Lematang	Pinang Belarik	90.31	87.00	383.00	4.24	6.15
58	Batang Anai	Batang Anai	Lubuk Simantung	67.20	67.00	42.00	0.63	1.00
59	Batanghari	Batang Tebo	Air Gemuruh	81.03	80.00	157.00	1.94	3.10
60	Ular	Ular	Pulau Tagor	72.03	71.00	79.00	1.10	2.32
61	Silau	Silau	Kisaranaga	93.00	92.00	102.00	1.10	2.80
62	Jambo Aye	Jambo Aye	Seureule	113.57	112.00	228.00	2.01	4.60
63	Jambo Aye	Jambo Aye	Pantai Balai	96.02	93.00	364.00	3.79	4.80

Table 2. (continued)

No.	River system	River	Site name	P (m)	W_b (m)	A (m ²)	R_b ($\approx d_m$) (m)	d_b (m)
64	Krueng Arakundo	Krueng Arakundo	Tj. Tuk Beulang	91.13	88.00	339.00	3.72	5.50
65	Manuhing	Manuhing	Tumbang Talaken	43.38	41.50	117.00	2.70	4.15
66	Sesayap	Sesayap	Jembatan Malinau	211.15	210.00	1145.00	5.42	7.95
67	Sesayap	Sesayap	Tanjung Lapang	182.24	180.00	758.00	4.16	5.85
68	Kayan	Kayan	Mara	263.01	260.00	1898.00	7.22	9.40
69	Selor	Selor	Jelera	112.40	110.00	445.00	3.96	6.20
70	Pimping	Pimping	Salimbatu	164.27	162.00	796.00	4.85	6.20
71	Kayan	Kayan	Salimbatu	296.19	295.00	1309.00	4.42	8.00
72	Mahakam	Mahakam	Kota Bangun	257.63	250.00	3640.00	14.13	26.00
73	Mahakam	Mahakam	Muara Pahu	107.18	101.00	699.00	6.52	12.60
74	Mahakam	Mahakam	Penyenggahan	266.10	255.00	3350.00	12.59	17.40
75	Mahakam	Mahakam	Muara Kaman	463.59	450.00	6040.00	13.03	16.10
76	Mahakam	Mahakam	Muara Pela	218.11	211.00	1542.00	7.07	10.50
77	Kayan	Selangket	Selangket	405.70	405.00	1051.00	2.59	6.10
78	Kayan	Kayan	Long Beluah	222.05	220.00	1323.00	5.96	7.86
79	Kayan	Kayan	Antutan	312.33	310.00	1989.00	6.37	8.20
80	Kayan	Kayan	Belayan	288.75	281.79	2896.00	10.03	15.62
81	Mahakam	Mahakam	Samarinda	540.93	537.66	7432.00	13.74	18.00
82	Riam Kanan	Riam Kanan	Awang Bangkal	52.46	51.50	104.00	1.98	2.55
83	Mahakam	Mahakam	Long Iram	165.75	160.00	1240.00	7.48	8.70
84	Mahakam	Mahakam	Melak	274.09	270.00	2760.00	10.07	15.28
85	Mahakam	Mahakam	Tenggarong	809.35	805.26	5483.00	6.77	12.48
86	Mentaya	Mentaya	Kuala Kuayan	108.53	108.00	183.00	1.69	2.26

Table 3. Relative percentages of spatial distribution of river bed and bank materials in Java, Sumatra, and Kalimantan islands.

Types of river bed–bank materials	Relative area coverage (%)		
	Java (127,151 km ²)	Sumatra (433,326 km ²)	Kalimantan (532,854 km ²)
Type 1: Quaternary volcanic deposits	46%	33%	0
Type 2: Quaternary alluvial–coastal deposits	37%	35%	44%
Type 3: Neogene–Paleogene sedimentary rocks	17%	28%	26%
Type 4: Mesozoic sedimentary rocks	0	0	16%
Type 5: pre-Neogene igneous and metamorphic rocks	0	4%	14%

Table 4. List of symbols used in the present study.

W_b	Bankfull channel width (m)
W_c	Bankfull channel width (m)
Q_{mean}	Mean annual discharge (m^3s^{-1})
Q_b	Bankfull discharge (m^3s^{-1})
P	Wetted perimeter (m)
A	Cross-sectional area (m^2)
R_h	Hydraulic radius (m)
d_m	Mean bankfull-channel depth (m)
d_b	Bankfull-channel depth (m)
S_n	Channel sinuosity
h	Thickness of bar deposits (m)
ϕ	half of maximum paleocurrent range (radian)
R^2	Coefficient of determination
r	Correlation coefficient
N	Number of data
p	Level of significance (from F -ratio for W_b , d_b , d_m)

Table 5. Width–discharge relationships in river channels in the Indonesian islands.

Region	Equation	N	r	R^2	p	Applicable range
A						
Java rivers	$Q_{\text{mean}} = 0.04W_b^{1.612}$	338	0.771	0.595	7.3×10^{-68}	$4 \leq W_b \leq 202$ m
Northward-flowing rivers (Java)	$Q_{\text{mean}} = 0.036W_b^{1.653}$	233	0.769	0.592	8.0×10^{-47}	$4 \leq W_b \leq 202$ m
Southward-flowing rivers (Java)	$Q_{\text{mean}} = 0.057W_b^{1.498}$	105	0.779	0.607	1.3×10^{-22}	$4 \leq W_b \leq 168$ m
Sumatra rivers	$Q_{\text{mean}} = 0.174W_b^{1.457}$	247	0.721	0.706	4.2×10^{-67}	$7 \leq W_b \leq 466$ m
Westward-flowing rivers (Sumatra)	$Q_{\text{mean}} = 0.281W_b^{1.232}$	86	0.781	0.610	7.1×10^{-19}	$9 \leq W_b \leq 126$ m
Eastward-flowing rivers (Sumatra)	$Q_{\text{mean}} = 0.169W_b^{1.511}$	161	0.872	0.766	5.5×10^{-52}	$7 \leq W_b \leq 466$ m
Kalimantan rivers	$Q_{\text{mean}} = 0.072W_b^{1.776}$	64	0.920	0.847	6.2×10^{-27}	$11 \leq W_b \leq 350$ m
Indonesian rivers (all data)	$Q_{\text{mean}} = 0.06W_b^{1.645}$	649	0.781	0.610	1.6×10^{-134}	$4 \leq W_b \leq 466$ m
B						
Java rivers	$Q_b = 0.95W_b^{1.426}$	338	0.827	0.684	6.1×10^{-86}	$4 \leq W_b \leq 202$ m
Northward-flowing rivers (Java)	$Q_b = 0.984W_b^{1.431}$	233	0.840	0.706	3.0×10^{-63}	$4 \leq W_b \leq 202$ m
Southward-flowing rivers (Java)	$Q_b = 0.760W_b^{1.456}$	105	0.794	0.796	5.8×10^{-24}	$4 \leq W_b \leq 168$ m
Sumatra rivers	$Q_b = 1.560W_b^{1.362}$	247	0.921	0.889	6.5×10^{-93}	$7 \leq W_b \leq 466$ m
Westward-flowing rivers (Sumatra)	$Q_b = 2.838W_b^{1.17}$	86	0.867	0.752	3.8×10^{-27}	$9 \leq W_b \leq 126$ m
Eastward-flowing rivers (Sumatra)	$Q_b = 1.278W_b^{1.428}$	161	0.925	0.846	1.7×10^{-66}	$7 \leq W_b \leq 466$ m
Kalimantan rivers	$Q_b = 1.078W_b^{1.441}$	64	0.969	0.923	2.0×10^{-27}	$11 \leq W_b \leq 350$ m
Indonesian rivers (all data)	$Q_b = 1.09W_b^{1.420}$	649	0.858	0.737	1.2×10^{-189}	$4 \leq W_b \leq 466$ m

Table 6. Width–depth relationships in river channels in the Indonesian islands.

Region	Equation	N	r	R^2	p
A					
Java rivers	$R_h (\approx d_m) = 0.59 d_b$	45	0.929	0.862	4.3×10^{-28}
Sumatra rivers	$R_h (\approx d_m) = 0.66 d_b$	19	0.972	0.933	1.4×10^{-10}
Kalimantan rivers	$R_h (\approx d_m) = 0.66 d_b$	22	0.945	0.888	1.8×10^{-12}
Indonesian rivers (all data)	$R_h (\approx d_m) = 0.65 d_b$	86	0.970	0.941	5.3×10^{-61}
B					
Java rivers	$W_b = 49.44 d_m^{0.62}$	45	0.657	0.542	8.4×10^{-9}
Sumatra rivers	$W_b = 75.27 d_m^{0.36}$	19	0.674	0.308	1.4×10^{-2}
Kalimantan rivers	$W_b = 60.73 d_m^{0.70}$	22	0.428	0.365	2.9×10^{-3}
Indonesian rivers (all data)	$W_b = 52.88 d_m^{0.70}$	86	0.711	0.674	3.7×10^{-22}
C					
Java rivers	$W_b = 33.57 d_b^{0.65}$	45	0.614	0.506	4.3×10^{-8}
Sumatra rivers	$W_b = 52.73 d_b^{0.49}$	19	0.756	0.411	3.1×10^{-3}
Kalimantan rivers	$W_b = 41.47 d_b^{0.74}$	22	0.433	0.424	1.0×10^{-3}
Indonesian rivers (all data)	$W_b = 33.63 d_b^{0.77}$	86	0.707	0.673	4.5×10^{-22}

Table 7. Empirical equations for the relationships between discharge parameters (Q_{mean} and Q_b) and bankfull channel width (W_b) and channel depth (d_m) and channel width (W_b) obtained from different regions.

Equation	Reference	Applicable range	Remarks
Channel width–mean discharge relationships			
$Q_{\text{mean}} = 0.06W_b^{1.645}$	Present study	$4 \leq W_b \leq 466$ m	Data are obtained from 649 measurement sites along various rivers in Java, Sumatra and Kalimantan islands.
$Q_{\text{mean}} = 0.0055W_b^{2.17}$	Carlston (1965)	–	Meandering river in central U.S.A. Cited by Shibata and Ito (2014).
$Q_{\text{mean}} = 0.027W_b^{1.17}$	Osterkamp and Hedman (1982)	$0.8 \leq W_b \leq 430$ m	Missouri river basin, U.S.A.
$Q_{\text{mean}} = 0.06W_b^{1.66}$	Williams (1984a)	$1.8 \leq W_b \leq 67$ m	Meandering rivers in Sweden.
$Q_{\text{mean}} = 0.09W_b^{1.11}$	Shibata and Ito (2014)	$35 \leq W_b \leq 1135$ m	Rivers in the Japanese islands. Data are obtained from 367 measurement sites along various rivers in Japan.
Channel width–bankfull discharge relationships			
$Q_b = 1.09W_b^{1.420}$	Present study	$4 \leq W_b \leq 466$ m	Data are obtained from 649 measurement sites along various rivers in Java, Sumatra and Kalimantan islands.
$Q_b = 0.126W_b^{1.84}$ ($W_b = 3.0825Q_b^{0.543}$)	Dury (1976)	$12 \leq Q_b \leq 290000$ m ³ s ⁻¹	Unbraided rivers in U.S.A, U.K., U.S.S.R., European mainland, China, Australia and India. Channel width defined by Dury as bed width and some data have been regarded as bankfull width by Williams (1984b). Discharges are most probable annual flood ($Q_{1.58}$).
$Q_b = 1.0W_b^{1.3}$	Williams (1984a)	$1.8 \leq W_b \leq 67$ m	Meandering rivers in Sweden, Q_b is the average annual peak discharge.
$Q_b = 0.05W_b^{2.04}$	Mackey (1993)	–	Cited by Bridge (2003).
$Q_b = 1.99W_b^{1.03}$	Shibata and Ito (2014)	$35 \leq W_b \leq 1135$ m	Rivers in the Japanese islands. Data are obtained from 356 measurement sites along various rivers in Japan.
Channel width–channel depth relationships			
$W_b = 52.88d_m^{0.70}$	Present study	$0.21 \leq d_m \leq 14.13$ m	Rivers in largest islands of west Indonesian. Data are obtained from 86 measurement sites along various rivers in Java, Sumatra, and Kalimantan islands.
$W_b = 47.00d_m^{0.98}$	Leopold and Maddock (1953)	$0.15 \leq d_m \leq 15.54$ m	Major river basins in U.S.A. (Yellowstone, Tennessee, Kansas, Missouri, Mississippi river basins).
$W_b = 12.82d_m^{1.59}$	Crane (1982)	$0.24 \leq d_m \leq 20.1$ m	Rivers in U.K., U.S.A, Canada, Australia, and India
$W_b = 21.3d_m^{1.45}$	Williams (1986)	$0.03 \leq d_m \leq 18$ m	Rivers in U.S.A, Sweden, U.S.S.R., Canada, Australia, and India.
$W_b = 8.88d_m^{1.82}$	Bridge and Mackey (1993)	–	

Table 8. Summary of paleohydrology parameters of the Bayah Formation.

Parameters	IV1 <i>n</i> = 48			IV2 <i>n</i> = 53			IV3 <i>n</i> = 24			IV4 <i>n</i> = 17			IV5 <i>n</i> = 30			IV6 <i>n</i> = 10			IV7 <i>n</i> = 25		
	Min.	Max.	Avg.	Min.	Max.	Avg.	Min.	Max.	Avg.	Min.	Max.	Avg.	Min.	Max.	Avg.	Min.	Max.	Avg.	Min.	Max.	Avg.
Max paleocurrent range	0.3 (rad)	2.6 (rad)	1.3 (rad)	0.1 (rad)	2.8 (rad)	1.3 (rad)	0.4 (rad)	1.7 (rad)	1.1 (rad)	0.1 (rad)	2.5 (rad)	1.3 (rad)	0.6 (rad)	1.8 (rad)	1.2 (rad)	0.8 (rad)	2.4 (rad)	1.6 (rad)	0.4 (rad)	2.7 (rad)	1.6 (rad)
Sinuosity	1.02	1.56	1.13	1.00	1.68	1.12	1.01	1.51	1.08	1.00	1.51	1.16	1.02	1.20	1.10	1.03	1.61	1.20	1.01	1.61	1.20
Avg. bar thickness	1.7 (m)	15.8 (m)	5.7 (m)	2.0 (m)	17.8 (m)	7.5 (m)	3.8 (m)	16.0 (m)	9.4 (m)	2.1 (m)	18.5 (m)	11.0 (m)	2.3 (m)	14.3 (m)	8.2 (m)	4.9 (m)	12.5 (m)	9.2 (m)	1.7 (m)	11.6 (m)	5.6 (m)
Max. bankfull depth	1.7 (m)	15.8 (m)	5.7 (m)	2.0 (m)	17.8 (m)	7.5 (m)	3.8 (m)	16.0 (m)	9.4 (m)	2.1 (m)	18.5 (m)	11.0 (m)	2.3 (m)	14.3 (m)	8.2 (m)	4.9 (m)	12.5 (m)	9.2 (m)	1.7 (m)	11.6 (m)	5.6 (m)
Mean bankfull depth	1.1 (m)	10.3 (m)	3.7 (m)	1.3 (m)	11.6 (m)	4.9 (m)	2.5 (m)	10.4 (m)	6.1 (m)	1.4 (m)	12.0 (m)	7.2 (m)	1.5 (m)	9.3 (m)	5.3 (m)	3.2 (m)	8.1 (m)	6.0 (m)	1.1 (m)	7.5 (m)	3.6 (m)
Channel width	57 (m)	270 (m)	132 (m)	64 (m)	294 (m)	160 (m)	100 (m)	272 (m)	188 (m)	65 (m)	302 (m)	210 (m)	71 (m)	252 (m)	171 (m)	120 (m)	229 (m)	185 (m)	57 (m)	217 (m)	131 (m)
Maximum bankfull discharge	337 (m ³ /s)	3090 (m ³ /s)	1122 (m ³ /s)	396 (m ³ /s)	3479 (m ³ /s)	1473 (m ³ /s)	750 (m ³ /s)	3129 (m ³ /s)	1844 (m ³ /s)	412 (m ³ /s)	3615 (m ³ /s)	2156 (m ³ /s)	463 (m ³ /s)	2799 (m ³ /s)	1610 (m ³ /s)	973 (m ³ /s)	2444 (m ³ /s)	1805 (m ³ /s)	337 (m ³ /s)	2273 (m ³ /s)	1102 (m ³ /s)